Control strategies of series active variable geometry suspension for cars

Cheng Cheng

Department of Electrical and Electronic Engineering

Imperial College London

This dissertation is submitted for the degree of

Doctor of Philosophy

January 2018

I would like to dedicate this thesis to my loving parents and my husband

Declaration of Originality

I hereby declare that this thesis is the result of my own work, all material in this dissertation which is not my own work has been properly acknowledged.

Cheng Cheng
January 2018

Declaration of Copyright

Cheng Cheng
January 2018

Acknowledgements

This thesis is the result of research work carried out at the Department of Electrical and Electronic Engineering, Imperial College London. First and foremost, I wish here to sincerely thank my supervisor, Dr. Simos Evangelou, who supported and guided me with patience and efforts during my whole PhD and Msc studies. His constant guidance and encouragement continuously motivated me to reach my objectives and provided me an excellent atmosphere for doing research. His attention to details and profound insights have been true inspiration to my research.

I would also like to thank Dr. Arana Carlos, for helping me become familiar with SAVGS concept and Autosim. Also thanks to Min Yu who has supported me by sharing his knowledge in vehicle dynamics. I am very fortunate to have had them as my research collaborator during my PhD. They made my research go more smoothly than what I expected.

Thanks to all the students and staff of the control and power research group for giving me an enriching and stimulating as well as friendly and warm environment during my stay here. Special gratitude goes to my friends, Boli Chen, Xuefang Li, Mingyang Sun, Dixi Liu, Jingye Sun, Zongxiang Wu, Yujie Wu, Yang Wang, Chen Wang, Hailing Fu, Yuan Qin, Hang Ren, Mayue Shi, Peng Li, Chengyuan Liu, Jingjing Jiang, Yunyang Wu, Yujian Ye, Ming Ge, Luxin Zhang, Fangjing Hu, for helping in different ways, and for the tea breaks, great lunches and dinners we had together in the past years.

I would also extend my gratitude to Tianjin University and Glasgow University for providing me the excellent undergraduate educational experience and leading me to the hall of knowledge.

Finally, I would like to express my deepest gratitude to my loving parents, for their everlasting love and unconditional support. And last, but not least, my thanks goes to my husband Yilun, who is taking the word worry out of my vocabulary and replacing it with happiness. I could not complete this work without his constant support and encouragement.

Abstract

This thesis develops control strategies of a new type of active suspension for high performance cars, through vehicle modelling, controller design and application, and simulation validation. The basic disciplines related to automotive suspensions are first reviewed and are followed by a brief explanation of the new Series Active Variable Geometry Suspension (SAVGS) concept which has been proposed prior to the work in this thesis. As part of the control synthesis, recent studies in suspension control approaches are intensively reviewed to identify the most suitable control approach for the single-link variant of the SAVGS.

The modelling process of the high-fidelity multi-body quarter- and full- vehicle models, and the modelling of the linearised models used throughout this project are given in detail. The design of the controllers uses the linearised models, while the performance of the closed loop system is investigated by implementing the controllers to the nonlinear models.

The main body of this thesis elaborates on the process of synthesising $\mathcal{H}_\infty$ control schemes for quarter-car to full-car control. Starting by using the quarter-car single-link variant of the SAVGS, an $\mathcal{H}_\infty$ -controlled scheme is successfully constructed, which provides optimal road disturbance and external force rejection to improve comfort and road holding in the context of high frequency dynamics. This control technique is then extended to the more complex full-car SAVGS and its control by considering the pitching and rolling motions in the context of high frequency dynamics as additional objectives. To improve the level of robustness to single-link rotations and remove the geometry nonlinearity away from the equilibrium position, an updated approach of the full-car SAVGS $\mathcal{H}_\infty$ -controlled scheme is then developed based on a new linear equivalent hand-derived full-car model. Finally, an overall SAVGS control framework is developed, which operates by blending together the updated $\mathcal{H}_\infty$ controller and an attitude controller, to tackle the comfort and road holding in the high frequency vehicle dynamics and chassis attitude motions in the low frequency vehicle dynamics simultaneously.

In all cases, cascade inner position controllers developed prior to the work in this thesis are employed at each corner of the vehicle and combined with the control systems developed in this thesis, to ensure that none of the physical or design limitations of the actuator are violated under any circumstances.

Table of contents

Acronyms and Abbreviation **xvi**

List of figures **xix**

List of tables **xxvii**

1 Introduction **1**
1.1 A Brief Background 1
1.2 Research aims 3
1.3 Outline of thesis 4

2 Literature review **7**
2.1 Suspension functions 7
2.2 Classification of suspension systems 9
2.2.1 Passive suspension 12
2.2.2 Semi-active suspension 14
2.2.3 Active suspension 16
2.2.4 Brief review of previous SAVGS studies 20
2.3 Vehicle Models and Suspension Performance Indices 22
2.3.1 Quarter-car model 23
2.3.2 Half-car model 23
2.3.3 Full-car model 24
2.3.4 Multibody models 25
2.3.5 Suspension Performance Indices 26
2.4 Classification of suspension control methodologies 28
2.4.1 PID control 28
2.4.2 Adaptive control 28
2.4.3 Optimal control 29
2.4.4 Fuzzy logic and Neural Network control 31

2.4.5 Robust control and the review of H_∞ Control for Vehicle Active Suspension Systems . . . 33
2.5 Conclusions . . . 41

3 Vehicle Modelling 43
3.1 Vehicle models . . . 43
3.1.1 Software . . . 43
3.1.2 Types of models . . . 44
3.1.3 Reference frames . . . 46
3.1.4 Symbols for vehicle models . . . 47
3.1.5 SAVGS quarter-car multi-body model (QC) . . . 48
3.1.6 SAVGS full-car multi-body model (FC) . . . 49
3.1.7 SAVGS Autosim quarter-car linearised model (QCL) . . . 52
3.1.8 SAVGS Autosim full-car linearised model (FCL) . . . 53
3.1.9 SAVGS hand-derived quarter-car linearised model (QECL) . . . 53
3.1.10 SAVGS full-car hand-derived linear equivalent model (FECL) . 56
3.2 Vehicle and SAVGS parameters . . . 66
3.2.1 Main vehicle parameters . . . 66
3.2.2 SAVGS parameters . . . 66
3.3 Road models . . . 67
3.3.1 Sinusoidal input . . . 67
3.3.2 Smoothed bump input . . . 69
3.3.3 Random road profiles . . . 69
3.4 Type of closed-loop control schemes . . . 70
3.4.1 Quarter-car closed-loop control schemes . . . 72
3.4.2 Full-car closed-loop control schemes . . . 72
3.5 Conclusions . . . 73

4 $\mathcal{H}_\infty$ control synthesis for quarter-car comfort and road holding enhancement 75
4.1 Quarter-car multi-body model (QC) . . . 76
4.2 General Control Scheme . . . 76
4.3 $\mathcal{H}_\infty$ control synthesis framework . . . 77
4.3.1 Quarter-car Autosim linearized model (QCL) . . . 77
4.3.2 Frequency response . . . 80
4.3.3 Controller design . . . 84
4.4 Simulation results . . . 88

4.4.1 Quarter-car simulation results . . . 88
4.4.2 Full-car simulation results with quarter-car controller . . . 97
4.5 Conclusions . . . 101

5 $\mathcal{H}_\infty$ CONTROL SYNTHESIS FOR FULL-CAR COMFORT AND ROAD HOLDING ENHANCEMENT 107
5.1 Full-car multi-body model (FC) . . . 108
5.2 General Control Scheme . . . 108
5.3 $\mathcal{H}_\infty$ control synthesis framework . . . 111
5.3.1 Full-car Autosim linearized model (FCL) . . . 111
5.3.2 Controller design . . . 112
5.4 Full-car simulation results and comparison . . . 115
5.4.1 Controllers for comparison . . . 117
5.4.2 Random road profile . . . 117
5.4.3 Smoothed bump profile . . . 121
5.4.4 Inner position controller performance . . . 123
5.5 Conclusions . . . 126

6 $\mathcal{H}_\infty$ CONTROL SYNTHESIS WITH HAND-DERIVED MODEL FOR FULL-CAR COMFORT AND ROAD HOLDING ENHANCEMENT 129
6.1 Full-car model . . . 130
6.1.1 SAVGS nonlinear multi-body model . . . 130
6.1.2 SAVGS linear hand-derived equivalent model . . . 130
6.2 $\mathcal{H}_\infty$ control design . . . 137
6.2.1 Control objectives . . . 137
6.2.2 Robust control scheme . . . 138
6.3 Nonlinear control scheme . . . 145
6.4 Simulation results and comparison . . . 146
6.4.1 Response to random road profiles . . . 147
6.4.2 Response to a smoothed bump . . . 150
6.4.3 Position controller performance . . . 152
6.5 Conclusions . . . 153

7 FULL-CAR OVERALL CONTROL FOR COMBINED ATTITUDE CONTROL, COMFORT AND ROAD HOLDING IMPROVEMENT 155
7.1 Overall control framework for comfort, road holding enhancement and attitude control . . . 156

7.1.1 Overall SAVGS control framework 156
7.1.2 Attitude control 157
7.2 Simulation results and comparisons 159
7.2.1 Random road profiles 160
7.2.2 Smoothed bump 163
7.2.3 Steady-state cornering 164
7.2.4 Step steer 165
7.2.5 Pure longitudinal accelerating and braking 166
7.2.6 Position controller performance 168
7.3 Conclusions 170

8 Conclusions and future work **173**
8.1 Conclusions 173
8.2 Future work 175

References **177**

Acronyms and Abbreviation

ABC	Active Body Control
CM	Centre of sprung mass
DOF	Degree of Freedom
FC	Full Car
FCL	Full Car Linear
FECL	Full Car Equivalent Linear
HC	Hub Carrier
ICE	Internal Combustion Engine
ISO	International Organisation for Standardisation
GT	Grand Tourer
LQG	Linear Quadratic Gaussian
LQR	Linear Quadratic Regulator
LMI	Linear Matrix Inequality
LW	Lower Wishbone
MIMO	Multi-input multi-output
MPC	Model Predictive Control
PID	Proportional-Integral-Derivative
PMSM	Permanent Magnet Synchronous Machine
PSD	Power Spectral density
QC	Quarter Car
QCL	Quarter Car Linear
QECL	Quarter Car Equivalent Linear
RMS	Root Mean Square
SAVGS	Series Active Variable Geometry Suspension
SD	Spring-damper
SL	Single-link
SISO	Single Input Single Output
UW	Upper Wishbone
WH	Wheel
RHI	Road Holding Index
RCI	Road Comfort Index

List of figures

2.1 Conventional suspension configuration [26] 8
2.2 A solid axle beam dependent leaf-spring suspension system [129] 10
2.3 Examples of independent suspension system. Image from [2, 35, 41, 128] 11
2.4 Double wishbone independent suspension system 12
2.5 Quarter-car passive suspension configuration. 13
2.6 Schematic configuration of the Electrorheological (left) and Magnetorheological (right) shock absorbers [33, 182]. 15
2.7 Quarter-car semi-active suspension configuration. 15
2.8 An example of electromagnetic active suspension system [65]. 19
2.9 Single-link variant of the SAVGS [10]. (a) Passive equilibrium position, T_{SAVGS}; (b) Rotated configuration. 22
2.10 (a) Passive double-wishbone suspension, and (b) SAVGS-retrofitted suspension. 22
2.11 Quarter-car active automotive suspension. The particular case of an actuator in series with a passive spring is shown. 24
2.12 Half-car active automotive suspension. The particular case of an actuator in series with a passive spring is shown. 24
2.13 Full-car active automotive suspension. The particular case of an actuator in series with a passive spring is shown. 25
2.14 Generalized bock diagram of $\mathcal{H}_\infty$ syntheses. $P(s)$ is the car model and $K(s)$ is the $\mathcal{H}_\infty$ controller. The inputs $d(s)$ and outputs $z(s)$ of P are vector valued signals. The components of $d(s)$ are the exogenous input disturbances. The components of $z(s)$ are the performance variables of interest to be minimised. The measurement signals that are used by controller $K(s)$ are denoted $y(s)$ and the controlled inputs generated by the controller are denoted $u(s)$. 36
2.15 Classic unity feedback structure [150]. 39

2.16 The new generalised plant $P_w(s)$ with weighting functions W_d and W_p . 40

3.1 SAE vehicle axis system [154]. 46

3.2 Global and local reference frames of full-car SAVGS configuration and the external forces acting on the the vehicle during acceleration and cornering, in x-y (top), y-z (middle) and x-z (bottom) planes respectively. The reference frames used in this project are the right-hand orthogonal axis system. Positive lateral and longitudinal accelerations are shown in this case (i.e, a_x, $a_y > 0$). 47

3.3 Quarter-car arrangement. Points A, C and G are attached to the chassis; points E and F are fixed to the spring-damper unit; and points B,D, H and I are fixed to the wheel. The length of the spring-damper unit and its orientation can be continuously controlled through the rotation of the single-link with respect to its default equilibrium position [9]. . . . 50

3.4 Full-car multi-body structure [11]. Except for the chassis, S, which has six degree of freedom, the other bodies shown in this model only have a rotational degree of freedom. LW and UW are the lower and upper wishbones. AHC and HC represent the hub carriers. WH refers to wheels and PIN refers to steering pinion. ICE is the internal combustion engine, and CRW and DFG are the crown wheel and the gears in the differential, respectively. 51

3.5 One corner (rear right) configurations of the GT. (a) Passive suspension configuration; (b) the extension of the passive suspension by employing the variant of the SAVGS; and (c) dynamic equilibrium, in where the SAVGS compensates for the increased tire load and ensures that the wishbones remain in their desired positions. 52

3.6 Nonlinear damper force versus damper extension rate. c_0 at the front axles is 12980Ns/m and c_0 at the rear axles is 24236Ns/m. c_0 is chosen such that the frequency responses of the linearised GT model to an average quality random road match well the PSDs of the nonlinear GT model for the same road. 53

3.7 SAVGS suspension and equivalent hand-derived model. 54

3.8 Full-car hand-derived linear equivalent model for the study of vehicle dynamic response. 57

3.9 Ferrari F430, the high performance sports car used in this thesis. 66

3.10 Example PSDs for road profiles with roughness A and C considered in this chapter, shown in red and green lines, which correspond to good and average quality road. G_d is the displacement power spectral density as a function of spatial frequency, n. Classification of roads A to H are defined in [ISO 8608:1995] [85]. 71

4.1 Nonlinear control scheme (QA-SAVGS) for the quarter-car model. . . 77

4.2 Details of position control, K_{slp}, of the single-link shown in Fig. 4.1. Starting from the position error signal, controllers B, C1 and C2 are combined with several dynamic saturation blocks and feedback loops in order to generate suitable voltage commands for the bridge converter that drives the PMSM actuator. The proposed scheme provides good position tracking performance and ensures that none of the physical or design limitations of the actuator are violated under any circumstances. Further details can be found in [10]. 77

4.3 Bode plots of the quarter-car model from single-link angle and nominal single-link offset angle $\Delta\theta_{SL}^{(ne)}$ to (a) sprung mass acceleration, (b) suspension deflection, and (c) tyre deflection. 78

4.4 Magnitude Bode plots of the quarter-car vehicle plant. From vertical road speed (top row) , external vertical force acting on the sprung mass (second row) and single-link rotational velocity (third row) to dynamic tyre deflection (left column), sprung mass acceleration (middle column) and dynamic suspension deflection (right column). 81

4.5 New $\mathcal{H}_\infty$ control scheme for disturbance rejection showing weighting functions, W_{perf1}, W_{perf2}, W_{perf3}, W_{act1}, W_{act2}, W_{act3}, W_{dist1}, W_{dist2}. . . 84

4.6 Singular value plots for the closed-loop (dotted) and open-loop (solid) systems with all the frequency weights. 87

4.7 Frequency response of the designed $\mathcal{H}_\infty$ controller. 87

4.8 Quarter-car time responses under 2 Hz sinusoidal roadway displacement with amplitude of 0.01 m, for the passive suspension and SAVGS $\mathcal{H}_\infty$-controlled configurations. 89

4.9 Random road profile for 30.6 m/s forward vehicle speed. 90

4.10 Quarter-car time responses for the random road excitation in Fig. 4.9, for the passive suspension and SAVGS $\mathcal{H}_\infty$-controlled configurations. Results obtained for the passive suspension and SAVGS $\mathcal{H}_\infty$-controlled configurations 91

4.11 Bode magnitude plots for the nonlinear quarter car model with random road disturbance inputs to the outputs: a) body vertical acceleration, b) tyre deflection and c) suspension travel. 92
4.12 Quarter-car time responses when running over a road bump of 0.05 m height at 5.56 m/s forward vehicle speed, for the passive suspension and SAVGS $\mathcal{H}_\infty$-controlled configurations. 94
4.13 Quarter-car time responses with a sinusoidal external force disturbance with forward velocity $5.56m/s$, for the passive suspension and SAVGS $\mathcal{H}_\infty$-controlled configurations. 95
4.14 Random external vertical force profile 96
4.15 Bode magnitude plots for the nonlinear quarter car model with random external force disturbance to the outputs: a) body vertical acceleration, b) suspension deflection and c) tyre deflection. 96
4.16 Output torque vs. single-link speed characteristics for bump and random disturbance forcing events of the nonlinear quarter-car with SAVGS, presented in Figs. 4.12, 4.10, 4.13 and 4.15. The actuator limit boundaries are symmetric about the horizontal axis. 97
4.17 Vertical acceleration at each corner of the full-car vehicle when running over a road bump at 20 m/s forward speed, for the SAVGS $\mathcal{H}_\infty$ scheme and the passive suspension. The bump starts at 0.5 s. 99
4.18 Tyre deflection of each corner at the full-car vehicle when running over a road bump at 20 m/s forward speed, for the SAVGS $\mathcal{H}_\infty$ scheme and the passive suspension. The bump starts at 0.5 s. 100
4.19 Suspension deflection at each corner of the full-car vehicle when running over a road bump at 20 m/s forward speed, for the SAVGS $\mathcal{H}_\infty$ scheme and the passive suspension. The bump starts at 0.5 s. 101
4.20 Rotational angle at each corner of the full-car vehicle when running over a road bump at 20 m/s forward speed, for the SAVGS $\mathcal{H}_\infty$ scheme and the passive suspension. The bump starts at 0.5 s. 102
4.21 Vertical acceleration at each corner of the full-car vehicle for a brake in turn event. Braking starts at 0.5 s. 103
4.22 Tyre deflection at each corner of the full-car vehicle for a brake in turn event. Braking starts at 0.5 s 104
4.23 Single-link angles for a brake in turn event. Braking starts at 0.5 s . . . 104
4.24 Pitch and roll angles for passive and SAVGS cases during a brake-in-turn event. Braking starts at 0.5 s 105

5.1 Responses at the rear left wheel of the GT. Power spectral density (PSD) plots of the reference single-link velocity and the actual velocity generated by the actuator undergoing random road classes A and C. . . 109
5.2 General full-car control scheme (F-SAVGS). 110
5.3 Bode plots of the full-car linearised model. The gains correspond to the nominal offset angle $\theta_{\mathrm{SL}}^{ne} = \theta_{\mathrm{SL}}^{min} + \Delta\theta_{\mathrm{SL}}$ when $\Delta\theta_{\mathrm{SL}} = 90°$. The responses are from the inputs: vertical road speeds (first row), exogenous torques at the mass centre (second row), and SL angular speed. To outputs: vertical acceleration, suspension deflection and tyre deflection at the rear-left wheel (first three columns), as well as pitching (forth column) and rolling (fifth column) accelerations at centre of mass of the GT. . . 112
5.4 $\mathcal{H}_\infty$ control scheme. 114
5.5 Singular value plot of the designed $\mathcal{H}_\infty$ controller. 116
5.6 Singular value plots for the weighted systems: closed-loop system with dotted line and open-loop system with solid line. 116
5.7 Sprung mass vertical acceleration PSDs for each corner of the GT under uneven an random disturbance (Road class C). The results of the aforementioned controllers in 5.4.1 are compared with passive suspension. 119
5.8 Sprung mass vertical acceleration PSDs for each corner of the GT under uneven random disturbance (Road class A). The results of the aforementioned controllers in 5.4.1 are compared with passive suspension. 120
5.9 Pitching and rolling accelerations PSD plots at the mass centre of the GT under an uneven random disturbance (Road class C). Results of the controllers in 5.4.1 are compared with passive suspension. 121
5.10 Pitching and rolling accelerations PSD plots at the mass centre of the GT under uneven an random disturbance (Road class A). Results of the controllers in 5.4.1 are compared with passive suspension. 122
5.11 The 5 s to 10 s time series simulation results under random road class A. The plots are: 1) road profile; 2) single-link angle; and 3) vertical acceleration at the rear-right wheel; 4) pitching; and 5) rolling accelerations at the sprung mass centre. 123
5.12 Response at the rear-left wheel while running over a smoothed bump at the left wheels. Passive suspension and SAVGS $\mathcal{H}_\infty$-controlled system (F-SAVGS) are undergoing the same smoothed bump excitation with a $5\,cm$ height and $2\,m$ width. The other three wheels have similar simulation results. 124

5.13 Rotational accelerations (F-SAVGS and PASSIVE) at the mass centre under smooth bump disturbance at the left wheels: (a) pitching acceleration; and (b) rolling acceleration. 124
5.14 The boundaries of the output torques vs. single-link speeds characteristics for random road C of the $\mathcal{H}_\infty$ controlled SAVGS system (F-SAVGS). 1, 2, 3, and 4 match actuators in the different corners presented in Fig.3.2. 125

6.1 A new model with better robustness to single-link rotation 131
6.2 SAVGS-retrofitted double-wishbone suspension (left) and equivalent hand-derived model of the rear left corner of the GT (right). The full-car equivalent schematic has been shown in Figure 3.8. 132
6.3 Evolution of a_f (front axle) and a_r (rear axle) as a function of the single-link angle $\Delta\theta_{SL} = \theta_{SL} - \theta_{SL}^{(min)}$. Red lines represent the curves of a_f and a_r at the nominal equilibrium position in which $\Delta\theta_{LW} = 0.1881\,rad$. The gray bands indicate the influence of lower wishbone angular change around the nominal case, $\Delta\theta_{LW} \in [0, 0.3]\,rad$. 134
6.4 Evolution of $k_{eq_{f/r}}$ (top row) and $c_{eq_{f/r}}$ (bottom row). The red lines represent the curves of $k_{eq_{f/r}}$ and $c_{eq_{f/r}}$ at the nominal equilibrium position in which $\Delta\theta_{LW} = 0.1881\,rad$. 135
6.5 Frequency response from the exogenous disturbances (i.e. road speed at four corners (top), pitch and roll torque at CM (middle), and the speeds for the equivalent linear actuators (bottom), to suspension velocity and tyre deflection at the rear left corner of the GT (left two columns), and vertical, pitching and rolling accelerations at CM (right three columns). The results are obtained at the nominal single-link angle $\theta_{SL}^{(ne)} = \theta_{SL}^{min} + 90°$. 136
6.6 Interconnection for $\mathcal{H}_\infty$ control synthesis. 139
6.7 Bode magnitude plot of controller, from 11 measurement signals $\mathbf{y}$ to the first control effort $u_1 = \dot{z}_{lin1}^*$ at the front left corner of the vehicle. The other three corners of the vehicle have very similar results to the shapes of these curves. 144
6.8 General nonlinear control scheme (FE-SAVGS). 145
6.9 Evolution of β_f and β_r as a function of $\Delta\theta_{SL}$. 147
6.10 PSDs for sprung mass vertical, pitching and rolling accelerations at the mass centre of the GT with road class A (bottom row) and C (top row). 149
6.11 PSDs for tyre deflections of four corners of vehicle systems with road class C. 150

6.12 Response time histories of vehicle systems for random class C during a 5 s period simulation. 151
6.13 Response time histories of vehicle systems for one side bump disturbances: (a) road inputs at four corners; (b) vertical accelerations at mass centre; (c) pitching accelerations; (d) rolling accelerations; (e) tyre deflection at rear left wheel; (f) single-link rotation for SAVGS controlled systems at rear left wheel. 152
6.14 Output torque vs. single-link velocity characteristics for random road class C (only shows the boundaries), presented in Figure 6.12. The black envelop is the actuator limit boundaries. 153

7.1 Overall SAVGS control framework (FE-PID-SAVGS). 157
7.2 PSDs for sprung mass vertical, pitching and rolling accelerations at the mass centre of the GT with random road sections of class C (top row) and A (bottom row). 162
7.3 Response time histories of vehicle systems for random class C during a 20 s period simulation. 164
7.4 Response time histories of vehicle systems for one sided bump disturbances: (a) road inputs at four corners; (b) vertical accelerations at mass centre; (c) pitching accelerations; (d) rolling accelerations; (e) tyre deflection at rear left wheel; (f) single-link rotation for SAVGS controlled systems at rear left wheel. 165
7.5 Roll reduction during steady-state cornering at different lateral accelerations. 166
7.6 Roll peak angle reduction for different lateral accelerations during step steer. 167
7.7 Forward speed velocity profiles for the longitudinal accelerating and braking manoeuvre. 167
7.8 Simulation results for the longitudinal and braking manoeuvre: (a) pitch angles; (b) pitching accelerations; (c) sprung mass vertical acceleration at the rear left wheel; and (d) single-link angle of the rear left wheel. 169
7.9 Output torque vs. single-link velocity characteristics for: (a) random road class C (only shows the boundaries); (b) longitudinal acceleration and braking event of the nonlinear simulations, presented in Figures 7.3 and 7.8. Black envelope is the actuator limit boundaries. 170

List of tables

2.1 Advantages and disadvantages of hydraulic actuators in vibration control systems. 18
2.2 Advantages and disadvantages of electromagnetic actuators in the vibration control systems. 19

3.1 Vehicle models used for the work of this thesis 45
3.2 Symbols of the SAVGS and hand-derived full-car model 48
3.3 The main assumptions in the multi-body quarter-car model [13]. 49
3.4 The main constraints and assumptions in the linear quarter-car model . 52
3.5 Full-car vehicle parameters 67
3.6 SAVGS parameters 68
3.7 Full-car nonlinear control schemes in this thesis 73

4.1 Quarter-car SAVGS symbols 78
4.2 Ride comfort analysis (SI units) 93
4.3 Road holding analysis (SI units) 93

5.1 full-car SAVGS symbols 108
5.2 Ride comfort index (m/s^2) at four corners ((%) = Performance Improvement (%) compared to Passive) 118
5.3 Peak values of tyre deflection (cm) at four corners, ((%) = Performance Improvement (%) compared to Passive) 118
5.4 Mass centre comfort index (MCI) (m/s^2), ((%) = Performance Improvement (%) compared to Passive) 121
5.5 Power losses in the actuator 125

7.1 Attitude control gains 159
7.2 RMS of vertical, pitching and rolling accelerations ((%) = Performance Improvement (%) compared to Passive) 163

Chapter 1

Introduction

1.1 A Brief Background

As many other vehicle systems, the development of suspensions has been influenced by the evolution of the transportation technology. In the early years, carts were not having any type of suspension at all. Until the eighteenth century, the primitive suspension was an iron chain. Metal springs and leaf springs were first designed at that time period. Various implementations have been developed until the last century, which saw the development of the suspension with the following basic components: a spring and a damper [132]. Ride comfort was the first performance shown in the studies that can date back to the 1920s and 1930s [105, 124]. The analysis of handling and steering followed during the mid-1950s and was successfully in applying control theory, which was previously used in aircraft studies [116]. In the following decades, the compromises between ride and handling behaviour of the vehicle were a critical aspect of the importance of subjective evaluation in vehicle dynamics for both customers and manufacturers. With the evolution of digital computers, the complexity of vehicle models were grown at full speed due to the greater processing power. In particular, the software environment for the multi-body system contributes to the formulation of motion equations for complex models which could never have been tackled by hand [37].

A vehicle suspension system provides ride comfort and road holding properties as the suspension supports the vehicle body and transmits load forcing by road excitation between the chassis and the wheels. The suspension design seeks to resolve the conflict of improving ride comfort and road holding simultaneously [149]. Essentially suspensions can be categorised into three main types: passive [122], semi-active [33, 126, 182], and active suspension systems [91, 183]. A passive suspension consists of a spring and

a damper, which can only store or dissipate energy. However such single spring and damper combination is not capable of simultaneously achieving the many purposes of the suspension system. A semi-active suspension is one with no external force sources employed, but where some control is achieved by switching the characteristics of the passive suspension components. The concept of active vehicle suspension has attracted great interest in both the academic and industrial fields since the late 1960s; see [58, 67, 114, 149] and the references therein. The primary advantage of active suspension, compared with the passive and the semi-active suspension presented in most of today's cars, is its ability of reducing the conflict between achieving passenger comfort and road holding [137]. However, despite their advanced capabilities, active suspensions have not had a significant impact in the automotive market due to several disadvantages, related to power requirements, weight, size and complexity [54].

The research focus of this project is to develop control strategies for a new concept of mechatronic vehicle active suspension, namely the series active variable geometry suspension (SAVGS). This suspension concept has been initially proposed in a patent [51] at Imperial College London as a solution with the potential to provide better suspension performance than passive/semi-active suspensions and avoid the inherent disadvantages of active suspensions regarding to less weight and less energy consumption. Then, the thesis [13] and the corresponding publications [9–11] have further studied the SAVGS concept for cars through: 1) developing virtual and experimental tools to better understand its behaviour, advantages and weaknesses; and 2) investigating the interdependence between the vehicle properties and the requirements for the main SAVGS components to enable system dimensioning. The successful design of the SAVGS is also determined by choosing a suitable control strategy to simultaneously obtain excellent ride comfort and handling, with some initial control design also conducted in [9–11].

The issue of control in active suspension has attracted attention of researchers for many years. Typically, linear control methods such as PID [104], model predictive control (MPC) [97, 112] and $H_2/\mathcal{H}_\infty$ [160] control have been developed in several studies and widely applied to industry due to their simplistic design. To manage a more complex model, backstepping [156] and adaptive sliding-mode [107] nonlinear control techniques are commonly used. Regarding to highly-nonlinear systems in which the models are more complex, fuzzy logic and neural network control have been successfully applied, as for example in [108, 184]. This project will focus on the design of a control scheme for a car model with SAVGS. More importantly, this controller will then be applied to the real test rig of a high performance car over a wide range of road

input conditions and uncertainties in the future work. Therefore, since the car model is nonlinear and complex, nonlinear control will not be considered in the present work. Instead, $\mathcal{H}_\infty$ techniques are found to be more suitable as a powerful tool when solving robust control problems, which has been applied to active suspension controls since 1980s [56, 72, 174, 181]. Meanwhile, $\mathcal{H}_\infty$ techniques have the advantage over classical control techniques because they are multi-input multi-outputs (MIMO) control techniques that are applicable to solve multivariable problems in the frequency domain. Demonstrations of $\mathcal{H}_\infty$ based design techniques to active suspension system have been reported in the literature to guarantee stable and robust operation of the system in [181]. In this work, a comprehensive approach to development and verification of the control strategies of the SAVGS are conducted using the $\mathcal{H}_\infty$ technique.

1.2 Research aims

The main research aims of the work described in this thesis are summarised as follows:

- to identify the best control techniques that will solve the multi-objective SAVGS control problem and achieve stabilisation with guaranteed performance,
- to model the high-fidelity multi-body quarter- and full-vehicle nonlinear models (with passive and SAVGS-retrofitted suspensions) to virtually test the control algorithms and compare the performance of different controllers,
- to linearise the nonlinear vehicle models at the equilibrium position or to develop simple hand-derived equivalent models for control synthesis,
- to formulate $\mathcal{H}_\infty$ control synthesis for the quarter-car single-link variant of the SAVGS, with the aim of providing optimal road disturbance and external force rejection to improve passenger ride comfort and road holding in the context of high frequency vehicle dynamics,
- to apply the quarter-car $\mathcal{H}_\infty$ control technique experience to the full-car SAVGS vehicle control by considering the addition of the pitching and rolling motions to the high-frequency suspension functions as additional objectives,
- to develop an attitude control scheme with the full-car SAVGS for the mitigation of pitch and roll motions to the low-frequency suspension functions during turning manoeuvres or longitudinal acceleration/braking, and

- to develop an overall full-car SAVGS control scheme to assess the overall requirements by blending the $\mathcal{H}_\infty$ and attitude control together, in terms of improving the combined ride comfort, road holding and vehicle attitude motions control simultaneously.

1.3 Outline of thesis

Chapter 2 contains a thorough literature review of the state-of-the-art in the field of vehicle suspension systems, together with a brief explanation of the new Series Active Variable Geometry Suspension (SAVGS) [51] concept. A review of recent studies on control approaches to active suspension is also completed and compared.

Chapter 3 forms the foundation of this project, providing the modelling of the multi-body quarter- and full-car nonlinear models and the linearisation of the quarter- and full-car models. The selection of the software packages (AutoSim and MATLAB) used for the development of the models and the testing of the control systems are also justified in this chapter. Also, lists of the vehicle parameters and actuator components used for the high performance car in subsequent chapters are supplied. Moreover, the system performance indexes used to compare the performance of different systems and the modelling of the road disturbances to excite the vibration of the vehicle are explained.

Chapter 4 details the development of a SAVGS $\mathcal{H}_\infty$ -controlled scheme based on a quarter-car model, which is the linearisation of the nonlinear quarter-car in AutoSim at a trim state. The closed-loop controlled system aims to tackle comfort and road holding objectives simultaneously and the tuning process of the controller design is discussed in detail. The simulation results of the passive and SAVGS $\mathcal{H}_\infty$ -controlled nonlinear quarter-car are presented to characterise the behaviour of the system and to quantify control performance with a range of road and external load disturbances. The obtained quarter-car $\mathcal{H}_\infty$ controller is then equipped at each corner of the active suspension to control the full-vehicle model. Simulation results are carried out, which contribute a good reference point for the development of the full-car specific controller in the subsequent chapters.

Chapter 5 details the development of a SAVGS $\mathcal{H}_\infty$ -controlled scheme based on a full-car model which is the linearisation of the nonlinear full-car in AutoSim at a trim state. The closed-loop controlled system aims to minimise vertical accelerations and tyre deflections for all corners of the vehicle simultaneously, as well as considering the pitching and rolling motions in the context of high frequency vehicle dynamics, as

additional objectives. This is a more complex control problem due to the larger number of states, inputs, and outputs, as well as the interaction of the SAVGS dynamics of the four corners of the vehicle. Thorough simulation tests are conducted to verify its performance and robustness characteristics, as well as the satisfaction of constraints, in a more realistic context than with a quarter-car.

Chapters 6 and 7 finalise an overall full-car SAVGS control scheme that assesses the overall requirements.

In Chapter 6, another approach for full-car SAVGS control in the context of high frequency vehicle dynamics with higher level of robustness to single-link rotations is proposed. This approach is developed based on a new linear equivalent hand-derived full-car model that manages to remove the main geometric nonlinearity associated with the AutoSim linearised model mentioned in Chapter 5. In addition, in the full-car SAVGS $\mathcal{H}_\infty$ -controlled scheme, extra exogenous inputs are designed for tracking the single-link position commands of higher level controllers.

In Chapter 7, an attitude controller for studying the effectiveness of the control of SAVGS attitude motions, in the context of low frequency vehicle dynamics, for the mitigation of pitch and roll motions in standard test manoeuvres is presented. The outputs of the attitude controller are used as exogenous inputs that feed to the $\mathcal{H}_\infty$ -controlled scheme developed in Chapter 6. The final overall SAVGS control framework chosen operates by blending the $\mathcal{H}_\infty$ controller and attitude controller together to tackle comfort and road holding in high frequency vehicle dynamics and chassis attitude motion in low frequency vehicle dynamics simultaneously.

Finally, Chapter 8 summarises the main conclusions attained in this thesis and outlines the main areas for further research.

Chapter 2

Literature review

Active suspension control has been a popular subject in the automotive industry in the past few decades [49, 106, 163, 164]. It plays a vital role to improving the compromise between the conflicting ride and handling measures of vehicle performance. The design and development of control strategies for active suspension systems is a multi-disciplinary engineering approach that involves subjects that range from mechanical engineering to control theory.

In this chapter, the basic disciplines related to the control of active suspension systems for road vehicles are reviewed to understand the historical evolution of the suspension system and the current state-of-the-art in suspension systems. In sections 2.1 and 2.2, the basic tasks of the automotive suspension system on a vehicle are briefly explained and then a comprehensive comparison between passive, semi-active and active suspension (including SAVGS) is provided. In Section 2.3, the commonly used vehicle models in research studies and suspension performance indices are discussed. In section 2.4, recent studies of linear and nonlinear control approaches to the active suspension are illustrated and compared. At the end of this chapter, section 2.5 provides a brief discussion and summary to identify the most suitable control approach for the SAVGS.

2.1 Suspension functions

A suspension in a conventional configuration (see Fig. 2.1) contains three main elements: 1) A coil spring is used for delivering a force opposite and proportional to the elongation of the suspension. This part also carries all the external static force loading. 2) A damping element is used for delivering a dissipative force opposite and proportional to the elongation speed of the suspension. Even if the dissipative force

is negligible at steady-state; it plays a central role in the dynamic behaviour of the suspension. 3) A set of mechanical components is used for connecting the sprung mass (chassis) to the unsprung mass (wheels) [140].

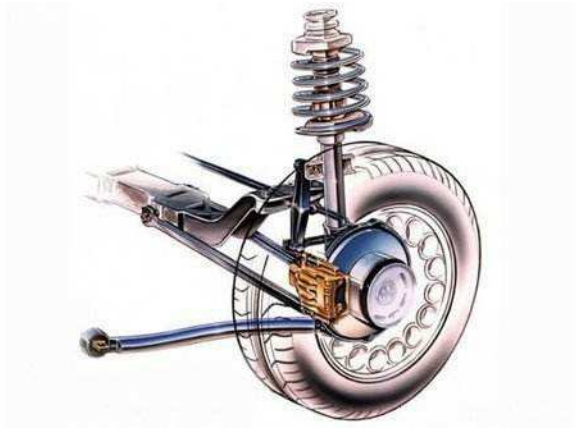

Fig. 2.1 Conventional suspension configuration [26]

A typical suspension on a vehicle has the following basic functions [24, 42, 130, 168]:

1. *To isolate external road disturbances to achieve good passenger comfort*

   Passenger ride comfort is determined by the vertical acceleration at the passenger locations. Therefore, a well-designed suspension system should be able to reduce the vibratory forces transmitted from the axle to the vehicle body (sprung mass), which means minimising the vehicle body accelerations.

2. *To minimise the tyre deflection to keep good road holding ability*

   Optimal road holding ability of a suspension can be qualified by the vehicle tyre deflection performance. Tyre deflection can be directly calculated from the variations in normal tyre load, as a tyre model can be roughly assumed as a spring unit in response to vertical tyre loads. Minimising the normal tyre load will improve the road holding by producing better cornering, braking and traction performance. Road holding and ride comfort have always been a compromise in conventional passive suspension systems.

3. *To minimise pitch and roll motion in order to provide good handling*

   The vehicle handling ability can be judged by the roll and pitch accelerations of a vehicle during cornering, acceleration and braking as well as on the vehicle's directional stability when driving in steady state condition. Half- and full-car

models are normally used to investigate the pitch and roll performance of a vehicle. In the automotive industry, good handling ability is a major aspect for a vehicle's safety. Thus a good suspension system should be able to keep the roll and pitch motion small while driving.

4. *To operate within the rattle space limitations to support the vehicle static weight*

   Another important objective of the suspension system in automotive road vehicles is to support the body static weight by ensuring the suspension rattle space (suspension deflection) is minimised. Rattle space is the maximum relative displacement of the suspension components between the sprung mass (chassis) and unsprung mass (wheels). A good suspension system should ensure suspension deflection is within a vehicle's rattle space.

To meet the mainstream passenger's requirements, engineers adjust the suspension systems with better driver and passenger comfort. Sports cars may emphasise stability, road holding and handling over passenger comfort and space. The existence of a suspension establishes the link between the road and the vehicle chassis which affects the entire dynamic behaviour of a vehicle. In addition to dominating the vertical dynamics, the behaviour of the suspension also manages the rotational dynamics (roll, pitch) caused by its unsynchronised motions. Therefore, suspension systems affect most aspects of the passenger feeling and driving ability.

2.2 Classification of suspension systems

To fulfil these functions, researchers have established several suspension designs to achieve variable trade-off between ride comfort and handing characteristics of vehicles [5].

Consequently, suspension systems can be categorised into two types according to the geometric layout: dependent suspension system (rigid axle) and independent suspension system [42]. A typical four-wheel vehicle has the two front wheels connected by the front axle and the two rear wheels connected by the rear axle, which means that a vehicle may have two arrangements of suspension on the front and back. The arrangement is classified by whether a solid axle beam binds the wheels or whether the wheels are permitted to move independently. The former is known as the dependent suspension system and the latter is called the independent suspension system:

- *Dependent suspension system (solid axle)*

Dependent suspension system is the system in which the vertical motions of one wheel are directly affected by the motions of the other wheel because of the solid axle beam. A solid axle dependent leaf-spring rear suspension system is shown in Fig. 2.2. It is fixed under the front/rear axle of the car like a solid bar and clamped with leaf springs and shock absorbers. The leaf springs and shock absorbers are then attached to the vehicle body. Dependent suspensions are simple and have low-price.

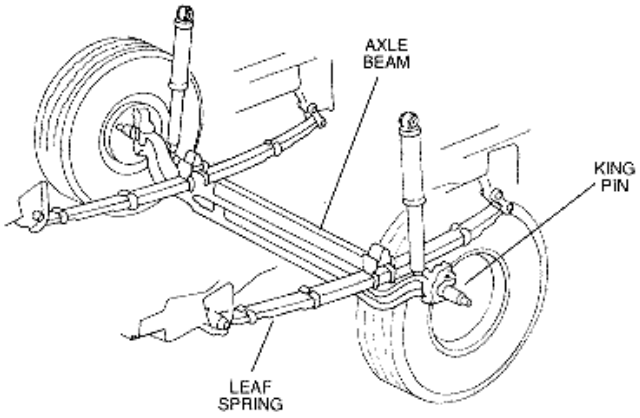

Fig. 2.2 A solid axle beam dependent leaf-spring suspension system [129]

Recently, dependent front suspensions have not been used in mainstream cars. Only heavy vehicles are still equipped with dependent suspensions, such as front dependent suspensions on trucks. In the case of dependent suspensions, the left and right wheels cannot be simplified as independent unsprung masses.

- *Independent suspension system*

  Vehicles mostly have independent front suspension and many of them also have independent rear suspensions. Independent suspension represents a broad range of automobile suspension system in which each wheel on the same axle could have completely independent movement under road disturbances. A fully independent suspension has both front and rear independent suspension.

  Even with higher manufacturing costs and development efforts, the independent suspension offers several advantages over dependent suspension which include better ride quality and handling performance as well as the better control ability of each wheel during steady and straight-line motion, cornering and braking situations. Independent suspensions are further classified into: swing axle; sliding pillar; MacPherson Strut; Double Wishbone; Multi link; Trailing and Semi-trailing, etc.. (see in Fig. 2.3).

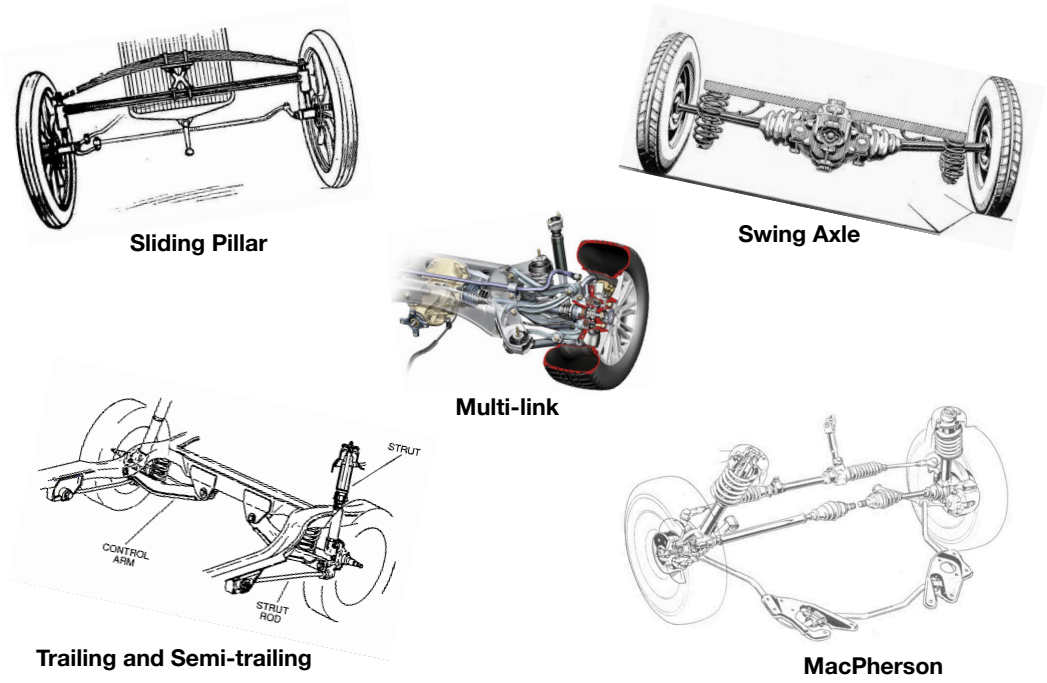

Fig. 2.3 Examples of independent suspension system. Image from [2, 35, 41, 128]

Double Wishbone Independent Suspension

In this project, the mechanical vehicle model is developed based on an existing vehicle with double wishbone suspension retrofitted with the SAVGS. The double wishbone suspension has become one of the most commonly used solutions in both front and rear axles (shown in Fig. 2.4). This type of suspension is also known as short long arm suspension as its upper and lower arms have unequal length [138]. The upper and lower arms are connected to the chassis and steering knuckle by means of revolute joints and spherical joints, respectively. Arms are also the control links guiding the motion of wheels. The upper arm is usually designed to be shorter than lower arm to produce negative camber as the suspension jounces. The negative camber provided by the shorter upper arm of the outside wheel when the vehicle is in a turning manoeuvre tends to cancel the positive camber gain on the inside wheel. This design attempts to have the tires perpendicular to the ground. Double wishbone designs provide the engineers with more tuneable options than other types of independent suspensions. It is fairly easy to optimise the wheel motion by controlling the camber angle, caster angle, toe pattern and roll centre height.

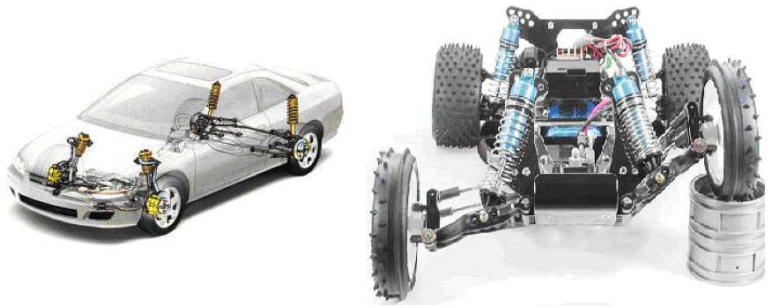

Fig. 2.4 Double wishbone independent suspension system

The double wishbone suspension is an optimal choice when considering the ratio of kinematic versatility vs. complexity, it has larger numbers of design parameters than other systems such as the McPherson strut and slightly simpler and less expensive than others such as multi-link suspensions [29]. Compared to the McPherson strut, the double wishbone suspension has more parameters to fulfil more design requirements; it also has lower friction forces that are caused by the sliding motions; In addition, it is easier to reinforce the chassis base due to a lower position of chassis attachment points [153]. Conversely, it takes more space and is more complex than other suspensions such as the McPherson struct. At the other end of the scale, multi-link suspension system is considered as the evolution of the double wishbone suspension as it offers more design choice for a specific vehicle. However, it normally costs more and is more complex than double wishbone.

All of the suspension systems in full and quarter-car models mentioned in this project are independent suspensions and can be represented by unsprung masses.

Alternatively, suspension systems also can be classified according to the nature of their force-producing elements: passive suspensions, semi-active suspensions and active suspensions. These suspensions are explained in detail in the following subsections:

2.2.1 Passive suspension

Traditional passive suspensions are the most widely used suspensions in road vehicles. This type of suspension is called passive suspension because the suspension passively adapts to the road profile. In a passive suspension system, the units producing force are coil springs and dampers. Shock energy resulting from road perturbation

can be absorbed by the spring unit; and the damper unit then dissipates the stored energy and prevents excessive oscillation [89]. The relationship between the force and velocity characteristic of the shock absorber is also usually nonlinear [115]. The spring and damper are placed in parallel with each other and normally such a spring-damper united is known as a *"strut"*. There are no sensors, electronics, or controllers implemented in passive suspension [115].

A passive suspension configuration is shown in Fig. 2.5, using an example of the linear quarter-car model. The dynamic equations and the features of this quarter-car model are illustrated in the next subsection.

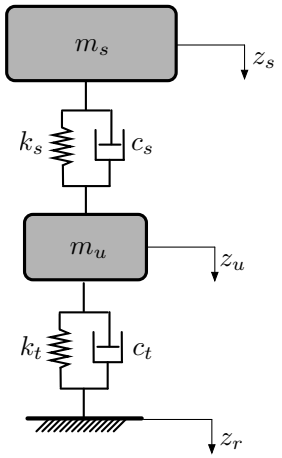

Fig. 2.5 Quarter-car passive suspension configuration.

The basic limitation of passive suspensions as indicated in [94, 135, 159] includes that it is not possible to eliminate the conflict between the ride comfort and handling even by using nonlinear springs or additional cross coupling by devices such as anti-roll bars. A suspension with large damping coefficient has good vehicle handling performance. However, it transfers much of the load to the vehicle body which might result in a harsh ride experience, especially when the vehicle traveling at low speed on a rough road or at high speed in a straight line. On the other hand, a suspension with low damping coefficient offers a more comfortable ride but it sacrifices the stability when the vehicle in turns and lane change manoeuvres. The limitation also comes from vehicle with passive suspension that will not keep best performance when passively response to the changing road roughness levels and speeds due to the elements (spring and damper) values are not tune-able [73]. Even under the same road and speed conditions, when vehicle equipped with soft passive suspension suffering relatively high static load changes, it may cause attitude control problems in cornering and

braking and lateral stability and control problems. Therefore, a good design of passive suspension can optimise ride and stability to some extent but cannot eliminate the compromise between these different requirements [71].

Compared with the limitations of passive suspension, semi-active and active suspensions could offer greater freedom to optimise the variety of performance requirements.

2.2.2 Semi-active suspension

The concept of semi-active suspension was first developed by Karnopp [39, 92, 93] and dates back to the 1970s'. This type of suspension was initially introduced as an alternative to the costly, complex and power-consuming active systems at that time. As yet, semi-active suspension can be categorised as three classes, which are with variable damper, variable lever arm, and variable stiffness [170]. Variable lever arm semi-active suspensions are achieved by moving the point of force application to adjust the force transfer ratio [8, 171, 173], therefore, they have a variable stiffness feature.

Moreover, the variable damper type semi-active suspension, known as the general semi-active suspension, has been the main focus of researchers in semi-active suspension designs in the past [39, 145, 147]. A variable damper type semi-active suspension is identical to the passive except that the damping coefficient can be adjusted actively. Thus, the characteristics of dampers that determine the damping coefficient, such as fluid viscosity, can be switched according to different driving conditions. Electrorheological (ER) and magnetorheological (MR) have been mentioned in [39] for the types of viscosity in the dampers.

An ER damper is typically constructed from pneumatic or hydraulic piston/cylinder combinations and controlled by an electromechanical unit of an orifice. ER dampers application have been employed in the market since the 1980s, initially implemented in Toyota Soarers's Toyota electronic modulated suspension model[102]. Another implementation of ER damper is found in the recent model of Lincoln's contunuous controlled damping system in 2006 [123], which monitores the suspension motion, body movement, braking and steering inputs by a group of sensors and changes the damper coefficient in milliseconds. This ER damper application provides improved driving comfort and dynamics, and better isolation of road harshness. The MR fluid damper is another implementation of semi-active type suspension, which is characterised by faster response time in changing the force across the actuator with electronical control. This method is limited with short fluid life which increased service concerns. An example is the 2003 Chevrolet Corvette whose MR damper is co-developed with Delphi and Lord Corporations [69]. The damping variable can be adjusted in milliseconds with

the imposed magnetic field to force the iron particles to align with the direction of the imposed field. The central idea of using MR damper is to distribute the damping forces in a very short response time to mitigate the closed-loop vehicle oversteer or understeer tendencies during quick transient manoeuvres through the control of lateral and longitudinal load transfer characteristics of the suspension [20, 68].

Examples of the ER and MR damper are shown in Fig. 2.6 and a variable damper type semi-active suspension configuration is shown in Fig. 2.7.

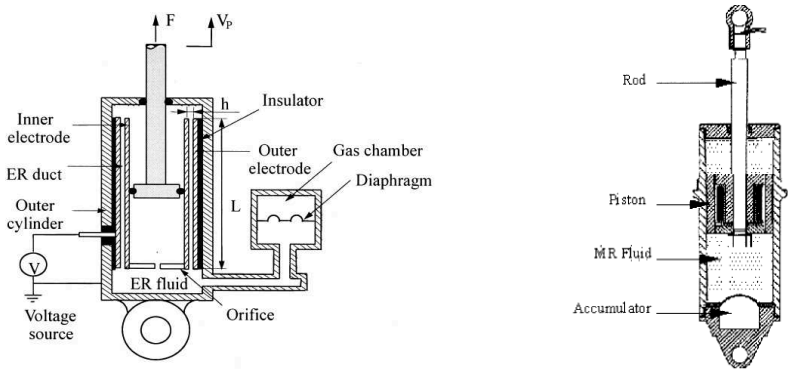

Fig. 2.6 Schematic configuration of the Electrorheological (left) and Magnetorheological (right) shock absorbers [33, 182].

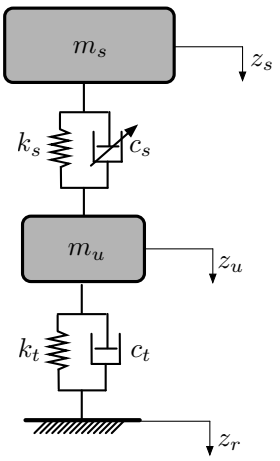

Fig. 2.7 Quarter-car semi-active suspension configuration.

Therefore, semi-active suspensions adjust the damping coefficient according to the driving condition but cannot introduce any force into the system [87, 152, 166]. They only react to the damper compression or extension.

2.2.3 Active suspension

The design of active suspension for road vehicles has been investigated by researchers for many years [71, 96, 162, 178]. The actuator in an active suspension provides energy to the system to improve dynamic behaviour [149]. It differs from passive suspensions, in which components are fixed. In addition, the design of active suspensions has been shown to offer the best suspension performance, in terms of both comfort and road holding, compared to passive and semi-active systems [73, 147]. The main advantages are summarised as follows:

- If the suspension working space is plenty in comparison with the road roughness, active suspension offers better performance in ride comfort and road holding compared with passive suspension. In this situation, semi-active suspension performs as good as the active suspension due to the fast response of the damper unit.

- If the suspension working space is restricted in comparison with the road roughness, the performance differences between fully active suspension and passive/semi-active suspension increase. Active suspension can adjust the suspension parameters through different circumstances to provide a desired combination of ride comfort and dynamic tyre deflection control and to offer better attitude control by being responsive to manoeuvring. However, the fixed parameter passive system suffers the weakness of having no external forces and non-adjustable components. Thus it is only optimal for one designed operating condition. However, the semi-active performance is between active and passive system, and the substantial performance differences between active and semi-active occurre in extreme rough road conditions.

- Another benefit of using active suspension is its self-levelling and height adjusting feature used to control the vehicle pitch and roll motions in manoeuvring. In the same situation, without self-levelling, the semi-active and passive systems would have static deflections due to the large payload, especially the system with soft suspension [21, 148].

Actuator Bandwidth

Actuator dynamics is a very important aspect when considering the practical application of control of active suspension systems. The idealised active suspension actuator, at the optimisation analyses stage, is capable of delivering any force with

an infinity response time. However, in practice, it is a very challenging task to obtain a high-fidelity actuation without a full understanding of underlying system dynamics and a mastery of mechatronic design skills [79]. In general, active suspensions can be classified into two major types according to the control bandwidth of the actuation systems: a) narrow bandwidth, and b) broad bandwidth [4, 78, 176]. More precisely, this system bandwidth filters the actuator force feedback to the system, which filters all the possible motions outside the bandwidth at the actuator mounting points. The narrow bandwidth systems attempt to control the relatively slow body mode around the sprung mass resonance frequency and as such the bandwidth is between 3 and 7 Hz [111]. In this case, the actuator system is positioned in series between the passive spring and the chassis. Broad bandwidth systems, on the other hand, attempt to address the body mode and wheel-hop and the bandwidth is above 15-20 Hz [101]. In this case, the actuator is installed is parallel with the passive spring.

Both the narrow and broad bandwidth suspensions are mostly in the research and development stage, while only fewer models can be seen in the commercial marketplace. Commercial examples are found as the 2000 Mercedes "active body control " [113] narrow-bandwidth active suspension and the 1989 Ford Thunderbird [111] broad-bandwidth active suspension.

In general, broad bandwidth is expected to be more difficult to implement compared to narrow bandwidth suspension due to higher costs, complexities and fuel consumption when operating under a wider frequency range [75]. Therefore, the narrow bandwidth suspensions attract more attention from car makers although it is subjected to compliant actuator structure and higher load from the vehicle because it is installed in series [37, 60].

Actuator classification

As is well known, the main differences between active and passive suspension systems are the use of an actuator. The parameters in active suspensions are varied, primarily depending on their applications, which can be classified as hydraulic, hydropneumatic, electromagnetic, or mechatronic. Within these categories, hydraulic actuator is the mostly widely considered by car makers.

Hydraulic actuator systems are more commonly used in vibration control systems as compared to electromagnetic actuators. The basic arrangement of components of various hydraulic fully active suspensions includes the following [161]: a source of hydraulic fluid at pressure with accumulators; a servo valve to control the flow of hy-

draulic fluid; a hydraulic piston for the conversion of hydraulic pressure to the force between wheels and chassis; an oil cooler to dissipate the heat generated by the hydraulic actuator; a series of sensors to measure the control objectives and feedback signals; a controller to generate control signals for the servo valve computed based on feedback signals.

The main advantages and disadvantages of hydraulic actuator systems can be summarised as shown in Table 2.1 [53, 64, 109].

Table 2.1 Advantages and disadvantages of hydraulic actuators in vibration control systems.

Hydraulic Actuator	
Advantages	Generating high forces
	Simplicity of control and compact design
	Market ready of the various parts and commercial maturity
	Little sensitivity to temperature changes
Disadvantages	Complex nonlinear dynamics
	Relatively low efficiency
	High system time constant
	Environment unfriendly due to hose leaks and toxic hydraulic fluids
	Heavy and bulky

Hydraulic systems proved their potential in commercial systems. One application of hydraulic actuator is implemented in the BMW-ARC system [155] to improve vehicle roll behaviour and ride control by directly controlling the force density of the actuators. Compared to the hydraulic active suspension systems, the main drawback of the electromagnetic systems are the limited force density. However, this can be overcome by the proper choice of design, materials and geometrical optimisation [63].

Electromagnetic actuators have increasingly become attractive replacements for passive, semi-active and hydraulic active suspension systems due to their relatively high efficiency, high control bandwidth and decreasing costs in recent years [110]. An example of an electromagnetic suspension system with the basic components of the electromagnetic actuator, is shown in Fig. 2.8.

More precisely, the main advantages and disadvantages of electromagnetic actuator systems can be summarised as shown in Table 2.2 [32, 64, 117, 172].

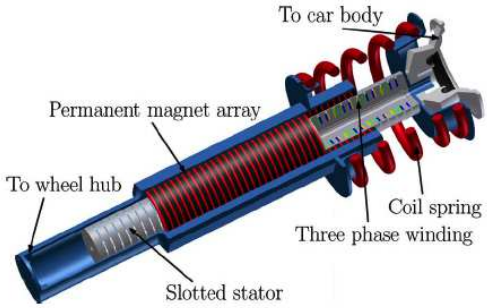

Fig. 2.8 An example of electromagnetic active suspension system [65].

Table 2.2 Advantages and disadvantages of electromagnetic actuators in the vibration control systems.

Eletromagnetic Actuator	
Advantages	Power regeneration capabilities (energy saving)
	High efficiency
	Ease of control
	Accurate force control
	Environmental friendly
Disadvantages	Relatively high current required
	Cost and packaging
	Low force density

This type of active suspension system can be found in a Bose suspension system [90] that uses a linear electromagnetic motor to generate force according to the feedback signals from the control algorithms. Recently, in [117], an active electromagnetic suspension system that has a linear combination of skyhook and groundhook control strategies is investigated and the desired performance has been obtained while energy can be regenerated from the road excitation and transformed into electric energy.

Variable geometry active suspensions

Variable geometry active suspensions are a relatively new concept of fully active suspension systems with both variable spring and variable damping characteristics [13]. The automatic/manual control of suspension damper characteristics has already become a mature technology and can be found on some production cars [75]. However,

the effect of variable stiffness springs, which normally are pneumatic or air springs, could bring additional complicating factors to the system, such as heavy auxiliary components and slow response [146]. Therefore, it is very desirable to obtain a new concept of suspension that could employ variable spring and damping elements into passive suspension and provide performance that is sufficiently good in comparison with passive, semi-active or other active suspension systems.

Variable geometry active suspensions may achieve this effect by changing the leverage of the passive spring-damper units with wheel motions. The main idea behind variable geometry is to adjust the ratio of wheel movement to spring movement and to do it continuously by introducing actuators that are perpendicular to the main suspension forces. Consequenctly, the actuator potentially has smaller and lighter geometry and less energy consumption while having the capacity to offer better attitude control and vibration performance.

The earliest implementation of variable geometry active suspension that has been proposed in the literature is the 1965 Velocette Thruxton motorcycle with the upper/damper mount located in a curved track to adjust the ratio of wheel and spring. Another form of leverage arrangement is the Delft Active suspension which is described in [52, 171]. This arrangement aims to change the orientation of the spring with a cone mechanism. A recent implementation of the variable geometry active suspension for motorcycles is found in [50]. The rear wheel monoshock suspension arrangement is modified and extended to adjust the suspension leverage between the spring-damper unit and wheel motion by varying the displacement between two rubbing surfaces. Simulation results show that the active suspension control offers better performance in terms of weave oscillations reduction within a range of operating conditions, including high-speed and low-lean operation, in which weave is likely to respond vigorously to road forcing.

2.2.4 Brief review of previous SAVGS studies

In addition to the implementations above, the SAVGS is a new promising concept for the variable geometry active suspension, that provides better suspension performance than passive/semi-active suspensions and avoids the inherent disadvantages of active suspensions regarding to less weight and less energy consumption. In this concept, which has been initially proposed in the patent [51], the actuator is mounted for displacing the end of the compressible member displaceable in a displacement direction. In this case, the displacement adjusts the geometry of the suspension and thereby vary the compression. The variable-geometry suspension apparatus in this patent is

suggested to be implemented on cars and motorcycles. Based on this foundation, recent publications [9–11] further studied, developed and tested the SAVGS concept and its attitude control strategies, with the aims: 1) to propose a new application of the active variable geometry suspension, 2) to develop vehicle and actuator models that involve the components dimensioning process, an inner controller scheme to optimise the SAVGS performance as well as satisfying the system constraints (torque, power, current and voltage), and 3) to propose an attitude control scheme and test the vehicle performance through a set of open-loop test manoeuvres.

The configuration of SAVGS is shown in Fig. 2.9. The new concept is to extend a conventional passive double wishbone suspension by introducing a short rigid link in series with the end eye of the spring-damper unit (Point F) and the chassis (Point G) that could rotate. Any rotation of the single-link by the actuation torque T_{SAVGS} modifies the spring-damper force and the suspension installation ratio. The torque is provided by an electromechanical actuator that is fixed to the chassis and installed adjacent to the single-link [11]. Based on the torque and single-link speed requirement, the optimum actuator in this work is selected as a permanent magnet synchronous motor (PMSM) and an epicyclic gearbox.

The main advantages of the SAVGS in comparison with other suspension methodologies can be summarised as follows:

- Fail safe operation
- Power regeneration capability
- Potentially low power and energy consumption
- No unsprung mass increase and small sprung mass increase
- Use of existing well-developed electro-mechanical components
- Flexible packaging

A schematic of the passive and retrofitted double-wishbone suspension arrangements used in this work is shown in Figure 2.10. Figure 2.10(a) represents the static equilibrium passive suspension configuration. Figure 2.10(b) shows that the SAVGS is the extension of this passive suspension retrofitted with the single-link variant. Points A, C and G are attached to the chassis; points E and F are fixed to the spring-damper unit; and points B,D, H and I are fixed to the wheel. The length of the spring-damper unit and its orientation can be continuously controlled through the rotation of the single-link with respect to its default equilibrium position [9].

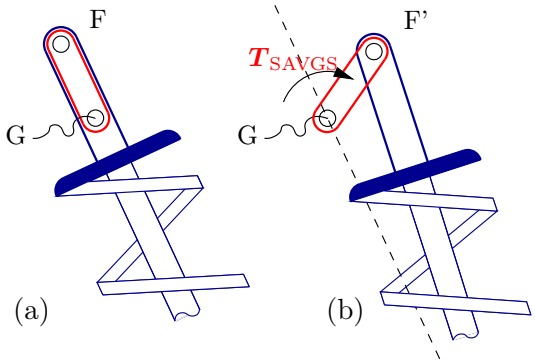

Fig. 2.9 Single-link variant of the SAVGS [10]. (a) Passive equilibrium position, T_{SAVGS}; (b) Rotated configuration.

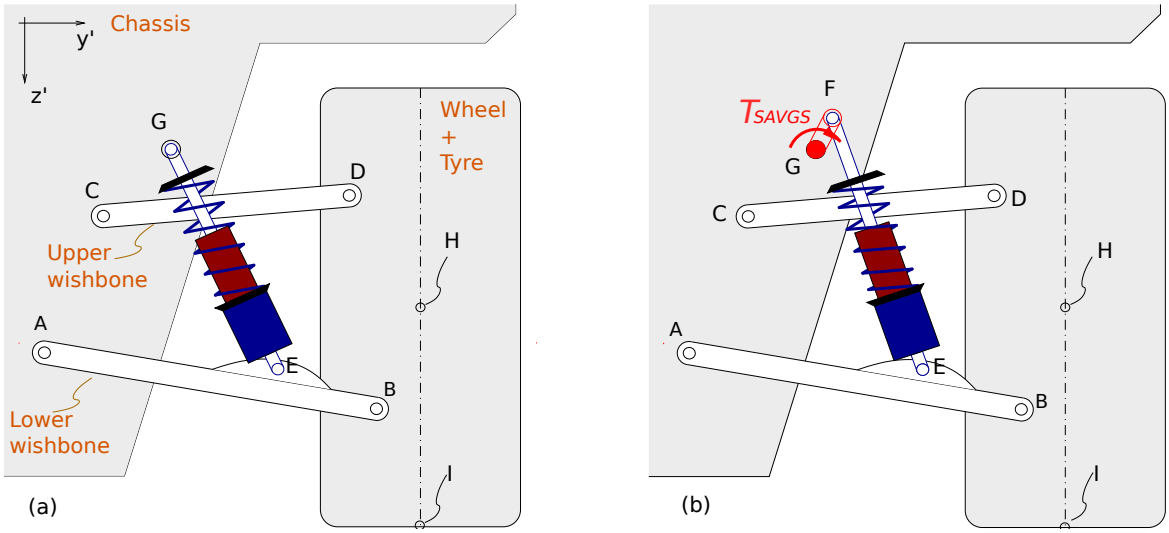

Fig. 2.10 (a) Passive double-wishbone suspension, and (b) SAVGS-retrofitted suspension.

2.3 Vehicle Models and Suspension Performance Indices

Vehicles, similar to other complex mechanical systems, have many degrees of freedom and consist of linear or nonlinear spring, various types of damping characteristic and actuators. The vehicle body is supported on the wheels through the active suspension elements (spring-damper units and actuators) and the wheels, which are supported through the tyres which are consists of springs and dampers in contact with the road. Sections 2.3.1-2.3.3 describe the well-known full, half and quarter models of the vehicle. The following assumptions are introduced with the relevant models: 1) the

vehicle comprises four types of components: masses, springs, damping elements and actuator forces; and 2) the frequency range is considered lower than 15 Hz, therefore the deformation of vehicle body can be neglected. In Section 2.3.4, a review of the multi-body model which can accommodate all kinematic effects and nonlinearities is given. Finally, in Section 2.3.5, the performance indices such as ride comfort, handling, attitude performance that allow the engineer to compare different control strategies for active suspensions are explained.

2.3.1 Quarter-car model

The quarter-car suspension system is a two-degree-of-freedom system, which represents the suspension system at each corner of the vehicle [129] i,e. the motion of the axle and the vehicle body at any one of the four wheels. The quarter-car model is often used when the controller design of the suspension system is considered. The quarter-car model does not contain the whole-car geometric effects such as wheelbase filtering and lateral equivalent, and does not offer the longitudinal interconnection properties. However, it still preserves the most basic features of wheel mass and body mass that are required for meaningful suspension analysis. Compared with more complex models such as half- and full-car configurations, the advantages of this quarter-car model are summarised as follows [129, 145]:

- Represented by fewer design parameters.
- Requires fewer performance specifications (human-body comfort and road holding).
- Reduces the difficulty in applying optimal control theory and the difficulty in evaluating operation performance.

In this project, controller design will progress from the quarter-car model and then it will base on the more-complex full-car models. A two-degree-of-freedom quarter-car automotive suspension system is shown in Fig. 2.11.

2.3.2 Half-car model

A half-car suspension model has four degrees of freedom, and it is a natural extension of a quarter-car model that includes pitch or roll dynamics. The basic half-car model is simply the linking of two quarter-car models (front and rear or the left and right). The four degrees of freedom are namely the vertical displacement of the front and rear axles as well as the pitch and heave motions of the vehicle body. There is a

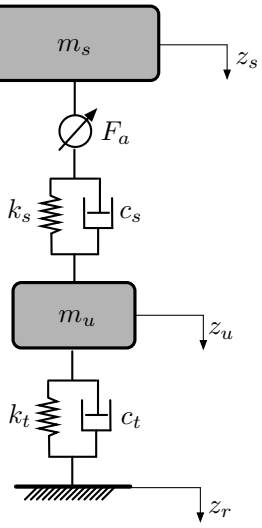

Fig. 2.11 Quarter-car active automotive suspension. The particular case of an actuator in series with a passive spring is shown.

kinematic correlation between the rear and front positions of the chassis. Therefore, this model is commonly used when analysing front/rear load transfer, such as acceleration or breaking [141]. A four-degree-of-freedom "half-car" automotive suspension system is shown in Fig. 2.12.

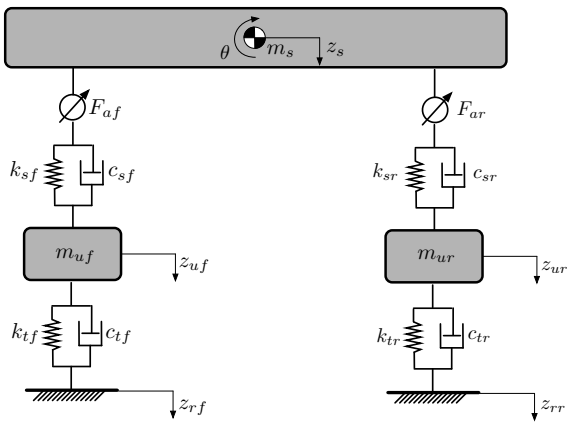

Fig. 2.12 Half-car active automotive suspension. The particular case of an actuator in series with a passive spring is shown.

2.3.3 Full-car model

A full-car model has seven degrees of freedom (heave, pitch, and roll motions of the vehicle body and the vertical translation at each corner of the four unsprung masses),

and it is an extension of the quarter-car model that includes additional rolling and pitching dynamics. A seven-degree-of-freedom full-car automotive suspension system is shown in Fig. 2.13. The vehicle body is represented as a rigid plate with uniform mass distribution which is attached with four masses representing the wheels at each corner of the vehicle.

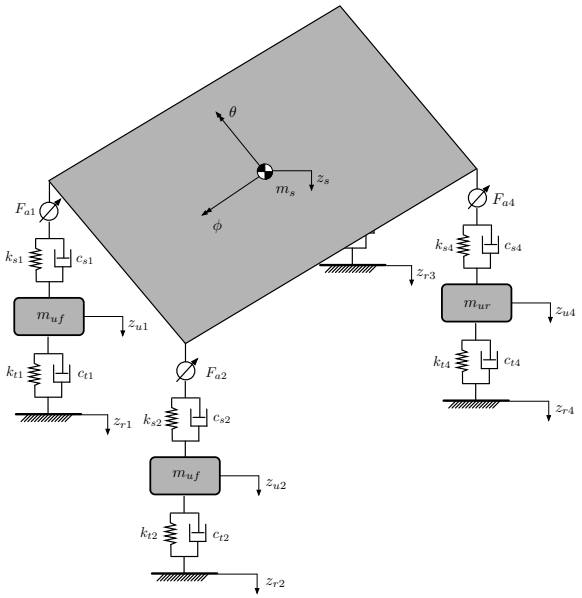

Fig. 2.13 Full-car active automotive suspension. The particular case of an actuator in series with a passive spring is shown.

2.3.4 Multibody models

While the theory of mechanical system dynamics has been well understood for nearly two centuries [125], the application of computational dynamics and related disciplines have become popular only recently in vehicles studies as several multibody systems analysis programmes. Compared with the simplified models in the previous sections, the multibody vehicle models can represents all kinematic effects and nonlinearities. The advantages of multibody systems computer analysis for gaining insight into the system performance include: fast turnaround and low cost investigations; reduced risk of dangerous solutions as with experiments on the real vehicle; prediction of experimental and field test results to assist in the design of test schedules; monitoring, diagnostics and failure prediction of operational systems [19, 37, 103, 143].

In the early years, programmes such as MSC.ADAMS (Automated Dynamic Analysis of Mechanical Systems) have been developed with a view of commercial gaining and assembling a physical description of the vehicle model rather than writing equations of motion [17, 18, 134]. Another vehicle-specific system known as VDAS (Vehicle Dynamics Analysis Software) was developed under the supervision of Crolla [38] in which most of the common dynamics studies have been incorporated into the programmes. Other examples of recently developed programs are MESA VERDE [177] and RASNA applied motion software [76] which formulate the equations algebraically and use a symbolic approach. AUTOSIM [121, 142, 144] is another programme developed as a symbolic code to analyse the handling of complex vehicle models with very fast simulation speed. Individual subsystems embodied within the multibody models developed by such aforementioned programmes include aerodynamics, drivers, seat characteristics, steering system, propulsion and braking system, suspension systems, tyre forces and moments and road profiles.

2.3.5 Suspension Performance Indices

In control theory, system performance evaluation aims to evaluate system effectiveness. Regarding the suspension systems (passive, semi-active and active), the factors used to evaluate system performance include ride comfort, working space, road holding, actuator force requirement and power consumption.

Ride comfort and road holding

The two main aspects that are of great interest in testing the efficiency of a suspension system include: 1) ride comfort characteristics and 2) road-holding characteristics. From a general perspective, comfort-feeling analysis is focussed on the behaviour of acceleration and displacement of the chassis with respect to external road impacts [85]. Compared with the ride comfort specifications, the road holding represents the ability of the vehicle to handle the wheel status in response to road unevenness and guarantees wheel contact with the road. Road holding is essential since longitudinal, lateral and yaw dynamics strongly depend on the forces related to wheel load due to road irregularities. In most cases, the tire deflection minimisation problem is considered the main road-holding objective. This project provides general methodologies and metrics to evaluate and analyse the performance of a controlled or uncontrolled system in the time and frequency domain. In previous studies that analysed suspension systems [137, 141], it is noted that the interesting range for road comfort and road

holding is 0-10 Hz. This frequency range refers to the greatest human sensitivity to vertical vibration defined in [ISO 2631-1:1997] [82]. In frequency domain performance evaluations, the performance index is usually computed through the integration of the power spectral density (PSD), which used to describes the distribution of power into frequency components composing that response, from lower to upper bounds of the frequency of interest. In the time domain, the performance evaluation is commonly evaluated through the weighted RMS value [82].

In addition, several global studies on the effects of realistic road unevenness on the suspension model, such as bump, step and random road excitations, should be tested to extend the results obtained from the frequency domain. The objective of these experiments is to evaluate the suspension under multi-frequency excitations through one simulation, while previous frequency domain tests only excite one specific frequency each time.

Suspension travel/rattle space

In practice, the available suspension travel of a vehicle is limited. Therefore, suspension travel is also worth measuring to ensure that the maximum deflection is smaller than its upper limitation [149]. Similar to the ride comfort and road holding, the suspension travel can be evaluated by calculating the RMS values of suspension displacement, especially for random and stochastic road disturbances.

Attitude control

Vehicle attitude control could help enhance both the ride and handling performance of road vehicles. Attitude control can be characterised according to peak angle or RMS values of pitch and roll angles compared with the default conditions [11, 23, 47].

Actuator performance

For active suspension performance evaluation, force requirement and power consumption can be measured through the peak values and RMS values during operation [11].

2.4 Classification of suspension control methodologies

In academic and industrial fields, the issue of control in active suspensions has attracted the attention of researchers for many years. Academic publications written about suspension systems show that several types of controllers have been developed to enhance vehicle performance. Broadly speaking, the most widely control theories employed to cope with the active suspension systems can be grouped into these families:

- PID control
- Adaptive control
- Optimal control
- Fuzzy and Neural Network control
- Robust control

The following paragraphs will give some qualitative insights into each of these control techniques:

2.4.1 PID control

In industry, PID (proportional-integral-derivative) control remains the most preferred control method because of its simplicity and simplistic design [40, 180]. The PID controller is used as a feedback loop by adjusting the 'error' signal and then sending back new optimised input to the plant to drive the measured output value back to the desired setpoint quickly. The PID controller can be designed without knowing the structure of the system or the process and without knowing the knowledge of advanced mathematics that is different from other types of optimal control theory. PID control is inadequate in dealing with changing behaviour processes, and large system disturbances and uncertainties, thus present low robustness. Therefore, in several research studies, a PID controlled system is optimised by developing a robust design approach or by incorporating an additional adaptive loop [15, 46, 70].

2.4.2 Adaptive control

Adaptive controllers are used if the parameters of the system dynamic models are unknown and/or time varying, and a fixed-parameter controller would not yield acceptable results. Typical adaptive control can be thought as the control of a system

with on line estimation of uncertain parameters that can improve the system performance by using the measured varying uncertain parameters in the control action [151]. The objective of adaptive control is to maintain system performance while the system is impacted by unknown variations in its parameters. The implementation of the adaptive algorithms to active/semi-active suspension can be found in several studies [4, 28, 98, 158], in which the controllers are possible to adapt to the changes of the variation of the vehicle parameters and the road disturbances. Two main approaches exist to design adaptive controllers, which are model-reference adaptive control and self-tuning adaptive control. Model-reference adaptive control aims to set the ideal response of the system, and the error between the ideal and the actual response is used as the input to the adoption law. Sunwoo et al. [158] developed a model reference adaptive controller for the vehicle active suspension subsystems. In this work, the controller tunes the active suspension to reduce the disturbance and vibration of a vehicle to an "ideal" conceptual suspension reference model. The second, self-tuning adaptive control approach is achieved by measuring the inputs and outputs of the plant which are used for the estimation of the parameters. Chen [28] and Yu [186] have designed a self-tuning controller for active vehicle suspensions which can adapt to both external and internal disturbances. The feasibility and performance improvement of the proposed self-tuning systems were investigated and proved by simulation results. Adaptive control can also be added to other control approaches to solve problem when the system dynamic models with large parameter variations. These control strategies on active suspension can be found in [119, 127, 157].

2.4.3 Optimal control

The optimal control problem of the active/semi-active suspension had been studied in the past 20 years [48, 66, 77]. In general, the optimal control technique was initially applied in the aerospace industry since the 1950s before finding its application in the study of active suspension [120]. The most widely optimal suspension design problems found use Linear quadratic regulator (LQR) control and Model predictive control (MPC) methods.

Linear quadratic regulator (LQR) and Linear quadratic estimator (LQG) control

If the control design problem is posed as that of minimising the impact of the system outputs for the system white noise inputs, it can be defined as a linear quadratic

regulator (LQR) control problem [43]. However, the LQR problem is unrealistic, as additional measurement noise and process noise always exists within a suspension system. To estimate the true state when noise is added to the uncertain linear system as additive white Gaussian noise, a linear-quadratic estimator, also known as a Kalman filter, needs to be employed to work synergistically with the LQR. This control strategy combines the Kalman filter and LQR control, which are collectively called the linear quadratic Gaussian regulator. Here, the Kalman filter can apply to a time-varying system, enabling the LQG control to design a linear feedback controller based on a non-linear uncertain system.

Ulsoy et al. [167] and Ray et al. [131] presented detailed analysis of the LQG control for second- and higher- order active suspension systems. They performed the stability analyse of the system with estimators, with uncertain input and output dynamics. For the estimator (Kalman filter) design of a quarter-car active suspension, the disturbance and measurement noise are white Gaussian processes, which are produced based on the roughness of the road and forward velocity of the vehicles. The basic design requirement for a linear-quadratic controller is to create a cost function with performance indexes that weights sprung-mass acceleration, suspension travel, tyre deflection and the control element [163, 167, 188]. By providing matrices with appropriate gains for the estimator and controller and by adjusting the scalar weighting parameters, this linear-optimal control theory can produce a system with guaranteed stability phase and gain margins. LQG optimality, however, does not automatically ensure good robustness properties. Therefore, in many circumstances, LQG and LQR controls are widely implemented with other control methods for better robustness properties.

Model Predictive Control

To incorporate all hard constraints of the states, output variables and states of the systems in real time, the MPC method seems to be the appropriate control strategy [59]. MPC techniques are very ideal for multivariable control, and can deal with both linear and nonlinear behaviours of the systems and constraints. MPC controller design aims to minimise a cost function over the receding prediction horizon and calculate an optimal sequence of control laws by consideration of constraints on the control variables. The basic idea of the MPC with receding horizon control concept is that the desired actuator inputs at time $k+1$ are taken as the optimal solution of the control variables, which are calculated with regard to the cost function at time k. This procedure is repeated in the next sampling time util the end of the simulation

[175]. In [31, 139, 175], the preview information for road profiles in front of the wheels is assumed to be available to the controller, which provides the data for improving the efficiency of the active suspension controller. The majority of applications for MPC approaches are for active suspension linear models. When dealing with nonlinear black-box models or highly-nonlinear suspension systems, MPC is usually used with the neural network technique to obtain a simple structure which directly describes the relations between input and output variables. In this way, it does not require nonlinear differential equations at each sampling time and it is not necessary to solve complicated problem during the on-line control process. This kind of technique for active suspension control can be found in the research studies in [136, 185].

2.4.4 Fuzzy logic and Neural Network control

In recent years, to deal with the nonlinear and ill-defined dynamic systems, fuzzy logic and neural networks have emerged as innovative and promising techniques, and several studies have been reported for active suspension systems.

Neural Network Control

The neural network control method offers robust performance when dealing with various types of system uncertainties and road disturbances. The reason for choosing a neural network for suspension control is because of its simplicity, satisfactory performance, and easy-to-understand system model without previous knowledge. Typically, the neural network plant is trained with a static back-propagation algorithm, which became widespread after the 1980s [133]. Compared to other training algorithms, back-propagation is a high-speed computation technology due to its requirement of minimal on-line computation [7]. Basically, the training of a neural network can be regarded as solving an optimisation problem with an appropriately defined cost function. The cost function generally incorporates body acceleration, suspension travel and tire force or deflection. The logic of the optimisation procedure can be described as follows [3]. The weights are initialized with random values. Given an input, the output pattern is probably unable to match the desired output pattern. Then, the desired output makes a comparison with the output, and the back-propagation training algorithm is introduced to adjust the pattern until the weights errors become small enough. Guclu [62] proposed a neural network controller for a nonlinear full-car vehicle model using a permanent magnet synchronous motor (PMSM). This controller successfully provides

excellent ride comfort. Moreover, this model implements the same motor used in the SAVGS system, which can be used as a reference for the following design.

Fuzzy Logic Control

Similar to neural network control, fuzzy logic control also has advantages over other traditional control theories when it is applied to complex and highly-nonlinear systems. This is because fuzzy control theory is a rule-based system that does not require the mathematical model of the system. A standard FL (fuzzy logic) system configuration can be found in [88]. The design of a fuzzy logic controller typically has the following three stages. 1) Fuzzification: the inputs in this step are converted to fuzzy values by using the membership functions (MFs). 2) Inference mechanism: in this step, the fuzzified inputs are computed to high-level descriptions of the outputs by using a rule-base. 3) Defuzzification: the fuzzy outputs are transformed back to crispy values of the outputs. Fuzzy logic as an important technique for intelligent control on active suspension systems has been successfully applied to many suspension systems. Cao [25] designed an adaptive fuzzy logic controller based on interval type-2 fuzzy methods for a quarter-car vehicle active suspension system. Ting [165] combined the sliding mode control frame with FLC for an active suspension. The fuzzy logic theory is used to reduce the chattering from the sliding mode control and this control scheme can reduce sprung mass accelerations and suspension deflections. In addition, there are many ways to combine neural network and fuzzy logic together, which has been successfully applied in [16, 34, 55].

Overall, each of these control approaches can bring some useful perspective and insight. However, the performance of PID control is likely too poor when dealing with the situation when the system encounters to multiple challenges from the operating conditions of the system, such as temperature, weather, power surge, etc. The linear optimal control theory is mainly concentrated on the improvements obtainable for a particular set of road profile (i.e. LQG control theory) and forward preview road information (i.e. model predictive control). The present work will focus on the design of a control scheme for a car model with SAVGS. More importantly, this controller will then be applied to the real test rig of a high performance car over a wide range of road input conditions and uncertainties in the future work. Therefore, since the car model is nonlinear and complex, nonlinear control will not be considered in the present work. Instead, linear robust control techniques described in the next section and more suitable and will be employed.

2.4.5 Robust control and the review of H_∞ Control for Vehicle Active Suspension Systems

Robust control is often associated with variable structure control (VSC) and H_∞ control, which have been developed as a consequence of the derivation of various mathematical methods, such as the state space equation, the phase plane method, and the Lyapunov stability theory. The main mode of variable structure control operation is sliding mode control. In this work, the H_∞ control strategy is considered.

Sliding Mode Control

It is well known that the sliding-mode control is an effective robust control approach for nonlinear systems. Sliding mode control (SMC) has been widely applied to the control of active suspension systems after Utkin [169] published a paper in 1977. SMC aims to develop a variable structure controller, which could drive the system to move into the neighbourhood of a designed sliding surface, and then constrain the system slide along this surface. One of the remarkable advantages of SMC is that the sliding surface can be specifically selected and switched based on the dynamic behaviour of the system [14]. Also, with a well-designed sliding mode controller, the closed-loop system is able to be insensitive to particular types of parameter variations such as disturbances and uncertainties [14, 179].

The difficulties of applying the sliding mode scheme includes the need to know the reference nonlinear model, and that it has high-frequency switching (chartering) [14]. Whilst it is difficult to deal with and define a highly nonlinear system, fuzzy logic and neural networks techniques have been developed in recent years to solve this problem [81]. Therefore, several research studies have been undertaken in order to combine the advantages of sliding mode control and neural network or fuzzy logic control. Nizar [3] proposed a sliding mode neural network inference fuzzy logic controller for an active suspension system. In addition, Huang and Lin [3, 81] designed a fuzzy sliding mode controller applied to a quarter-car test model. Regarding this controller, the input and output of the fuzzy logic controller are chosen as the sliding function and the control signal, respectively.

H_∞ Control

The concept of H_∞ theory was initially proposed in a published paper in 1981 [189]. H_∞ synthesis has been known as a powerful tool when solving robust control problems, but was not very easy to apply to the real system until Doyle et al. proposed a solution

based on solving two Riccati equations [45] and Gahinet and Apkarian proposed the linear matrix inequalities (LMIs) for solving these kinds of problems [57].

In recent years, H_∞ synthesis has been applied to active suspension controls. In 1994, Yamashita et al. [181] presented a control law for a full-car model based on the H-infinity control theory. Simulation results showed that the vehicle performance is better when the closed-loop controlled system is perturbed by disturbances. Hayakawa et al. (1999) [72] presented a robust H_∞ output feedback control scheme to a full-car active suspension model. They proved that output feedback control is a powerful tool to deal with the disturbance attenuation problems of active suspensions. Wang et al. (2005) [174] proposed an H_∞ control scheme for a full-vehicle active suspension system to improve ride-comfort and handling control. H_∞ synthesis is also applied with other types of control techniques for active suspension system. An example can be found in [56] by Fukao, where the combination of the H_∞ and adaptive nonlinear control technique has been developed. H_∞ is designed to improve the ride comfort, and the adaptive nonlinear controller is designed to overcome the nonlinearities and the uncertainties of the actuator.

$\mathcal{H}_\infty$ techniques have the advantage over classical control techniques in that they are a type of multiple-input, multiple-output (MIMO) control techniques and are applicable to solve multivariable problems in the frequency domain. More demonstrations of $\mathcal{H}_\infty$-based design techniques for active suspension systems have been reported in the literature to improve performance and guarantee robust operation of the system in [156, 181]. A depth investigation of multi-objective H_∞ robust control strategies for quarter- and full- car models will be provided in this project. The basic principle of $\mathcal{H}_\infty$ control is described as follows.

$\mathcal{H}_\infty$ norm

First define the linear, time-invariant, stable system with a transfer function matrix [44]:

$$G(s) = C(sI - A)^{-1}B \tag{2.1}$$

$\|G\|_\infty$ is the $\mathcal{H}_\infty$ norm which is defined as:

$$\|G\|_\infty = \sup_\omega \sigma_{max}[G(j\omega)] \tag{2.2}$$

where $\sigma(\cdot)$ is the singular value, and the 'sup' represents the upper bound of the function $\sigma_{max}[G(j\omega)]$. Therefore, the $\mathcal{H}_\infty$ norm of $G(s)$ is the maximum value of

$\sigma_{max}[G(j\omega)]$ over all frequency ranges ω. To compute the $\mathcal{H}_\infty$ norm, a state-space procedure is given as follows:

Let $\|G\|_\infty = \gamma_{min}$. *For the Eq. 2.1 with a stable A matrix and* $\gamma > 0$. *The Hamiltonian matrix is defined as*

$$H = \begin{bmatrix} A & \frac{1}{\gamma^2}BB^T \\ -C^TC & -A^T \end{bmatrix} \tag{2.3}$$

in where, $\sigma_{max}[G(j\omega)] < \gamma$ *exists if and only if there are no eigenvalues on the* $j\omega-axis$ *of the Hamiltonian matrix Eq. 2.3.*

The way to find γ_{min} is through an iterative computation process. A $\gamma > 0$ is initially selected, and then tested to see if there are any eigenvalues on the $j\omega$-$axis$. If there are no eigenvalues, decrease the γ and compute the eigenvalues of H again. If there are eigenvalues on the $j\omega$-$axis$, increase γ and compute again. Continue this process until a satisfied γ is obtained within the desired tolerance. This process can be computed automatically in the MATLAB environment.

Output feedback $\mathcal{H}_\infty$ control

In practice, with the different road disturbances and loads, some of the state information for active suspension systems may not be directly measurable (i.e., tyre deflection). Therefore, in recent years, many researchers investigated the $\mathcal{H}_\infty$ control design problem for active suspension systems with an output feedback controller [27, 181]. In Figure. 2.14, $y(s)$ is used as the feedback signals that is measured and used by controller $K(s)$. $d(s)$ and $z(s)$ are the input and output vectors. The control inputs are denoted as u(s). All of this information is considered into the plant P, which is used for the controller synthesis. All the formulas in the following analysis will be based on the state-space realisation of system P. P can be partitioned:

$$P \triangleq \left[\begin{array}{c|cc} A & B_1 & B_2 \\ \hline C_1 & D_{11} & D_{12} \\ C_2 & D_{21} & D_{22} \end{array}\right] .$$

Which is an alternative representative of the following system of equations:

$$\dot{x}(t) = Ax(t) + B_1 d(t) + B_2 u(t) \tag{2.4}$$

$$z(t) = C_1 x(t) + D_{11} d(t) + D_{12} u(t) \tag{2.5}$$

$$y(t) = C_2 x(t) + D_{21} d(t) + D_{22} u(t)\,. \tag{2.6}$$

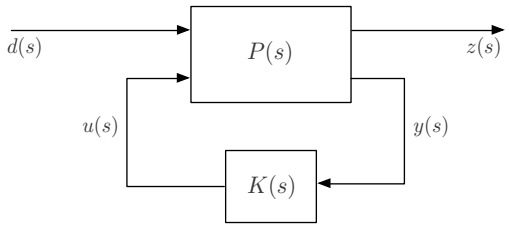

Fig. 2.14 Generalized bock diagram of $\mathcal{H}_\infty$ syntheses. $P(s)$ is the car model and $K(s)$ is the $\mathcal{H}_\infty$ controller. The inputs $d(s)$ and outputs $z(s)$ of P are vector valued signals. The components of $d(s)$ are the exogenous input disturbances. The components of $z(s)$ are the performance variables of interest to be minimised. The measurement signals that are used by controller $K(s)$ are denoted $y(s)$ and the controlled inputs generated by the controller are denoted $u(s)$.

Additionally, the following assumptions for the elements of P have to be satisfied to ensure the existence of a stabilising controller (assumptions 1 and 2) and to guarantee the Riccati equations related to the optimal controllers have positive semidefinite solutions (assumption 3 and 4).

Assumptions on P

1. $\left[\begin{array}{cc} A & B_2 \end{array}\right]$ is stabilizable
2. $\left[\begin{array}{cc} A & C_2 \end{array}\right]$ is detectable
3. $V = \left[\begin{array}{c} B_1 \\ D_{21} \end{array}\right] \left[\begin{array}{cc} B_1^\top & D_{21}^\top \end{array}\right] \triangleq \left[\begin{array}{cc} V_{xx} & V_{xy} \\ V_{xy}^\top & V_{yy} \end{array}\right] \geq 0$ with $V_{yy} > 0$
4. $R = \left[\begin{array}{c} C_1^\top \\ D_{12}^\top \end{array}\right] \left[\begin{array}{cc} C_1^\top & D_{12} \end{array}\right] \triangleq \left[\begin{array}{cc} R_{xx} & R_{xu} \\ R_{xu}^\top & R_{uu} \end{array}\right] \geq 0$ with $R_{uu} > 0$

Theorem 2.4.1 $\mathcal{H}_\infty$ ***Output Feedback***
A further, assumption is that $d(t)$ is a bounded $\mathcal{L}_2$ signal, so that $\int_{-\infty}^{\infty} d^\top(t)d(t)dt < \infty$. A stabilising controller which satisfies $\left\|T_{zd}\right\|_\infty < \gamma$ is

$$K_\infty \triangleq \left[\begin{array}{c|c} A_\infty & -Z_\infty L_\infty \\ \hline F_\infty & 0 \end{array}\right] \tag{2.7}$$

where

$$A_\infty = A + (B_1 + L_\infty D_{21})W_\infty + B_2 F_\infty + Z_\infty L_\infty C_2 + Z_\infty L_\infty D_{22} F_\infty$$

where

$$\begin{aligned} F_\infty &= -R_{uu}^{-1}(R_{xu}^\top + B_2^\top X_\infty) \\ L_\infty &= -(Y_\infty C_2^\top + V_{xy})V_{yy}^{-1} \\ W_\infty &= \frac{1}{\gamma^2}B_1^\top X_\infty \\ Z_\infty &= (1 - \frac{1}{\gamma^2}Y_\infty X_\infty)^{-1} \end{aligned}$$

in where X_∞ *and* Y_∞ *are the stabilising solutions to the Riccati equations* (2.8) *and* (2.9)

$$0 = X_\infty A_r + A_r^\top X_\infty + R_{xx} - R_{xu}R_{uu}^{-1}R_{xu}^\top - X_\infty(B_2 R_{uu}^{-1}B_2^\top - \frac{1}{\gamma^2}B_1 B_1^\top)X_\infty \tag{2.8}$$

$$0 = A_e Y_\infty + Y_\infty A_e^\top + V_{xx} - V_{xy}V_{yy}^{-1}V_{xy}^\top - Y_\infty(C_2^\top V_{yy}^{-1}C_2 - \frac{1}{\gamma^2}C_1^\top B_1)Y_\infty \tag{2.9}$$

Meanwhile, the solutions are necessary to satisfy the following conditions

1. $X_\infty \geq 0$ *and* $Y_\infty \geq 0$

2. *The Hamiltonian matrix for Eq.* (2.8)

$$\begin{bmatrix} A - B_2 R_{uu}^{-1}R_{xu}^\top & -B_2 R_{uu}^{-1}B_2^\top + \frac{1}{\gamma^2}B_1 B_1^\top \\ -R_{xx} + R_{xu}R_{uu}^{-1}R_{xu}^\top & -(A - B_2 R_{uu}^{-1}R_{xu}^\top)^\top \end{bmatrix}$$

   has no $j\omega$*-axis eigenvalues*

3. *The Hamiltonian matrix for Eq.* (2.9)

$$\begin{bmatrix} (A - V_{xy}V_{yy}^{-1}C_2)^\top & -C_2^\top V_{yy}^{-1}C_2 + \frac{1}{\gamma^2}C_1^\top C_1 \\ -V_{xx} + V_{xy}V_{yy}^{-1}V_{xy}^\top & -A + V_{xy}V_{yy}^{-1}C_2^\top \end{bmatrix}$$

   has no $j\omega$*-axis eigenvalues*

4. $\rho(Y_\infty X_\infty) < \gamma^2$ *, where* $\rho(\cdot) = \max_i |\lambda(\cdot)|$ *is the spectral radius*

An optimal $\mathcal{H}_\infty$ controller which satisfies all the conditions from 1 to 4 is K_∞ with γ value equal to the smallest value of $\gamma > 0$ and $\left\|T_{zd}\right\|_\infty < \gamma$.

Generalized $\mathcal{H}_\infty$ problem

In $\mathcal{H}_\infty$ syntheses, both performance and robustness specifications can be incorporated into the standard generalised regulator feedback structure [61], as shown in Figure 2.14.

The general control objective in this framework is to generate a controller that will keep the performance outputs, $z(s)$, as small as possible in the presence of the external disturbance signals, $d(s)$. Hence, the closed-loop transfer function, denoted as $T_{zd}(s)$, will decide the disturbance rejection performance from $d(s)$ to $z(s)$. Thus, minimising the $\mathcal{H}_\infty$ norm of $T_{zd}(s)$ is the control objective of this framework.

The plant, P, is a linear time-invariant system representing the linear half/full-car SAVGS model in the controller design process. It is also applicable to nonlinear time-domain studies containing a nonlinear system, actuator, and sensor dynamics, at the controller validation stage. Based on plant P, this work is about the design of closed-loop SAVGS controlled systems to meet frequency-domain performance specifications, such as excellent ride, handling, attitude and steering properties, while undergoing system external disturbances.

With plant P partitioned as

$$P(s) = \begin{bmatrix} P_{11}(s) & P_{12}(s) \\ P_{21}(s) & P_{22}(s) \end{bmatrix} \tag{2.10}$$

the overall system can then be represented in the following transfer function form as

$$\begin{bmatrix} z(s) \\ y(s) \end{bmatrix} = \begin{bmatrix} P_{11}(s) & P_{12}(s) \\ P_{21}(s) & P_{22}(s) \end{bmatrix} \begin{bmatrix} d(s) \\ u(s) \end{bmatrix} \tag{2.11}$$

$$u = K(s)y \tag{2.12}$$

where $K(s)$ is the $\mathcal{H}_\infty$ feedback controller to be designed.

Hence, the closed-loop transfer function matrix between exogenous, d, and performance variables, z, under plant perturbations is represented as

$$T_{zd} = P_{11} + P_{12}K\left[I - P_{22}K\right]^{-1} P_{21} \tag{2.13}$$

As a disturbance rejection problem, the control design aims to obtain a stabilising controller K to minimise the $\mathcal{H}_\infty$-norm of $T_{zd}(s)$ in the presence of road disturbances

[61] :

$$\|T_{zd}\|_{\infty} = \sup_{\omega} \bar{\sigma}[T_{zd}(j\omega)] < \gamma. \tag{2.14}$$

where $\bar{\sigma}(\cdot)$ is the largest singular value of T_{zd} for a given ω. $\bar{\sigma}(\cdot)$ should be stable and bounded by a relative small real number γ.

Figure 2.15 shows a classic unity-feedback setup of the generalised plant in this section where the inputs (d) and outputs (z) might be used in control design. Plant $G(s)$ is the vehicle body. There are three types of generalised disturbance inputs: 1) r represents the reference inputs; 2) n represents the sensor noise; and 3) d_0 represents the system-input disturbance. There are also three generalised performance variables, including: 1) control effort, e; 2) tracking error, o; and 3) control objectives, u. The variables y and u represent the control inputs and controller outputs of the generalised plant P, respectively.

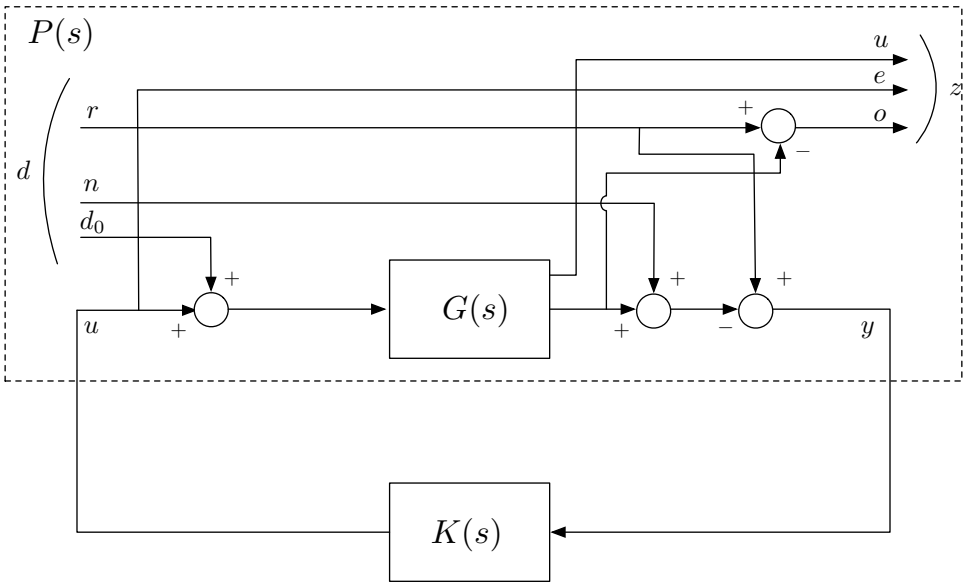

Fig. 2.15 Classic unity feedback structure [150].

Frequency weighting functions

During the $\mathcal{H}_{\infty}$ design process, the generalised plant P in Figure. 2.14 is often necessary to incorporate extra information about the plant such as system stability and performance requirements. In this project, for example, it may be assumed that the attenuation of vehicle body acceleration only focuses on certain low frequencies according to the human sensitivity. This extra information can be augmented to the

generalised plant P as "frequency weighting functions" after the outputs and before the inputs. This type of $\mathcal{H}_\infty$ design has been applied to several examples, both theoretical and practical in, [80, 100]. An example of the generalised plant P with weighting functions is shown in Figure 2.16. P_w is the new generalised plant, which is the replacement of the plant P in Figure. 2.14, with frequency-dependent weightings W_d and W_p.

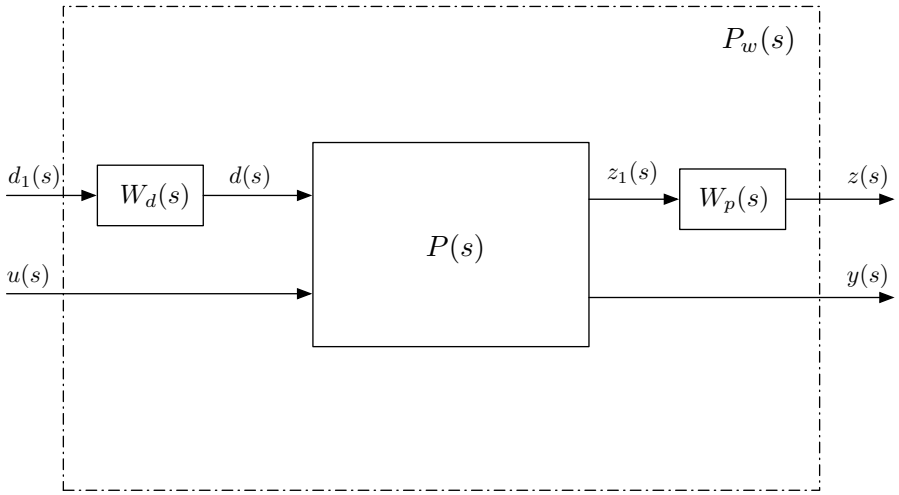

Fig. 2.16 The new generalised plant $P_w(s)$ with weighting functions W_d and W_p

The new plant P_w is partitioned as

$$P_w(s) = \begin{bmatrix} W_p(s)P_{11}(s)W_d(s) & W_p(s)P_{12}(s) \\ P_{21}(s)W_d(s) & P_{22}(s) \end{bmatrix}, \tag{2.15}$$

where P_w is the state-space model that is ready for $\mathcal{H}_\infty$ control design and analysis. W_d and W_p have to be formulated into the state-space representation of P_w. This can be done via MATLAB commands “augw", “sysic" or “iconnect".

More specifically, weighting functions W_d on the generalised disturbance vectors $d(s)$ emphasise the frequency regions, and the strength of these system disturbances. Here, $d_{(s)} = W_d(s)d_1(s)$. There are two aspects that have to be considered when defining the proper weightings $W_d(s)$: 1) $W_d(s)$ are usually selected as active filters to emphasise certain variables in specific frequency domains based on the understanding of the design specifications. For example, reference inputs normally consisting of low frequencies and noise inputs are often associated with high frequencies on the other hand. These $W_d(s)$ should be selected as low- and high- pass filters, respectively; and 2) except for the filter characteristics, the gains of $W_d(s)$ are related to the maximum

expected input values. For example, for a vehicle system, the unit of road disturbance is m and the maximum road disturbance is normally assumed to be smaller than 0.5m. The load transfer on the vehicle is at a magnitude of kN, however. Therefore, the gain of the various components of $W_p(s)$ has to be considered with the understanding of the nature of the disturbances.

Weighting functions W_p on the generalised performance vectors emphasise the importance of the control objectives in the frequency domain, similar to the weighting functions for the inputs vectors. The frequency interest regions of W_p are dependent on the understanding of the design specifications. Vehicle body acceleration, as an example, only affects passenger comfort at low frequencies according to the ISO standard. Therefore, this part of W_p is usually chosen as a low-pass filter. The control effort is sometimes used at high frequencies and this part of W_p is chosen as high-pass filter instead. The gain of different parts of W_p represents the importance of the corresponding design specifications. For example, assuming weighting functions for body acceleration and tyre deflection are all low-pass filters, if the design of the $\mathcal{H}_\infty$ controller is focused on increasing the ride comfort rather than road holding, the gain of the frequency weight on body acceleration has to be higher than the one on tyre deflection. The relationship of the weighting functions on the outputs z should make sense as a whole.

It is also noted that Figure. 2.16 is a typical example of augmented plant with weighting functions. In addition to W_d and W_p, other weighting functions might be also employed before and after the controller, such as some weighting functions used to represent the dynamics of actuators that should be inserted between the controller and the vehicle. These frequency weights should be finally absorbed into the controller by post- and pre- multiplying in state-space representation.

2.5 Conclusions

This chapter has reviewed the state of the art of suspension systems classification and the control algorithms of active suspensions. As the foundation of this project, the previous studies of the SAVGS concept have also been reviewed. The commonly basic quarter-, half-, and full-vehicle models are generally described. In next Chapter, the modelling process of the double-wishbone quarter- and full-car SAVGS-retrofitted models which adapted to high performance sports used in this thesis will be descried in detail.

Chapter 3

Vehicle Modelling

Developing accurate models of vehicle systems is the foundation of this project. As explained in the last section, the nonlinear quarter- and full- car SAVGS/passive models can represent the vehicle for the SAVGS and assess its performance in the context of comfort, road holding, and attitude control. In addition, for the development of the $\mathcal{H}_\infty$ controller, linearised models are most convenient for representing the accuracy in the range of operating conditions of interest for the study of the input-output relationships in the frequency domain.

In Section 3.1.1, the starting point will be a description of the software packages used for the development of multi-body vehicle models and for the validation of closed-loop controlled SAVGS systems. The modelling of the multi-body quarter- and full-car nonlinear models and the liberalisation of the quarter- and full-car models used in this thesis then follows. Also, in Sections 3.2.1 and 3.2.2, a summary of the vehicle parameters and actuator components, selected for the high-performance car used in this study are provided. Section 3.3.3 describes the road modelling imposed on the tyres at each corner of the vehicle and the relevant ISO standards are also explained. Finally, a step-by-step guide of the closed-loop $\mathcal{H}_\infty$ -controlled schemes developed in this thesis in subsequent chapters are summarised for a better understanding of the thesis structure.

3.1 Vehicle models

3.1.1 Software

The following software is used for the work of this thesis:

Autosim Quarter- and full- car vehicle models as well as the actuators have been built by the multi-body simulation code *Autosim* [6]. The linearised state-space equations in Chapters 4 and 5 for analysis and controller development in MATLAB or the nonlinear C-MEX code for the nonlinear simulation , can also been generated in Autosim. In the latter case it writes the simulation code in C language and C-MEX code that contains all the nonlinear equations of motion of the SAVGS, which are then included into a Simulink block as an S-function for controller validation purpose.

MATLAB + Simulink This project applies $\mathcal{H}_\infty$ control theory in the SAVGS controller design and application, and makes considerable use of MATLAB and the Simulink Toolbox. Both MATLAB and Simulink have been extensively used in this project in the following ways:

- Building in MATLAB the dynamic equations of the hand-derived (equivalent) linearised quarter- and full- car models described in Chapter 6. MATLAB is also used for the numerical calculation of equivalent parameters.
- Synthesis of $\mathcal{H}_\infty$ controllers in MATLAB with the linearised models for the performance improvement of ride comfort, road holding and attitude control properties (Chapters 4 to 6).
- Simulink provides the test environment for the linear and nonlinear simulation to validate the effectiveness of the $\mathcal{H}_\infty$ controllers (Chapters 4 to 7).

3.1.2 Types of models

The models developed and used in this project can be classified into two groups: linearised models for the $\mathcal{H}_\infty$ control design and nonlinear models for assessing and comparing the performance of the vehicle systems. All the models that will be used in the present work are listed in Table 3.1. Some of these models are based on previous work [9, 11, 12] and some are newly developed (Sections 3.1.8 and 3.1.10).

The purpose and application of the (1) - (8) models in Table 3.1 are summarised as follows:

- Linear models (1), (2), (3), (4) are used for the design of the $\mathcal{H}_\infty$ controllers from Chapters 4 to 7. More specifically, quarter-car model (1) is initially used for the application of the $\mathcal{H}_\infty$ control to the SAVGS problem to improve the ride comfort and road holding performance in a vertical direction. This is the first step to

Table 3.1 Vehicle models used for the work of this thesis

Vehicle Model Types			**No.**	**Name**
Linear models	Quarter-car	AutoSim SAVGS linearised model (Generated in Autosim)	①	QCL
		Hand-derived SAVGS model (Equivalent model)	②	QECL
	Full-car	AutoSim SAVGS linearised model (Generated in Autosim)	③	FCL
		Hand-derived SAVGS model (Equivalent model)	④	FECL
Nonlinear, multi-body models	Quarter-car	Passive quarter-car model	⑤	Passive
		SAVGS quarter-car model	⑥	QC
	Full-car	Passive full-car model	⑦	PASSIVE
		SAVGS ful-car model	⑧	FC

evaluate the suitability and effectiveness of the $\mathcal{H}_\infty$ synthesis to the SAVGS concept. Full-car model ③ is then used for the full-car SAVGS $\mathcal{H}_\infty$ control design where the movement at the mass centre, such as pitching and rolling motions, are incorporated into the control scheme. Model ② and ④ are the SAVGS hand-derived linear models that have proved to have better robustness and smaller state-space equation size to single-link rotations, compared with ① and ③ in Chapter 4 and 6, respectively. Therefore, a quarter-car SAVGS $\mathcal{H}_\infty$ controller for the hand-derived quarter-car model based on ②, which has been obtained in previous work [13] will be compared with the controllers in this thesis in Chapter 4. Meanwhile, Chapter 6 proposeds a full-car SAVGS $\mathcal{H}_\infty$ controller for the hand-derived full-car model ④.

- Nonlinear models ⑤, ⑥, ⑦, ⑧ are employed to validate the performance, and to compare the active control results with the passive configurations. Nonlinear models ⑥ and ⑧ are employed to assess the performance of the linearised SAVGS $\mathcal{H}_\infty$ controllers, which are developed based on the models ① to ④. This is done by simulation and the results are also compared with the passive configurations ⑤, ⑦. More specifically, quarter-car models ⑤ and ⑥ are used for ride comfort and road holding studies in a vertical direction. Full-car models ⑦ and ⑧ are used for assessing the vehicle's more dynamic responses such as pitching and rolling motions during turning manoeuvres.

3.1.3 Reference frames

The reference frames used in this project are the right-hand orthogonal axis system. The definition of this axis systems is initially presented in [SAE J670] [154] and the coordinates centre is attached to the vehicle mass centre. When moving forward in a straight line on the road, the axis system is with a positive x-axis substantially horizontal and pointing forward, a y-axis pointing to the driver's right, and a z-axis pointing downwards, as shown in Figure 3.1.

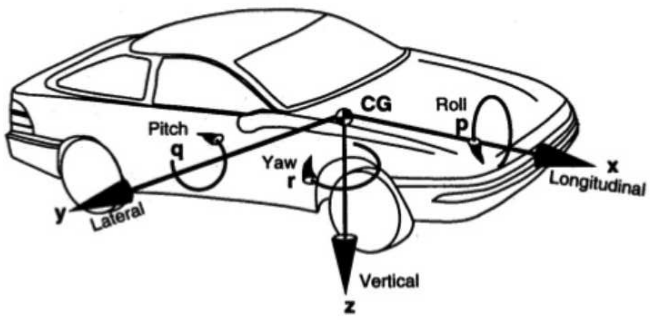

Fig. 3.1 SAE vehicle axis system [154].

- **Axis system for quarter-car models:** The quarter-car models are used in Chapter 4. The origin of the coordinate system is named as $O^{'}$, and it is attached to the sprung mass. The axes have been named to $x^{'}$, $y^{'}$ and $z^{'}$. As in [SAE J670], the $x^{'}$-axis designed to the vehicle's horizontal direction, the $z^{'}$-axis points downwards, and the $y^{'}$-axis points outwards the wheel and parallel to the road surface.

- **Axis system for full-car models:** The full-car models are used in Chapters 5 to 7. Assuming the global reference frame is assume as xyz and local reference frames are assumed as $x'y'z'$. At each corner of the vehicle, the frame transformations are shown in Figure 3.2 and defined as: 1) front left($i = 1$) and rear left($i = 3$) wheels: $x' = -x$, $y' = -y$, $z' = z$, 2) front right($i = 2$) and rear right($i = 4$) wheels: $x' = x$, $y' = y$, $z' = z$ [11].

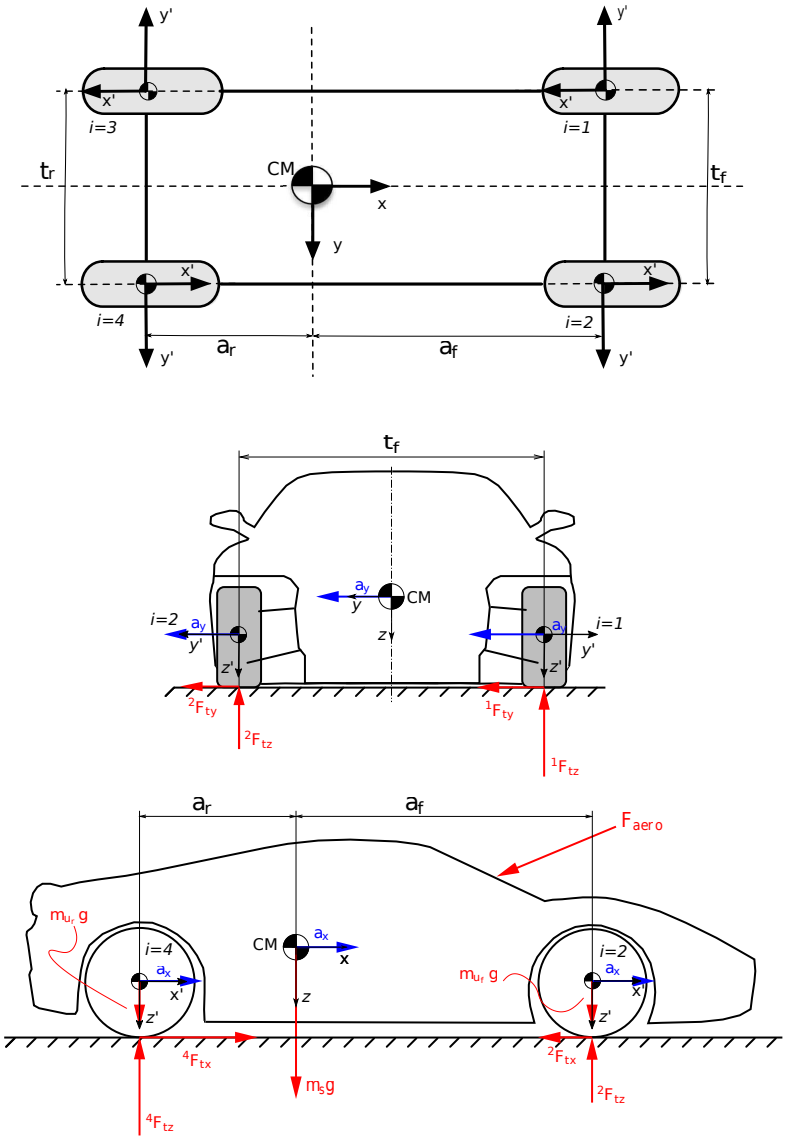

Fig. 3.2 Global and local reference frames of full-car SAVGS configuration and the external forces acting on the the vehicle during acceleration and cornering, in x-y (top), y-z (middle) and x-z (bottom) planes respectively. The reference frames used in this project are the right-hand orthogonal axis system. Positive lateral and longitudinal accelerations are shown in this case (i.e, a_x, $a_y > 0$).

3.1.4 Symbols for vehicle models

The symbols used in this chapter for nonlinear model and the full-car SAVGS linear hand-derived model are given in Table 3.2.

Except for the symbols given in Table 3.2, the following notations are used:

a_f *and* a_r *are the longitudinal distances between each axle and the centre of mass*

Table 3.2 Symbols of the SAVGS and hand-derived full-car model

Symbols	Physical Meanings	Unit
$\ddot{z}_{si}$	the ith sprung mass acceleration	m/s^2
Δl_{ti}	the ith tyre deflection	m
Δl_{si}	the ith suspension deflection	m
$\Delta \dot{l}_{si}$	the ith suspension velocity	m/s
z_{ri}	the ith vertical road displacement	cm
$\dot{z}_{ri}$	the ith vertical road height change	m/s
z_{lini}	the ith equivalent linear actuator displacement	m
$\dot{z}_{lini}$	the ith speed for the equivalent linear actuator	m/s
$z^{(e)}_{lini}$	the ith reference equivalent linear actuator displacement	m
$\dot{z}^{*}_{lini}$	the ith reference speed for the equivalent linear actuator	m/s
θ^{*}_{refi}	the ith single-link reference angle	deg
$\Delta\theta_{SLi}$	the ith single-link angle	deg
$\ddot{\theta}, \ddot{\phi}$	pitching and rolling accelerations at CM	rad/s^2
θ, ϕ	the rolling and pitching angles at CM	rad
$\ddot{z}_{CM}$	vertical mass acceleration at CM	m/s^2
z_{CM}	vertical mass displacement at CM	m
T_p, T_r	pitch/roll torque at mass centre	$N.m$
$T_{\text{SAVGS}i}$	the ith actuation torque	$N.m$
m_s	total sprung mass	kg
$m_{u_f}g, m_{u_r}g$	front and rear unsprung mass	kg
${}^iF_{tx}$	the ith tyre force in the longitudinal direction	N
${}^iF_{ty}$	the ith tyre force in the lateral direction	N
${}^iF_{tz}$	the ith tyre force in the vertical direction	N
a_x, a_y	longitudinal and lateral acceleations	m/s^2

(CM).
t_f and t_r are the track widths, which is the lateral distance between the points of contact of the tyres in each axle.
k_{eq} and c_{eq} are the equivalent parameters of the spring and damper.

3.1.5 SAVGS quarter-car multi-body model (QC)

The SAVGS concept in this work is adapted to a high performance sports car with double-wishbone arrangements. The AUTOSIM programme has been used to develop the quarter- and full- car multi-body SAVGS models by C.Arana in [11, 13]. For a comprehensive understanding of the development of these multi-body models and the associated code, the reader can refer to the work in [11, 13].

The quarter-car model is used to evaluate the controller's performance to in a vertical direction to improve passenger ride comfort and road holding. The passive configuration comprises five major parts: 1) a rigid double-wishbone; 2) a rigid wheel spindle; 3) a vertically compliant tyre; 4) a suspension spring and 5) a suspension damper. The concept and principle of the SAVGS has been illustrated in Section 2.2.4. To build the multi-body model in AUTOSIM, the main assumptions are shown in Table. 3.3 [13]:

Table 3.3 The main assumptions in the multi-body quarter-car model [13].

Suspension	Spring is linear and damper is non-linear.
	Spring-damper (SD) unit can only produce forces along the axis between points E and G.
	Spring and damper act in parallel and are assembled together.
Tyre model	Comprises a linear vertical spring and a linear vertical damper that act in parallel between the road and point I.
	The movement of the wheel is restricted within the local y'z' plane.
Unsprung mass	Point H is the mass center of all the unsprung mass.
Others	All joints are ideal revolutes.

The quarter car model used in this thesis extends the conventional quarter car to include a double wishbone arrangement as shown in Fig. 3.3.

It involves a sprung mass (chassis) that is allowed to move vertically and an unsprung mass (wheel) that is connected to it via a massless double wishbone kinematic linkage. A road tyre compression force F_{tz} proportional to the tyre deflection (the difference between the unsprung mass vertical displacement, z_t, and road input vertical displacement, z_r), acts on the unsprung mass to support the overall mass of the quarter car and to introduce the road forcing. A conventional suspension strut is combined with the new SAVGS components (single-link and actuator) and to introduce the road forcing that suspends the sprung mass on the unsprung mass.

3.1.6 SAVGS full-car multi-body model (FC)

The full-car multi-body model has been developed based on the quarter-car models. That is, a 6 DOF chassis model has the same suspension system at each corner of the vehicle. In addition, to evaluate the performance of the SAVGS on the attitude motions and directional response of the vehicles, other subsystems are incorporated, such as

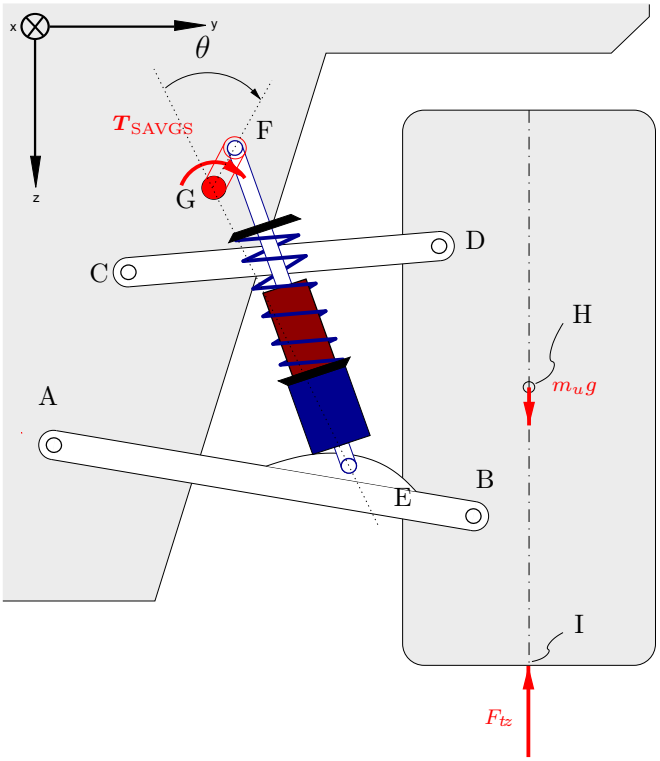

Fig. 3.3 Quarter-car arrangement. Points A, C and G are attached to the chassis; points E and F are fixed to the spring-damper unit; and points B,D, H and I are fixed to the wheel. The length of the spring-damper unit and its orientation can be continuously controlled through the rotation of the single-link with respect to its default equilibrium position [9].

aerodynamic forces, steering system, powertrain, braking system, tyres and virtual drivers. The final tree structure of the full-vehicle model is depicted in Figure 3.4 and the details of these subsystems can be found in C.Arana's work [11]. Diamond-head arrows represent the commands sent from the virtual drivers, the thick black arrows represent the tyre and braking forces and the dotted lines mean there are kinematic constraints between these bodies. The x, y and z symbols show the rotational motion allowed between a body and its parent body.

One quarter-car (rear left wheel) double wishbone arrangement of the full-car GT is shown in Figure 3.5. Figure 3.5 (a) and (b) represent the passive and active configurations for the vehicle operating with nominal payload and driving with a constant forward speed, no longitudinal or lateral acceleration. Typically, in Figure 3.5 (b), a single-link variant of the SAVGS is inserted between points G and F that is controlled by a actuation torque T_{SAVGS} to the longitudinal axis that act through point G. The nominal equilibrium of the active configuration is when the single-link at its nominal

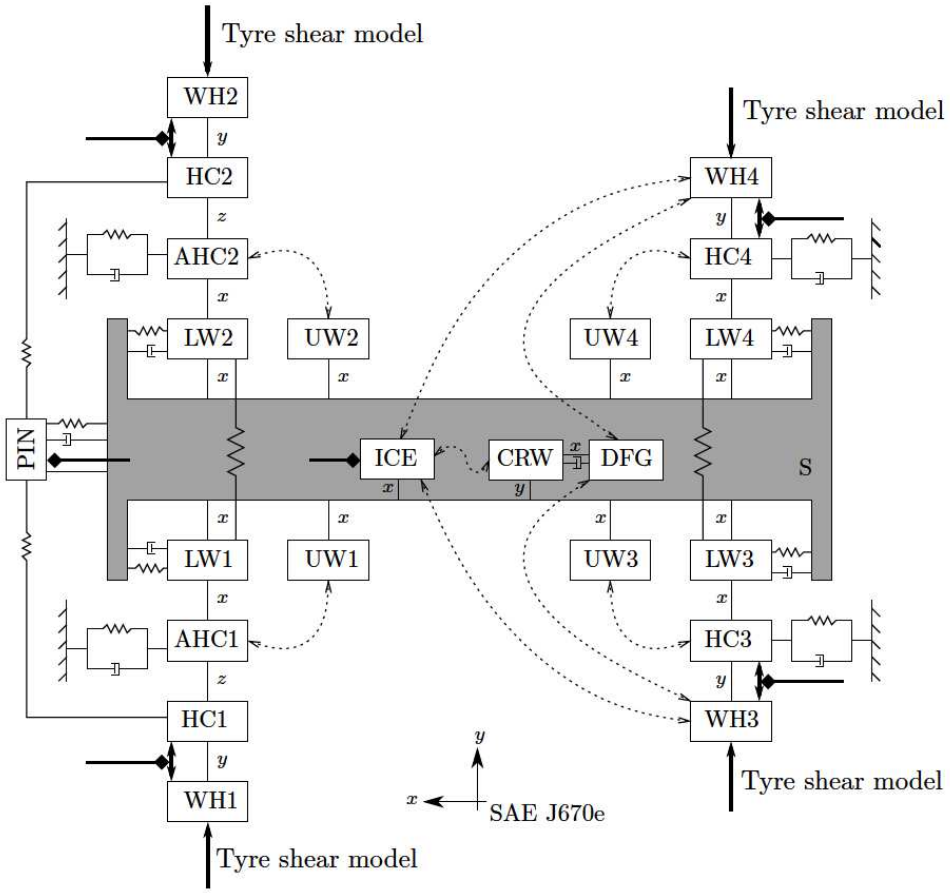

Fig. 3.4 Full-car multi-body structure [11]. Except for the chassis, S, which has six degree of freedom, the other bodies shown in this model only have a rotational degree of freedom. LW and UW are the lower and upper wishbones. AHC and HC represent the hub carriers. WH refers to wheels and PIN refers to steering pinion. ICE is the internal combustion engine, and CRW and DFG are the crown wheel and the gears in the differential, respectively.

angle $\theta_{\mathrm{SL}}^{(\mathrm{ne})}$, in where $\theta_{\mathrm{SL}}^{(\mathrm{ne})} \approx \theta_{\mathrm{SL}}^{(\mathrm{min})} + \Delta\theta_{\mathrm{SL}}$. $\Delta\theta_{\mathrm{SL}}$ is the single-link angle. When $\Delta\theta_{\mathrm{SL}}$ equals to 90°, the transfer function of the vehicle system has superior gains in the frequency domain that indicates the linearised controller developed at this position could offer the maximum control authority. The rotation of the single-link angle from its nominal angle alters the length of the spring-damper unit and the system installation ratio. Figure 3.5 (c) shows dynamic equilibrium position that the vehicle drive with a given payload, longitudinal or later acceleration. The SAVGS operates to compensates for the variation of the tire load and stabilise the vehicle motion with respect

Table 3.4 The main constraints and assumptions in the linear quarter-car model

Sprung and unsprung mass	Constrained to move vertically without rotation
Lateral tyre force	Neglected
Vertical tyre force	Act along the same line as the Spring-damper unit
Damping coefficient	$c = 0.41 * c_0$, c_0 is the maximum slope in the nonlinear damping force vs. damper extension speed (see Figure 3.6)

to the cornering conditions or the speeding changing in longitudinal directions. The reference frames used in this model are identical to the frames in Section 3.1.3.

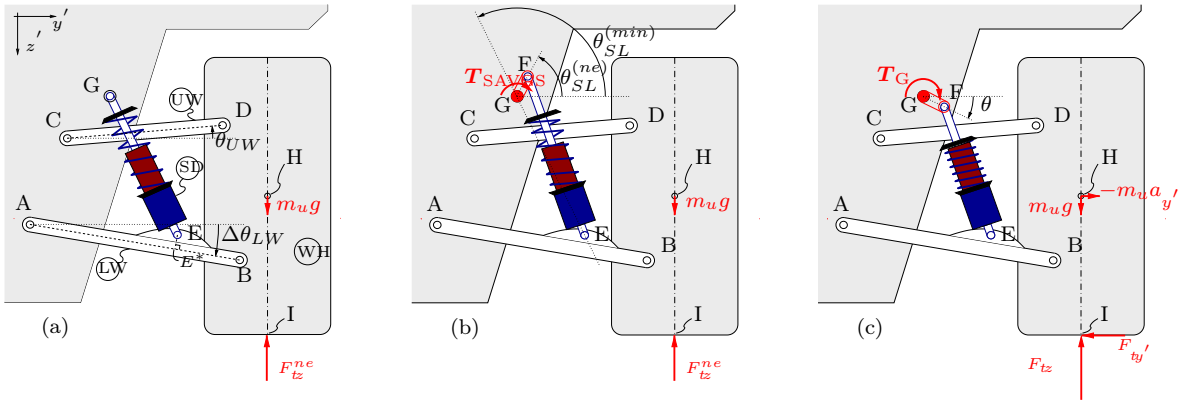

Fig. 3.5 One corner (rear right) configurations of the GT. (a) Passive suspension configuration; (b) the extension of the passive suspension by employing the variant of the SAVGS; and (c) dynamic equilibrium, in where the SAVGS compensates for the increased tire load and ensures that the wishbones remain in their desired positions.

3.1.7 SAVGS Autosim quarter-car linearised model (QCL)

The SAVGS Autosim quarter-car linearised model can be generated automatically in Autosim by linearising at a trim state of the nonlinear quarter-car SAVGS multi-body model described in Section 3.1.5. When the vehicle parameters are converted from multi-body model to the linear suspension model, there are several differences between the linear and multi-body representations of the quarter-car. The main constraints and assumptions in the linear quarter-car model, are [13]:

In the multi-body system, the d and f are vectors of the generalised coordinates and speeds. By defining the state variables, $x = \begin{bmatrix} d \\ f \end{bmatrix}$, the linearised state-space equa-

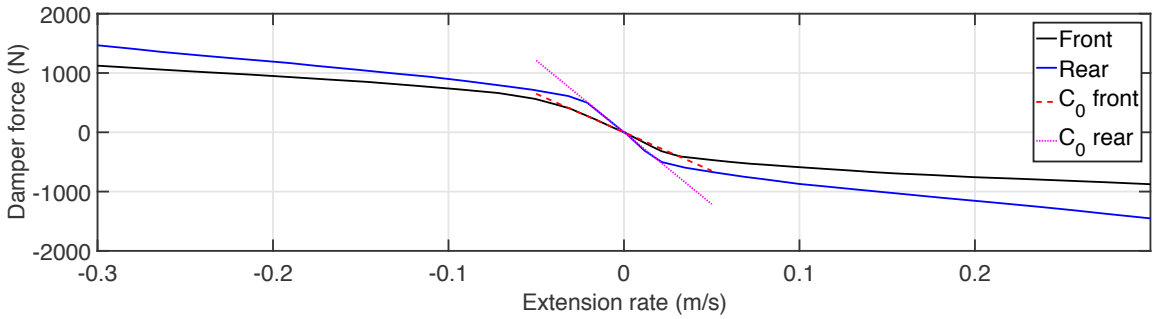

Fig. 3.6 Nonlinear damper force versus damper extension rate. c_0 at the front axles is 12980Ns/m and c_0 at the rear axles is 24236Ns/m. c_0 is chosen such that the frequency responses of the linearised GT model to an average quality random road match well the PSDs of the nonlinear GT model for the same road.

tion of the quarter-car model at $\Delta\theta_{\mathrm{SL}} = 90°$ can then be expressed as follows:

$$\dot{x} = Ax + Bu$$
$$y = Cx + Du$$

where the inputs u and outputs y of the plant are considered according to the multiple control objectives.

3.1.8 SAVGS Autosim full-car linearised model (FCL)

Similar to the QCL model, the SAVGS full-car linearised model can also be generated by Autosim from the nonlinear full-car multi-body model presented in Section 3.1.6. In addition to the previous constraints and assumptions of the QCL model, some more assumptions are made when converting the vehicle dynamics from a nonlinear model to a linear model, including: 1) fours wheel are fixed to the ground, therefore the vehicle has no movement in lateral and longitudinal directions at the four corners; 2) the aerodynamic effects are neglected; and 3) the vehicle front-rear mass distribution ratio is 57 to 43.

3.1.9 SAVGS hand-derived quarter-car linearised model (QECL)

The SAVGS hand-derived quarter-car linearised model has been developed in [13] with the aim to remove the main geometric nonlinearity associated with the single-link rotation of the SAVGS. Control design based on this model is used in subsequent work

in this thesis for comparison purposes and the work is briefly summarised here. An idea of the desired model for control synthesis is given in Figure. 3.7 (b). Instead of taking single-link velocity $\dot{\theta}_{SL}$ in the Autosim model as the control effort, this hand-derived model uses a new signal u. An external look-up table $\alpha^{-1}(u)$ is inserted between the vehicle plant (QC) and u, which is the function of single-link angle to extract the nonlinearities from the QC model. When doing so, the relationship between u and y becomes independent of the single-link angle.

The representative of the equivalent hand-derived model of the model in Figure 3.7 (b) is shown in Figure 3.7 (c). As compared to the SAVGS-retrofitted double-wishbone suspension in Figure 3.7 (a), the effect of the single-link (point G to F) can be incorporated into the equations of motion in the hand-derived model by treating it as a displacement input (z_{lin}). Therefore, the suspension deflection (i.e. the distance between the sprung and unsprung masses) can now be calculated by the sum of the deflection of the equivalent spring-damper unit (k_{eq} and c_{eq}) and the displacement of an equivalent linear actuator (z_{lin}).

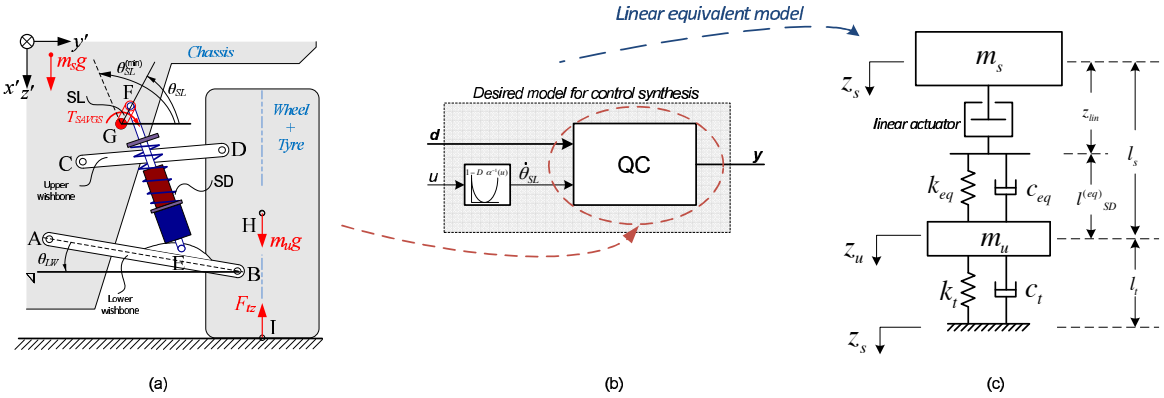

Fig. 3.7 SAVGS suspension and equivalent hand-derived model.

The calculation of these equivalent properties z_{lin}, k_{eq} and c_{eq} is taken from [13]. The relationship between $\dot{z}_{lin}$ and α can be expressed as:

$$\dot{z}_{lin} = \alpha \dot{\theta}_{SL}\,, \tag{3.1}$$

in where α is a function of the lower wishbone angle ($\Delta\theta_{LW}$) and single-link angle ($\Delta\theta_{SL}$), and:

$$\alpha = -\frac{1}{R_{SD}}\frac{\mathrm{d}l_{SD}}{\mathrm{d}\theta_{SL}}, \text{ and } R_{SD} = \frac{\mathrm{d}l_{SD}}{\mathrm{d}\theta_{LW}}\frac{\mathrm{d}\theta_{LW}}{\mathrm{d}z_H} \tag{3.2}$$

in where R_{SD} is the installation ratio of the spring-damper and l_{SD} is the actual spring-damper length of the real suspension. The term $\frac{\mathrm{d}\theta_{LW}}{\mathrm{d}z_H}$ can be calculated based on the

passive suspension geometry and can be treated as a parameter. The term $\frac{\mathrm{d}l_{SD}}{\mathrm{d}\theta_{LW}}$ is a function of $\Delta\theta_{LW}$ and $\Delta\theta_{SL}$. In this thesis, the effect of $\Delta\theta_{LW}$ will be neglected as the maximum change of α is less than 4% with respect to the nominal α ($\Delta\theta_{LW} = 0.1881$), which has been proved in the previous work [13]. Therefore,

$$\alpha = \alpha(\Delta\theta_{LW}, \Delta\theta_{SL}) \approx \alpha(\Delta\theta_{SL}) \tag{3.3}$$

In both real and equivalent suspension systems, the motion between the sprung and unsprung masses is the single factor that effects the energy stored in the suspension spring and the energy dissipated from the suspension damper. Assume the sprung mass is fixed and the unsprung mass moves with the wishbones. It is convenient to consider that the vertical motion of the equivalent unsprung mass is equal to the vertical motion of point H in Figure 3.7. It is also noted that the rate of change of the energy stored in the real and equivalent suspension springs must be equal to each other. In the meantime, the rate of energy dissipated from the real and equivalent linear dampers also must be equal. Thus, the spring stiffness and damper coefficient of the equivalent suspension to be used in QECL can be calculated as follows:

$$\begin{aligned} k_{eq} &= k_s\, R_{SD}^2 - F_{SD}\frac{\mathrm{dR_{SD}}}{\mathrm{dz_H}} \\ c_{eq} &= c_s\, R_{SD}^2 \end{aligned} \tag{3.4}$$

where c_s and k_s are the spring and damping coefficients in the real SAVGS-retrofitted double-wishbone suspension. F_{SD} is the force exerted by the real spring. Both coefficients depend on the change of lower wishbone angle ($\Delta\theta_{LW}$) and single-link angle ($\Delta\theta_{SL}$).

With the system state vectors and inputs/outputs defined as follows:

$$\begin{aligned} x^\top &= [\dot{z}_s\,, \dot{z}_u\,, \Delta l_s\,, \Delta l_t\,, z_{lin}]\,, \\ u^\top &= [\dot{z}_r\,, \dot{z}_{lin}]\,, \\ y^\top &= [\ddot{z}_s\,, \Delta l_s\,, \Delta l_t]\,, \end{aligned}$$

the state-space equation for the SAVGS hand-derived quarter-car linearised model is given by:

$$\left[\begin{array}{c|c} A & B \\ \hline C & D \end{array}\right] = \left[\begin{array}{ccccc|cc} -\frac{c_{eq}}{m_s} & \frac{c_{eq}}{m_s} & \frac{k_{eq}}{m_s} & 0 & -\frac{k_{eq}}{m_s} & 0 & -\frac{c_{eq}}{m_s} \\ \frac{c_{eq}}{m_u} & -\frac{c_{eq}+c_t}{m_u} & -\frac{k_{eq}}{m_u} & \frac{k_t}{m_u} & \frac{k_{eq}}{m_u} & \frac{c_t}{m_u} & \frac{c_{eq}}{m_u} \\ -1 & 1 & 0 & 0 & 0 & 0 & 0 \\ 0 & -1 & 0 & 0 & 0 & 1 & 0 \\ 0 & 0 & 0 & 0 & 0 & 0 & 1 \\ \hline -\frac{c_{eq}}{m_s} & \frac{c_{eq}}{m_s} & \frac{k_{eq}}{m_s} & 0 & -\frac{k_{eq}}{m_s} & 0 & -\frac{c_{eq}}{m_s} \\ 0 & 0 & 1 & 0 & 0 & 0 & 0 \\ 0 & 0 & 0 & 1 & 0 & 0 & 0 \end{array}\right].$$

3.1.10 SAVGS full-car hand-derived linear equivalent model (FECL)

The full-car hand-derived linear equivalent model is the (non-trivial) expansion of the SAVGS hand-derived quarter-car linearised model in Section 3.1.9. The configuration of the equivalent model is shown in Figure 3.8 and it is a contribution of this thesis. This is a 7-DOF model where the sprung mass is defined to be a rigid body with in vertical, pitching, and rolling freedoms (z_{CM}, θ, ϕ), while a vertical displacement freedom is also defined for each of the four unsprung masses (z_{u1}, z_{u2}, z_{u3}, z_{u4}). Two external actions, namely the exogenous pitching and rolling moments (T_p, T_r), are added to the chassis to simulate the movement of the vehicle with load transfer.

The state-space form of the equivalent full-car SAVGS model can be written as:

$$\dot{x} = Ax + Bu$$
$$y = Cx + Du$$

The state vector is chosen as the follows for the minimal realisation of linear system:

$$x^T = [\dot{z}_{CM}, \dot{\theta}, \dot{\varphi}, \dot{z}_{u1}, \dot{z}_{u2}, \dot{z}_{u3}, \dot{z}_{u4}, \Delta l_{s1}, \Delta l_{s2}, \Delta l_{s3}, \Delta l_{s4}, \Delta l_{t1}, \Delta l_{t2}, \Delta l_{t3}, \Delta l_{t4}, z_{lin1}, z_{lin2}, z_{lin3}, z_{lin4}]$$

The input vector u includes disturbances (time derivatives of the vertical road profiles, the exogenous pitching and rolling torques) and control inputs (the actuator velocities

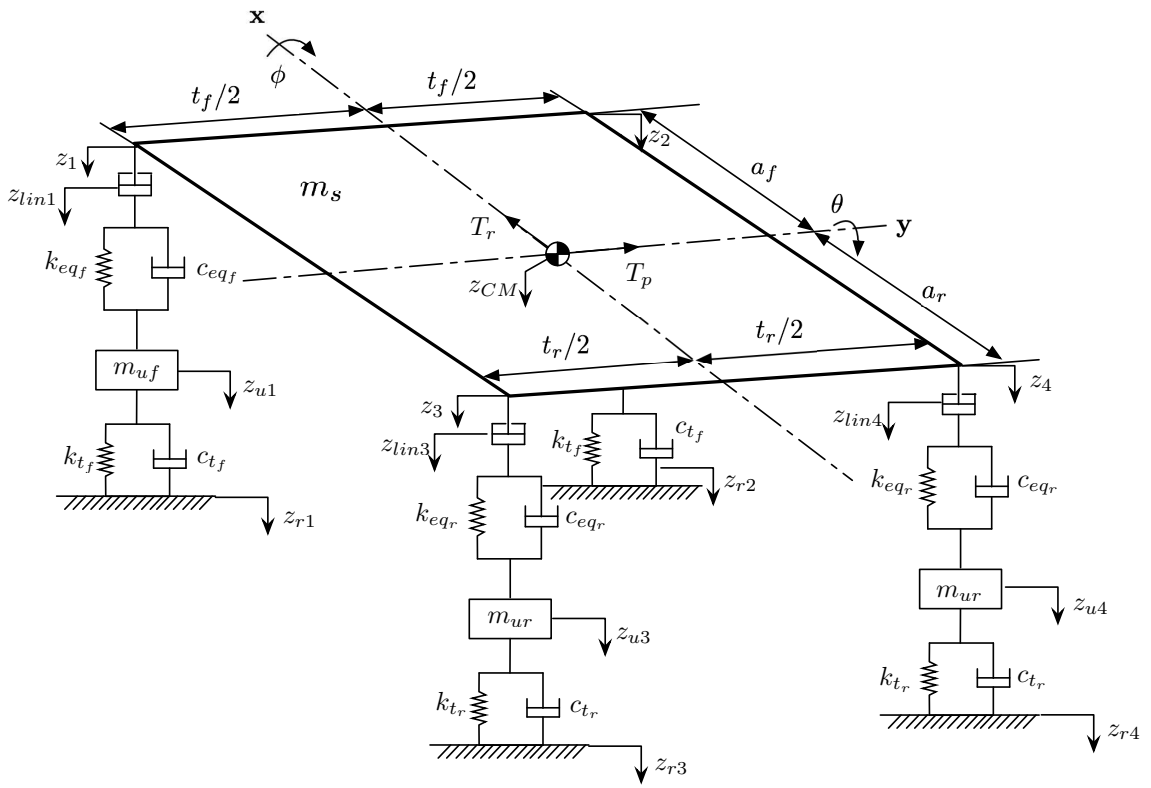

Fig. 3.8 Full-car hand-derived linear equivalent model for the study of vehicle dynamic response.

regarding to the single-link rotations):

$$u^T = [\dot{z}_{r1}, \dot{z}_{r2}, \dot{z}_{r3}, \dot{z}_{r4,} T_p, T_r, \dot{z}_{lin1}, \dot{z}_{lin2}, \dot{z}_{lin3}, \dot{z}_{lin4}]$$

The outputs are selected as the displacements of equivalent linear actuators, the tyre deflections, and mass centre accelerations (vertical, pitch and roll directions). The list of these variables can be modified according to different control objectives:

$$y^T = \left[z_{lin1}, z_{lin2}, z_{lin3}, z_{lin4}, \Delta l_{t1,} \Delta l_{t2,} \Delta l_{t3}, \Delta l_{t4}, \Delta \dot{l}_{s1}, \Delta \dot{l}_{s2}, \Delta \dot{l}_{s3}, \Delta \dot{l}_{s4}, \ddot{z}_{CM}, \ddot{\theta}, \ddot{\phi}\right]$$

Basic assumption of the linear equivalent model:
The linearised equations for the position and speeds of the sprung masses at each corner of the vehicle are (subscripts f and r refer to the front and rear axes):

$$z_1 = z_{CM} - a_f\theta - \left(\frac{t_f}{2}\right)\phi,$$

$$z_2 = z_{CM} - a_f\theta + \left(\frac{t_f}{2}\right)\phi,$$

$$z_3 = z_{CM} + a_r\theta - \left(\frac{t_r}{2}\right)\phi,$$

$$z_4 = z_{CM} + a_r\theta + \left(\frac{t_r}{2}\right)\phi,$$

The suspension deflections and deflection rates can therefore be calculated through:

$$\Delta l_{s1} = z_{u1} - z_1 = z_{u1} - z_{CM} + a_f\theta + \left(\frac{t_f}{2}\right)\phi, \dot{\Delta} l_{s1} = \dot{z}_{u1} - \dot{z}_{CM} + a_f\dot{\theta} + \left(\frac{t_f}{2}\right)\dot{\phi}$$

$$\Delta l_{s2} = z_{u2} - z_2 = z_{u2} - z_{CM} + a_f\theta - \left(\frac{t_f}{2}\right)\phi, \dot{\Delta} l_{s2} = \dot{z}_{u2} - \dot{z}_{CM} + a_f\dot{\theta} - \left(\frac{t_f}{2}\right)\dot{\phi}$$

$$\Delta l_{s3} = z_{u3} - z_3 = z_{u3} - z_{CM} - a_r\theta + \left(\frac{t_r}{2}\right)\phi, \dot{\Delta} l_{s3} = \dot{z}_{u3} - \dot{z}_{CM} - a_r\dot{\theta} + \left(\frac{t_r}{2}\right)\dot{\phi}$$

$$\Delta l_{s4} = z_{u4} - z_4 = z_{u4} - z_{CM} - a_r\theta - \left(\frac{t_r}{2}\right)\phi, \dot{\Delta} l_{s4} = \dot{z}_{u4} - \dot{z}_{CM} - a_r\dot{\theta} - \left(\frac{t_r}{2}\right)\dot{\phi}$$

Tyre deflections and deflection rates are simply $\Delta l_{ti} = z_{ri} - z_{ui}$ and $\dot{\Delta} l_{ti} = \dot{z}_{ri} - \dot{z}_{ui}$ respectively. The suspension forces produced by the spring-damper and the actuator acting on the sprung mass as well as the tyre forces acting on the unsprung masses are given by:

$$F_{SD1} = k_{eqf}\left(\Delta l_{s1} - z_{lin1}\right) + c_{eqf}\left(\dot{\Delta} l_{s1} - \dot{z}_{lin1}\right),$$
$$F_{SD2} = k_{eqf}\left(\Delta l_{s2} - z_{lin2}\right) + c_{eqf}\left(\dot{\Delta} l_{s2} - \dot{z}_{lin2}\right),$$
$$F_{SD3} = k_{eqr}\left(\Delta l_{s3} - z_{lin3}\right) + c_{eqr}\left(\dot{\Delta} l_{s3} - \dot{z}_{lin3}\right),$$
$$F_{SD4} = k_{eqr}\left(\Delta l_{s4} - z_{lin4}\right) + c_{eqr}\left(\dot{\Delta} l_{s4} - \dot{z}_{lin4}\right),$$

and

$$F_{t1} = k_{tf}\left(z_{r1} - z_{u1}\right) + c_{tf}\left(\dot{z}_{r1} - \dot{z}_{u1}\right),$$
$$F_{t2} = k_{tf}\left(z_{r2} - z_{u2}\right) + c_{tf}\left(\dot{z}_{r2} - \dot{z}_{u2}\right),$$
$$F_{t3} = k_{tr}\left(z_{r3} - z_{u3}\right) + c_{tr}\left(\dot{z}_{r3} - \dot{z}_{u3}\right),$$
$$F_{t4} = k_{tr}\left(z_{r4} - z_{u4}\right) + c_{tr}\left(\dot{z}_{r4} - \dot{z}_{u4}\right).$$

Equations of motion: The equations of motions are derived by using Newton's second law to the chassis and unsprung masses. Hence, the final equations of motion of the SAVGS equivalent full-car model can be formalised as:

$$\begin{aligned}
\ddot{z}_{u1} = \frac{F_{t1} - F_{SD1}}{M_{uf}} = \; & \tfrac{1}{m_{uf}}(c_{eqf}\dot{z}_{CM} - c_{eqf}a_f\dot{\theta} - c_{eqf}\left(\tfrac{t_f}{2}\right)\dot{\phi} - (c_{tf} + c_{eqf})\,\dot{z}_{u1} \\
& -k_{eqf}\Delta l_{s1} + k_{tf}\Delta l_{t1} + c_{tf}\dot{z}_{r1} + k_{eqf}z_{lin1} + c_{eqf}\dot{z}_{lin1})\,, \\
\ddot{z}_{u2} = \frac{F_{t2} - F_{SD2}}{M_{uf}} = \; & \tfrac{1}{m_{uf}}(c_{eqf}\dot{z}_{CM} - c_{eqf}a_f\dot{\theta} + c_{eqf}\left(\tfrac{t_f}{2}\right)\dot{\phi} - (c_{tf} + c_{eqf})\,\dot{z}_{u2} \\
& -k_{eqf}\Delta l_{s2} + k_{tf}\Delta l_{t2} + c_{tf}\dot{z}_{r2} + k_{eqf}z_{lin2} + c_{eqf}\dot{z}_{lin2})\,, \\
\ddot{z}_{u3} = \frac{F_{t3} - F_{SD3}}{M_{ur}} = \; & \tfrac{1}{m_{ur}}(c_{eqr}\dot{z}_{CM} + c_{eqr}a_r\dot{\theta} - c_{eqr}\left(\tfrac{t_r}{2}\right)\dot{\phi} - (c_{tr} + c_{eqr})\,\dot{z}_{u3} \\
& -k_{eqr}\Delta l_{s3} + k_{tr}\Delta l_{t3} + c_{tr}\dot{z}_{r3} + k_{eqr}z_{lin3} + c_{eqr}\dot{z}_{lin3})\,, \\
\ddot{z}_{u4} = \frac{F_{t4} - F_{SD4}}{M_{ur}} = \; & \tfrac{1}{m_{ur}}(c_{eqr}\dot{z}_{CM} + c_{eqr}a_r\dot{\theta} + c_{eqr}\left(\tfrac{t_r}{2}\right)\dot{\phi} - (c_{tr} + c_{eqr})\,\dot{z}_{u4} \\
& -k_{eqr}\Delta l_{s4} + k_{tr}\Delta l_{t4} + c_{tr}\dot{z}_{r4} + k_{eqr}z_{lin4} + c_{eqr}\dot{z}_{lin4})\,, \\
\ddot{z}_{CM} = \frac{\sum F_{SDi}}{m_s} = \; & \tfrac{1}{m_s}(k_{eqf}\Delta l_{s1} + k_{eqf}\Delta l_{s2} + k_{eqr}\Delta l_{s3} + k_{eqr}\Delta l_{s4} - k_{eqf}z_{lin1} \\
& -k_{eqf}z_{lin2} - k_{eqr}z_{lin3} - k_{eqr}z_{lin4} - c_{eqf}\dot{z}_{lin1} - c_{eqf}\dot{z}_{lin2} \\
& -c_{eqr}\dot{z}_{lin3} - c_{eqr}\dot{z}_{lin4} + c_{eqf}\dot{z}_{u1} + c_{eqf}\dot{z}_{u2} + c_{eqr}\dot{z}_{u3} \\
& +c_{eqr}\dot{z}_{u4} - 2(c_{eqf} + c_{eqr})\dot{z}_{CM} + 2(c_{eqf}a_f - c_{eqr}a_r)\dot{\theta})\,, \\
\ddot{\theta} = \frac{\sum M_y}{I_{yy}} = \; & \tfrac{1}{I_{yy}}\left(-a_f\left(F_{SD1} + F_{SD2}\right) + a_r\left(F_{SD3} + F_{SD4}\right) + T_P\right) \\
= \; & \tfrac{1}{I_{yy}}(2\left(c_{eqf}a_f - c_{eqr}a_r\right)\dot{z}_{CM} - 2\left(c_{eqf}a^2{}_f + c_{eqr}a^2{}_r\right)\dot{\theta} - a_f c_{eqf}\dot{z}_{u1} \\
& -a_f c_{eqf}\dot{z}_{u2} + a_r c_{eqr}\dot{z}_{u3} + a_r c_{eqr}\dot{z}_{u4} - a_f k_{eqf}\Delta l_{s1} - a_f k_{eqf}\Delta l_{s2} \\
& +a_r k_{eqr}\Delta l_{s3} + a_r k_{eqr}\Delta l_{s4} + a_f k_{eqf}z_{lin1} + a_f k_{eqf}z_{lin2} - a_r k_{eqr}z_{lin3} \\
& -a_r k_{eqr}z_{lin4} + a_f c_{eqf}\dot{z}_{lin1} + a_f c_{eqf}\dot{z}_{lin2} - a_r c_{eqr}\dot{z}_{lin3} - a_r c_{eqr}\dot{z}_{lin4} + T_p)\,,
\end{aligned}$$

$$
\begin{aligned}
\ddot{\phi} = \frac{\sum M_x}{I_{xx}} = & \quad \tfrac{1}{I_{xx}} \left(\tfrac{t_f}{2} \left(-F_{SD1} + F_{SD2} \right) + \tfrac{t_r}{2} \left(-F_{SD3} + F_{SD4} \right) + T_r \right) \\
= & \quad \tfrac{1}{I_{xx}} (-\tfrac{1}{2} \left(c_{eqf} t^2{}_f + c_{eqr} t^2{}_r \right) \dot{\phi} - \tfrac{t_f}{2} c_{eqf} \ \dot{z}_{u1} + \tfrac{t_f}{2} c_{eqf} \dot{z}_{u2} - \tfrac{t_r}{2} c_{eqr} \dot{z}_{u3} \\
& + \tfrac{t_r}{2} c_{eqr} \dot{z}_{u4} - \tfrac{t_f}{2} k_{eqf} \Delta l_{s1} + \tfrac{t_f}{2} k_{eqf} \Delta l_{s2} - \tfrac{t_r}{2} k_{eqr} \Delta l_{s3} + \tfrac{t_r}{2} k_{eqr} \Delta l_{s4} \\
& + \tfrac{t_f}{2} k_{eqf} z_{lin1} - \tfrac{t_f}{2} k_{eqf} z_{lin2} + \tfrac{t_r}{2} k_{eqr} z_{lin3} - \tfrac{t_r}{2} k_{eqr} z_{lin4} + \tfrac{t_f}{2} c_{eqf} \dot{z}_{lin1} \\
& - \tfrac{t_f}{2} c_{eqf} \ \dot{z}_{lin2} + \tfrac{t_r}{2} c_{eqr} \dot{z}_{lin3} - \tfrac{t_r}{2} c_{eqr} \dot{z}_{lin4} + T_r) \, ,
\end{aligned}
$$

$$
\begin{aligned}
\ddot{z}_1 = & \quad \ddot{z}_{CM} - a_f \ddot{\theta} - \tfrac{t_f}{2} \ddot{\phi} \\
= & \quad \left(\tfrac{k_{eqf}}{m_s} + \tfrac{a_f^2 k_{eqf}}{I_{yy}} + \tfrac{t_f^2 k_{eqf}}{4 I_{xx}} \right) \Delta l_{s1} + \left(\tfrac{k_{eqf}}{m_s} + \tfrac{a_f^2 k_{eqf}}{I_{yy}} - \tfrac{t_f^2 k_{eqf}}{4 I_{xx}} \right) \Delta l_{s2} \\
& + \left(\tfrac{k_{eqr}}{m_s} - \tfrac{a_f a_r k_{eqr}}{I_{yy}} + \tfrac{t_f t_r k_{eqr}}{4 I_{xx}} \right) \Delta l_{s3} + \left(\tfrac{k_{eqr}}{m_s} - \tfrac{a_f a_r k_{eqr}}{I_{yy}} - \tfrac{t_f t_r k_{eqr}}{4 I_{xx}} \right) \Delta l_{s4} \\
& + \left(\tfrac{c_{eqf}}{m_s} + \tfrac{a_f^2 c_{eqf}}{I_{yy}} + \tfrac{t_f^2 c_{eqf}}{4 I_{xx}} \right) \dot{z}_{u1} + \left(\tfrac{c_{eqf}}{m_s} + \tfrac{a_f^2 c_{eqf}}{I_{yy}} - \tfrac{t_f^2 c_{eqf}}{4 I_{xx}} \right) \dot{z}_{u2} \\
& + \left(\tfrac{c_{eqr}}{m_s} - \tfrac{a_f a_r c_{eqr}}{I_{yy}} + \tfrac{t_f t_r c_{eqr}}{4 I_{xx}} \right) \dot{z}_{u3} + \left(\tfrac{c_{eqr}}{m_s} - \tfrac{a_f a_r c_{eqr}}{I_{yy}} - \tfrac{t_f t_r c_{eqr}}{4 I_{xx}} \right) \dot{z}_{u4} \\
& + \left(-\tfrac{1}{m_s} - \tfrac{a_f^2}{I_{yy}} - \tfrac{t_f^2}{4 I_{xx}} \right) k_{eqf} z_{lin1} + \ \left(-\tfrac{1}{m_s} - \tfrac{a_f^2}{I_{yy}} + \tfrac{t_f^2}{4 I_{xx}} \right) k_{eqf} z_{lin2} \\
& + \left(-\tfrac{1}{m_s} + \tfrac{a_f a_r}{I_{yy}} - \tfrac{t_f t_r}{4 I_{xx}} \right) k_{eqr} z_{lin3} + \left(-\tfrac{1}{m_s} + \tfrac{a_f a_r}{I_{yy}} + \tfrac{t_f t_r}{4 I_{xx}} \right) k_{eqr} z_{lin4} \\
& + \left(\tfrac{1}{m_s} - \tfrac{a_f^2}{I_{yy}} - \tfrac{t_f^2}{4 I_{xx}} \right) c_{eqf} \dot{z}_{lin1} + \left(\tfrac{1}{m_s} - \tfrac{a_f^2}{I_{yy}} + \tfrac{t_f^2}{4 I_{xx}} \right) c_{eqf} \dot{z}_{lin2} \\
& + \left(\tfrac{1}{m_s} + \tfrac{a_r a_f}{I_{yy}} - \tfrac{t_f t_r}{4 I_{xx}} \right) c_{eqr} \dot{z}_{lin3} + \left(\tfrac{1}{m_s} + \tfrac{a_r a_f}{I_{yy}} + \tfrac{t_f t_r}{4 I_{xx}} \right) c_{eqr} \dot{z}_{lin4} \\
& + \left(-\tfrac{2}{m_s} \left(c_{eqr} + c_{eqf} \right) - \tfrac{2 a_f}{I_{yy}} \left(c_{eqf} a_f - c_{eqr} a_r \right) \right) \dot{z}_{CM} \\
& + \left(\tfrac{2}{m_s} \left(c_{eqf} a_f - c_{eqr} a_r \right) + \tfrac{2 a_f}{I_{yy}} \left(c_{eqf} a_f^2 + c_{eqr} a_f^2 \right) \right) \dot{\theta} \\
& + \tfrac{t_f}{4 I_{xx}} \left(c_{eqf} t_f^2 + c_{eqr} t_f^2 \right) \dot{\phi} - \tfrac{a_f}{I_{yy}} T_p - \tfrac{t_f}{2 I_{xx}} T_r \, ,
\end{aligned}
$$

$$
\begin{aligned}
\ddot{z}_2 = \;& \ddot{z}_{CM} - a_f\ddot{\theta} + \tfrac{t_f}{2}\ddot{\phi} \\
= \;& \left(\tfrac{k_{eqf}}{m_s} + \tfrac{a_f^2 k_{eqf}}{I_{yy}} - \tfrac{t_f^2 k_{eqf}}{4I_{xx}}\right)\Delta l_{s1} + \left(\tfrac{k_{eqf}}{m_s} + \tfrac{a_f^2 k_{eqf}}{I_{yy}} + \tfrac{t_f^2 k_{eqf}}{4I_{xx}}\right)\Delta l_{s2} \\
& + \left(\tfrac{k_{eqr}}{m_s} - \tfrac{a_f a_r k_{eqr}}{I_{yy}} - \tfrac{t_f t_r k_{eqr}}{4I_{xx}}\right)\Delta l_{s3} + \left(\tfrac{k_{eqr}}{m_s} - \tfrac{a_f a_r k_{eqr}}{I_{yy}} + \tfrac{t_f t_r k_{eqr}}{4I_{xx}}\right)\Delta l_{s4} \\
& + \left(\tfrac{c_{eqf}}{m_s} + \tfrac{a_f^2 c_{eqf}}{I_{yy}} - \tfrac{t_f^2 c_{eqf}}{4I_{xx}}\right)\dot{z}_{u1} + \left(\tfrac{c_{eqf}}{m_s} + \tfrac{a_f^2 c_{eqf}}{I_{yy}} + \tfrac{t_f^2 c_{eqf}}{4I_{xx}}\right)\dot{z}_{u2} \\
& + \left(\tfrac{c_{eqr}}{m_s} - \tfrac{a_f a_r c_{eqr}}{I_{yy}} - \tfrac{t_f t_r c_{eqr}}{4I_{xx}}\right)\dot{z}_{u3} + \left(\tfrac{c_{eqr}}{m_s} - \tfrac{a_f a_r c_{eqr}}{I_{yy}} + \tfrac{t_f t_r c_{eqr}}{4I_{xx}}\right)\dot{z}_{u4} \\
& + \left(-\tfrac{1}{m_s} - \tfrac{a_f^2}{I_{yy}} + \tfrac{t_f^2}{4I_{xx}}\right)k_{eqf} z_{lin1} + \left(-\tfrac{1}{m_s} - \tfrac{a_f^2}{I_{yy}} - \tfrac{t_f^2}{4I_{xx}}\right)k_{eqf} z_{lin2} \\
& + \left(-\tfrac{1}{m_s} + \tfrac{a_f a_r}{I_{yy}} + \tfrac{t_f t_r}{4I_{xx}}\right)k_{eqr} z_{lin3} + \left(-\tfrac{1}{m_s} + \tfrac{a_f a_r}{I_{yy}} - \tfrac{t_f t_r}{4I_{xx}}\right)k_{eqr} z_{lin4} \\
& + \left(\tfrac{1}{m_s} - \tfrac{a_f^2}{I_{yy}} + \tfrac{t_f^2}{4I_{xx}}\right)c_{eqf}\dot{z}_{lin1} + \left(\tfrac{1}{m_s} - \tfrac{a_f^2}{I_{yy}} - \tfrac{t_f^2}{4I_{xx}}\right)c_{eqf}\dot{z}_{lin2} \\
& + \left(\tfrac{1}{m_s} + \tfrac{a_r a_f}{I_{yy}} + \tfrac{t_f t_r}{4I_{xx}}\right)c_{eqr}\dot{z}_{lin3} + \left(\tfrac{1}{m_s} + \tfrac{a_r a_f}{I_{yy}} - \tfrac{t_f t_r}{4I_{xx}}\right)c_{eqr}\dot{z}_{lin4} \\
& + \left(-\tfrac{2}{m_s}\left(c_{eqr} + c_{eqf}\right) - \tfrac{2a_f}{I_{yy}}\left(c_{eqf}a_f - c_{eqr}a_r\right)\right)\dot{z}_{CM} \\
& + \left(\tfrac{2}{m_s}\left(c_{eqf}a_f - c_{eqr}a_r\right) + \tfrac{2a_f}{I_{yy}}\left(c_{eqf}a_f^2 + c_{eqr}a_f^2\right)\right)\dot{\theta} \\
& - \tfrac{t_f}{4I_{xx}}\left(c_{eqf}t_f^2 + c_{eqr}t_f^2\right)\dot{\phi} - \tfrac{a_f}{I_{yy}}T_p + \tfrac{t_f}{2I_{xx}}T_r\,,
\end{aligned}
$$

$$
\begin{aligned}
\ddot{z}_3 = \;& \ddot{z}_{CM} + a_f\ddot{\theta} - \tfrac{t_f}{2}\ddot{\phi} \\
= \;& \left(\tfrac{k_{eqf}}{m_s} - \tfrac{a_f^2 k_{eqf}}{I_{yy}} + \tfrac{t_f^2 k_{eqf}}{4I_{xx}}\right)\Delta l_{s1} + \left(\tfrac{k_{eqf}}{m_s} - \tfrac{a_f^2 k_{eqf}}{I_{yy}} - \tfrac{t_f^2 k_{eqf}}{4I_{xx}}\right)\Delta l_{s2} \\
& + \left(\tfrac{k_{eqr}}{m_s} + \tfrac{a_f a_r k_{eqr}}{I_{yy}} + \tfrac{t_f t_r k_{eqr}}{4I_{xx}}\right)\Delta l_{s3} + \left(\tfrac{k_{eqr}}{m_s} + \tfrac{a_f a_r k_{eqr}}{I_{yy}} - \tfrac{t_f t_r k_{eqr}}{4I_{xx}}\right)\Delta l_{s4} \\
& + \left(\tfrac{c_{eqf}}{m_s} - \tfrac{a_f^2 c_{eqf}}{I_{yy}} + \tfrac{t_f^2 c_{eqf}}{4I_{xx}}\right)\dot{z}_{u1} + \left(\tfrac{c_{eqf}}{m_s} - \tfrac{a_f^2 c_{eqf}}{I_{yy}} - \tfrac{t_f^2 c_{eqf}}{4I_{xx}}\right)\dot{z}_{u2} \\
& + \left(\tfrac{c_{eqr}}{m_s} + \tfrac{a_f a_r c_{eqr}}{I_{yy}} + \tfrac{t_f t_r c_{eqr}}{4I_{xx}}\right)\dot{z}_{u3} + \left(\tfrac{c_{eqr}}{m_s} + \tfrac{a_f a_r c_{eqr}}{I_{yy}} - \tfrac{t_f t_r c_{eqr}}{4I_{xx}}\right)\dot{z}_{u4} \\
& + \left(-\tfrac{1}{m_s} + \tfrac{a_f^2}{I_{yy}} - \tfrac{t_f^2}{4I_{xx}}\right)k_{eqf} z_{lin1} + \left(-\tfrac{1}{m_s} + \tfrac{a_f^2}{I_{yy}} + \tfrac{t_f^2}{4I_{xx}}\right)k_{eqf} z_{lin2} \\
& + \left(-\tfrac{1}{m_s} - \tfrac{a_f a_r}{I_{yy}} - \tfrac{t_f t_r}{4I_{xx}}\right)k_{eqr} z_{lin3} + \left(-\tfrac{1}{m_s} - \tfrac{a_f a_r}{I_{yy}} + \tfrac{t_f t_r}{4I_{xx}}\right)k_{eqr} z_{lin4} \\
& + \left(\tfrac{1}{m_s} + \tfrac{a_f^2}{I_{yy}} - \tfrac{t_f^2}{4I_{xx}}\right)c_{eqf}\dot{z}_{lin1} + \left(\tfrac{1}{m_s} + \tfrac{a_f^2}{I_{yy}} + \tfrac{t_f^2}{4I_{xx}}\right)c_{eqf}\dot{z}_{lin2} \\
& + \left(\tfrac{1}{m_s} - \tfrac{a_r a_f}{I_{yy}} - \tfrac{t_f t_r}{4I_{xx}}\right)c_{eqr}\dot{z}_{lin3} + \left(\tfrac{1}{m_s} - \tfrac{a_r a_f}{I_{yy}} + \tfrac{t_f t_r}{4I_{xx}}\right)c_{eqr}\dot{z}_{lin4} \\
& + \left(-\tfrac{2}{m_s}\left(c_{eqr} + c_{eqf}\right) + \tfrac{2a_f}{I_{yy}}\left(c_{eqf}a_f - c_{eqr}a_r\right)\right)\dot{z}_{CM} \\
& + \left(\tfrac{2}{m_s}\left(c_{eqf}a_f - c_{eqr}a_r\right) - \tfrac{2a_f}{I_{yy}}\left(c_{eqf}a_f^2 + c_{eqr}a_f^2\right)\right)\dot{\theta} \\
& + \tfrac{t_f}{4I_{xx}}\left(c_{eqf}t_f^2 + c_{eqr}t_f^2\right)\dot{\phi} + \tfrac{a_f}{I_{yy}}T_p - \tfrac{t_f}{2I_{xx}}T_r\,,
\end{aligned}
$$

$$
\begin{aligned}
\ddot{z}_4 = \;& \ddot{z}_{CM} + a_f\ddot{\theta} + \tfrac{t_f}{2}\ddot{\phi} \\
= \;& \left(\tfrac{k_{eqf}}{m_s} - \tfrac{a_f^2 k_{eqf}}{I_{yy}} - \tfrac{t_f^2 k_{eqf}}{4I_{xx}}\right)\Delta l_{s1} + \left(\tfrac{k_{eqf}}{m_s} - \tfrac{a_f^2 k_{eqf}}{I_{yy}} + \tfrac{t_f^2 k_{eqf}}{4I_{xx}}\right)\Delta l_{s2} \\
& + \left(\tfrac{k_{eqr}}{m_s} + \tfrac{a_f a_r k_{eqr}}{I_{yy}} - \tfrac{t_f t_r k_{eqr}}{4I_{xx}}\right)\Delta l_{s3} + \left(\tfrac{k_{eqr}}{m_s} + \tfrac{a_f a_r k_{eqr}}{I_{yy}} + \tfrac{t_f t_r k_{eqr}}{4I_{xx}}\right)\Delta l_{s4} \\
& + \left(\tfrac{c_{eqf}}{m_s} - \tfrac{a_f^2 c_{eqf}}{I_{yy}} - \tfrac{t_f^2 c_{eqf}}{4I_{xx}}\right)\dot{z}_{u1} + \left(\tfrac{c_{eqf}}{m_s} - \tfrac{a_f^2 c_{eqf}}{I_{yy}} + \tfrac{t_f^2 c_{eqf}}{4I_{xx}}\right)\dot{z}_{u2} \\
& + \left(\tfrac{c_{eqr}}{m_s} + \tfrac{a_f a_r c_{eqr}}{I_{yy}} - \tfrac{t_f t_r c_{eqr}}{4I_{xx}}\right)\dot{z}_{u3} + \left(\tfrac{c_{eqr}}{m_s} + \tfrac{a_f a_r c_{eqr}}{I_{yy}} + \tfrac{t_f t_r c_{eqr}}{4I_{xx}}\right)\dot{z}_{u4} \\
& + \left(-\tfrac{1}{m_s} + \tfrac{a_f^2}{I_{yy}} + \tfrac{t_f^2}{4I_{xx}}\right)k_{eqf} z_{lin1} + \left(-\tfrac{1}{m_s} + \tfrac{a_f^2}{I_{yy}} - \tfrac{t_f^2}{4I_{xx}}\right)k_{eqf} z_{lin2} \\
& + \left(-\tfrac{1}{m_s} - \tfrac{a_f a_r}{I_{yy}} + \tfrac{t_f t_r}{4I_{xx}}\right)k_{eqr} z_{lin3} + \left(-\tfrac{1}{m_s} - \tfrac{a_f a_r}{I_{yy}} - \tfrac{t_f t_r}{4I_{xx}}\right)k_{eqr} z_{lin4} \\
& + \left(\tfrac{1}{m_s} + \tfrac{a_f^2}{I_{yy}} + \tfrac{t_f^2}{4I_{xx}}\right)c_{eqf}\dot{z}_{lin1} + \left(\tfrac{1}{m_s} + \tfrac{a_f^2}{I_{yy}} - \tfrac{t_f^2}{4I_{xx}}\right)c_{eqf}\dot{z}_{lin2} \\
& + \left(\tfrac{1}{m_s} - \tfrac{a_r a_f}{I_{yy}} + \tfrac{t_f t_r}{4I_{xx}}\right)c_{eqr}\dot{z}_{lin3} + \left(\tfrac{1}{m_s} - \tfrac{a_r a_f}{I_{yy}} - \tfrac{t_f t_r}{4I_{xx}}\right)c_{eqr}\dot{z}_{lin4} \\
& + \left(-\tfrac{2}{m_s}\left(c_{eqr} + c_{eqf}\right) + \tfrac{2a_f}{I_{yy}}\left(c_{eqf}a_f - c_{eqr}a_r\right)\right)\dot{z}_{CM} \\
& + \left(\tfrac{2}{m_s}\left(c_{eqf}a_f - c_{eqr}a_r\right) - \tfrac{2a_f}{I_{yy}}\left(c_{eqf}a_f^2 + c_{eqr}a_f^2\right)\right)\dot{\theta} \\
& - \tfrac{t_f}{4I_{xx}}\left(c_{eqf}t_f^2 + c_{eqr}t_f^2\right)\dot{\phi} + \tfrac{a_f}{I_{yy}}T_p + \tfrac{t_f}{2I_{xx}}T_r \,,
\end{aligned}
$$

State-space equation:

The system matrices are $A \in \mathbb{R}^{19*19}$, $B \in \mathbb{R}^{19*10}$, $C \in \mathbb{R}^{15*19}$, $D \in \mathbb{R}^{15*10}$, and are shown below with their non-zero parameters:

$$
A = \begin{bmatrix}
* & * & 0 & * & * & * & * & * & * & * & * & 0 & 0 & 0 & 0 & * & * & * & * \\
* & * & 0 & * & * & * & * & * & * & * & * & 0 & 0 & 0 & 0 & * & * & * & * \\
0 & 0 & * & * & * & * & * & * & * & * & * & 0 & 0 & 0 & 0 & * & * & * & * \\
* & * & * & * & 0 & 0 & 0 & * & 0 & 0 & 0 & * & 0 & 0 & 0 & * & 0 & 0 & 0 \\
* & * & * & 0 & * & 0 & 0 & 0 & * & 0 & 0 & 0 & * & 0 & 0 & 0 & * & 0 & 0 \\
* & * & * & 0 & 0 & * & 0 & 0 & 0 & * & 0 & 0 & 0 & * & 0 & 0 & 0 & * & 0 \\
* & * & * & 0 & 0 & 0 & * & 0 & 0 & 0 & * & 0 & 0 & 0 & * & 0 & 0 & 0 & * \\
* & * & * & * & 0 & 0 & 0 & 0 & 0 & 0 & 0 & 0 & 0 & 0 & 0 & 0 & 0 & 0 & 0 \\
* & * & * & 0 & * & 0 & 0 & 0 & 0 & 0 & 0 & 0 & 0 & 0 & 0 & 0 & 0 & 0 & 0 \\
* & * & * & 0 & 0 & * & 0 & 0 & 0 & 0 & 0 & 0 & 0 & 0 & 0 & 0 & 0 & 0 & 0 \\
* & * & * & 0 & 0 & 0 & * & 0 & 0 & 0 & 0 & 0 & 0 & 0 & 0 & 0 & 0 & 0 & 0 \\
0 & 0 & 0 & * & 0 & 0 & 0 & 0 & 0 & 0 & 0 & 0 & 0 & 0 & 0 & 0 & 0 & 0 & 0 \\
0 & 0 & 0 & 0 & * & 0 & 0 & 0 & 0 & 0 & 0 & 0 & 0 & 0 & 0 & 0 & 0 & 0 & 0 \\
0 & 0 & 0 & 0 & 0 & * & 0 & 0 & 0 & 0 & 0 & 0 & 0 & 0 & 0 & 0 & 0 & 0 & 0 \\
0 & 0 & 0 & 0 & 0 & 0 & * & 0 & 0 & 0 & 0 & 0 & 0 & 0 & 0 & 0 & 0 & 0 & 0 \\
0 & 0 & 0 & 0 & 0 & 0 & 0 & 0 & 0 & 0 & 0 & 0 & 0 & 0 & 0 & 0 & 0 & 0 & 0 \\
0 & 0 & 0 & 0 & 0 & 0 & 0 & 0 & 0 & 0 & 0 & 0 & 0 & 0 & 0 & 0 & 0 & 0 & 0 \\
0 & 0 & 0 & 0 & 0 & 0 & 0 & 0 & 0 & 0 & 0 & 0 & 0 & 0 & 0 & 0 & 0 & 0 & 0 \\
0 & 0 & 0 & 0 & 0 & 0 & 0 & 0 & 0 & 0 & 0 & 0 & 0 & 0 & 0 & 0 & 0 & 0 & 0
\end{bmatrix}
$$

$$C = \begin{bmatrix}
0 & 0 & 0 & 0 & 0 & 0 & 0 & 0 & 0 & 0 & 0 & 0 & 0 & 0 & 0 & * & 0 & 0 & 0 \\
0 & 0 & 0 & 0 & 0 & 0 & 0 & 0 & 0 & 0 & 0 & 0 & 0 & 0 & 0 & 0 & * & 0 & 0 \\
0 & 0 & 0 & 0 & 0 & 0 & 0 & 0 & 0 & 0 & 0 & 0 & 0 & 0 & 0 & 0 & 0 & * & 0 \\
0 & 0 & 0 & 0 & 0 & 0 & 0 & 0 & 0 & 0 & 0 & 0 & 0 & 0 & 0 & 0 & 0 & 0 & * \\
0 & 0 & 0 & 0 & 0 & 0 & 0 & 0 & 0 & 0 & 0 & * & 0 & 0 & 0 & 0 & 0 & 0 & 0 \\
0 & 0 & 0 & 0 & 0 & 0 & 0 & 0 & 0 & 0 & 0 & 0 & * & 0 & 0 & 0 & 0 & 0 & 0 \\
0 & 0 & 0 & 0 & 0 & 0 & 0 & 0 & 0 & 0 & 0 & 0 & 0 & * & 0 & 0 & 0 & 0 & 0 \\
0 & 0 & 0 & 0 & 0 & 0 & 0 & 0 & 0 & 0 & 0 & 0 & 0 & 0 & * & 0 & 0 & 0 & 0 \\
* & * & * & * & 0 & 0 & 0 & 0 & 0 & 0 & 0 & * & 0 & 0 & 0 & 0 & 0 & 0 & 0 \\
* & * & * & 0 & * & 0 & 0 & 0 & 0 & 0 & 0 & 0 & * & 0 & 0 & 0 & 0 & 0 & 0 \\
* & * & * & 0 & 0 & * & 0 & 0 & 0 & 0 & 0 & 0 & 0 & * & 0 & 0 & 0 & 0 & 0 \\
* & * & * & 0 & 0 & 0 & * & 0 & 0 & 0 & 0 & 0 & 0 & 0 & * & 0 & 0 & 0 & 0 \\
* & * & 0 & * & * & * & * & * & * & * & * & 0 & 0 & 0 & 0 & * & * & * & * \\
* & * & 0 & * & * & * & * & * & * & * & * & 0 & 0 & 0 & 0 & * & * & * & * \\
0 & 0 & * & * & * & * & * & * & * & * & * & 0 & 0 & 0 & 0 & * & * & * & *
\end{bmatrix}$$

$$B = \begin{bmatrix}
0 & 0 & 0 & 0 & 0 & 0 & * & * & * & * \\
0 & 0 & 0 & 0 & * & 0 & * & * & * & * \\
0 & 0 & 0 & 0 & 0 & * & * & * & * & * \\
* & 0 & 0 & 0 & 0 & 0 & * & 0 & 0 & 0 \\
0 & * & 0 & 0 & 0 & 0 & 0 & * & 0 & 0 \\
0 & 0 & * & 0 & 0 & 0 & 0 & 0 & * & 0 \\
0 & 0 & 0 & * & 0 & 0 & 0 & 0 & 0 & * \\
0 & 0 & 0 & 0 & 0 & 0 & 0 & 0 & 0 & 0 \\
0 & 0 & 0 & 0 & 0 & 0 & 0 & 0 & 0 & 0 \\
0 & 0 & 0 & 0 & 0 & 0 & 0 & 0 & 0 & 0 \\
0 & 0 & 0 & 0 & 0 & 0 & 0 & 0 & 0 & 0 \\
* & 0 & 0 & 0 & 0 & 0 & 0 & 0 & 0 & 0 \\
0 & * & 0 & 0 & 0 & 0 & 0 & 0 & 0 & 0 \\
0 & 0 & * & 0 & 0 & 0 & 0 & 0 & 0 & 0 \\
0 & 0 & 0 & * & 0 & 0 & 0 & 0 & 0 & 0 \\
0 & 0 & 0 & 0 & 0 & 0 & * & 0 & 0 & 0 \\
0 & 0 & 0 & 0 & 0 & 0 & 0 & * & 0 & 0 \\
0 & 0 & 0 & 0 & 0 & 0 & 0 & 0 & * & 0 \\
0 & 0 & 0 & 0 & 0 & 0 & 0 & 0 & 0 & *
\end{bmatrix}, D = \begin{bmatrix}
0 & 0 & 0 & 0 & 0 & 0 & 0 & 0 & 0 & 0 \\
0 & 0 & 0 & 0 & 0 & 0 & 0 & 0 & 0 & 0 \\
0 & 0 & 0 & 0 & 0 & 0 & 0 & 0 & 0 & 0 \\
0 & 0 & 0 & 0 & 0 & 0 & 0 & 0 & 0 & 0 \\
0 & 0 & 0 & 0 & 0 & 0 & 0 & 0 & 0 & 0 \\
0 & 0 & 0 & 0 & 0 & 0 & 0 & 0 & 0 & 0 \\
0 & 0 & 0 & 0 & 0 & 0 & 0 & 0 & 0 & 0 \\
0 & 0 & 0 & 0 & 0 & 0 & 0 & 0 & 0 & 0 \\
0 & 0 & 0 & 0 & 0 & 0 & 0 & 0 & 0 & 0 \\
0 & 0 & 0 & 0 & 0 & 0 & 0 & 0 & 0 & 0 \\
0 & 0 & 0 & 0 & 0 & 0 & 0 & 0 & 0 & 0 \\
0 & 0 & 0 & 0 & 0 & 0 & 0 & 0 & 0 & 0 \\
0 & 0 & 0 & 0 & 0 & 0 & * & * & * & * \\
0 & 0 & 0 & 0 & * & 0 & * & * & * & * \\
0 & 0 & 0 & 0 & 0 & * & * & * & * & *
\end{bmatrix}$$

The non-zero parameters in matrix A are given as follows:

$A(1,1) = -2(c_{eqr} + c_{eqf})/m_s\,; A(1,2) = 2(c_{eqf}a_f - c_{eqr}a_r)/m_s\,;$
$A(1,4) = c_{eqf}/m_s\,; A(1,5) = c_{eqf}/m_s\,; A(1,6) = c_{eqr}/m_s\,;$
$A(1,7) = c_{eqr}/m_s\,; A(1,8) = k_{eqf}/m_s\,; A(1,9) = k_{eqf}/m_s\,;$
$A(1,10) = k_{eqr}/m_s\,; A(1,11) = k_{eqr}/m_s\,; A(1,16) = -A(1,8)\,;$
$A(1,17) = -A(1,8)\,; A(1,18) = -A(1,10)\,; A(1,19) = -A(1,10)\,;$
$A(2,1) = 2(c_{eqf}a_f - c_{eqr}a_r)/I_{yy}; A(2,2) = -2(c_{eqf}(a_f)^2 + c_{eqr}(a_r)^2)/I_{yy};$
$A(2,4) = -a_f c_{eqf}/I_{yy}; A(2,5) = A(2,4); A(2,6) = a_r c_{eqr}/I_{yy}; A(2,7) = A(2,6);$
$A(2,8) = -a_f k_{eqf}/I_{yy}; A(2,9) = A(2,8); A(2,10) = a_r k_{eqr}/I_{yy};$
$A(2,11) = A(2,10); A(2,16) = -A(2,8); A(2,17) = -A(2,8);$
$A(2,18) = -A(2,10); A(2,19) = -A(2,10);$
$A(3,3) = -0.5(c_{eqf}(t_f)^2 + c_{eqr}(t_r)^2)/I_{xx}; A(3,4) = -0.5t_f c_{eqf}/I_{xx};$
$A(3,5) = -A(3,4); A(3,6) = -0.5t_r c_{eqr}/I_{xx}; A(3,7) = -A(3,6);$
$A(3,8) = -0.5t_f k_{eqf}/I_{xx}; A(3,9) = -A(3,8); A(3,10) = -0.5t_r k_{eqr}/I_{xx};$
$A(3,11) = -A(3,10); A(3,16) = -A(3,8); A(3,17) = A(3,8);$
$A(3,18) = -A(3,10); A(3,19) = A(3,10);$
$A(4,1) = c_{eqf}/m_{uf}; A(4,2) = -c_{eqf}a_f/m_{uf}; A(4,3) = -0.5c_{eqf}t_f/m_{uf};$
$A(4,4) = -(c_{tf} + c_{eqf})/m_{uf}; A(4,8) = -k_{eqf}/m_{uf}; A(4,12) = k_{tf}/m_{uf};$
$A(4,16) = k_{eqf}/m_{uf};$
$A(5,1) = c_{eqf}/m_{uf}; A(5,2) = -c_{eqf}a_f/m_{uf}; A(5,3) = 0.5c_{eqf}t_f/m_{uf};$
$A(5,5) = -(c_{tf} + c_{eqf})/m_{uf}; A(5,9) = -k_{eqf}/m_{uf}; A(5,13) = k_{tf}/m_{uf};$
$A(5,17) = k_{eqf}/m_{uf};$
$A(6,1) = c_{eqr}/m_{ur}; A(6,2) = c_{eqr}a_r/m_{ur}; A(6,3) = -0.5c_{eqr}t_r/m_{ur};$
$A(6,6) = -(c_{tr} + c_{eqr})/m_{ur}; A(6,10) = -k_{eqr}/m_{ur}; A(6,14) = k_{tr}/m_{ur};$
$A(6,18) = k_{eqr}/m_{ur};$
$A(7,1) = c_{eqr}/m_{ur}; A(7,2) = c_{eqr}a_r/m_{ur}; A(7,3) = 0.5c_{eqr}t_r/m_{ur};$
$A(7,7) = -(c_{tr} + c_{eqr})/m_{ur}; A(7,11) = -k_{eqr}/m_{ur}; A(7,15) = k_{tr}/m_{ur};$
$A(7,19) = k_{eqr}/m_{ur};$
$A(8,1) = -1; A(8,2) = a_f; A(8,3) = 0.5t_f; A(8,4) = 1;$
$A(9,1) = -1; A(9,2) = a_f; A(9,3) = -0.5t_f; A(9,5) = 1;$
$A(10,1) = -1; A(10,2) = -a_r; A(10,3) = 0.5t_r; A(10,6) = 1;$
$A(11,1) = -1; A(11,2) = -a_r; A(11,3) = -0.5t_r; A(11,7) = 1;$
$A(12,4) = -1; A(13,5) = -1; A(14,6) = -1; A(15,7) = -1;$

The non-zero parameters in matrix B are given as:

$B(1,7) = -A(1,4); B(1,8) = -A(1,4); B(1,9) = -A(1,6); B(1,10) = -A(1,6);$
$B(2,5) = 1/I_{yy}; B(2,7) = -A(2,4); B(2,8) = -A(2,4); B(2,9) = -A(2,6);$
$B(2,10) = -A(2,6); B(3,6) = 1/I_{xx}; B(3,7) = -A(3,4); B(3,8) = A(3,4);$
$B(3,9) = -A(3,6); B(3,10) = A(3,6);$
$B(4,1) = c_{tf}/m_{uf}; B(4,7) = c_{eqf}/m_{uf}; B(5,2) = c_{tf}/m_{uf}; B(5,8) = c_{eqf}/m_{uf};$
$B(6,3) = c_{tr}/m_{ur}; B(6,9) = c_{eqr}/m_{ur}; B(7,4) = c_{tr}/m_{ur}; B(7,10) = c_{eqr}/m_{ur};$
$B(12,1) = 1; B(13,2) = 1; B(14,3) = 1; B(15,4) = 1; B(16,7) = 1; B(17,8) = 1; B(18,9) = 1; B(19,10) = 1;$

The non-zero parameters in matrix C are given as:

$C(1,16) = 1; C(2,17) = 1; C(3,18) = 1; C(4,19) = 1;$
$C(5,12) = 1; C(6,13) = 1; C(7,14) = 1; C(8,15) = 1;$
$C(9,1) = -1; C(9,2) = a_f; C(9,3) = t_f/2; C(9,4) = 1;$
$C(10,1) = -1; C(10,2) = a_f; C(10,3) = -t_f/2; C(12,5) = 1;$
$C(11,1) = -1; C(11,2) = -a_r; C(11,3) = t_r/2; C(12,6) = 1;$
$C(12,1) = -1; C(12,2) = -a_r; C(12,3) = -t_r/2; C(12,7) = 1;$
$C(13,1) = -2(c_{eqr} + c_{eqf})/m_s; C(13,2) = 2(c_{eqf}a_f - c_{eqr}a_r)/m_s;$
$C(13,4) = c_{eqf}/m_s; C(13,5) = c_{eqf}/m_s; C(13,6) = c_{eqr}/m_s;$
$C(13,7) = c_{eqr}/m_s; C(13,8) = k_{eqf}/m_s; C(13,9) = k_{eqf}/m_s;$
$C(13,10) = k_{eqr}/m_s; C(13,11) = k_{eqr}/m_s; C(13,16) = -C(13,8);$
$C(13,17) = -C(13,8); C(13,18) = -C(13,10); C(13,19) = -C(13,10);$
$C(14,1) = 2(c_{eqf}a_f - c_{eqr}a_r)/I_{yy}; C(14,2) = -2(c_{eqf}(a_f)^2 + c_{eqr}(a_r)^2)/I_{yy};$
$C(14,4) = -a_f c_{eqf}/I_{yy}; C(14,5) = C(14,4); C(14,6) = a_r c_{eqr}/I_{yy};$
$C(14,7) = C(14,6); C(14,8) = -a_f k_{eqf}/I_{yy}; C(14,9) = C(14,8);$
$C(14,10) = a_r k_{eqr}/I_{yy}; C(14,11) = C(14,10); C(14,16) = -C(14,8);$
$C(14,17) = -C(14,8); C(14,18) = -C(14,10); C(14,19) = -C(14,10);$
$C(15,3) = -0.5(c_{eqf}(t_f)^2 + c_{eqr}(t_r)^2)/I_{xx}; C(15,4) = -0.5t_f c_{eqf}/I_{xx};$
$C(15,5) = -C(15,4); C(15,6) = -0.5t_r c_{eqr}/I_{xx}; C(15,7) = -C(15,6);$
$C(15,8) = -0.5t_f k_{eqf}/I_{xx}; C(15,9) = -C(15,8); C(15,10) = -0.5t_r k_{eqr}/I_{xx};$
$C(15,11) = -C(15,10); C(15,16) = -C(15,8); C(15,17) = C(15,8);$
$C(15,18) = -C(15,10); C(15,19) = C(15,10);$

The non-zero parameters in matrix D are given as:

$D(13,7) = -C(13,4); D(13,8) = -C(13,4); D(13,9) = -C(13,6);$
$D(13,10) = -C(13,6); D(14,5) = 1/I_{yy}; D(14,7) = -C(14,4);$
$D(14,8) = -C(14,4); D(14,9) = -C(14,6); D(14,10) = -C(14,6);$

$D(15,6) = 1/I_{xx}; D(15,7) = -C(15,4); D(15,8) = C(15,4);$
$D(15,9) = -C(15,6); D(15,10) = C(15,6);$

3.2 Vehicle and SAVGS parameters

In this thesis, a vehicle representative of a Grand Tourer (GT) has been considered to explore the SAVGS performance. One of the representative models of the GT car is Ferrari F430, as shown in Figure 3.9.

Fig. 3.9 Ferrari F430, the high performance sports car used in this thesis.

3.2.1 Main vehicle parameters

The fundamental properties, such as masses, inertias and lengths, which determine the dynamic response of the high performance car used in this project, are summarised in Table 3.5. To see the selection process of the vehicle chassis and subsystems parameters, the reader is refered to the earlier work [11]. The QC model in Chapter 4 uses the rear wheel axle parameters.

3.2.2 SAVGS parameters

The selected actuator of the SAVGS in this thesis comprises one Kollmorgen AKM33H, which is a Permanent Magnet Synchronous Motor (PMSM), and one Danaher UT075-40, which is an epicyclic gearbox. The main properties of the single-link, PMSM, gearbox and converters selected for the GT are shown in Table 3.6. The details of the selection and sizing of the SAVGS components are found in [11].

Table 3.5 Full-car vehicle parameters

Parameter	Symbol	Units	Axle	Value
Sprung mass	m_s	kg	-	1325
Unsprung mass	m_{u_f}/m_{u_r}	kg	F/R	62.5/62.5
Wheelbase	l	m	-	2.6
Mass center height	h_{CM}	m	-	0.424
Weight distribution	%		F/R	57/43
Tyre track	t_f/t_r	m	F/R	1.669/1.615
Spring stiffness	k_{s_f}/k_{s_r}	N/mm	F/R	92/158
Damping coefficient*	c_{s_f}/c_{s_r}	Ns/m	F/R	5321/9937
Tyre stiffness	k_{t_f}/k_{t_r}	N/mm	F&R	275
Tyre damping	c_{t_f}/c_{t_r}	Ns/m	F&R	300
Chassis xx inertia	I_{xx}	kgm^2	-	300
Chassis yy inertia	I_{yy}	kgm^2	-	1500
Chassis zz inertia	I_{zz}	kgm^2	-	1500

$*$ Damping coefficient (Ns/m) for linear analyses

3.3 Road models

As the main excitation source, the modelling of the road profile is important for simulations of the vehicle models. The vehicle body accelerations, suspension travel, rotational motions, and vehicle displacements are all determined by the vehicle's dynamic responses to the road input. Road disturbances when analysing a vehicle dynamic's response can normally be classified into two groups:

- Deterministic roads, such as bump waves and sine waves, which are often used to analyse the response of the vehicle in the time domain when it travels at low speeds.
- Random roads, which allow for the validation of the responses of the vehicle in the time domain when it travels at high speeds.

3.3.1 Sinusoidal input

Vehicle motions are often studied using sinusoidal inputs. In Chapter 4, a $2\,Hz$ frequency is selected to investigate the superior improvement of the $\mathcal{H}_\infty$ controller near the natural frequencies of the quarter-car vehicle.

Table 3.6 SAVGS parameters

Component	Parameter	Units	Value
SAVGS	Single-link lengths (front/rear)	mm	15.0/11.0
	SL equivalent inertia (front & rear)	$\mathrm{kg\,m^2}$	0.16
	Actuator mass (front & rear)	kg	6
Gearbox	Gear ratio	-	40
	Efficiency	%	90
	Max. acceleration torque	Nm	205
	Static output torque	Nm	97
	Max. speed	rpm	137.5
PMSM	Static friction	Nm	0.026
	Winding (damping) coefficient	Nm s/rad	0.000038
	Number of pole pairs	-	4
	dp resistance	Ω	0.91
	dp inductance	mH	2.05
	Flux linkage due to the rotor magnets	mV s/rad	61.8
	Stray losses coefficient	mV s/rad	4.6
	Core resistance	Ω	250
	Max. cont. phase current amplitude	A	8.0
	Max. peak phase current amplitude	A	21.0
	Max. DC voltage	V	320
Converters	DC-DC converter efficiency	%	95
	DC-AC converter efficiency	%	98

3.3.2 Smoothed bump input

A smoothed bump change in the road height is another road perturbation used to evaluate the performance of the controllers. The step is given by the following expression in the time domain:

$$f(t) = \begin{cases} \frac{h_b}{2}\left(1 - \cos\left(2\pi\frac{V}{w_b}t\right)\right) & 0 \leq t \leq \frac{w_b}{V} \\ 0 & t > \frac{w_b}{V} \end{cases} \tag{3.5}$$

in which h_b is the height of the bump, w_b is the width of the bump, and V represents the forward velocity of the vehicle.

3.3.3 Random road profiles

In this work, two approaches to generating random road profiles, which can be expressed using power spectra density (PSD), are considered based on [ISO 8608:1995] [85].

- **First approach used in Chapter 4:** In this approach, the random road profile can be calculated through the integration of a random white noise signal that represents the road roughness with respect to the longitudinal velocity. As low frequencies are not expected in the suspension studies, a coloured noise source that limits the average power at low frequencies is used instead. In addition, a geometric filter that corresponds to the wheel radius of the vehicle is employed to emulated the effect of the tyre.

  The road disturbance can be characterised in terms of its displacement power spectral density (PSD), in $\mathrm{m}^2/(\mathrm{rad/m})$, which can be approximated to be [36]:

  $$\Phi(\omega) = \frac{(\sigma^2/\pi)\alpha V}{\omega^2 + \alpha^2 V^2}, \tag{3.6}$$

  in which ω is the angular spatial frequency in rad/m, σ^2 is the road roughness variance in m^2, V is the forward velocity of the car in m/s, and α depends on the quality of the road and has units of $\mathrm{rad\,s/m}^2$. The road disturbance with the PSD can be produced by solving the differential equation

  $$\dot{z}_r(t) + \alpha V z_r(t) = w(t), \tag{3.7}$$

in which z_r is the road vertical displacement disturbance and $w(t)$ is a white noise process with spectral density $2\sigma^2\alpha V$.

- **Second approach used in Chapters 5 to 7:** This approach can be obtained as the sum of a series of harmonic signals with varying amplitudes and spatial frequencies with respect to the vehicle longitudinal velocity. This approach is simpler than the previous approach and eliminates the high frequency interference in the previous case.

  Roads are modelled as the sum of harmonically related signals with varying spatial frequencies and amplitudes, which can be obtained in longitudinal direction, x, through:

$$h = \sum_{n_i=n_{min}}^{n_{max}} A_i cos(2\pi n_i x + \phi_i) \tag{3.8}$$

  where h is the random road height. Sinusoidal components are associated with the spatial frequency n_i, and the random phase ϕ_i which are distributed uniformly over the range (0, 2π). [n_{min}, n_{max}] = [0.1, 10] $cycles/m$ are defined as the lower and higher end of the spatial frequency in [ISO 8608:1995], which implies that frequencies outside this range are not relevant for the excitation of road vehicles. The amplitude, A_i, can be approximately derived from a given displacement power spectral density (PSD) [85]:

$$G_d(n_i) = G_d(n_0)(\frac{n_i}{n_0})^{-\omega} = \lim_{\Delta n \to 0} \frac{\Phi(n_i)^2}{\Delta n} \tag{3.9}$$

  in which n_0 is the reference spatial frequency, Δn is the spatial frequency step, and ω is a constant exponent. $\Phi(n_i)^2 = {A_i}^2/2$ represents the average power of a harmonic signal, and $G_d(n_0) = 10^{-6} \cdot 2^{2k}$ [85] where k corresponds to different road roughness A to H.

The power spectral density (PSD) plots of the random road profiles used in Chapters 5 to 7 based on this approach, with the values of the road parameters $n_0 = 0.1\, cycles/m$, $\Delta\, n = 0.005\, cycles/m$, $\omega = 2$, are depicted in Figure 3.10.

3.4 Type of closed-loop control schemes

In this thesis, three robust $\mathcal{H}_\infty$ control designs are formulated based on the models (1), (3) and (4) shown in Table 3.1 to solve the disturbance attenuation problem with

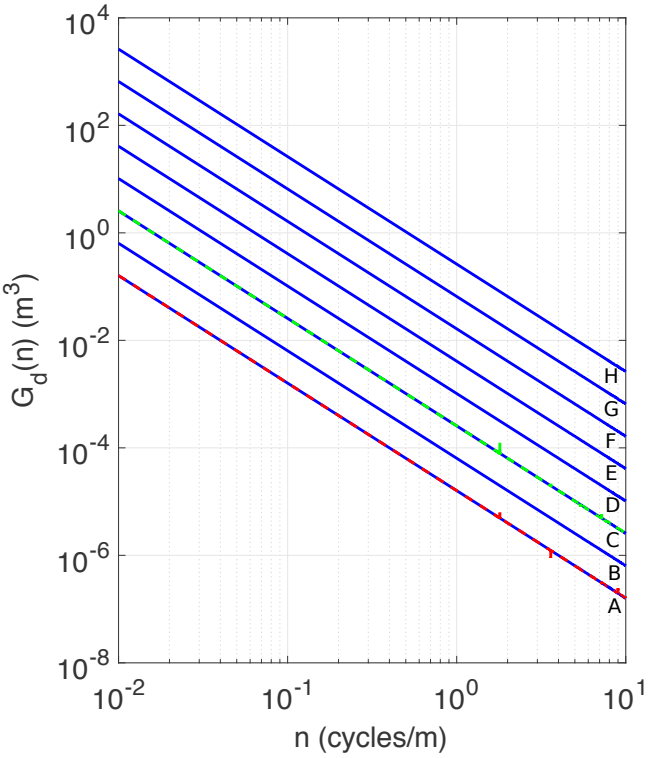

Fig. 3.10 Example PSDs for road profiles with roughness A and C considered in this chapter, shown in red and green lines, which correspond to good and average quality road. G_d is the displacement power spectral density as a function of spatial frequency, n. Classification of roads A to H are defined in [ISO 8608:1995] [85].

linearised quarter- and full- car models in the high-frequency suspension functions and an overall full-car control framework is also constructed for the purpose of tackling both the low- and high- frequency suspension functions. For a complete understanding the effectiveness of the $\mathcal{H}_\infty$ techniques on SAVGS control and to assess the potential of the SAVGS both the low- and high- frequency suspension functions, an $\mathcal{H}_\infty$ controller based on the hand-derived equivalent model (model (2) in Table 3.1) and a PID controller for the chassis attitude control proposed in the previous studies ([10] and [12]) are also introduced in Chapter 5 and 7 to help to identify the best control approach. More specifically, the $\mathcal{H}_\infty$ controller based on the hand-derived model is employed to confirm that the $\mathcal{H}_\infty$ synthesis for quarter-car hand-derived model has better level of robustness to single-link rotations, which is the motivation of the design in Chapter 6 of an $\mathcal{H}_\infty$ control synthesis for full-car hand-derived model. The latter one, the PID controller is employed to compared with the overall full-car control in the low-frequency suspension functions. As the overall full-car control in Chapter 7 is

achieved thoroughly blending an $\mathcal{H}_\infty$ controller (develop in Chapter 6) together with a new PID controller (develop in Chapter 7), the pure $\mathcal{H}_\infty$ -controlled scheme in Chapter 6 and the pure PID control scheme developed in previous studies [12] are compared to ensure that the overall control framework improves comfort and road holding in high frequency vehicle dynamics and chassis attitude motion in low frequency vehicle dynamics simultaneously while the different control objectives do not interfere with each other.

3.4.1 Quarter-car closed-loop control schemes

In Chapter 4, a SAVGS $\mathcal{H}_\infty$ -controlled scheme based on the Autosim quarter-car linearised model, denoted by QA-SAVGS, is proposed and investigated by nonlinear simulation for a range of disturbances. The results of the QA-SAVGS are compared with the passive quarter-car system, denoted by Q-Passive, to understand the effectiveness and potential of $\mathcal{H}_\infty$ synthesis with the SAVGS.

3.4.2 Full-car closed-loop control schemes

Six full-car closed-loop nonlinear control schemes in this thesis are listed in Table 3.7, in where the controllers developed in Chapters 4 to 7 are installed on the passive nonlinear full-car model, and their performance will be examined in the frequency and time domains for various operating manoeuvres. The goal of this project is to compare these closed-loop SAVGS $\mathcal{H}_\infty$ controlled schemes with the passive nonlinear full-car model (denoted as PASSIVE) to identify the final overall control approach, which could provide excellent ride comfort, road holding, and attitude control performance, simultaneously. In Table 3.7, F-SAVGS, Q1-SAVGS, and Q2-SAVGS will be compared in Chapter 5 to investigate whether the closed-loop control scheme with a full-car $\mathcal{H}_\infty$ linear controller performs better than the control scheme with four quarter-car $\mathcal{H}_\infty$ linear controllers equipped at four corners of the vehicle, in terms of ride comfort and road holding enhancement. Then, in Chapter 6, FE-SAVGS and F-SAVGS will be compared to assess whether the $\mathcal{H}_\infty$ controller developed based on the hand-derived full-car linear model performs better than the $\mathcal{H}_\infty$ controller based on the Autosim model due to its improved robustness to single-link rotations. Finally, in Chapter 7, FE-PID-SAVGS, FE-SAVGS, and PID-SAVGS, are compared to see whether the FE-PID-SAVGS could tackle both the dynamics under low frequencies for attitude control of PID-SAVGS and high frequencies for ride comfort and road holding enhancement of FE-SAVGS simultaneously.

Table 3.7 Full-car nonlinear control schemes in this thesis

Chapter	Control Scheme	Controller					Compare
		$\mathcal{H}_\infty$ controller based on				PID	
		QCL	QECL	FCL	FECL		
4	Q1-SAVGS	✓					♢
#	Q2-SAVGS		✓				♢
5	F-SAVGS			✓			♢ ∇
6	FE-SAVGS				✓		∇ □
#	PID-SAVGS					✓	□
7	FE-PID-SAVGS				✓	✓	□

- #: these control scheme were proposed in the previous SAVGS studies [10] and [12].
- ♢: indicates that these control schemes will be compared in Chapter 5.
- ∇: indicates that these control schemes will be compared in Chapter 6.
- □: indicates that these control schemes will be compared in Chapter 7.
- ✓: four quater-car $\mathcal{H}_\infty$ controllers are equipped at four wheels of the full-car model.

3.5 Conclusions

In this chapter, the linear and nonlinear multi-body models used in this thesis have been presented. The software packages used to build the multi-body models and validate the vehicle's system performance are introduced. The multi-body quarter- and full- models are high fidelity models that are representative of a high-performance sports car. Linearised vehicle models can be generated automatically by Autosim. In addition, quarter- and full- vehicle hand-derived models are another approach to derive the linearised models of the SAVGS in MATLAB. A summary of the main vehicle and the SAVGS parameters are also provided. Furthermore, the modelling of road profiles used to analyse the vehicle's dynamic responses is presented. Finally, the closed-loop control schemes in this thesis are briefly described. In the subsequent chapters, these closed-loop $\mathcal{H}_\infty$ -controlled schemes will be developed in detail.

Chapter 4

$\mathcal{H}_\infty$ CONTROL SYNTHESIS FOR QUARTER-CAR COMFORT AND ROAD HOLDING ENHANCEMENT

The previous chapters described the $\mathcal{H}_\infty$ synthesis and SAVGS modelling. In this chapter, the aim is to design a linear $\mathcal{H}_\infty$ scheme to control a nonlinear quarter car model with SAVGS, representative of one corner of a high performance car with a double wishbone suspension arrangement. More precisely, the objectives are to: 1) design control for vertical acceleration, tyre deflection and suspension travel using a linearised quarter car model; and 2) investigate the performance of the closed loop system by implementing the $\mathcal{H}_\infty$ controller to the nonlinear quarter car. This will result in a multi-objective $\mathcal{H}_\infty$ control strategy, which can provide optimal road disturbance and external vertical force rejection to improve passenger ride comfort and road holding. At the same time, the operating constraints of the suspension should be satisfied for a range of road and external vertical force disturbances.

The successful application of the SAVGS $\mathcal{H}_\infty$ control scheme in this chapter will provide a solid foundation for understanding the effectiveness and potential of $\mathcal{H}_\infty$ synthesis on the SAVGS. Furthermore, it would be an important step forward for full-vehicle control if the quarter-car SAVGS $\mathcal{H}_\infty$ control can provide promising simulation results.

This chapter is organised as follows: Section 4.1 describes the model of the SAVGS quarter car; Section 4.2 provides the control schematic of the nonlinear simulation; Section 4.3 details the development of the SAVGS $\mathcal{H}_\infty$ -controlled scheme based on the quarter-car linearised model; in Section 4.4, the simulation results of the passive and SAVGS $\mathcal{H}_\infty$ -controlled nonlinear quarter car are conducted and compared, for a range of road and external force disturbances; a full-car nonlinear model simulation

with the proposed quarter-car controller is investigated in Section 4.4.2; and finally, the key findings from this study and the brief instructions for future work are presented in Section 4.5.

4.1 Quarter-car multi-body model (QC)

The quarter car model used in this chapter extends the conventional quarter car to include a double wishbone arrangement, as has been described in Fig. 3.3 in Chapter 3.

4.2 General Control Scheme

Depending on the use of the quarter-car model the SAVGS part is added in one of two ways: (a) for linear analysis and control design, instead of using the torque T_{SAVGS} as described above, the velocity of the single-link is used as an input and controlled directly, and no actuator dynamics are employed; this allows to reduce the complexity of the $\mathcal{H}_\infty$ control design prior to installing it on the full nonlinear model, and (b) for nonlinear simulation purposes the actuator dynamics are included with the plant and the actuator torque T_{SAVGS} is generated by an inner control loop that aims to reduce the error between a single-link angle input reference value and the actual single-link angle; the angle reference is calculated by integrating the output of the designed $\mathcal{H}_\infty$ controller.

The control schematic of the nonlinear simulation is shown in Fig. 4.1. There are two control loops involved, as introduced above. Firstly, K_{slp} is the position control scheme for the angle of the single-link. It makes use of saturation functions to ensure that operating and design constraints of the real system, such as the maximum single-link rotation angle and the maximum actuator torque, speed and power, are respected under any circumstances. This controller has been presented in [9] and the relevant schematic is shown here in Fig. 4.2. Secondly, K_∞ is the $\mathcal{H}_\infty$ control scheme to be developed in this work which aims to reduce the body acceleration, tyre deflection and suspension deflection (defined as the vertical component of the distance between the centres of mass of the sprung and unsprung masses) under external road disturbance forcing. The design procedure will be explained in detail in the next section. θ^*_{ref} is the reference rotational angle of the single-link, which is generated by the integration of the output from the K_∞ block, and is subsequently tracked precisely by the inner

position control loop. The saturation block in front of θ^*_{ref} is needed to ensure that the rotation of the single-link remains between chosen design boundaries ($0° - 180°$).

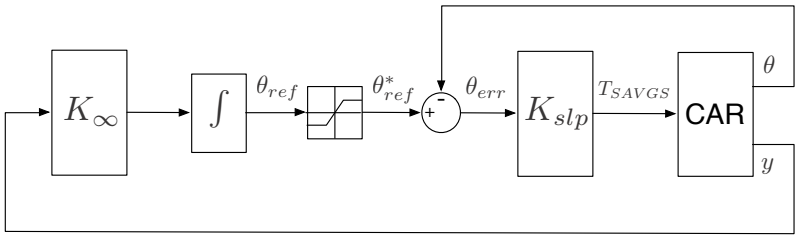

Fig. 4.1 Nonlinear control scheme (QA-SAVGS) for the quarter-car model.

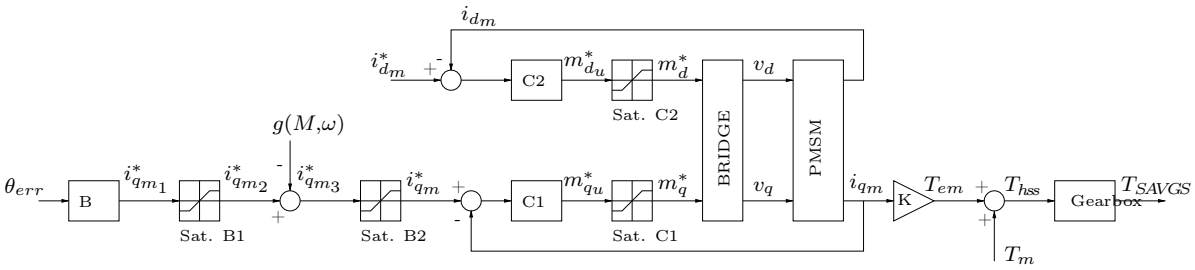

Fig. 4.2 Details of position control, K_{slp}, of the single-link shown in Fig. 4.1. Starting from the position error signal, controllers B, C1 and C2 are combined with several dynamic saturation blocks and feedback loops in order to generate suitable voltage commands for the bridge converter that drives the PMSM actuator. The proposed scheme provides good position tracking performance and ensures that none of the physical or design limitations of the actuator are violated under any circumstances. Further details can be found in [10].

The multibody modelling code AutoSim [6] is used to generate the overall quarter-car model. The control design is performed in Matlab and tested by simulation in the Simulink environment.

The symbols of the SAVGS model used in this chapter are listed in Table 4.1:

4.3 $\mathcal{H}_\infty$ control synthesis framework

4.3.1 Quarter-car Autosim linearized model (QCL)

For the purposes of control design the quarter-car equations of motion are linearised around a trim state of 90° single-link angle. The equilibrium state and equilibrium actuator torque are found by running a nonlinear simulation. Under the selected trim condition, the sensitivity of the suspension force increment to a single-link rotation is

Table 4.1 Quarter-car SAVGS symbols

Symbols	Physical Meanings	Unit
$\ddot{z}_s$	the sprung mass acceleration	m/s^2
Δl_t	the tyre deflection	cm
Δl_s	the suspension deflection	cm
z_r	the vertical road displacement	cm
$\dot{\theta}_{SL}$	the single-link reference velocity	rad/s
θ_{SL}	the single-link actual angle	deg
$\Delta\theta_{SL}$	the single-link angle	deg
T_{SAVGS}	the actuation torque	$N.m$
F_{exf}	the external vertical force	N

maximised and therefore, the controllability of the system is maximised. To investigate the effect of the nominal single-link angle to the SAVGS control ability, the rear left quarter-car frequency responses from the single-link speed to the sprung mass acceleration, dynamic suspension and tyre deflection as a function of the single-link angle $\Delta\theta_{\text{SL}}$ are provided in Fig. 4.3. It can be observed that the trim state when $\Delta\theta_{\text{SL}} = 90°$ offers the maximum control gains and the gains are able to maintain their level around this range, which implies that designing a controller at this trim state can offer the best control performance as well as be effective under a wide range of operating conditions.

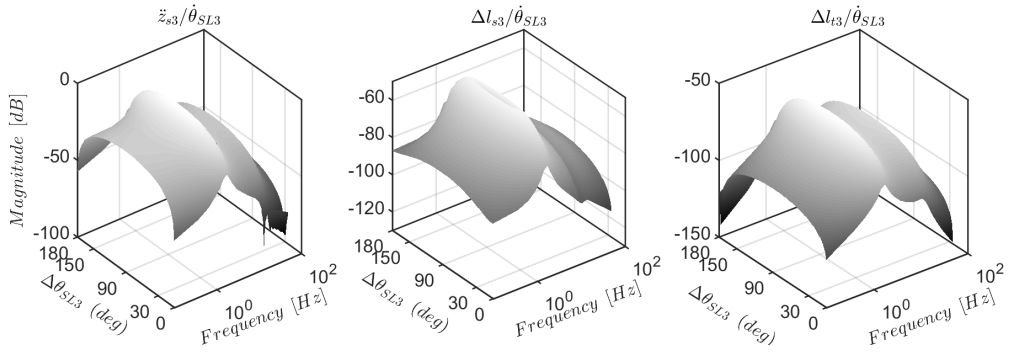

Fig. 4.3 Bode plots of the quarter-car model from single-link angle and nominal single-link offset angle $\Delta\theta_{SL}^{(ne)}$ to (a) sprung mass acceleration, (b) suspension deflection, and (c) tyre deflection.

The linearized Autosim quarter-car model (QCL) can be generated automatically in Autosim based on the nonlinear quarter-car SAVGS multi-body model (QC) at a trim point.

In the multi-body system, the d and f are vectors of the generalised coordinates and speeds, with the state variables defined as, $x = \begin{bmatrix} d \\ f \end{bmatrix}$, then the linearised state-space equation of quarter-car model at $\Delta\theta_{\mathrm{SL}} = 90^\circ$ is given as follows:

$$\dot{x} = Ax + Bu \tag{4.1}$$

$$y = Cx + Du \tag{4.2}$$

And

$$A = \begin{bmatrix} -1.227 & 10.54 & 0 & 0 \\ -10.54 & -1.227 & 0 & 0 \\ 0 & 0 & -14.91 & 74.28 \\ 0 & 0 & -74.28 & -14.91 \end{bmatrix}$$

$$B = \begin{bmatrix} -9.104 & -0.001107 & 0.1716 \\ -46.1 & 0.0008234 & 0.8578 \\ 35.47 & -0.0009173 & 2.434 \\ 324.4 & 0.003702 & 0.5751 \end{bmatrix}$$

$$C = \begin{bmatrix} 0.0005323 & -0.003532 & 0.0006099 & 0.002529 \\ 0.3827 & -2.429 & 0.5959 & -0.1897 \\ 0.002177 & 0.01821 & 0.0005254 & 0.002592 \end{bmatrix}$$

$$D = \begin{bmatrix} 0 & 0 & 0 \\ 0.05637 & 0.002535 & -0.06168 \\ 0 & 0 & 0 \end{bmatrix}$$

The inputs and outputs of the plant are considered according to the multiple control objectives:

- Plant inputs $u = [u_1\ u_2\ u_3]^T$ are chosen as the rate of change of the road height (also known as road irregularities), the external vertical force (represents the load transfer during acceleration in both longitudinal and lateral directions) acting on the sprung mass and the angular speed of the single-link (also known as the sinlge-link velocity).

- Plant outputs $y = [y_1 \ y_2 \ y_3]^T$ are chosen as dynamic tyre deflection, vertical acceleration of the sprung mass and suspension deflection for vehicle road holding and ride comfort enhancement.

4.3.2 Frequency response

In this chapter, the acceleration, suspension deflection and tire deflection are the control objectives of interest and their attenuation will be used to judge the effectiveness of the performance of the closed-loop suspension system. However, many research papers [74, 95] indicated that, based on the analysis from a two-degree-of-freedom model, there are some inherent performance limitations on the behaviour of suspension systems, whether they be active or passive. By analysing the frequency response functions of the quarter-car model, some 'invariant points' can be found at specified frequencies that depend only upon the tyre stiffness k_t, sprung mass m_s, and unsprung mass m_u. The invariant points of an active suspension indicate that at specified forcing frequencies, active parameters have no effect at all on certain important response, even the most aggressive control strategies are not omnipotent. The basic equations and main conclusions of the invariant points can be found in [22].

The input to output frequency responses of the plant P at the trim state where $\Delta\theta_{\mathrm{SL}} = 90^\circ$ are shown in Fig. 4.4, to help identify the principles of the selection of weighing functions in the $\mathcal{H}_\infty$ controller synthesis and to learn more about the quarter-car model by analysing its invariant points and the trade-off constraints.

From the frequency response plot above, the following points can be observed:

1. **Invariant points and their influence:** The transfer functions of these control objectives and their invariant points can be obtained through the following Laplace transformation ($s = j\omega$) of Equations (4.3) to (4.5) [22]:

   (a) *Acceleration transfer function ($H_A(j\omega_{inv1})$) and the invariant point (ω_{inv1}):*

   $$H_A(j\omega_{inv1}) \ = \ j\frac{\sqrt{m_u k_t}}{m_s} \ \ and \ \ \omega_{inv1} = \sqrt{\frac{k_t}{m_u}} \tag{4.3}$$

   (b) *Suspension deflection transfer function ($H_{SD}(j\omega_{inv2})$) and the invariant point (ω_{inv2}):*

   $$H_{SD}(j\omega_{inv2}) \ = \ j\frac{m_s + m_u}{m_u}\frac{\sqrt{m_s + m_u}}{k_t} \ \ and \ \ \omega_{inv2} = \sqrt{\frac{k_t}{m_s + m_u}} \tag{4.4}$$

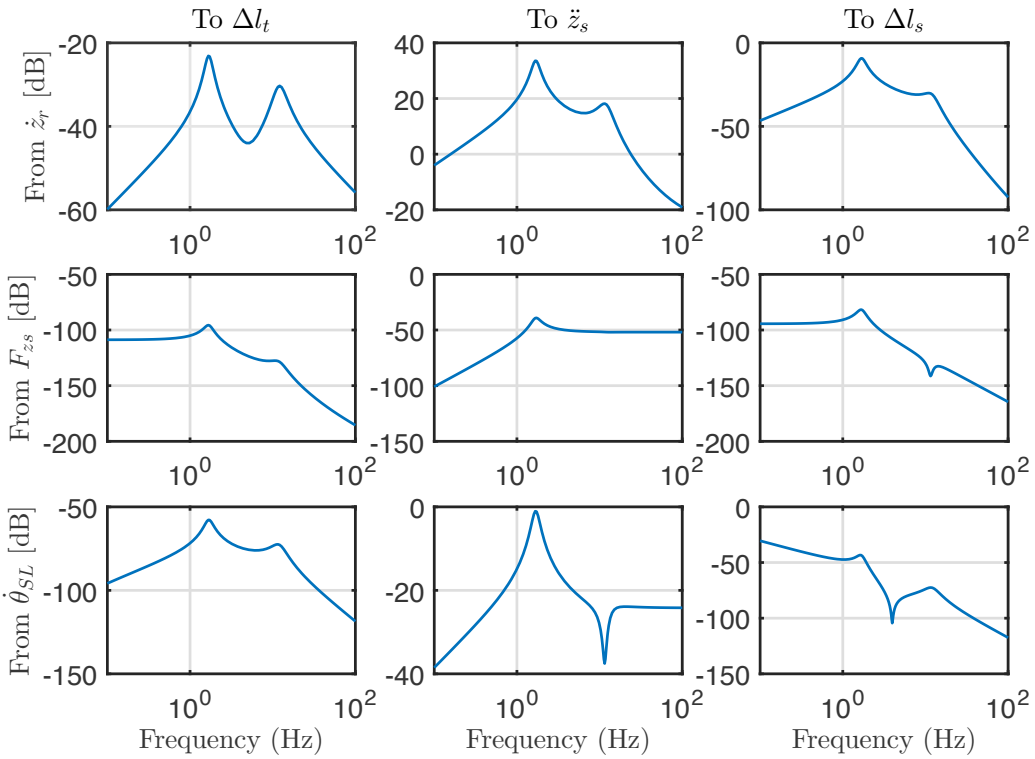

Fig. 4.4 Magnitude Bode plots of the quarter-car vehicle plant. From vertical road speed (top row) , external vertical force acting on the sprung mass (second row) and single-link rotational velocity (third row) to dynamic tyre deflection (left column), sprung mass acceleration (middle column) and dynamic suspension deflection (right column).

(c) *Tyre deflection transfer function ($H_{TD}(j\omega_{inv3})$) and the invariant point (ω_{inv3}):*

$$H_{TD}(j\omega_{inv3}) \;=\; 0 \;\; and \;\; \omega_{inv3} = 0 \tag{4.5}$$

where $m_s = 313\,kg$ and $m_u = 53\,kg$ represent the sprung and unsprung mass of the quarter-car vehicle body. The vertical stiffness of the tire is represented by the spring $k_t = 275000\,N/m$. For the values given above, invariant points of the acceleration and suspension deflection are at $\omega_{inv1} \approx 11.47\,Hz$ and $\omega_{inv2} \approx 4.36\,Hz$. From Equation (4.5), it can be seen that when $\omega > 0$ the tyre deflection transfer function does not process any invariant point.

In Fig. 4.4, for the case with road irregularities as input (first row), the plots are typically double-hump responses. The first peak is the sprung mass resonance frequency and the later peak is the unsprung mass resonance frequency. It can be

observed that the unsprung mass resonance frequency is approximately $11.5\,Hz$ which is close to the acceleration invariant point ω_{inv1}. Therefore, regardless of the values of the active suspension control law $\dot{\theta}_{SL}$ and the suspension stiffness k_s chosen, the sprung mass acceleration will not be changed at the unsprung mass resonance frequency. The suspension deflection invariant point ω_{inv2} also indicates that at about $4.36\,Hz$ the suspension deflection cannot be improved upon, irrespective of what active suspension forces are introduced.

2. **The trade-offs between the control objectives using invariant points:** $\mathcal{H}_\infty$ control aims to develop an optimal trade-off solution between the sprung mass acceleration, suspension deflection and tyre deflection. The relationship and constraints between the three transfer function and the invariant points should be analysed. The following asymptotic properties can be found [22]:

   (a) *Trade-off between ride comfort and road holding:* In [22], it is shown that changing the ride comfort transfer function ($\delta H_A(j\omega)$) will affect the change of the tyre deflection transfer function ($\delta H_{TD}(j\omega)$). The relation equation can be written as:

$$\delta H_{TD} = -\epsilon H_{TD}(j\omega) + \frac{\epsilon}{\alpha_1(\omega)} j r_1 \omega \tag{4.6}$$

   where

$$\alpha_1(\omega) = r_1(\omega^2 - \omega_{inv1}^2)\ ,\ r_1 = \frac{m_u}{m_s} \quad and \quad \epsilon = -\frac{\delta H_A(j\omega)}{H_A(j\omega)}$$

   In Equation (4.6), when the frequency in lower than ω_{inv1} ($\omega < 11.47\,\text{Hz}$), the second term is negligible and the first term will dominate the equation. Therefore, at a low frequency range, tyre deflection and sprung mass acceleration can be improved simultaneously.

   On the other hand, at high frequencies close to ω_{inv1} (acceleration is unchangeable at ω_{inv1}), the second term in Equation (4.6) will become extremely large. Any improvement in sprung mass acceleration will result in a dramatic deterioration in tyre deflection.

(b) *Trade-off between ride comfort and suspension deflection:* The relationship between the change in the acceleration transfer function ($\delta H_A(j\omega)$) and the suspension deflection transfer ($\delta H_{SD}(j\omega)$) function can be written as:

$$\delta H_{SD}(j\omega) = -\epsilon H_{SD}(j\omega) - \epsilon(\frac{m_s}{m_u} + 1)\frac{j\omega^2_{inv2}}{\omega(\omega^2 - \omega^2_{inv1})} \tag{4.7}$$

In Equation (4.7), when ω is close to 0 and $11.47\,Hz$ (ω_{inv1}) where the second term dominates, the acceleration can only be improved by sacrificing the performance in suspension deflection. At the other frequencies, both the sprung mass acceleration and suspension deflection can be improved simultaneously.

3. Consider the frequency response for the case with single-link velocity $\dot{\theta}_{SL}$ (third row in Fig.4.4) as the active suspension control law of this particular control problem.

   (a) The sprung mass acceleration and dynamic tyre deflection bode plots at low frequencies are with + 20 dB/decade, while the suspension deflection is drop off with -20 dB/decade. Hence, very little ride comfort and road holding performance improvement can be obtained at low frequencies. At low frequencies, it is best to concentrate on suspension deflection in terms of providing better attitude control.

   (b) It can be seen that the second and third frequency response plots at the third row in Fig. 4.4 have a zero at the sprung mass acceleration and suspension deflection invariant points, which are $\omega_{inv2} = 11.47\,Hz$ and $\omega_{inv1} = 4.36\,Hz$. When close to these invariant points, the ride comfort and suspension deflection of SAVGS cannot be improved compared with the passive case regardless of the value of the single-link velocity $\dot{\theta}_{SL}$.

   (c) The suspension deflection and tyre deflection transfer functions roll off at -40dB/decade at high frequencies, which indicates that it is very hard to improve the road holding properties at high frequencies. The sprung mass transfer function has a constant high frequency asymptote ($\omega > \omega_{inv1}$) that implies that ride comfort can be improved at high frequency range. However, as argued in Section 3.3 the very high frequencies are not considered in this project since they are outside the human sensitive frequency range in [ISO 2613-1:1997].

To improve ride comfort and road holding without deterioration in the suspension deflection, based on the above observations and analysis, the suggestions for the $\mathcal{H}_\infty$ control are:

1. Dynamic weighting functions should be selected to reduce the sprung mass acceleration at the sprung mass resonance frequency, which is approximately 2Hz for the vehicle under study.

2. Significant reduction should also be achieved in suspension deflection and tyre deflection at the sprung mass resonance frequency.

3. Avoid any deterioration in all three control objectives at the unsprung mass resonance frequency.

4. Avoid any control effort at very low and high frequencies.

4.3.3 Controller design

The design procedure involves the use of dynamic weighting functions to shape the plant transfer functions to meet the required design specifications. In the controller synthesis stage the plant transfer functions in Equation (4.2) are replaced with their frequency weighted versions. Figure 5.4 shows the control scheme structure and the weighting functions used.

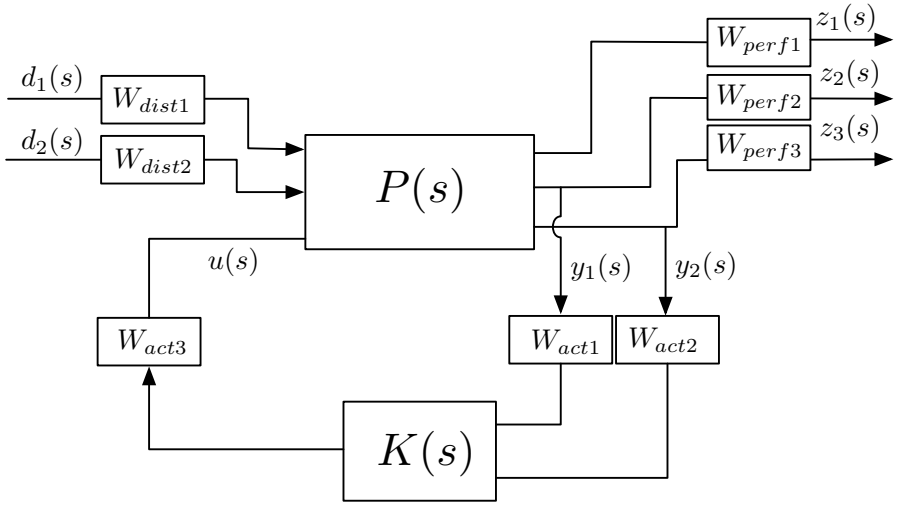

Fig. 4.5 New $\mathcal{H}_\infty$ control scheme for disturbance rejection showing weighting functions, W_{perf1}, W_{perf2}, W_{perf3}, W_{act1}, W_{act2}, W_{act3}, W_{dist1}, W_{dist2}.

In the figure, $d_1(s)$ and $d_2(s)$ represent the vertical road disturbance and vertical external force disturbance; $y_1(s)$ and $y_2(s)$ are the vertical body acceleration and suspension deflection used for feedback control; $u(s)$ is the controlled signal representative of the single-link velocity; and $z = [z_1\ z_2\ z_3]^T$ is the new output vector corresponding to tyre deflection, body acceleration, and suspension deflection. W_{perf1} , W_{perf2} and W_{perf3} are defined as low pass filters to penalise the appropriate low frequency ranges of tyre deflection, sprung mass acceleration and suspension deflection, corresponding to road holding, passenger comfort and rattle space respectively. W_{act1}, W_{act2} and W_{act3} are used for 'loop shaping' and are finally absorbed into the controller such that the final controller is found by post-multiplying. This means that the frequency properties of these two weights will be inherited by the controller. W_{act1} and W_{act2} are chosen as bandpass filters to concentrate the controller action in the frequency range of interest without expending much actuator power outside this range, while W_{act3} is a given constant value to keep the controller complexity low. Further design issues are the weight of the road disturbance input and external vertical force input, W_{dist1} and W_{dist2}, where it was found from trials that a non-dynamic function is adequate.

The final weighting functions are given as follows:

$$W_{perf1} = \frac{245(0.001s+1)}{s+314},$$

$$W_{perf2} = \frac{351.86(0.001s+1)}{s+628},$$

$$W_{perf3} = \frac{351.86(0.001s+1)}{s+314},$$

$$W_{act1} = \frac{3\cdot 10^5 s}{(s+1200)(s+1200)(s+180)},$$

$$W_{act2} = \frac{2\cdot 10^5 s}{(s+1200)(s+1200)(s+180)},$$

$$W_{act3} = 0.01, \quad W_{dist1} = 0.7, \quad W_{dist2} = 0.3.$$

The optimisation problem is defined in Matlab and the $\mathcal{H}_\infty$ problem is solved using the function `hinfsyn`. The controller that results has 16 states. Some iteration was involved in selecting the final weights by considering the performance of the lin-

ear closed-loop system and also by taking into account the resulting stability of the nonlinear closed loop system as found by simulation in the next section.

In order to analyse the frequency response of the linearised closed-loop SAVGS $\mathcal{H}_\infty$ -controlled system and the linearised open-loop vehicle system and to investigate the controller attenuation performance in the frequency domain, singular value plots are required. Similar to the Bode magnitude plot for single-input and single-out (SISO) system, singular values plots are the extension of the Bode magnitude response to analyse the robustness of MIMO systems. Define the augmented Autosim passive linearised quarter-car system with frequency weights as P_q and the augmented Autosim closed-loop $\mathcal{H}_\infty$ controlled quarter-car system as $F(P,K)$. Both systems are with 2 inputs (i.e. road height rate of change and external load transfer) and 3 outputs (i.e. tyre deflection, vertical body acceleration and suspension deflection). The input signals $u(t)$ with unit length is a complex exponential of the form $u(t) = \widetilde{u}e^{j\omega t}$, with $\widetilde{u} \in \mathbb{C}^2$. The output signals $y(t)$ is $y(t) = \widetilde{y}e^{j\omega t}$, with $\widetilde{y} \in \mathbb{C}^3$ [99].

Taking the Laplace transform of the state-space equations evaluated at $s = j\omega$:

$$\widetilde{y} = P_q(j\omega)\widetilde{u}$$
$$\widetilde{y} = F(P,K)(j\omega)\widetilde{u}$$

It is noted that the system state-space equations are changing with frequency ω. At a given frequency ω, the singular value decompositions of P_q and $F(P,K)$ are given by:

$$P_q = U_p(j\omega)\Sigma_p(j\omega)V_p^H(j\omega),$$
$$F(P,K) = U_f(j\omega)\Sigma_f(j\omega)V_f^H(j\omega)$$

where square matrices U_p and U_f with size 2×2 are the left singular input vectors, square matrices V_p^H and V_f^H with size 3×3 are the right singular output vectors, and Σ_p and Σ_f is a 2×3 matrix whose main diagonal is composed of the positive singular values of the systems. Singular value plots contain valuable information about the properties of the system. In particular, they represent the gains of the system and show the changing of the gains with frequency. In Figure, 4.6, the closed-loop ($F(P,K)$) and open-loop P_q systems are compared. It is observed that, in the frequency ranges of interest (2-8 Hz), the $\mathcal{H}_\infty$ controller proposed for the closed-loop system augmented with all the frequency weights in this chapter achieves significant gain reductions. The nonlinear simulation results and comparison will be shown in next section.

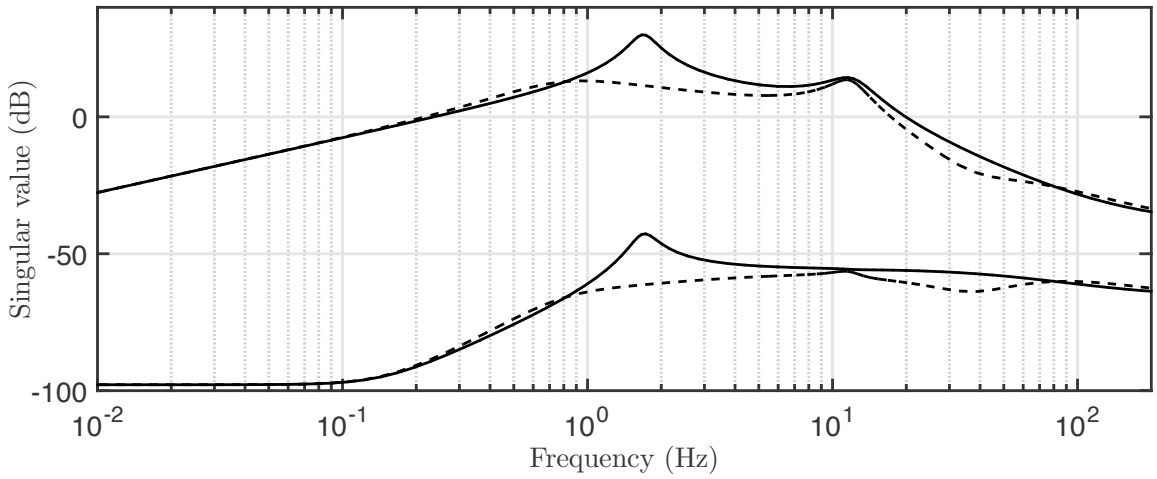

Fig. 4.6 Singular value plots for the closed-loop (dotted) and open-loop (solid) systems with all the frequency weights.

The frequency response of the resulting controller is shown in Fig. 4.7. As desired, the controller has a 'bandpass' nature and the transfer function from vertical body acceleration and suspension deflection to single-link velocity are rolling off at approximately 30 Hz.

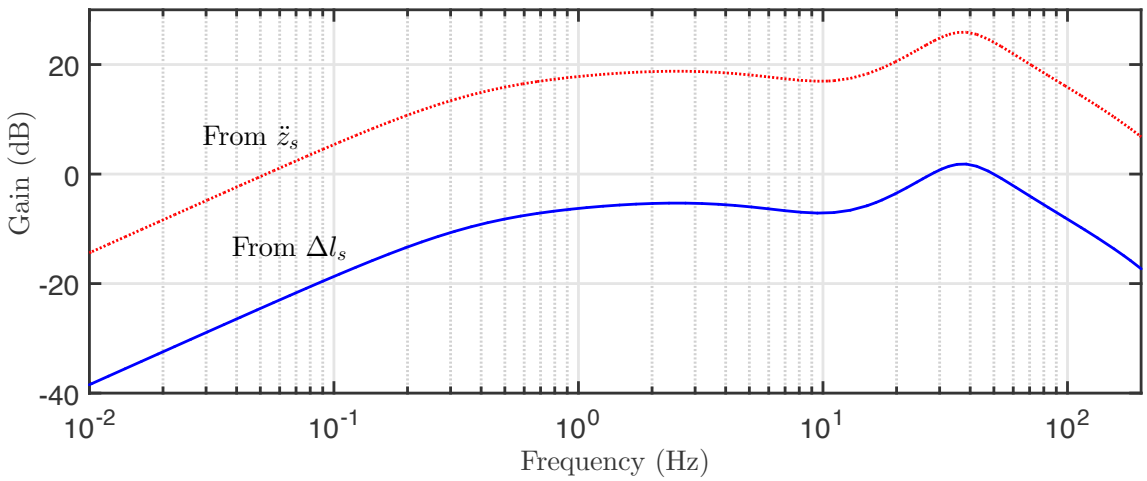

Fig. 4.7 Frequency response of the designed $\mathcal{H}_\infty$ controller.

4.4 Simulation results

4.4.1 Quarter-car simulation results

In this section, the performance of the proposed $\mathcal{H}_\infty$ controller is tested by simulation, using the configuration shown in Fig. 4.1. The appropriate interaction of the $\mathcal{H}_\infty$ controller and the inner position control loop is critically important for the success of the overall scheme. This generally means that the $\mathcal{H}_\infty$ controller is required to be designed with its frequency response gain not as large as to saturate too heavily the response of the inner loop.

A controlled nonlinear quarter-car model (denoted as QA-SAVGS) associated with a high performance sports car is used in the simulation. The selected actuator comprises one Kollmorgen AKM33H, which is a Permanent Magnet Synchronous Motor (PMSM), and one Danaher UT075-40, which is an epicyclic gearbox. The main vehicle and the SAVGS parameters for the quarter car control scheme can be found in Tables 3.5 and 3.6 in Chapter 3. The quarter car is run over a road surface with a) sinusoidal undulations ($0 - 30\,\text{Hz}$); b) a random road profile (ISO 8608:1995 [85]); c) smoothed bump; and d) an external vertical load transfer, to cover a wide range of operating conditions. The offset angle of the single-link has been set at 90° to correspond to the control design strategy in the previous section. For comparison purposes, the results for the quarter-car equiped with purely passive suspension (denoted as Q-Passive) are also obtained. Since the control objective is to improve ride comfort and road holding, the outputs selected and investigated in this section focus on body vertical acceleration, tyre deflection, and suspension travel.

Sinusoidal road forcing

Fig. 4.8 presents the time response results for the body acceleration, tyre deflection and suspension travel of the quarter-car in response to a sinusoidal road disturbance of 2 Hz, both for the passive (Q-Passive) and active suspension configuration (QA-SAVGS). The superiority of the SAVGS in reducing the amplitude of all output variables, as compared to the passive suspension, and leading to improved ride comfort and road holding is demonstrated. In particular, a reduction of approximately 65% in the amplitude of the body acceleration and tyre deflection, and a smaller reduction in the amplitude of the suspension travel, are observed. The figure also shows the single-link angle time history that achieves the SAVGS performance mentioned above. This angle needs to change between ±25° of its nominal offset value. Other simulations for

different frequencies from 1 Hz to 10 Hz have also been carried out demonstrate the positive performance of the SAVGS and $\mathcal{H}_\infty$ control scheme. Therefore the expectation is that the performance will be similarly improved in the case of more general road disturbances. This is investigated below.

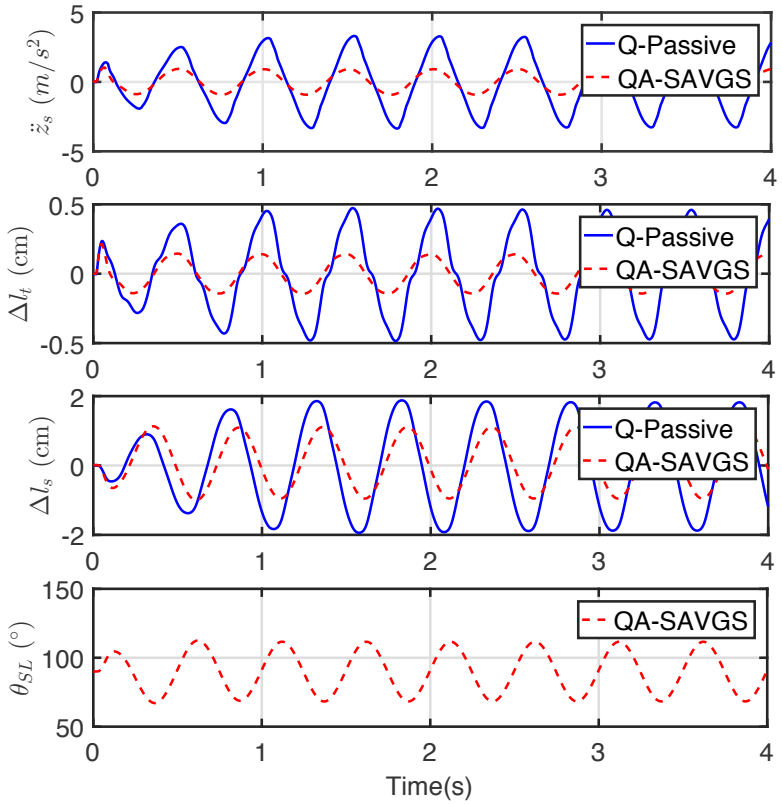

Fig. 4.8 Quarter-car time responses under 2 Hz sinusoidal roadway displacement with amplitude of 0.01 m, for the passive suspension and SAVGS $\mathcal{H}_\infty$-controlled configurations.

Random road forcing

The generation of a random road profile to be studied here is based on the ISO 8608:1995 standard [85]. The random road profile used in this section is identical to the expression of the first approach in Section 3.3.3 in Chapter 3. A typical highway road surface is generated by this expression in Simulink, with $V = 30.6\,\mathrm{m/s}$, $\alpha = 0.127\,\mathrm{rad\,s/m^2}$ and $\sigma = 7.5 \times 10^{-3}\,\mathrm{m}$. However, this road profile does not consider the geometry of the tyre.

Hence, a rigid ring tyre model with a fixed radius of 0.341 m is considered and a corresponding geometry filter is implemented to create a filtered version of the original road profile. Fig. 4.9 depicts the final filtered random disturbance to be used as the road input.

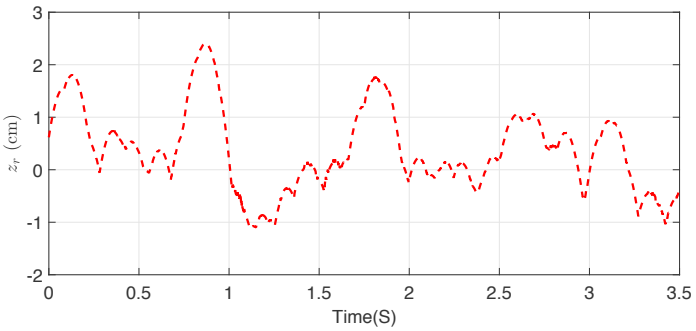

Fig. 4.9 Random road profile for 30.6 m/s forward vehicle speed.

Nonlinear simulation results examining the performance of the quarter-car with SAVGS undergoing the random road disturbance are presented in Fig. 4.10.

It can be seen in the first two plots that the body vertical acceleration and tyre deflection have reduced peak values once the SAVGS with $\mathcal{H}_\infty$ control scheme is employed, as compared to the passive suspension case. This indicates the improved comfort and road holding properties of the active scheme. Also, the third plot in Fig. 4.10 illustrates that the maximum and minimum values of the suspension travel are not negatively affected by utilising the active control scheme, while the final plot shows the corresponding usage of the single-link angle in the SAVGS.

The nonlinear quarter-car, regarding both passive and active configuration, PSDs are presented in Fig. 4.11 to examine and compare the frequency responses of the variables of interest. The frequency responses for the sprung-mass vertical acceleration, tyre deflection and suspension travel, for the passive and SAVGS cases, are calculated and presented in Fig. 4.11.

It can be seen in all three frequency responses associated with the passive system that the vertical dynamics of the vehicle exhibit the typical behaviour for this vehicle category, the dominant effect is the existence of two resonance peaks at approximately 2 Hz and 10 Hz, corresponding to sprung and unsprung mass resonances, respectively. The former peak falls in the range of frequencies where the human body is most sensitive to vertical acceleration (ISO 2361-1:1997 [82]). It is precisely in that frequency range that the $\mathcal{H}_\infty$ controller acts to reduce the vertical acceleration gain, as shown in Fig. 4.11 (a), to improve the ride comfort. The achieved reduction in acceleration gain

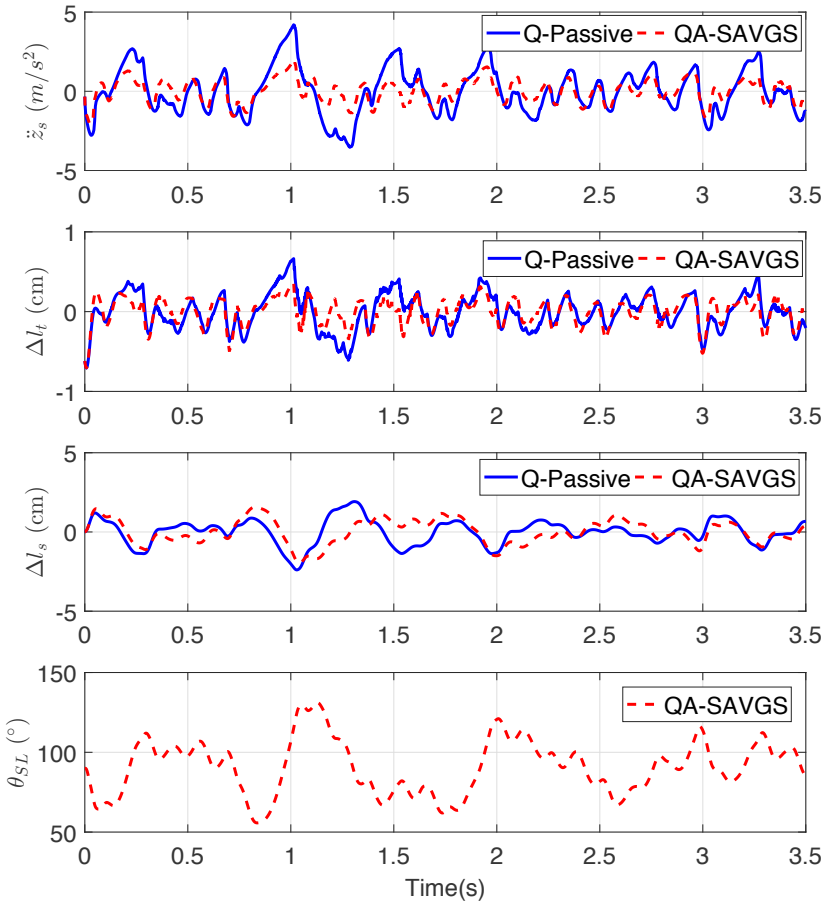

Fig. 4.10 Quarter-car time responses for the random road excitation in Fig. 4.9, for the passive suspension and SAVGS $\mathcal{H}_\infty$-controlled configurations. Results obtained for the passive suspension and SAVGS $\mathcal{H}_\infty$-controlled configurations

is up to approximately 8 dB at the resonance frequency near 2 Hz. Fig. 4.11 (b) shows that road holding is also improved since the SAVGS achieves a reduction in the tyre deflection gain at low frequencies ($1-7$ Hz) by up to 8 dB. This allows the tyre to run over the road with reduced variation in its normal load and therefore an improved grip. The frequency response presented in Fig. 4.11 (c) shows that overall, suspension travel is not adversely impacted while the controller is addressing the other two objectives. Its gain, as compared to the passive case, is even improved by up to 3 dB in the range of $1.7-4.4$ Hz, while at frequencies lower than 1.7 Hz its gain deteriorates. These results can be explained by Equation (4.7), which shows that in the frequency ω close to 0 Hz, there is a trade off between sprung mass acceleration and suspension

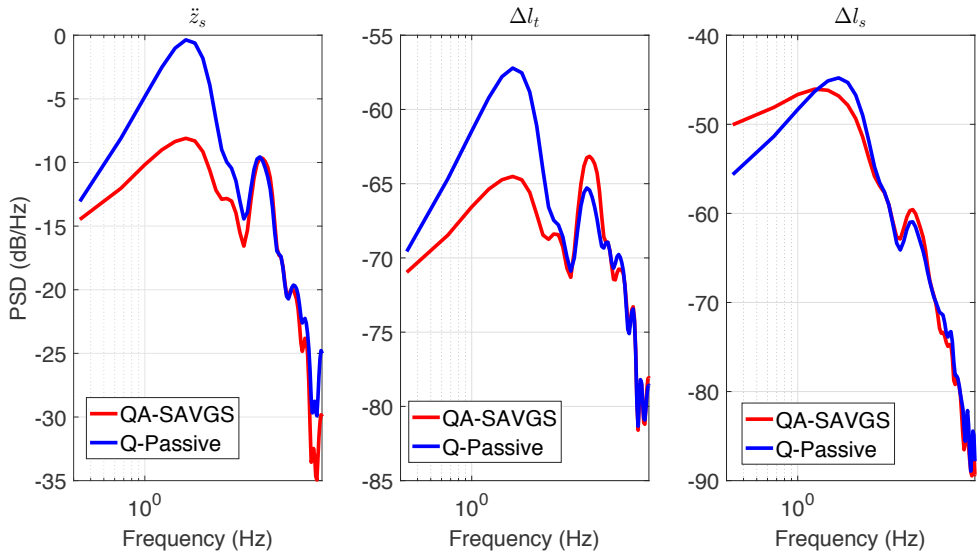

Fig. 4.11 Bode magnitude plots for the nonlinear quarter car model with random road disturbance inputs to the outputs: a) body vertical acceleration, b) tyre deflection and c) suspension travel.

deflection. Therefore, there is an amplification in suspension deflection to achieve a gain reduction in sprung mass acceleration at low frequencies for improvement in road comfort. However the gains involved are much smaller than at higher frequencies and the overall performance will not be impacted to a great extent.

The time responses are now analysed in more detail by making use of two standard fitness functions, the ride comfort and road holding indexes.

Ride comfort index (RCI) The ride comfort index is the rms bounce acceleration according to the ISO 2631-1:1997 standard [82]:

$$\mathrm{RCI} = \left[\frac{1}{T}\int_0^T a^2(t)\,\mathrm{d}t\right]^{\frac{1}{2}} \tag{4.8}$$

in which T is the vibration duration time and a is the body vertical acceleration.

Table 4.2 presents results for the RCI and a further fitness function, the maximum vertical acceleration, for the responses in Fig. 4.10. The calculated RCI for the quarter-car with SAVGS and $\mathcal{H}_\infty$ control is 49.7% less than for the passive system, and the maximum acceleration is similarly reduced by 50.7%. These results imply the improvement in the ride comfort due to the implementation of SAVGS with the $\mathcal{H}_\infty$ control feedback loop.

Table 4.2 Ride comfort analysis (SI units)

Fitness function	Passive	SAVGS	Improvement
RCI	1.4330	0.7213	49.7%
max($\|a\|$)	4.2013	2.0718	50.7%

Road holding index (RHI) The performance index for road holding is chosen to be the rms value of the tyre deflection z_{def} ($= z_t - z_r$) given by [141]:

$$\text{RHI} = \left[\frac{1}{T}\int_0^T z_{def}^2(t)\,\mathrm{d}t\right]^{\frac{1}{2}} \tag{4.9}$$

Table 4.3 presents results for the RHI and a further fitness function, the maximum tyre deflection, for the tyre deflection responses in Fig. 4.10. The RHI for the quarter-car with SAVGS and $\mathcal{H}_\infty$ control is reduced by 27.3% and the maximum tyre deflection is reduced by 22.6%, as compared to the passive system. This demonstrates that the $\mathcal{H}_\infty$ controller can enhance the road holding ability of the car.

Table 4.3 Road holding analysis (SI units)

Fitness function	Passive	SAVGS	Improvement
RHI	0.0022	0.0016	27.3%
max(z_{def})-min(z_{def})	0.0137	0.0106	22.6%

Smoothed road bump

The final road perturbation used to evaluate the performance of the controller is a bump change in the road height. To avoid numerical problems and to better represent the finite geometry of the tyre, the step is smoothed and is given by the following expression in the time domain:

$$f(t) = \begin{cases} \dfrac{h_b}{2}\left(1 - \cos\left(2\pi\dfrac{V}{w_b}t\right)\right) & 0 \le t \le \dfrac{w_b}{V} \\ \\ 0 & t > \dfrac{w_b}{V} \end{cases} \tag{4.10}$$

in which h_b is the height of the bump and w_b is the longitudinal distance to rise from zero to the step height value. In the present case, a low driving speed with

$V = 5.56\,\mathrm{m/s}$ over a road step change with dimensions $h_b = 0.05\,\mathrm{m}$ and $w_b = 2\,\mathrm{m}$, is considered.

Figure 4.12 presents the simulation results of the nonlinear passive and controlled systems.

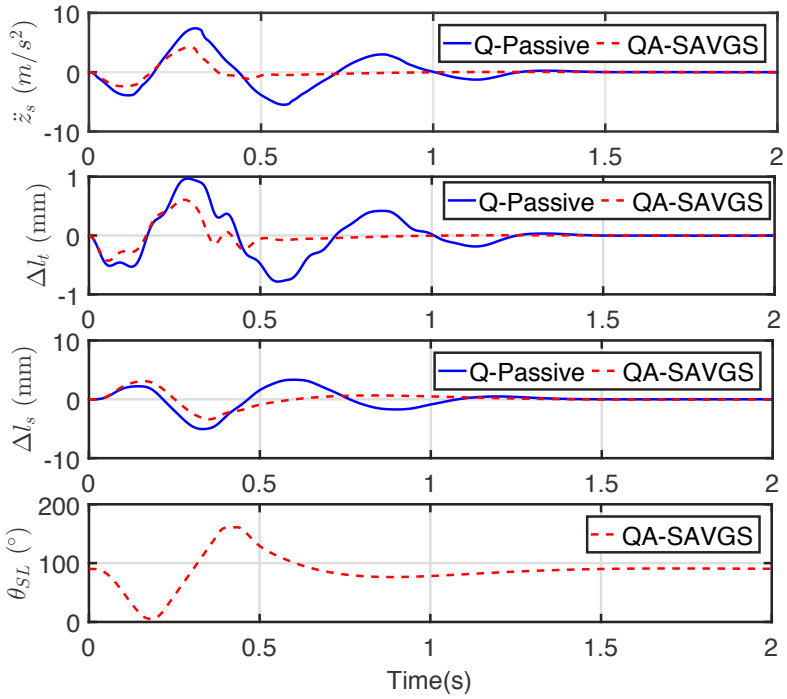

Fig. 4.12 Quarter-car time responses when running over a road bump of 0.05 m height at 5.56 m/s forward vehicle speed, for the passive suspension and SAVGS $\mathcal{H}_\infty$-controlled configurations.

Compared with the passive system, the SAVGS $\mathcal{H}_\infty$-controlled system offers a good disturbance attenuation and quick response with a short settling time; thus once again demonstrating its better comfort and road holding properties.

External vertical force

Fig. 4.13 and Fig. 4.15 assess the performance of the SAVGS $\mathcal{H}_\infty$-controlled system in the time and frequency domains respectively, when an external vertical force disturbance occurs.

Fig. 4.13 depicts the time histories for one cycle of a sinusoidal external force disturbance. The formulation of the disturbance is defined as: $F_{exf} = 2132\,sin(2\,\pi 2.8\,t)$ for $t \in [0, 1.8]\,s$. The results are as good as for the road bump as the SAVGS $\mathcal{H}_\infty$-controlled system significantly reduces the sprung mass acceleration for improved ride

comfort. The controller also produces a shorter settling time than the passive case during the impact of the vertical external force. The same trend is also observed for the tyre deflection and suspension deflection. The benefits of $\mathcal{H}_\infty$ control are evident in the time domain, and the performance of the $\mathcal{H}_\infty$ regarding external force disturbance in the frequency domain will be investigated next.

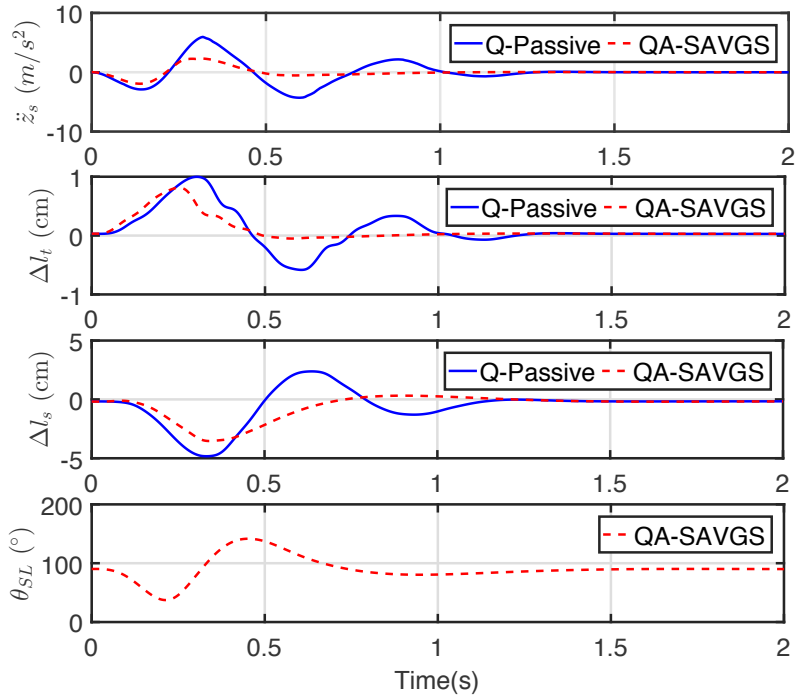

Fig. 4.13 Quarter-car time responses with a sinusoidal external force disturbance with forward velocity $5.56 m/s$, for the passive suspension and SAVGS $\mathcal{H}_\infty$-controlled configurations.

Fig. 4.15 shows the PSD plot in the frequency domain when the quarter-car operates on a random external force disturbance. The external vertical force profile is shown in Fig. 4.14.

The SAVGS $\mathcal{H}_\infty$-controlled system out-performs the passive system over most of the frequency ranges regarding the sprung mass acceleration, tyre deflection and suspension deflection. In the first plot regarding the sprung mass acceleration, the passive system exhibits one peak at chassis resonance ($\pm 2\,Hz$), and the SAVGS $\mathcal{H}_\infty$-controlled system performance is superior at this point, in that the amplitude is $8.5\,dB$ lower than the corresponding passive amplitude. The second and third plots regarding tyre and suspension deflection exhibit low pass features in the frequency domain; the presented results show that the SAVGS $\mathcal{H}_\infty$-controlled system responses are slightly better than

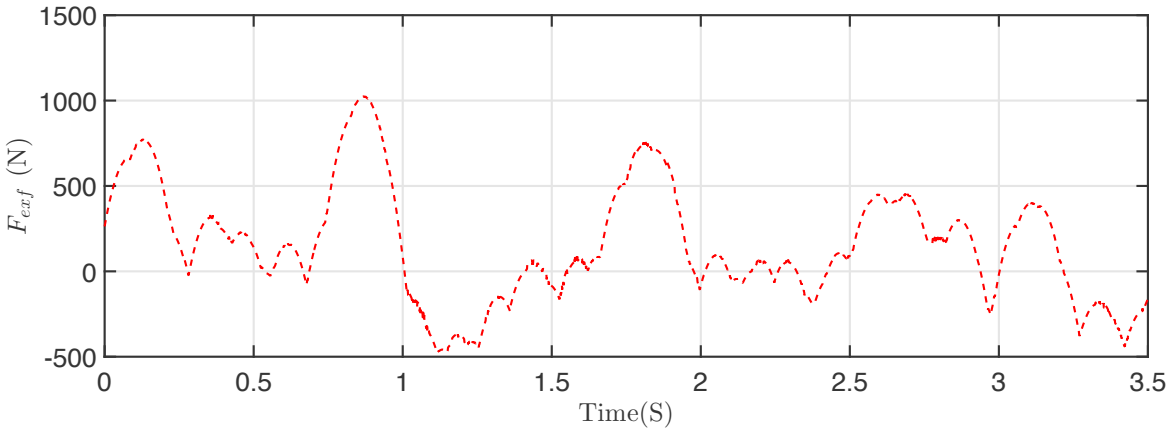

Fig. 4.14 Random external vertical force profile

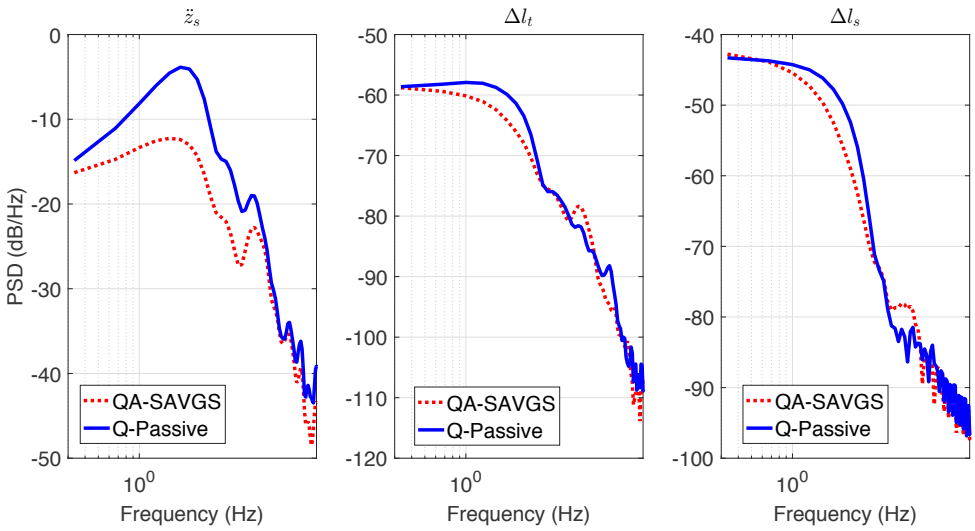

Fig. 4.15 Bode magnitude plots for the nonlinear quarter car model with random external force disturbance to the outputs: a) body vertical acceleration, b) suspension deflection and c) tyre deflection.

the passive responses. Consequently, the attenuation of the vertical external force disturbance in this case, proves the improved ride comfort and road holding properties of the SAVGS $\mathcal{H}_\infty$-controlled system.

Position controller performance

The position controller for the single-link angle presented in Section 4.2 and Fig. 4.2 is designed to maintain operational limits to protect the PMSM and its servo-drive, to avoid damage of the gearbox, and to set the desired electric power consumption by the controller. In the present control scheme, the maximum output torque (on the low

speed side of the gearbox) is limited to 200 Nm, which is the peak limit for the selected actuator to evaluate the potential of the $\mathcal{H}_\infty$ control synthesis. Thus it is possible to maintain the average power consumption below 220W for the bump and random road profile and external force input cases. The single-link rotational speed is constrained within a physical limit ± 13 rad/s, and a soft constraint of ± 1500 W is imposed on the electrical power flow from/to the PMSM.

Fig. 4.16 shows the evolution of the output torque against single-link speed for random road, random force, bump road, and bump force events studied using the simulation. It also shows the limit boundaries in actuator torque, speed and power. The figure clearly demonstrates that the operating points for all the simulations remain well within the design and operating constraints of the real system.

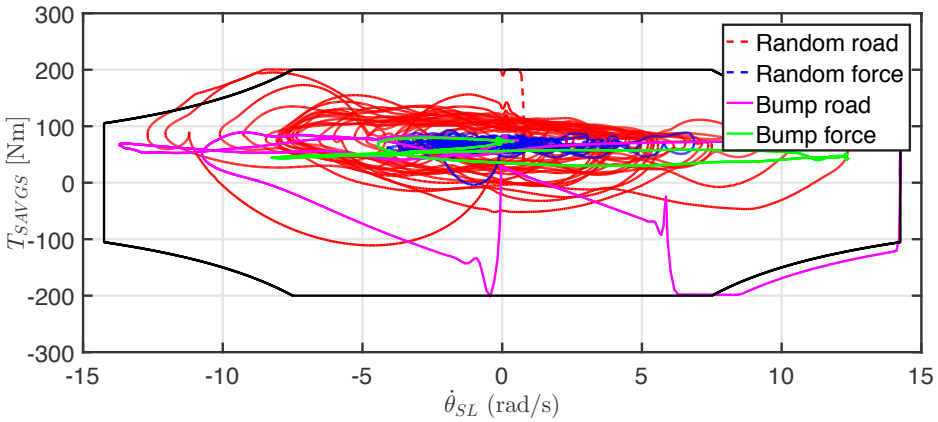

Fig. 4.16 Output torque vs. single-link speed characteristics for bump and random disturbance forcing events of the nonlinear quarter-car with SAVGS, presented in Figs. 4.12, 4.10, 4.13 and 4.15. The actuator limit boundaries are symmetric about the horizontal axis.

Overall, the results show that the $\mathcal{H}_\infty$ controller scheme can improve the performance of the suspension while satisfying the stringent actuator performance limits.

4.4.2 Full-car simulation results with quarter-car controller

The previous simulation shows that the SAVGS $\mathcal{H}_\infty$ control scheme has the potential to improve passenger ride comfort and road holding without deteriorating of suspension travel on the quarter-car multi-body model. In this section, this same controller is tested in the full-car nonlinear model, which is the first step to designing a suitable control scheme for the full-car $\mathcal{H}_\infty$ control.

Two basic types of full-car implementation methods are developed based on a comprehensive review of the literature:

1. The first method is straightforward. We design two quarter-car controllers for the front right and rear right corners of the car. Then, the full-car vehicle consists of these four quarter-car controllers at each corner, with the front right controller used twice in the front left and right, and the rear right controller used twice in the rear left and right. In this way, these four controllers will work independently under the same principle of the quarter-car.

2. The second method is to develop a new controller for the full-car model by implementing the proposed $\mathcal{H}_\infty$ control idea for the quarter-car design. We have successfully obtained the linear quarter-car $\mathcal{H}_\infty$ controller and are familiar with the designing and testing procedure in MATLAB. The selection and testing of dynamic weighting functions must consider the stability of the final nonlinear closed-loop system and balance the performance of different design objectives. This process is very time consuming and takes many iterations to be finalised. This step can be reduced by keeping the properties of the weighting functions consistent with the design for the quarter-car. For example, the output weightings need to maintain their 'lowpass' nature to penalise the appropriate low frequencies of vertical acceleration and tyre deflection, which correspond to passenger comfort and road holding. Additional weighting functions may be introduced for the pitching and rolling motions, as there are extra rotational DOF in the full-car model. This type of controller will be developed in Chapter 5, and the results of this method will be compared with the first method, which is developed in this section.

The first method is denoted as the Q1-SAVGS control scheme, while the passive full-car configuration is denoted as Passive. These two cases are compared in the following simulation results.

1. The equation of a typical bump road perturbation for the front wheels is the same as Equation. (4.10). In these equation, $h_b = 0.05\,m$ is the height of the bump and $\omega_b = 2\,m$ is the longitudinal distance of the bump. The forward velocity of driving is $V = 20\,m/s$. For the rear wheels, the motion caused by the same road perturbation is delayed. The delay time depends on the wheelbase length of the full-car vehicle. The nonlinear simulation results examining the performance of the full-car SAVGS with four $\mathcal{H}_\infty$ controller under bump disturbance are presented in Figs. 4.17 - 4.20

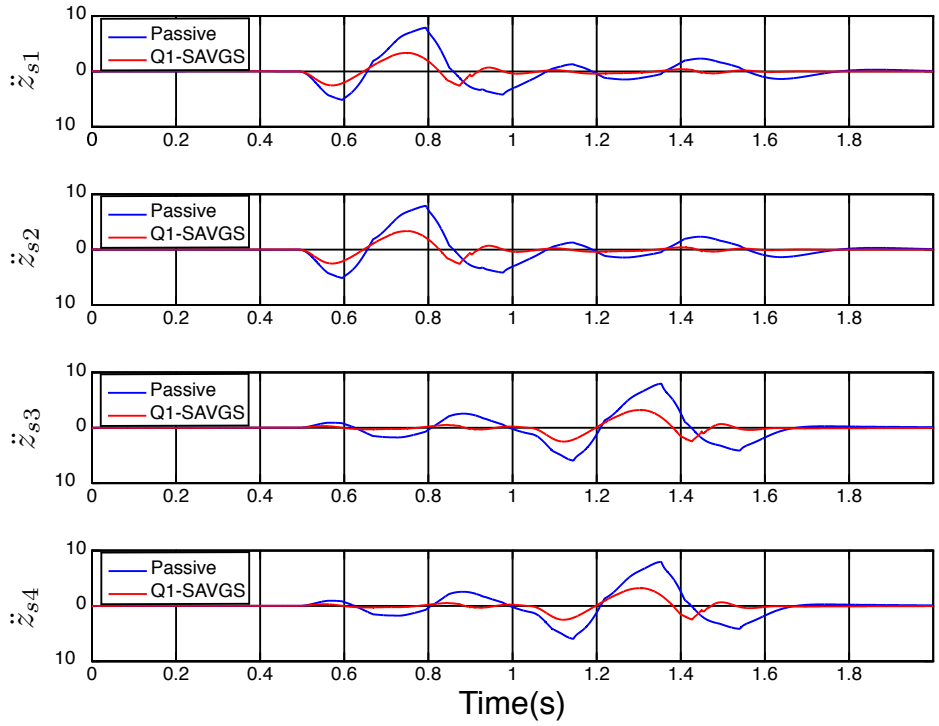

Fig. 4.17 Vertical acceleration at each corner of the full-car vehicle when running over a road bump at 20 m/s forward speed, for the SAVGS $\mathcal{H}_\infty$ scheme and the passive suspension. The bump starts at 0.5 s.

Figs. 4.17, 4.18, and 4.19 show that the body acceleration, tyre deflection, and suspension deflection are reduced once the SAVGS with $\mathcal{H}_\infty$ control scheme is employed to the full-car vehicle. Simulation results demonstrate the positive performance, which is similar to that of the quarter-car results. Fig. 4.20 contains the operation of the single-links at each corner, proving that the single-links are actively rotated to achieve the performance described above. The series of other tests for the quarter-car including random road, random external vertical force, smoothed bump and sinusoidal disturbances are also conducted using the full-car vehicle equipped with the previous $\mathcal{H}_\infty$ controller at four corners. The results are not shown here as they are comparable to the quarter-car simulation regarding ride comfort and road holding improvement in the vertical direction. The next simulation is made between the full-car SAVGS $\mathcal{H}_\infty$ -controlled scheme and passive suspension by considering the standard open-loop low frequency manoeuvres to assess the potential of the SAVGS for attitude control performance.

2. The second test is a braking event from steady-state circular motion based on ISO 7975:2006. Simulations have been obtained for evaluating the performance

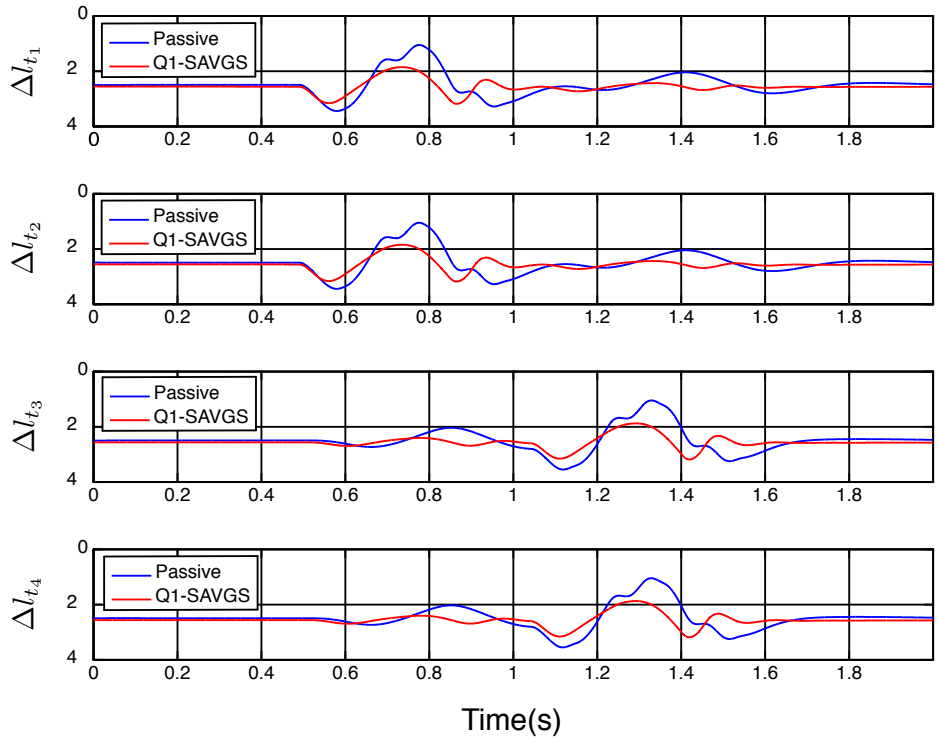

Fig. 4.18 Tyre deflection of each corner at the full-car vehicle when running over a road bump at 20 m/s forward speed, for the SAVGS $\mathcal{H}_\infty$ scheme and the passive suspension. The bump starts at 0.5 s.

of the SAVGS with $\mathcal{H}_\infty$ control for the full-car configuration. Initially, the car is driven at a constant speed of V=100 km/h and turned in a radius of R=100 m with a normal acceleration of $7\,m/s^2$. Then, maintaining the position of the steering wheel, with the deceleration of $6\,m/s^2$, the forward velocity is decreased from $27\,m/s$ to $3\,m/s$.

Figs. 4.21 to 4.24 depict the evolutions for SAVGS with $\mathcal{H}_\infty$ controlled vehicle and the passive cases. Similar to the previous cases, the acceleration and the tyre deflection are significantly reduced with respect to the passive case according to the rotation of the single-link presented in Fig. 4.23. Due to the turning behaviour, in Fig. 4.23, the single-link angles are distant from their offset angle (90°) before the deceleration phase begins. Pitch and roll evolutions are shown in Fig. 4.24. Roll and pitch do not perform better than the passive case but are also fully under control with the SAVGS $\mathcal{H}_\infty$ -controlled scheme. In addition to the braking event from steady-state circular manoeuvres, a step steering manoeuvre has also been investigated to understand the performance of the controller for

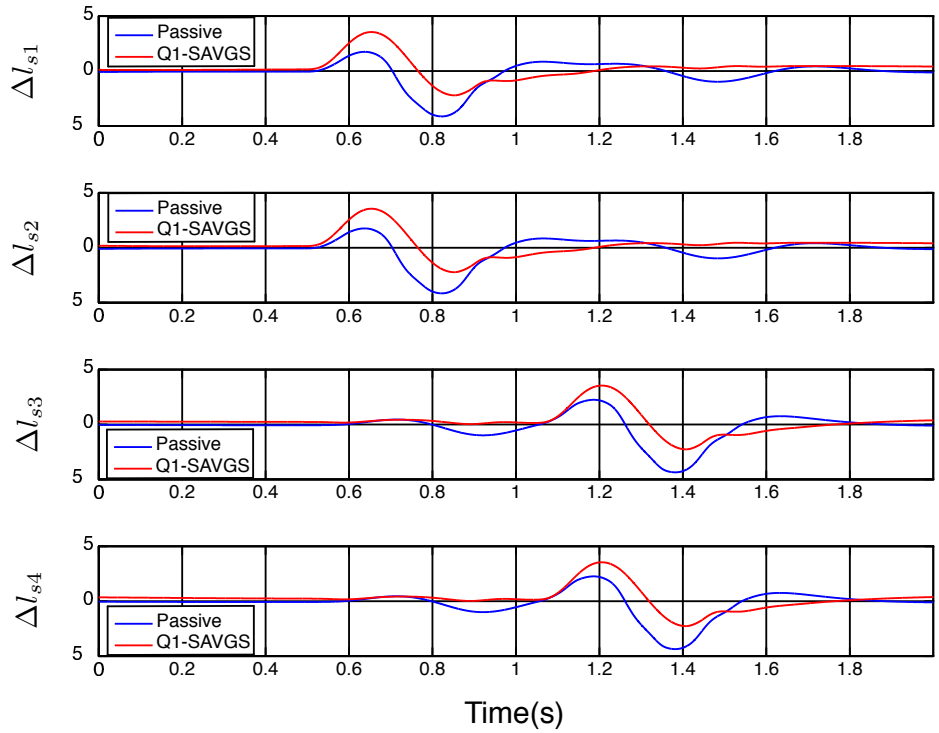

Fig. 4.19 Suspension deflection at each corner of the full-car vehicle when running over a road bump at 20 m/s forward speed, for the SAVGS $\mathcal{H}_\infty$ scheme and the passive suspension. The bump starts at 0.5 s.

roll mitigation. Similar to the case in this section, roll performance of the SAVGS $\mathcal{H}_\infty$ controlled full-car vehicle is much the same as the passive response. This is caused by the 'bandpass' nature of the controller as shown in Fig. 4.7, which doesn't act at low frequencies.

4.5 Conclusions

Using a quarter-car model of a high performance car with double wishbone kinematic linkage and series active variable geometry suspension, a linear $\mathcal{H}_\infty$ control scheme is developed in this chapter to reduce the impact of external road disturbances. The simulation results with and nonlinear controlled system, for a range of road and external vertical force input disturbances demonstrate that, as compared with a conventional passive suspension: a) the SAVGS with the proposed $\mathcal{H}_\infty$ controller offers a significant improvement in ride comfort and road holding of the vehicle, due to the reduction of body vertical acceleration and tire deflection, with limited impact on suspension travel, and b) the operation of the closed-loop system for realistic road con-

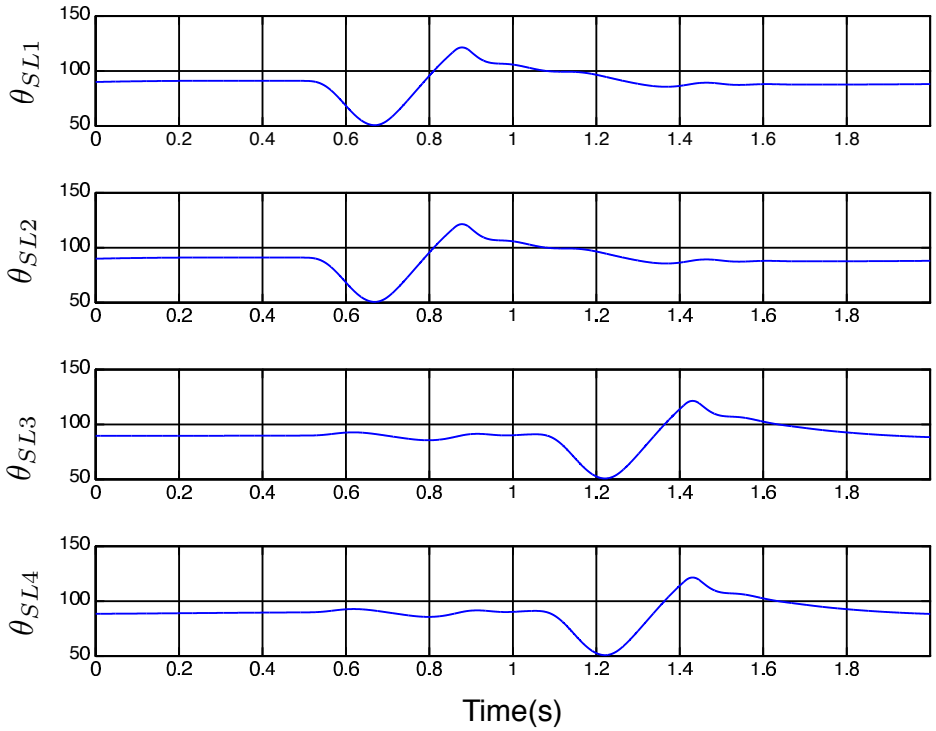

Fig. 4.20 Rotational angle at each corner of the full-car vehicle when running over a road bump at 20 m/s forward speed, for the SAVGS $\mathcal{H}_\infty$ scheme and the passive suspension. The bump starts at 0.5 s.

ditions requires low power consumption and satisfies the torque and speed constraint characteristics of relatively small actuators, already available on the market.

Other conclusions of this work and the suggestion for future work are summarised as follows:

- The magnitude of the Bode plots in Fig. 4.3 show that $\Delta\theta_{\mathrm{SL}} = 90°$ has the maximum gain and maximum control authority and the bode plot remains largely unchanged around 90°. Hence, the linearised quarter-car model (QCL) should be obtained at this trim state and the SAVGS control scheme based on this model could offer the best control performance. This finding is also applicable to later research on the linearised full-car model (FCL).

- The suspension system has two invariant points: 1) one for vertical body acceleration, and 2) one for the suspension deflection transfer function. The analysis of these invariant points shows the trade-off within the control objectives. To improve ride comfort and road holding without impacting the suspension travel, the following points can be considered while designing the controller: 1) achieve significant reduction in vertical body acceleration, suspension deflection and tyre

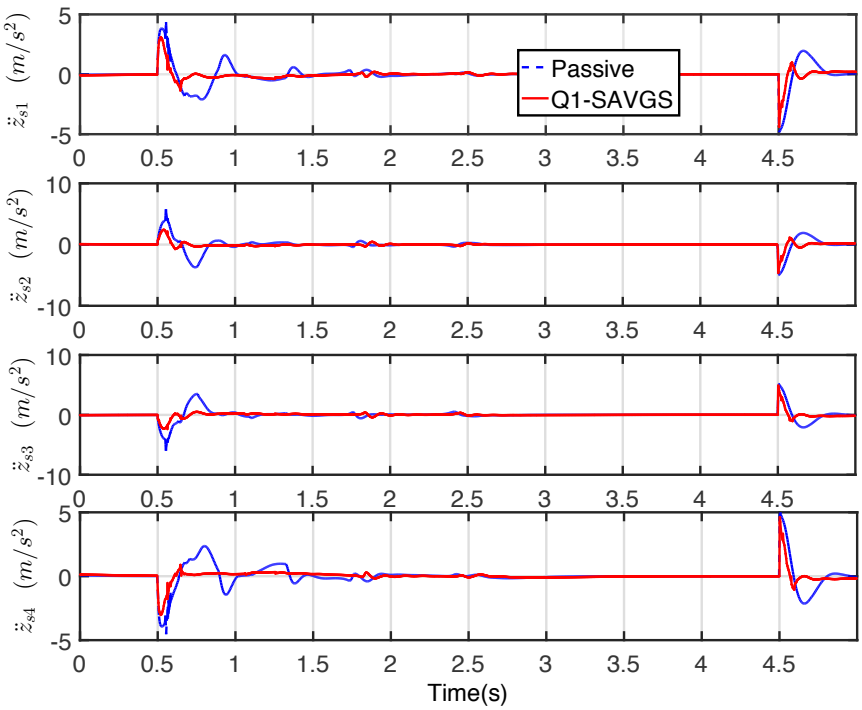

Fig. 4.21 Vertical acceleration at each corner of the full-car vehicle for a brake in turn event. Braking starts at 0.5 s.

deflection at the sprung mass resonance frequency; 2) avoid any deterioration in all three control objectives at the unsprung mass resonance frequency; and 3) avoid any control effort at extremely low and high frequencies.

- The bandpass nature in the frequency domain of the proposed $\mathcal{H}_\infty$ controller is expected since the desired controller should avoid expending much power outside the frequency range of interest. A small gain in the low frequency range ($\omega < 1\,Hz$) is desired since the $\mathcal{H}_\infty$ -controlled scheme could guarantee a short settling time (e.g, in bump disturbance). Furthermore, the analysis of the invariant point shows that a trade-off exists between ride comfort and rattle space when ω is close to $0\,Hz$. The improvement in acceleration for the low frequencies can only be obtained with a deterioration in rattle space.

  However, the full-car simulation in Section 4.4.2 indicates that small gain in low frequency is not able to provide significant roll and pitch correction the during turning manoeuvres. In Chapter 6 and 7, this will be solved by introducing separate PID controllers for the control of chassis attitude motions, which work together with the $\mathcal{H}_\infty$ controllers for the full car. In this case, mitigation of

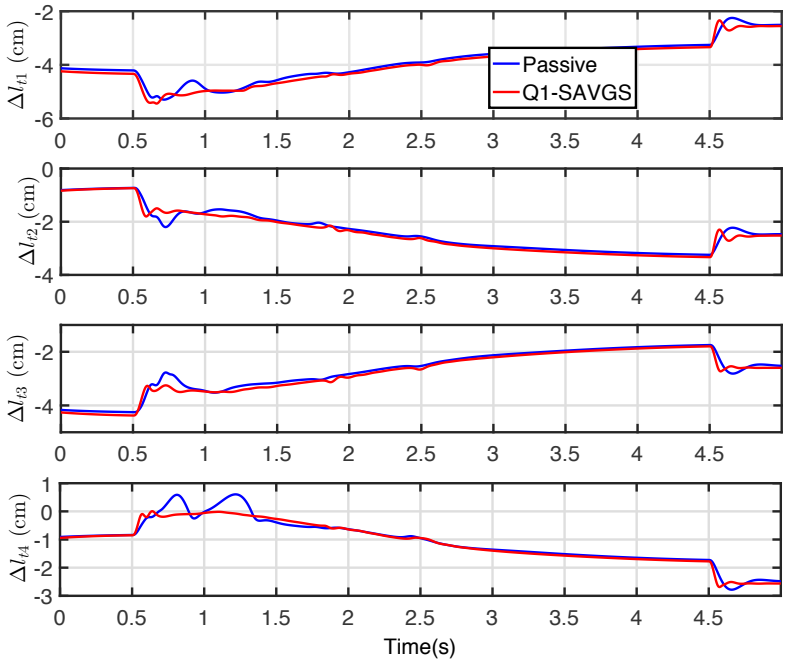

Fig. 4.22 Tyre deflection at each corner of the full-car vehicle for a brake in turn event. Braking starts at 0.5 s

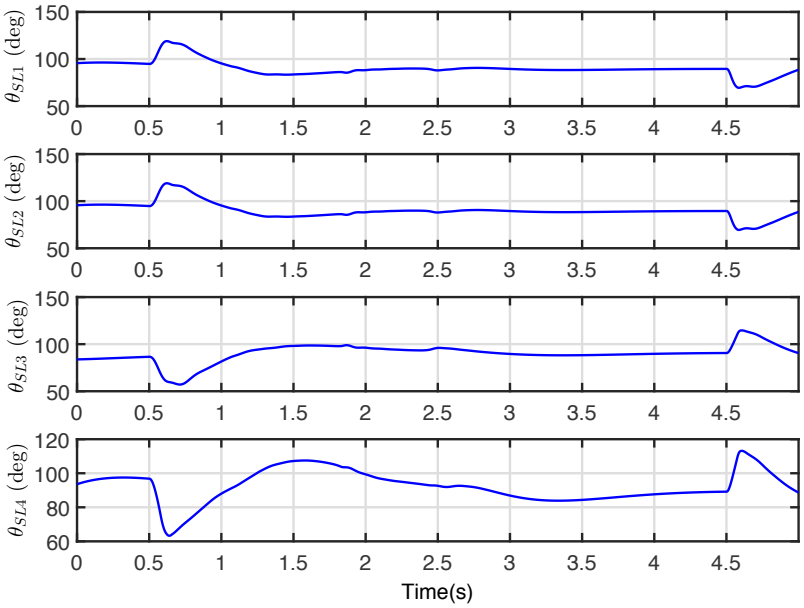

Fig. 4.23 Single-link angles for a brake in turn event. Braking starts at 0.5 s

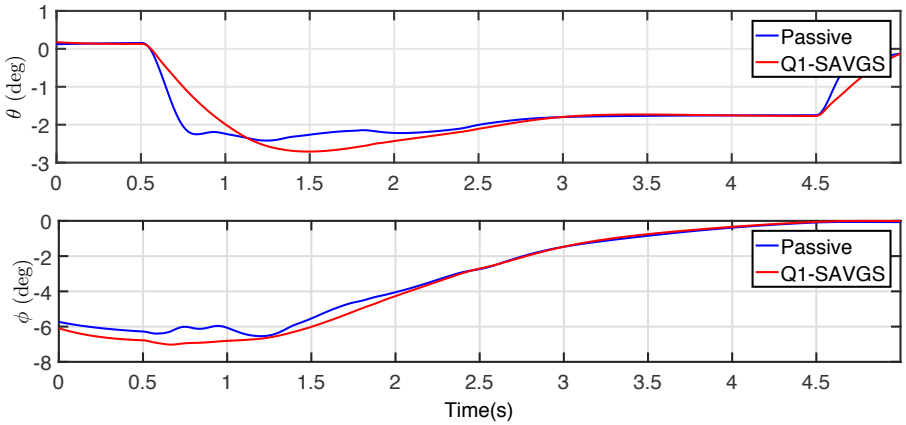

Fig. 4.24 Pitch and roll angles for passive and SAVGS cases during a brake-in-turn event. Braking starts at 0.5 s

attitude motions, as well as comfort and road holding enhancement are simultaneously considered as control objectives.

- The controller obtained for the quarter-car model has been applied to test the full-car nonlinear model and represent a good reference point for developing full-car specific controllers. In the next chapter, full-car $\mathcal{H}_\infty$ control requires additional weighting functions for the pitching and rolling motions at the vehicle mass centre. The selection of the rest of the weighting functions can be tuned based on the experience of this chapter.

Chapter 5

$\mathcal{H}_\infty$ CONTROL SYNTHESIS FOR FULL-CAR COMFORT AND ROAD HOLDING ENHANCEMENT

The previous chapter explored the effectiveness of $\mathcal{H}_\infty$ control applications on the SAVGS quarter-car, thereby laying the foundation for applying the same control methodology to a full-car vehicle. In the latter case it is envisioned to have one SAVGS system retrofitted at each of the four corners of a full vehicle with conventional independent passive double-wishbone suspension. In addition to the quarter-car control objectives involving vertical motions and according to ISO standard [82], rotational motions are also important in assessing comfort when considering full-car vehicle responses.

Thus, this chapter provides a comprehensive study of a full-car SAVGS model and its control in the context of high frequency vehicle dynamics, to demonstrate the optimal road disturbance rejection that improves passenger ride comfort and road holding. The performance objectives are achieved by constructing the full-car linear $\mathcal{H}_\infty$ multi-objective control framework to minimize vertical accelerations and tire deflections for all corners of the vehicle simultaneously, and also to minimize variables related to the pitching and rolling motions of the chassis. This is a significantly more complex control problem than what has been tackled in previous work due to the much larger number of states, inputs and outputs of the full-car model as compared to those of the quarter-car model, but also due to the interacting SAVGS dynamics among the four corners of the vehicle. The developed controller is ultimately tested in this work by simulation with the nonlinear full-car model with SAVGS, under various types of road disturbances, to verify its performance, robustness characteristics and satisfaction of

actuator and suspension operating constraints, in a more realistic context that with a quarter-car.

This chapter is organised as follows: Section 5.1 describes the full-car SAVGS model. Section 5.2 and Section 5.3 respectively, provide the general control scheme, and detail the $\mathcal{H}_\infty$ control synthesis and the multi-objective approach to $\mathcal{H}_\infty$ controller design with weighting functions. In Section 5.4.1, a Grand Tourer (GT) vehicle with SAVGS is used for the assessment of performance. The proposed full-car controller in this chapter is virtually tested through standard simulations and compared with the results of the full-car model equipped with the quarter-car controllers developed in [30] and [12] at four corners. Finally, conclusions are drawn and the suggested next steps are outlined in Section 5.5.

5.1 Full-car multi-body model (FC)

The vehicle model used in this chapter is the full-car SAVGS multi-body model (FC), which has been described previously in Section 3.1.6 in Chapter 3.

Table 5.1 full-car SAVGS symbols

Symbols	Physical Meanings	Unit
$\ddot{z}_{si}$	the ith sprung mass acceleration	m/s^2
Δl_{ti}	the ith tyre deflection	cm
Δl_{si}	the ith suspension deflection	cm
z_{ri}	the ith vertical road displacement	cm
$\dot{\theta}_{SLi}$	the ith single-link reference velocity	rad/s
$\Delta\theta_{SLi}$	the ith single-link angle	deg
$\ddot{\theta}, \ddot{\phi}$	pitch/roll mass centre acceleration	rad/s^2
$\ddot{Z}$	vertical mass centre acceleration	m/s^2
T_p, T_r	pitching/rolling torque at mass centre	$N.m$
$T_{\text{SAVGS}i}$	the ith actuation torque	$N.m$

5.2 General Control Scheme

The objective of this work is to develop a controller based on the full-car dynamics, which can control the rotation of the single-link angle to achieve the desired performance under certain conditions. The full-car SAVGS model will be used differently via two stages, corresponding to the development and validation of the controller:

a) For the linear analysis and robust controller design, which will be explained in the next section, the velocities of the single-links are selected as the controlled inputs. The actuator dynamics (PMSM and gear box) providing torque, T_{SAVGS}, are not included in the linearised SAVGS model. This allows for reduced complexity of the $\mathcal{H}_\infty$ control design prior to installing it on the full nonlinear model. Fig. 5.1 demonstrates the feasibility and reliability of this simplification. The reference for the single-link velocity is provided by the robust controller and the changing of this velocity is induced by random road excitations. Good quality road A and poor quality road C, detailed later in this chapter, are investigated. It can be seen that the small tracking error implies that the reference single-link velocity is traced precisely and quickly by the inner position control loop of the actuator.

b) For nonlinear validation purposes, the nonlinear SAVGS model contains the actuator dynamics which is the approximation of the real car. Torque T_{SAVGS} is provided by the actuator to track the reference angular position for the single-link.

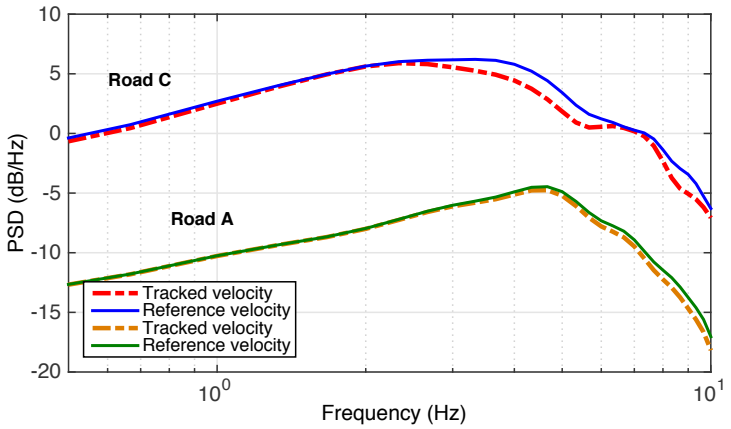

Fig. 5.1 Responses at the rear left wheel of the GT. Power spectral density (PSD) plots of the reference single-link velocity and the actual velocity generated by the actuator undergoing random road classes A and C.

The general control scheme for this work is shown in Fig. 5.2. The closed-loop SAVGS involves two controllers which are connected in series to tackle multiple control objectives.

1. The inner position control loop contains the actuator (PMSM and gear box) and the single-link position controller (K_{slpi}) at each corner of the vehicle. It

measures the rotational error (θ_{erri}) and generates the aforementioned T_{SAVGS} to follow the rotational references ($\theta^*{}_{refi}$) while satisfying all the physics and design constrains of the real systems (i.e., voltage, power, current, speed and single-link rotation limits). θ^*_{refi} is obtained by the integration of the output ($\dot{\theta}_{\text{SL}i}$) of the $\mathcal{H}_\infty$ controller. Saturation blocks have been placed between the integrators and the reference angles to guarantee the single-links operate within the chosen rotational limits. In this work, to improve the efficiency of the controller, we define the allowable range as $\theta^*_{refi} \in [\theta^{(\text{min})}_{\text{SL}}, \theta^{(\text{max})}_{\text{SL}} - 20°]$, since the recent work [11] indicates that the final 20° to $\theta^{(\text{max})}_{\text{SL}}$ ($=\theta^{(\text{min})}_{\text{SL}} + 180°$) offers small installation ratio changes. The details of K_{slpi} has been explained in [9], and the relevant schematic has been presented in Fig. 4.2 in the previous section.

2. The outer loop $\mathcal{H}_\infty$ controller takes the measurement signals (y) of the vehicle as the feedback input, and produces the reference single-link velocities ($\dot{\theta}_{\text{SL}i}$) as controlled input. The controller to be developed in this work aims to reduce the body accelerations and tyre deflections in terms of improving ride comfort and road holding properties, respectively, while simultaneously constraining the suspensions to move within their travel limits.

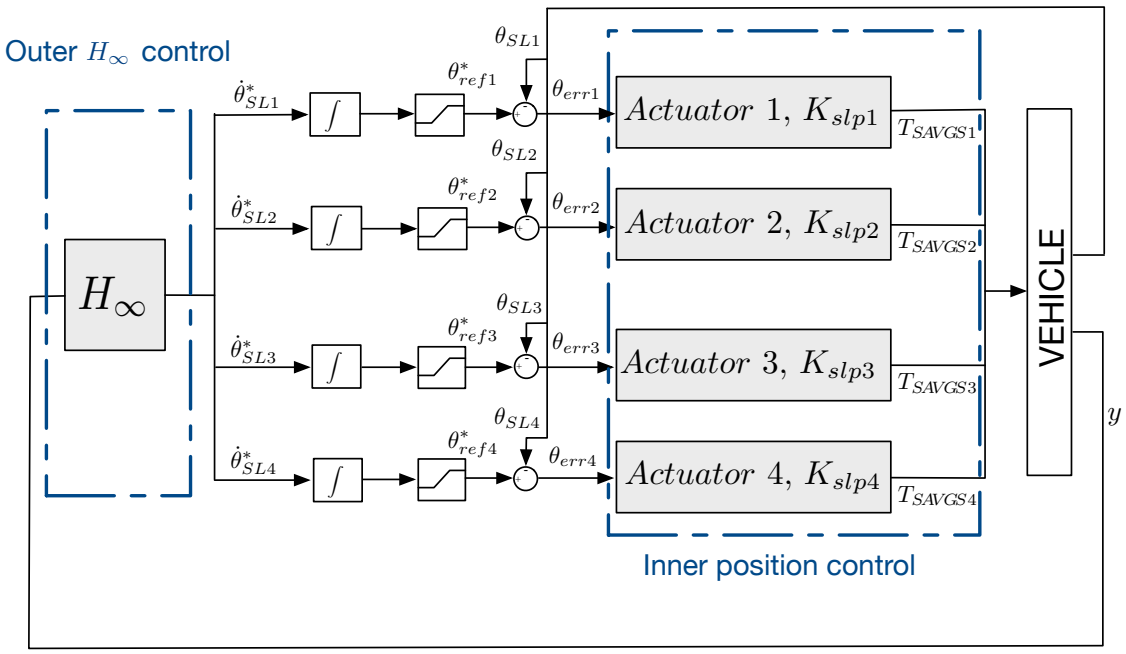

Fig. 5.2 General full-car control scheme (F-SAVGS).

The full-car model (FL) [9] is a high-fidelity dynamic system that has been developed using *Autosim* [6]. The Autosim model is first used to generate a state-space equation for the linear analysis, and the controller will be designed with Matlab at a defined trim condition. As explained in the previous section, in Fig. 4.3, the trim condition is selected as $\Delta\theta_{\mathrm{SL}} = 90°$, in which the linearised system offers the best control authority. The Autosim model can also can be written in C format code containing all the nonlinear equations of the SAVGS, which will be included in a Simulink block as an S-function for numerical integration and controller validation purposes.

5.3 $\mathcal{H}_\infty$ control synthesis framework

5.3.1 Full-car Autosim linearized model (FCL)

Frequency response

Frequency domain analysis makes system analysis much more straightforward and provides hints in next section for tuning weighting functions. Bode magnitude plots of the linear full-car model (Fig. 5.3) show the behaviors of the SAVGS system; this helps to investigate the relationship between performance factors (outputs) and control parameters (inputs) over a wide range of frequencies. Fig. 5.3 represents the response of both the rear left corner and the mass centre at the trim state, $\Delta\theta_{\mathrm{SL}} = 90°$. The other three corners have similar shapes and magnitudes. The inputs at the four corners are considered the rate of change of the road heights (to represent the exogenous road disturbances), the angular speeds of SL (to represent the control effort) and the exogenous pitching and rolling torques applied at the mass centre (to excite the rotational movements). The output performance factors are chosen as the sprung mass accelerations (i.e., corners, pitching and rolling), suspension deflections and tyre deflections, which are related to the main control objectives in terms of comfort, suspension travel limit, and road holding respectively.

The shapes of the bode plots in the first row of Fig. 5.3 reflect the typical double resonant peaks around 2 Hz and 10 Hz, that are associated with the vertical motion of the cabin and the tyres, respectively. In the bode plots of the second row, dominant peaks are found at and close to 1 Hz, which is associated with the exogenous torques with regards to the rotational motions. The bode plots in the third row indicate the control capability of the robust controller to be developed. It can be seen that: 1) the gains roll-up with a slope of +20 dB/dec at low frequencies (≤ 2 Hz) for vertical and rotational accelerations and remain as constant gains at high frequencies with small

dips close to 12 Hz; 2) the gains roll-down with a slope of -20 dB/dec and -40 dB/dec at low and high frequencies for tyre and suspension deflections. These observations imply that the closed-loop SAVGS controlled scheme has the potential of improving ride comfort and road holding at low frequencies. At high frequencies, even if the road holding will not be improved due to small control gains, the ride comfort performance still has the capability to be further enhanced.

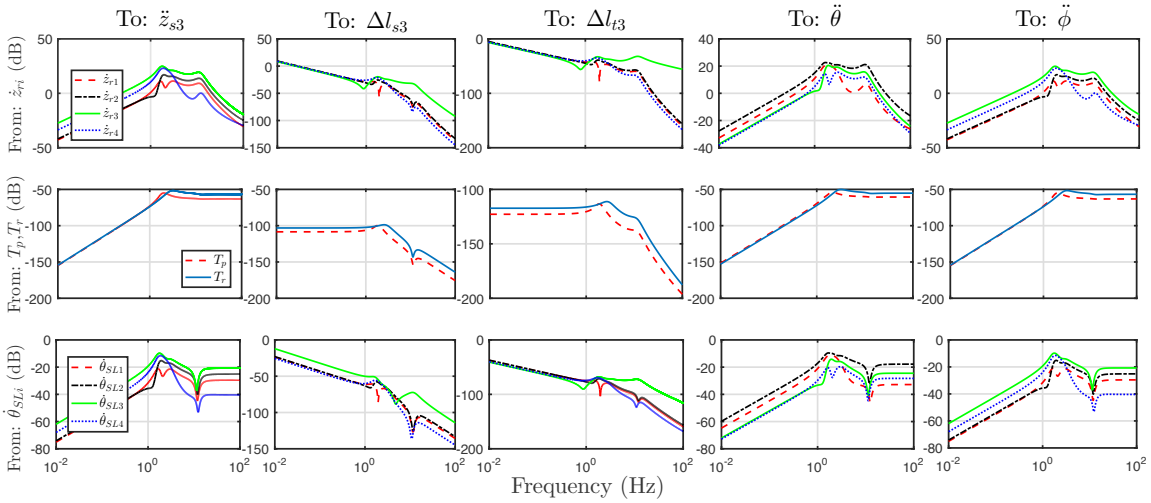

Fig. 5.3 Bode plots of the full-car linearised model. The gains correspond to the nominal offset angle $\theta_{\text{SL}}^{ne} = \theta_{\text{SL}}^{min} + \Delta\theta_{\text{SL}}$ when $\Delta\theta_{\text{SL}} = 90°$. The responses are from the inputs: vertical road speeds (first row), exogenous torques at the mass centre (second row), and SL angular speed. To outputs: vertical acceleration, suspension deflection and tyre deflection at the rear-left wheel (first three columns), as well as pitching (forth column) and rolling (fifth column) accelerations at centre of mass of the GT.

5.3.2 Controller design

Multiple control objectives

The main control objectives of this study are to improve ride comfort and road holding. These specifications correspond to minimising the body accelerations (i.e., vertical, pitching, and rolling) and tyre deflections of the vehicle, which is achieved by designing an effective H_∞ controller to isolate the vibrations caused by road irregularities. The suspension deflections and the actuator limits (i.e., power, torque and single-link speed limits) will be evaluated after the controller design.

Robust control scheme

Fig. 5.4 shows the H_∞ control scheme structure and the weighting functions based on the required design specifications. The mass centre of the linearised car model with zero forward velocity and tyres do not leave the ground. To estimate all the possible situations of the car, road displacements at the four corners and the pitching and rolling torques must be considered. The input vector containing these disturbances is then defined as $d = [d_1 \ \dots \ d_6]^T = [z_{r1}\, z_{r2},\, z_{r3},\, z_{r4},\, T_p,\, T_r]^T$.

For outputs, the ride comfort is qualified by the root mean square (RMS) of vehicle body accelerations at the four corners and the mass centre. Additionally, road holding is qualified by the tyre deflections at each corner of the vehicle. Hence, the vector of the regulated output variables minimised by the control system is chosen as: $z = [z_1 \ \dots \ z_{11}]^T = [\ddot{z}_{s1},\, \ddot{z}_{s2},\, \ddot{z}_{s3},\, \ddot{z}_{s4},\, \Delta l_{t1},\, \Delta l_{t2},\, \Delta l_{t3},\, \Delta l_{t4},\, \ddot{Z},\, \ddot{\theta},\, \ddot{\phi}]^T$.

The measurement signals, y, to be fed to the controller are chosen based on the availability of the sensors in our lab and the literature review of common sensors used for active suspension control. In summary, uniaxial accelerometers are used to detect the accelerations with regards to passenger ride comfort, and position sensors are used to measure the suspension deflections pertaining to the road holding performance. Thus, the vector of measurement signals is defined as $y = [y_1 \ \dots \ y_7]^T = [\Delta l_{s1},\, \Delta l_{s2},\, \Delta l_{s3},\, \Delta l_{s4},\, \ddot{Z},\, \ddot{\theta},\, \ddot{\phi}]^T$. Finally, as explained in the previous section, the controlled inputs are chosen as the single-link velocities $u = [\dot{\theta}^*_{\mathrm{SL1}},\, \dot{\theta}^*_{\mathrm{SL2}},\, \dot{\theta}^*_{\mathrm{SL3}},\, \dot{\theta}^*_{\mathrm{SL4}}]^T$ in the linearised model to be tracked by the car.

Selection of the weighting functions

In the $\mathcal{H}_\infty$ framework, dynamic frequency weightings are employed to shape the plant transfer functions to achieve the closed-loop performance and robustness specifications that can be expressed in the frequency domain. In Fig. 5.4, the plant $\mathbf{P}$ and final controller $\mathbf{K}$ are the generalised plants in Equation (2.14) multiplied by frequency-dependent design weights. The output weightings between $\bar{z}$ and z are used to penalise the body accelerations and tyre deflections for particular frequency ranges. Based on the ISO 2351-1 [82], humans are more sensitive to vibrations acting in the frequency range of 1∼8 Hz and 1∼2 Hz for the vertical and rotational accelerations and 1∼4 Hz for tyre deflection. Fig. 4.3 also shows that the body resonances of acceleration and tyre deflection at each corner of the vehicle is lower than 10 Hz. Therefore, the weightings are defined as low and band pass filters with cut-off frequencies, which cover these frequency ranges. The scaling factors in the front of the weighting functions reflect

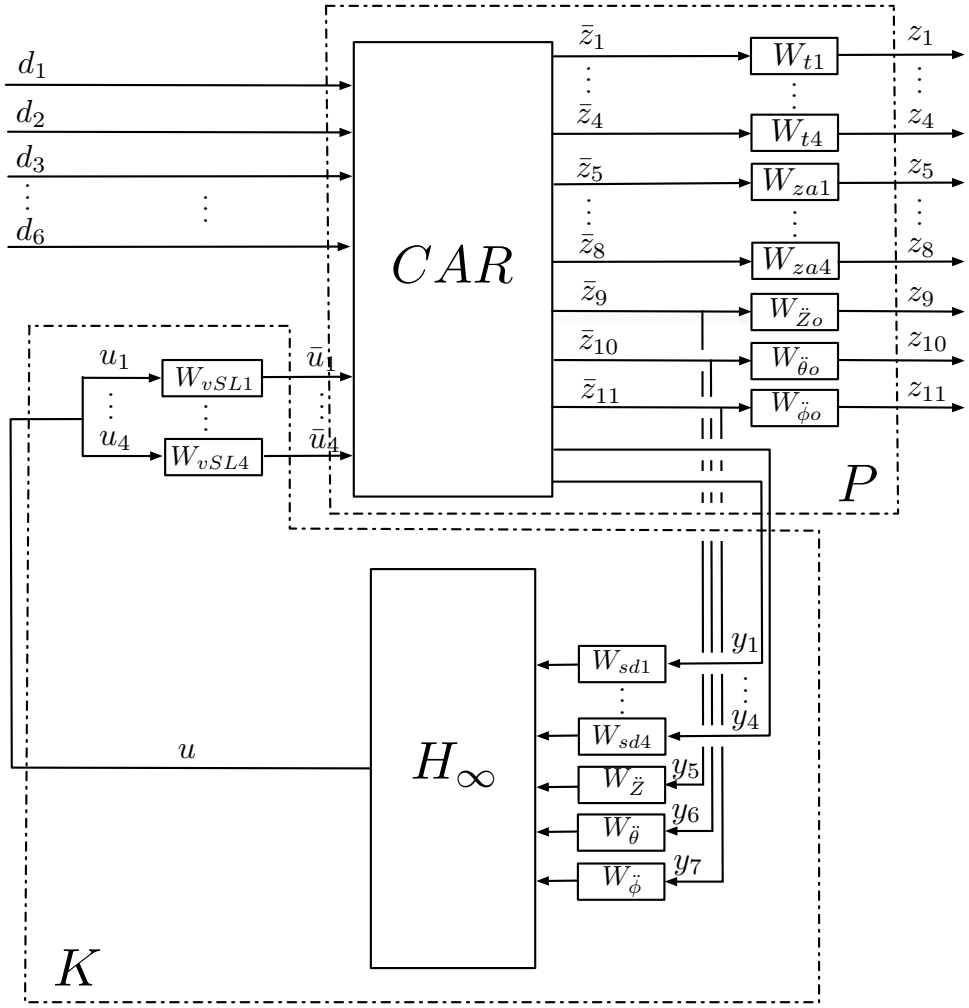

Fig. 5.4 $\mathcal{H}_\infty$ control scheme.

the relative importance of each regulated output:

$$W_{t1} = \frac{21.98(0.01s + 10)}{s + 62.8},$$

$$W_{t2} = W_{t3} = W_{t4} = W_{t1}$$

$$W_{za1} = \frac{40.82(0.01s + 10)}{s + 125.6},$$

$$W_{za2} = W_{za3} = W_{za4} = W_{\ddot{Z}o} = W_{za1},$$

$$W_{\ddot{\theta}o} = \frac{204.1s}{(s + 3.5)(s + 3.5)(s + 3.5)}, \quad W_{\ddot{\phi}o} = W_{\ddot{\theta}o}.$$

Controller $\mathcal{H}_\infty$ is solved by computing the minimum $\mathcal{H}_\infty$ norm of the closed-loop SAVGS system using an algebraic riccati method. The pre- and post-weighting functions in the series of the controller are used for 'loop-shaping' and will be absorbed by the $\mathcal{H}_\infty$ controller. The pre-weightings for suspension deflections and accelerations are defined as band-pass filters to avoid the controller expending too much power to extreme low- and high-frequencies. Moreover, to reduce the complexity of this control problem, the following non-dynamic scalar weightings are selected to modify the controlled input:

$$W_{vSL1} = W_{vSL2} = W_{vSL3} = W_{vSL4} = 0.25,$$

$$W_{sd1} = \frac{100s}{(s+100)(s+100)(s+100)},$$

$$W_{sd2} = W_{sd3} = W_{sd4} = W_{sd1},$$

$$W_{\ddot{\theta}} = \frac{200s}{(s+100)(s+100)(s+100)}, \quad W_{\ddot{\phi}} = W_{\ddot{\theta}}.$$

The closed-loop SAVGS controlled scheme is formulated in Matlab and the $\mathcal{H}_\infty$ optimal controller is computed by using the function `hinfsyn`. Arriving at the final satisfactory controller involves several iterations over the tuning of the frequency weightings by evaluating the performance and robustness specifications of the linear closed-loop system, as well as the analysis of the resulting stability of the nonlinear closed-loop system that was found by the simulation described in the next section. The singular value plot of the obtained $\mathcal{H}_\infty$ controller is shown in Figure. 5.5. The singular value plot of the closed-loop and open-loop weighted system is shown in Figure. 5.6. The next section will demonstrate the effectiveness of the proposed control system using full-car nonlinear Autosim models.

5.4 Full-car simulation results and comparison

In this section, two kinds of road forcing have been carried out to assess the potential of the proposed $\mathcal{H}_\infty$ controller equipped in a high-performance sports full-car nonlinear model: 1) two sets of random road profiles representative of good roughness road A and poor roughness road C at a constant longitudinal velocity of $100\,km/h$. Each set of road level roughness (road A or C) also includes two different profiles acting on the left and right wheels to observe the pitch and roll motions; and 2) a

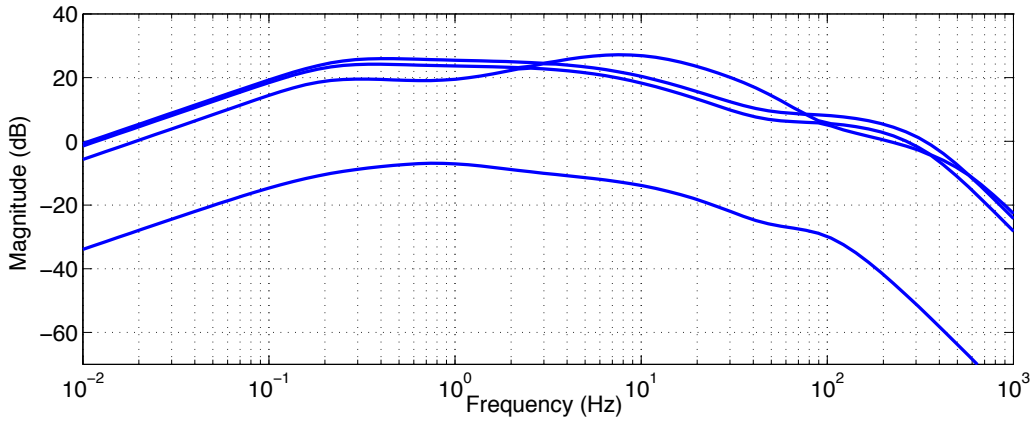

Fig. 5.5 Singular value plot of the designed $\mathcal{H}_\infty$ controller.

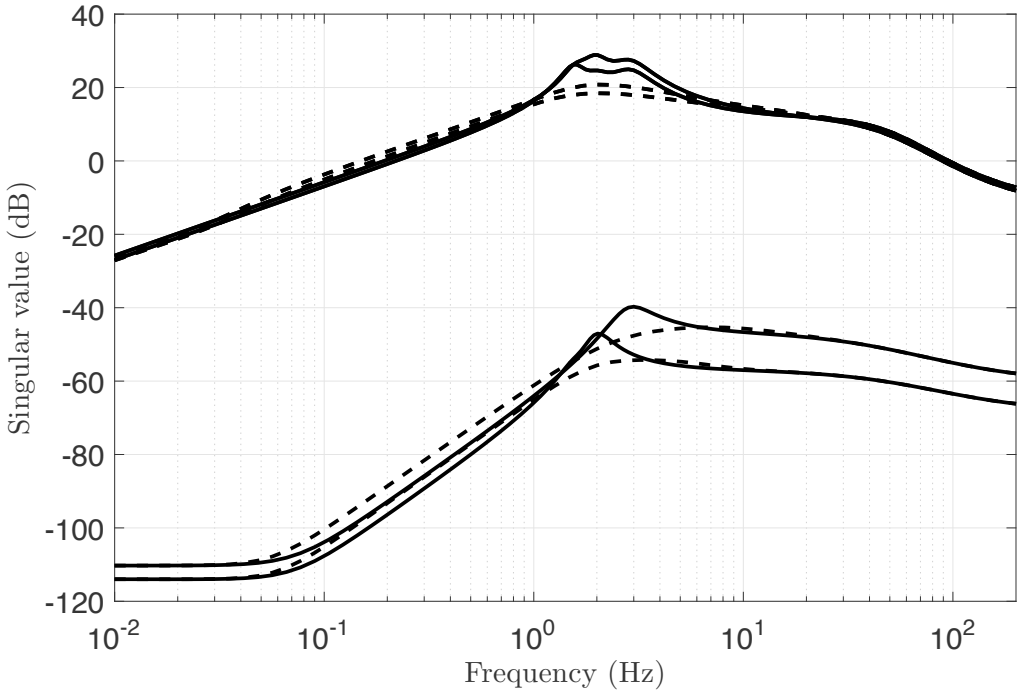

Fig. 5.6 Singular value plots for the weighted systems: closed-loop system with dotted line and open-loop system with solid line.

smooth bump disturbance with a low-speed constant velocity of $20\,km/h$. The model in [11] is a high-fidelity dynamic system and the main objective is to improve passenger comfort and road holding properties. Since the full-car model contains nonlinear factors, including a dynamic actuator, a well designed controller must also maintain

the actuator limits to protect the motor and gearbox. The relevant full-car GT and SAVGS parameters can be found in Tables 3.5 and 3.6 in Chapter 3.

5.4.1 Controllers for comparison

To investigate the effect of the proposed SAVGS $\mathcal{H}_\infty$ controlled scheme, three other suspension simulation results subjected to random road roughness are carried out and presented for comparison purposes. Then Power Spectral Density (PSD) plots of frequency domain are provided to analyse the suppressive effect over the human body sensitive frequency range. The full-car SAVGS with full-car $\mathcal{H}_\infty$ controller scheme (denoted by F-SAVGS) proposed in this work is compared to: 1) the full-car SAVGS with the original quarter-car $\mathcal{H}_\infty$ controller obtained in [30] which is equipped at the four corners of the vehicle (denoted by Q1-SAVGS), 2) the full-car SAVGS with the quarter-car $\mathcal{H}_\infty$ controller based on a new hand-derived quarter-car model in [12] (denoted by Q2-SAVGS), and 3) the passive configuration (denoted by PASSIVE).

5.4.2 Random road profile

Based on the equations (3.8) and (3.9) in Chapter 3.3.3, 1 km long random disturbances with road roughness A and C are generated for the simulation, with $n_0 = 0.1\,cycles/m$, $\Delta n = 0.005\,cycles/m$, $\omega = 2$ and forward velocity $V = 100\,km/h$. Level A and C represent the very good and average road profile, respectively for a high performance car. In each simulation, random road disturbances passing the left and right side wheels of the vehicle are assumed to be different, but exhibit the same level of roughness (A/C). The response of the rear wheels is delayed according to the wheelbase and the height between the right and left wheels varies according to the randomness of the two sides of the road. Hence, together with the responses of the vehicle at the four corners, pitching and rolling accelerations at the sprung mass centre will also be evaluated as additional assessments of comfort.

To analyse these results in time time domain, Tables 5.2 and 5.3 present the numerical results. The ride comfort index (RCI) used to assess the ride comfort is the RMS bounce acceleration according to the ISO 2631-1:1997 standard [82, 86, 118]:

$$\mathrm{RCI} = \left[\frac{1}{T}\int_0^T a^2(t)\,\mathrm{d}t\right]^{\frac{1}{2}} \tag{5.1}$$

in which T is the vibration duration time and a is the body vertical acceleration at each corner of the vehicle. The road holding index is selected as changes in the

peak-to-peak tyre defection [1]. For poor quality road C, the results show that RMS accelerations have reduced by approximately $\sim$ 13% for front wheels and $\sim$ 23% for rear wheels, and peak-to-peak tyre deflections can be maintained at the passive level and exhibit a minor improvement for the F-SAVGS case. For a quality road A, the vertical acceleration RMS values of the three controlled SAVGS suspensions are consistently improved when compared with the passive system. It also can be observed that F-SAVGS has the best road disturbance attenuation performance due to the largest RMS reductions. The tire defections on such a high quality road are reasonably small ($\leq$0.5 cm) and are irrelevant to compare.

Table 5.2 Ride comfort index (m/s^2) at four corners ((%) = Performance Improvement (%) compared to Passive)

Road A							
	Passive	Q2-SAVGS	(%)	Q1-SAVGS	(%)	F-SAVGS	(%)
$\ddot{z}_{s1}$	0.78463	0.67381	14.12	0.64993	17.16	0.5716	27.14
$\ddot{z}_{s2}$	0.81504	0.71001	12.89	0.68897	15.46	0.5915	27.14
$\ddot{z}_{s3}$	0.68165	0.56032	17.80	0.55994	17.85	0.3998	41.35
$\ddot{z}_{s4}$	0.68165	0.56032	17.80	0.55994	17.85	0.3998	41.25
Road C							
	Passive	Q2-SAVGS	(%)	Q1-SAVGS	(%)	F-SAVGS	(%)
$\ddot{z}_{s1}$	2.0773	1.8054	13.09	1.8014	13.28	1.8741	12.63
$\ddot{z}_{s2}$	2.1384	1.8566	13.18	1.8529	13.35	1.8741	12.63
$\ddot{z}_{s3}$	2.1439	1.6393	23.54	1.7108	20.57	1.6411	23.45
$\ddot{z}_{s4}$	2.1439	1.6393	23.54	1.7108	20.57	1.6411	23.45

Table 5.3 Peak values of tyre deflection (cm) at four corners, ((%) = Performance Improvement (%) compared to Passive)

Road C							
	Passive	Q2-SAVGS	(%)	Q1-SAVGS	(%)	F-SAVGS	(%)
$\mid \Delta l_{t1} \mid$	3.18	3.24	-1.89	3.30	-3.77	3.12	1.89
$\mid \Delta l_{t2} \mid$	2.97	2.94	1.01	3.00	-1.11	3.05	2.69
$\mid \Delta l_{t3} \mid$	3.02	2.87	4.87	2.80	7.28	2.96	1.99
$\mid \Delta l_{t4} \mid$	3.02	2.83	6.29	2.89	4.30	2.97	1.66

To further analyse the frequency domain, Fig. 5.7 and 5.8 present the PSD plots for vertical acceleration at the four corners of the vehicle for road classes C and A, concerning the passenger comfort on different seats. For poor quality road C and good quality road A, the figures show that the F-SAVGS design in this approach is the most effective, because: 1) F-SAVGS has relatively smaller gains than Q1-SAVGS

at the dominant range of human sensitive frequencies (1∼8 Hz) [82], especially for random road class A, which indicates a better vibration attenuation performance; and 2) the PSD magnitudes of the Q2-SAVGS are highly regulated in the frequency range 1∼5 Hz; however, the F-SAVGS approach in this work covers a wider frequency range of the sensitivity of the human body to vibrations. Therefore, the full-car SAVGS control approach is highly significant to improve the comfort of the human body. More specifically, compared to the passive case, the gain reductions of F-SAVGS are up to 6.5 dB and 7.3 dB for good road A regarding the front and rear axles near the sprung mass resonance peak (2 Hz) and with 4.3 dB and 7.1 dB maximum reductions for the front and rear axles for poor road C.

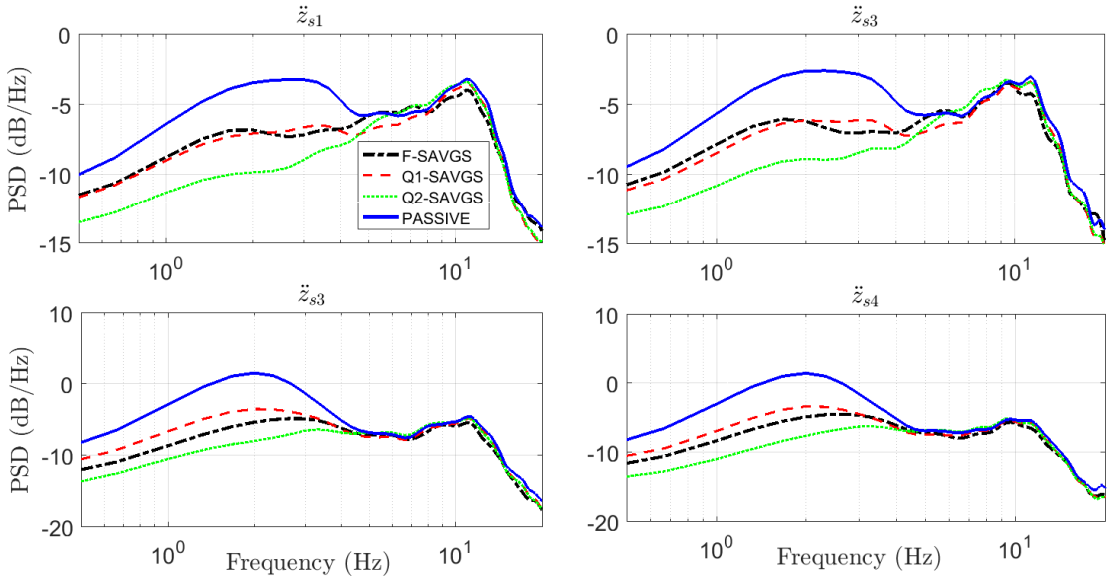

Fig. 5.7 Sprung mass vertical acceleration PSDs for each corner of the GT under uneven an random disturbance (Road class C). The results of the aforementioned controllers in 5.4.1 are compared with passive suspension.

To investigate the performance of $\mathcal{H}_\infty$ control scheme at the mass centre of the vehicle, Figs. 5.9 and 5.10 present the PSD for pitching and rolling accelerations. Similar to Figs. 5.7 and 5.8, the magnitude of the pitching and rolling accelerations of the three $\mathcal{H}_\infty$ controlled systems decreased over a wide frequency range, especially for the low-frequency range (≤2 Hz), thus, affecting human comfort with rotational variations [82]. Compared to the passive suspension, the pitching acceleration gain reduction achieved by the F-SAVGS is up to approximately 3.7 dB and 6.1 dB near the resonant peaks for pitching close to 1 Hz [82], with respect to road classes A and C. In terms of rolling acceleration, an even higher reduction (4.4 dB and 3.9 dB) is

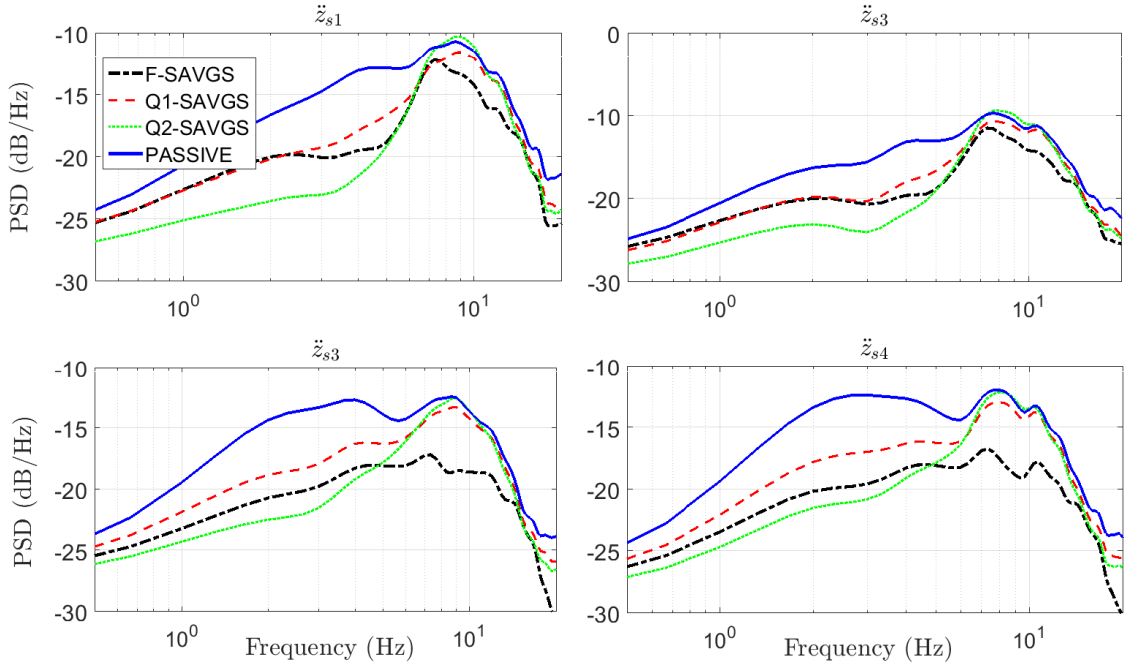

Fig. 5.8 Sprung mass vertical acceleration PSDs for each corner of the GT under uneven random disturbance (Road class A). The results of the aforementioned controllers in 5.4.1 are compared with passive suspension.

achieved. To analyse in a time domain, the mass centre comfort index (MCI) can be calculated by an expression similar to Eq. 5.1, given as:

$$\mathrm{MCI} = \left[\frac{1}{T}\int_0^T a_{\mathrm{mc}}^2(t)\,\mathrm{d}t\right]^{\frac{1}{2}} \tag{5.2}$$

where a_{mc} is the total acceleration at the mass centre calculated as the root-sum-of-squares value with respect to pitching and rolling accelerations:

$$a_{\mathrm{mc}}(t) = \left(a_p^2(t) + a_r^2(t)\right)^{\frac{1}{2}} \tag{5.3}$$

where a_p and a_r are the pitching and rolling accelerations at time t. The numerical results are shown in Table.5.4 with promising improvement. The reductions of F-SAVGS approach in this work are larger than Q1-SAVGS and Q2-SAVGS, which illustrate the ride comfort improvement of rotational motions due to the implementation of the SAVGS and the full-car $\mathcal{H}_\infty$ control scheme.

Fig. 5.11 presents 5 s time history simulation results for the rear-right wheel and sprung mass centre undergoing random road class A of F-SAVGS. The first plot is the

Table 5.4 Mass centre comfort index (MCI) (m/s^2), ((%) = Performance Improvement (%) compared to Passive)

Road A							
	Passive	Q2-SAVGS	(%)	Q1-SAVGS	(%)	F-SAVGS	(%)
MCI	1.0015	0.8691	13.22	0.8506	15.06	0.4304	57.02
Road C							
	Passive	Q2-SAVGS	(%)	Q1-SAVGS	(%)	F-SAVGS	(%)
MCI	2.5296	2.2316	11.78	2.2132	12.46	2.0513	18.91

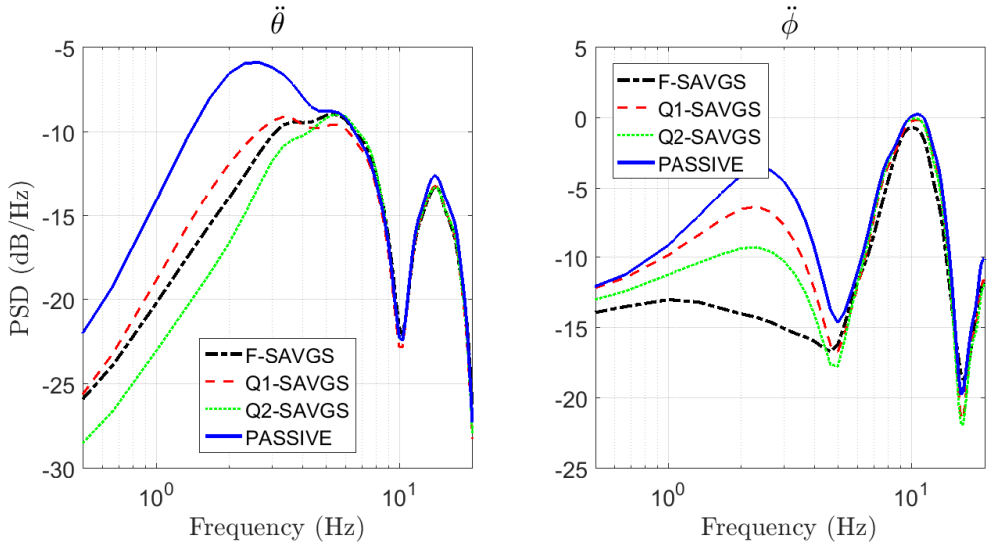

Fig. 5.9 Pitching and rolling accelerations PSD plots at the mass centre of the GT under an uneven random disturbance (Road class C). Results of the controllers in 5.4.1 are compared with passive suspension.

random road profile. The second plot is the rotation angle of the single-link from its equilibrium offset $\theta_{\mathrm{SL}}^{(\mathrm{ne})}$. It can be noted that the actuator is actively reacting and is rapid within its operation limit. A comparison reveals that by using the proposed $\mathcal{H}_\infty$ controller, most of the peaks in the SAVGS corner, pitching and rolling accelerations are reduced with respect to the passive suspension.

5.4.3 Smoothed bump profile

The smoothed bump event in this section is identical to the expression in 4.10 in Chapter 3, in which $V = 20\,km/h$ is the forward speed with bump height $h = 5\,cm$ and width $w = 2\,m$. For the purpose of evaluating the pitch and roll mitigation, the

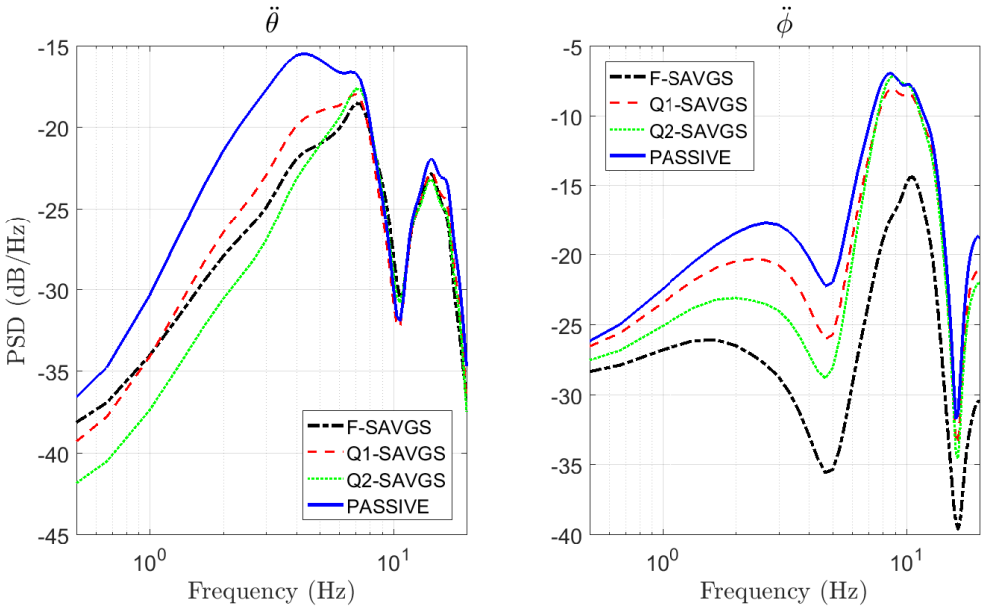

Fig. 5.10 Pitching and rolling accelerations PSD plots at the mass centre of the GT under uneven an random disturbance (Road class A). Results of the controllers in 5.4.1 are compared with passive suspension.

$\mathcal{H}_\infty$-controlled SAVGS full-car system only undergoes bump disturbance through the left wheels of the vehicle.

Fig. 5.12(a) and 5.12(b) investigates the disturbance attenuation of the sprung mass vertical acceleration and tyre deflection, which corresponds to ride comfort and road holding objectives. The blue lines demonstrate that the full-car SAVGS $\mathcal{H}_\infty$-controlled system performs as desired. Improvements in terms of RMS values are more than 32% for vertical acceleration and more than 25% for tyre deflection. Fig. 5.12(c) depicts that the maximum suspension deflection is reduced by 21%, which demonstrates that the performance enhancement does not degenerate the suspension working limits. Fig. 5.12(d) shows that the single-link angle operates quickly and effectively within its allowable range (0-160 deg) to achieve the desired performance. Once the bump is over, the single-link reverts back to its offset position without activating any further undesirable dynamics. Similar results are also observed in the plots of the other three wheels, which demonstrates the overall improvement in ride comfort and road holding due to the implementation of SAVGS with the $\mathcal{H}_\infty$-control full-car feedback loop.

Fig. 5.13 presents the results for the pitch and roll motions at the mass centre over this smoothed bump. RMS values for pitch and roll accelerations in the SAVGS suspension are reduced by 44% and 67% with respect to the passive case.

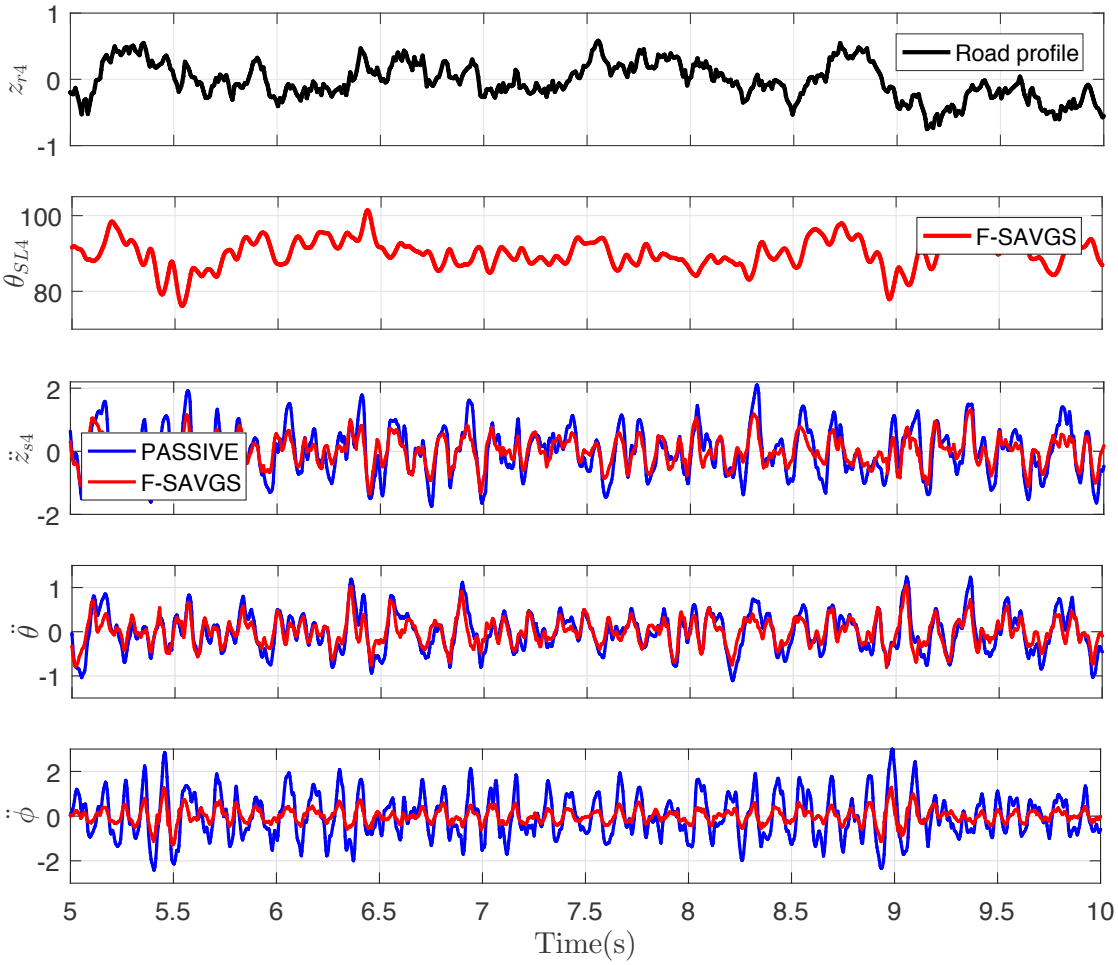

Fig. 5.11 The 5 s to 10 s time series simulation results under random road class A. The plots are: 1) road profile; 2) single-link angle; and 3) vertical acceleration at the rear-right wheel; 4) pitching; and 5) rolling accelerations at the sprung mass centre.

5.4.4 Inner position controller performance

As mentioned in Fig. 4.2, the inner position controller scheme is used to limit the operation of the single-link inside the gearbox and motor duty zone to protect the gearbox and motor under any circumstances and to set the maximum electric power consumption by the controller. The robustness of the controller is validated by the plot of the output torque against a single-link speed under the condition of random road C (worse roughness than road A and operates more aggressive than bump excitation), which shows the single-link operation boundaries of the four corners of the car. In Fig.

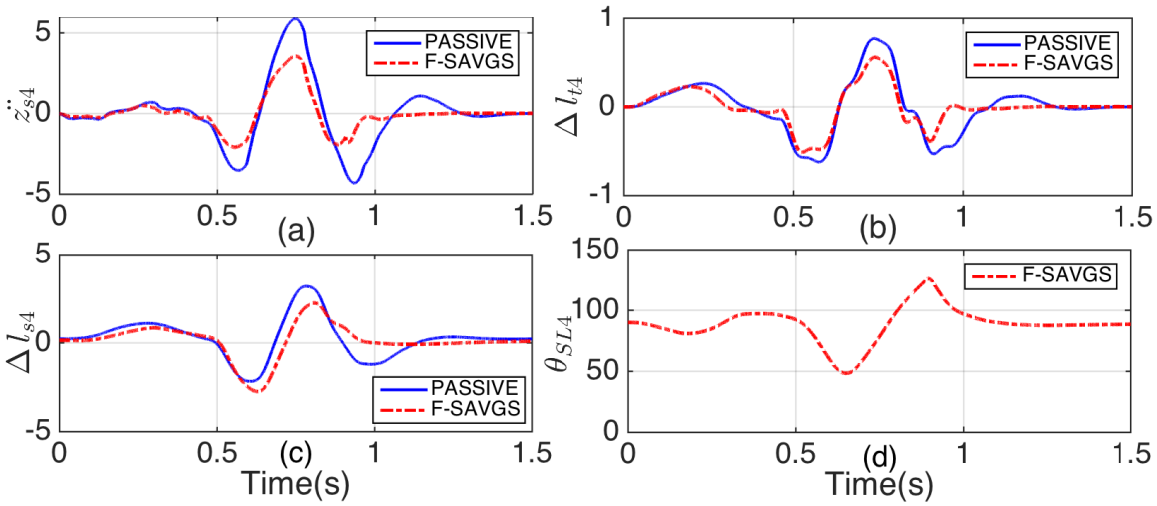

Fig. 5.12 Response at the rear-left wheel while running over a smoothed bump at the left wheels. Passive suspension and SAVGS $\mathcal{H}_\infty$-controlled system (F-SAVGS) are undergoing the same smoothed bump excitation with a $5\,cm$ height and $2\,m$ width. The other three wheels have similar simulation results.

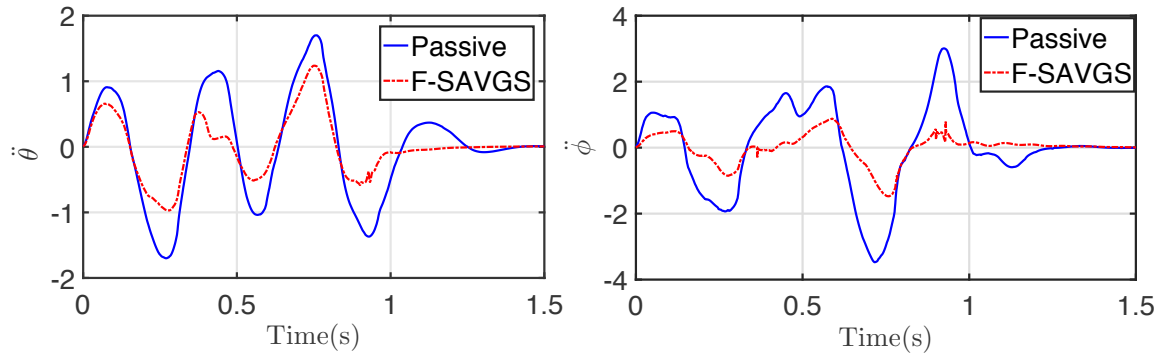

Fig. 5.13 Rotational accelerations (F-SAVGS and PASSIVE) at the mass centre under smooth bump disturbance at the left wheels: (a) pitching acceleration; and (b) rolling acceleration.

5.14, the operating envelope consists of the maximum actuation torque (on the low speed side of the gearbox) $\pm 200\,N.m$, the soft constraint of the electric power $\pm 500\,\mathrm{W}$ in the driving mode (flow from the PMSM) and $\pm 1500\,\mathrm{W}$ in the regenerating mode (flow to the PMSM). The maximum single-link rotational speed is set to $\pm 13\,rad/s$. The operating locus is located inside these boundaries. Small distances between the operation edges and the power constraints exist due to the power losses in the PMSM and gearbox, which are summarised in Table. 5.5. The expression of the these losses in the actuator can be found in [11].

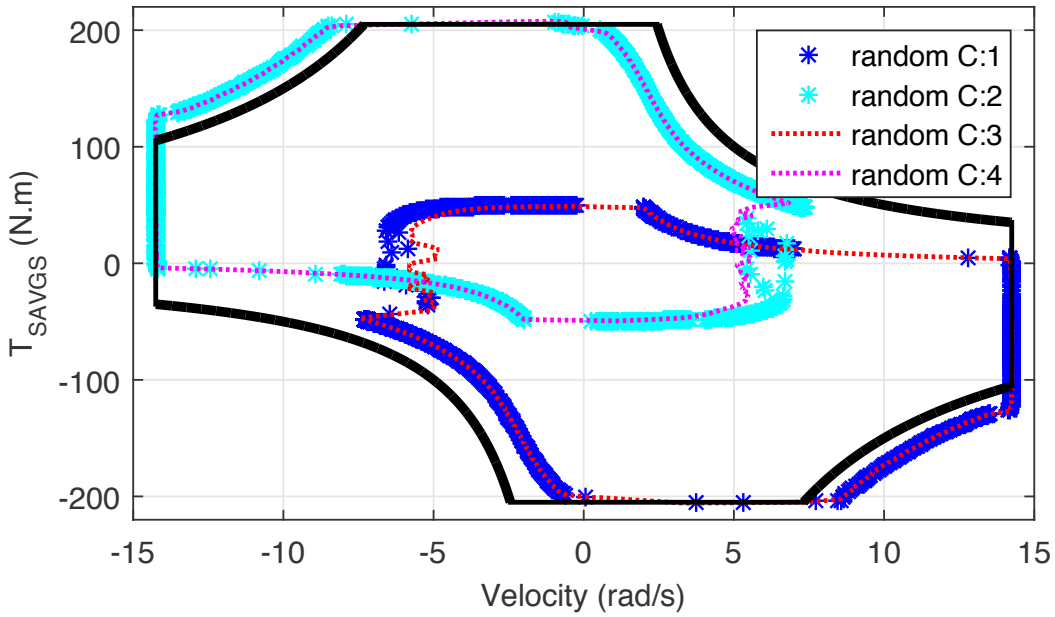

Fig. 5.14 The boundaries of the output torques vs. single-link speeds characteristics for random road C of the $\mathcal{H}_\infty$ controlled SAVGS system (F-SAVGS). 1, 2, 3, and 4 match actuators in the different corners presented in Fig.3.2.

Table 5.5 Power losses in the actuator

Component	Power losses
PMSM	Copper (resistive)
	Core (eddy current & hysteresis)
	Stray
	Mechanical (friction & windage)
Gearbox	Roller bearings, gears, seals

Fig. 5.14 clearly demonstrates that the operating points for all the simulations remain within the design and operating constraints of the real system. It also shows that under the excitation of rough road class C, the SAVGS controlled system can reach the physical limit boundaries but not to exceed them. This proves that the $\mathcal{H}_\infty$ controller can make the most efficient use of the gearbox to achieve performance specifications without sacrificing system stability. Moreover, the energy consumption of all the simulations in driving mode is less than 500 W (below rated power of the selected PMSM). This is relatively lower than the maximum energy demand (1-7 kW) of other active partially/fully loaded suspensions [54].

5.5 Conclusions

A high-performance full-car vehicle with a new concept of series active variable geometry suspension (SAVGS) has been presented in this chapter. A linear $\mathcal{H}_\infty$ SAVGS control scheme is then formulated as a closed-loop optimisation problem. Dynamic saturations and proper gains of the controller are considered to guarantee the physical and design constraints of the nonlinear SAVGS model. Through proper selection of the weighting functions, a multi-objective $\mathcal{H}_\infty$ controller is successfully obtained. The performance of the designed controller has been verified in frequency and time domain through nonlinear full-car simulations. Compared with a conventional passive suspension and the two $\mathcal{H}_\infty$ controllers obtained in previous works, the results of this $\mathcal{H}_\infty$ controlled SAVGS system, under random and bump disturbances, demonstrates the significant improvement in ride comfort and road holding of the vehicle, due to the reduction of body acceleration and tyre deflection. Moreover, to validate the robustness of the controller in realistic situations, the operation points of the controlled system have been analysed. The results show that the torque, speed, power, and single-link rotation satisfy the constraints of the actuators (PMSM+gearbox). This indicates the robust behaviour of the proposed $\mathcal{H}_\infty$ controller.

Some suggestions for future work, are:

- The outputs regarding the control objectives in this chapter are selected as sprung mass accelerations, four wheels tyre deflections, and four wheel vertical body accelerations. Among them, the sprung mass accelerations including vertical body acceleration, pitching, and rolling accelerations have a certain degree of repetition with the four wheel vertical body accelerations. In the next design, it is suggested to remove one such group of objectives to decrease the complexity of the controller design.

- Further effort can be done to improve the performance of the full-car $\mathcal{H}_\infty$ controller through extensive frequency weight tuning.

- In this Chapter and the previous Chapter, the $\mathcal{H}_\infty$ control synthesis is obtained with Autosim linearised vehicle models. The results presented in these two chapters of the SAVGS $\mathcal{H}_\infty$ -controlled schemes show that the Autosim linearised models are a good representation of the vehicle model. Meanwhile, another hand-derived linearised quarter-car model of the SAVGS was carried out by C.Arana in his work [13] which introduces another exogenous input to track the single-link position command provided by higher level controller. This enables the controller

to tackle the low frequencies disturbances to improve the suspension performance such as step steering or other cornering manoeuvres. The next chapter will focus on the construction of the full-car hand-derived vehicle SAVGS model and then investigate the SAVGS full-car $\mathcal{H}_\infty$ control scheme (FE-SAVGS) performance based on the new obtained hand-derived model.

Chapter 6

$\mathcal{H}_\infty$ CONTROL SYNTHESIS WITH HAND-DERIVED MODEL FOR FULL-CAR COMFORT AND ROAD HOLDING ENHANCEMENT

The previous chapter explored the potential of the SAVGS for ride comfort, road holding enhancement and pitching and rolling motion enhancement of the chassis in the context of high frequency vehicle dynamics. The full-car linear $\mathcal{H}_\infty$ multi-objective control framework is developed based on the linearised Autosim full-car model. The developed final controller is ultimately tested by simulations with the nonlinear full-car model with SAVGS, results are compared with the nonlinear full-car model equipped with the quarter-car controllers obtained in previous work [30] and [12] at four corners of the vehicles. The conclusion drawn from these results are that, the proposed controller in the last chapter provides the best road holding and ride comfort performance as well as the largest gain reduction for pitching and rolling motions of the chassis.

This chapter introduces a new linear equivalent hand-derived full-car model that successfully removes the main geometric nonlinearity associated with the single-link rotation of the Autosim linearised full-car model, which achieves a higher level of robustness to single-link rotations. In addition, higher level controller references are introduced for tracking of the single-link position commands as exogenous references, which are provided by the PID controller in the next chapter for good attitude control capabilities. $\mathcal{H}_\infty$ control synthesis is applied to this linear equivalent hand-derived full-car model to minimise vertical accelerations and tire deflections for all corners

of the vehicle simultaneously, and to minimise variables related to the pitching and rolling motions of the chassis.

Section 6.1.2 provides the schematic of the SAVGS linear equivalent hand-derived full-car model and the equations of motion. The frequency response of the equivalent hand-derived model at the nominal equilibrium position is also analysed. Section 6.2 constructs a linear multi-objective $\mathcal{H}_\infty$ control framework by selecting proper frequency weights. The nonlinear control scheme (FE-SAVGS) is depicted in Section 6.3, and simulation results and a comparison are provided in Section 6.4.1. Finally, conclusions are drawn in Section 6.5.

6.1 Full-car model

6.1.1 SAVGS nonlinear multi-body model

The vehicle model used in this chapter is the full-car SAVGS multi-body model (FC), which has been described previously in Section 3.1.6 in Chapter 3.

6.1.2 SAVGS linear hand-derived equivalent model

The full-car model (FL) described in Chapter 3 [9] is a high-fidelity dynamic nonlinear system that has been developed using *AutoSim* [6], which is an excellent model for virtually testing the SAVGS, to assess its performance in the context of comfort, road holding, and attitude control. However, the nonlinear full-car model is not the most suitable model for control synthesis. For the development of the $\mathcal{H}_\infty$ controller, linear models are good representative models for depicting the accuracy in the range of operating conditions of interest and for the study of the input-output relationships in the frequency domain.

In [30], a linearised AutoSim quart-car model of the SAVGS-retrofitted suspensions has been used for $\mathcal{H}_\infty$ control synthesis and the results proved that it is a good representative of the system for the SAVGS. One concern of this linearised AutoSim quarter-car model is whether this is the best representation of the system when the system is far away from its trim state (i.e. when the single-link is rotated from its default position ($\theta_{SL}^{(ne)} = 90^\circ$) or operational limits are reached). To analyse this problem, refer to Figure 4.3 in Chapter 4, where the bode plot of the quarter-car AutoSim model at the rear left corner of the GT as a function of the nominal angle offset, $\Delta\theta_{SL}^{(ne)}$, is presented. The plot depicts the effect of the nominal single-link angle on the frequency response of the SAVGS. It is observed that when the single-link rotation

angle is close to the trim state for $\mathcal{H}_\infty$ control design with $\theta_{SL}^{(ne)} = 90°$ less than $\pm 40°$, system gains are not very insensitive to single-link angle. Outside this range, the nominal AutoSim model cannot precisely estimate the gains from single-link speed, $\dot{\theta}_{SL}$, to the corresponding outputs.

In this chapter, a new full-car model with better robustness to single-link rotation is derived (see the concept in Figure 6.1), which idea is based on the previous work [12] for the quarter-car model. Instead of taking single-link velocity $\dot{\theta}_{SL\mathrm{i}}$ as the control effort, this hand-derived model introduces new signals u_{i}. External look-up tables $\alpha_{f/r}^{-1}(u)$ for front and rear axles are inserted between the vehicle plant (FC) and u_{i} that lump the main geometric nonlinearity associated with the single-link rotation of the SAVGS. When doing so, the relationship between the control effort u and system outputs y becomes strongly independent of the single-link angle. d represents the exogenous disturbances that are unrelated to the single-link position.

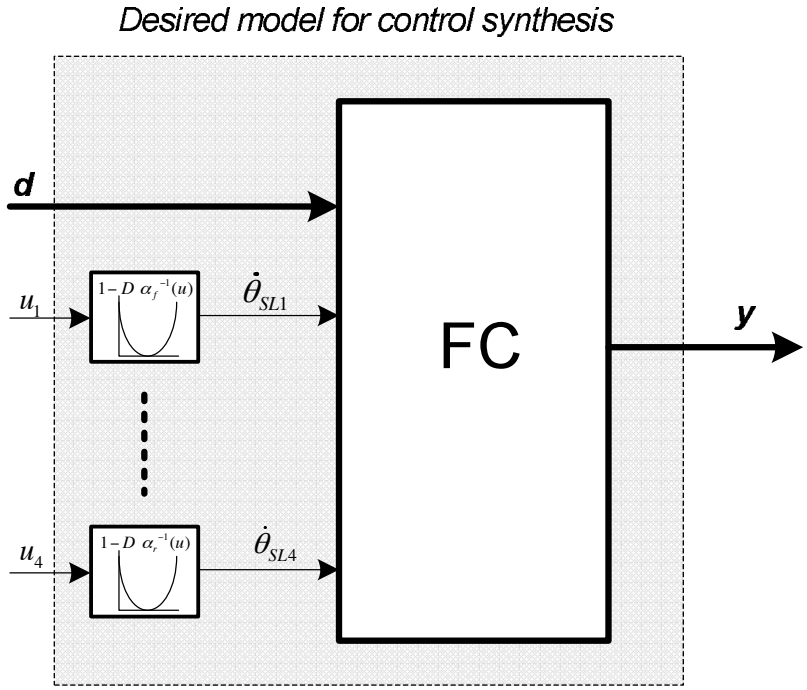

Fig. 6.1 A new model with better robustness to single-link rotation

The proposed model at the rear left corner of the GT, called the hand-derived equivalent model, is shown in Figure 6.2. Compared to the SAVGS-retrofitted double-wishbone suspension, the effect of the single-link (point G to F) can be incorporated into the equation of motions in the hand-derived model by treating it as a displacement input. Therefore, the suspension deflection (i.e. l_{s3}, the vertical distance between the centers of the sprung and unsprung masses) can now be calculated using the sum of

the deflection of the equivalent spring-damper unit (l_{SD3}) and the displacement of an equivalent linear actuator (z_{lin3}).

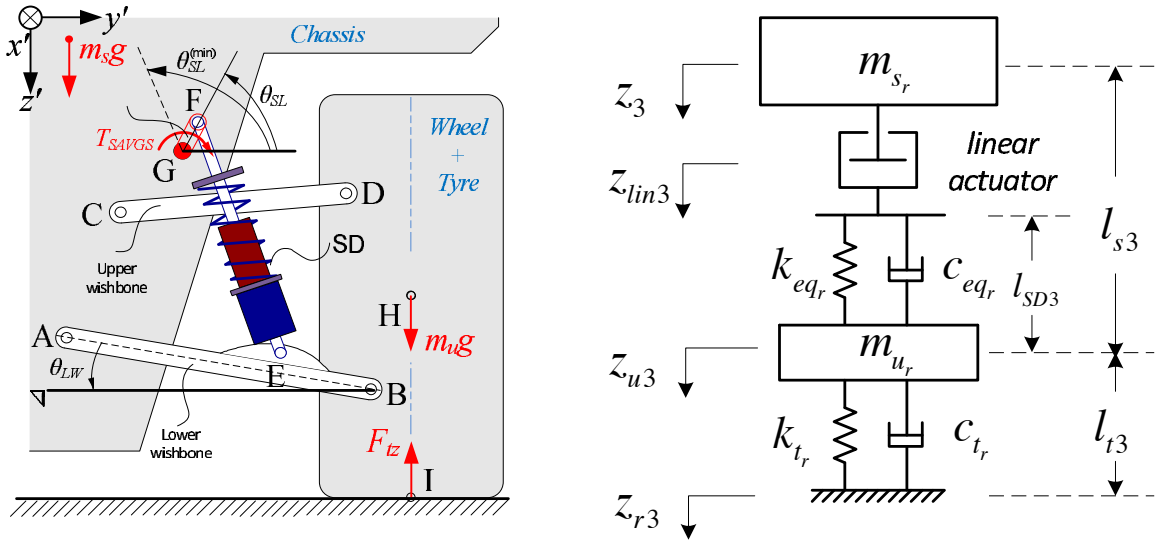

Fig. 6.2 SAVGS-retrofitted double-wishbone suspension (left) and equivalent hand-derived model of the rear left corner of the GT (right). The full-car equivalent schematic has been shown in Figure 3.8.

The schematic of the SAVGS full-car linear hand-derived model and the equations governing the dynamic motion of the hand-derived equivalent full-car model equipped with SAVGS have been described in detail in Chapter 3 Section 3.1.10. In addition, the symbols used in this chapter for the full-car SAVGS nonlinear multi-body model and linear hand-derived model has also been given in Table 3.2 in Chapter 3. In summary, by defining the following state, control input, and disturbance vectors:

$$x^T = [\dot{z}_{CM}, \dot{\theta}, \dot{\phi}, \dot{z}_{u1}, \dot{z}_{u2}, \dot{z}_{u3}, \dot{z}_{u4}, \Delta\dot{l}_{s1}, \Delta\dot{l}_{s2}, \Delta\dot{l}_{s3}, \Delta\dot{l}_{s4}, \Delta\dot{l}_{t1}, \Delta\dot{l}_{t2}, \Delta\dot{l}_{t3}, \Delta\dot{l}_{t4}, z_{lin1}, z_{lin2}, z_{lin3}, z_{lin4}]$$

$$u^T = [\dot{z}_{r1}, \dot{z}_{r2}, \dot{z}_{r3}, \dot{z}_{r4}, T_p, T_r, \dot{z}_{lin1}, \dot{z}_{lin2}, \dot{z}_{lin3}, \dot{z}_{lin4}]$$

$$y^T = \left[z_{lin1}, z_{lin2}, z_{lin3}, z_{lin4}, \Delta\dot{l}_{t1}, \Delta\dot{l}_{t2}, \Delta\dot{l}_{t3}, \Delta\dot{l}_{t4}, \Delta\dot{l}_{s1}, \Delta\dot{l}_{s2}, \Delta\dot{l}_{s3}, \Delta\dot{l}_{s4}, \ddot{z}_{CM}, \ddot{\theta}, \ddot{\phi}\right]$$

the state-space equations of the hand-derived equivalent full-car model can be written as:

$$\begin{aligned} \dot{x} &= Ax + Bu \\ y &= Cx + Du \end{aligned}$$

where $A \in \mathbb{R}^{19*19}$, $B \in \mathbb{R}^{19*10}$, $C \in \mathbb{R}^{15*19}$, $D \in \mathbb{R}^{15*10}$ are system matrices.

Equivalent parameters

The full-car vehicle parameters for the GT have been listed in Table 3.5 in Chapter 3. In addition, in this equivalent car model, the effects of the single-link in active suspension are considered as equivalent speed inputs (i.e. $\dot{z}_{lin1}, \dot{z}_{lin2}, \dot{z}_{lin3}$ *and* $\dot{z}_{lin4}$ in Figure 3.8), rather than the single-link velocity inputs in the SAVGS double-wishbone model. The suspension deflection is the sum of two parts: 1) the deflection of the equivalent spring-damper unit with equivalent coefficients $k_{eq_{f/r}}$ and $c_{eq_{f/r}}$, and 2) the displacement of the equivalent linear actuators, $z_{lin1}, z_{lin2}, z_{lin3}$ *and* z_{lin4}, which accounts for the contribution of the single-link angle at each corner of the vehicle.

The calculation of these equivalent properties $z_{lin\text{i}}$, $k_{eq_{f/r}}$ and $c_{eq_{f/r}}$ can be found in the SAVGS dimensioning equations (3.1) and (3.4) in Chapter 3. Figure 6.3 depicts the curves of a_f and a_r as a function of the single-link angle, $\Delta\theta_{SL} = \theta_{SL} - \theta_{SL}^{(min)}$, for the front and rear axle of the GT. The shape of a_f and a_r can be approximated to a negative parabola function with zeros at $\Delta\theta_{SL} = 0°$ and 180°, and with peak values of ∼25 mm/rad ($a_f^{(peak)}$) and ∼18.5 mm/rad ($a_r^{(peak)}$) at $\Delta\theta_{SL} = 90°$. Compared to the single-link rotation, the influence of the variation of the lower wishbone angle is reasonably small and can be neglected, as the grey bands (see Figure 6.3), which show only ∼4% difference with respect to the nominal equilibrium position (red lines), $\Delta\theta_{LW} = 0.1881\, rad$.

Figure 6.4 depicts the evolution of $k_{eq_{f/r}}$ (top row) and $c_{eq_{f/r}}$ as the function of the single-link angle $\Delta\theta_{SL}$ and the lower wishbone angle $\Delta\theta_{LW}$. To obtain a linear time invariant (LTI) model, the influence of the variation of lower wishbone angle and the single-link angle on $a_{f/r}$, $k_{eq_{f/r}}$ and $c_{eq_{f/r}}$ will be neglected. Thus, the equivalent properties in Figure 6.3 and 6.4 at the nominal equilibrium position ($\Delta\theta_{SL}^{(ne)} = \frac{\pi}{2}$ and $\Delta\theta_{LW}^{(ne)} = 0.1881$) will be used in the rest of this chapter.

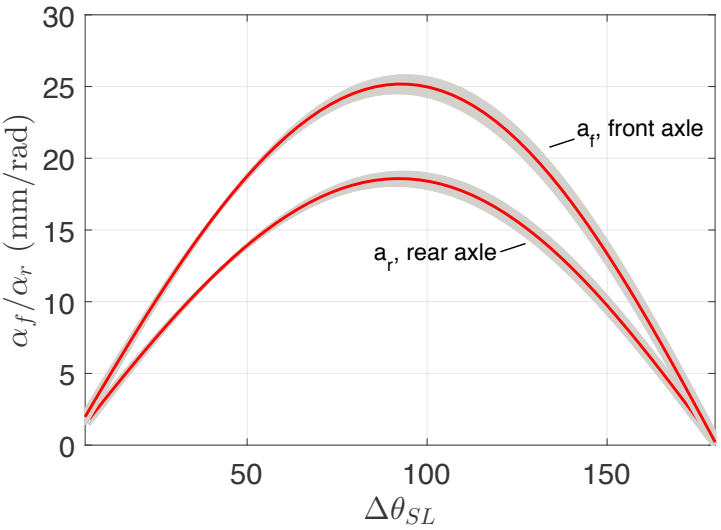

Fig. 6.3 Evolution of a_f (front axle) and a_r (rear axle) as a function of the single-link angle $\Delta\theta_{SL} = \theta_{SL} - \theta_{SL}^{(min)}$. Red lines represent the curves of a_f and a_r at the nominal equilibrium position in which $\Delta\theta_{LW} = 0.1881\, rad$. The gray bands indicate the influence of lower wishbone angular change around the nominal case, $\Delta\theta_{LW} \in [0, 0.3]\, rad$.

Frequency response of the equivalent hand-derived model

Based on the observations of Figure 4.3 in Chapter 4, the trim state of the AutoSim model corresponding to $\theta_{SL}^{(ne)} = \theta_{SL}^{min} + \Delta\theta_{SL}$ and $\Delta\theta_{SL} = 90°$ provides the best control performance. Therefore, the trim state of the linear hand-derived equivalent model can also be derived at a trim state corresponding to $\Delta\theta_{SL} = 90°$, at the four corners of the vehicle. To obtain a LTI system for linear control synthesis, the equivalent coefficients $k_{eq_{f/r}}$ and $c_{eq_{f/r}}$ can be computed through (3.4) at $\Delta\theta_{SL}^{(ne)} = \frac{\pi}{2}$ and $\Delta\theta_{LW}^{(ne)} = 0.1881$.

For the front axle:

$$\begin{aligned} k_{eq_f}^{(ne)} &= k_{eq_f}(\Delta\theta_{SL}^{(ne)} = \frac{\pi}{2}, \Delta\theta_{LW}^{(ne)} = 0.1881) = 3.5409 * 10^4 N/m \\ c_{eq_f}^{(ne)} &= c_{eq_f}(\Delta\theta_{SL}^{(ne)} = \frac{\pi}{2}, \Delta\theta_{LW}^{(ne)} = 0.1881) = 1.4925 * 10^3 Ns/m \end{aligned}$$

And for the rear axle:

$$\begin{aligned} k_{eq_r}^{(ne)} &= k_{eq_r}(\Delta\theta_{SL} = \frac{\pi}{2}, \Delta\theta_{LW} = 0.1881) = 5.8963 * 10^4 N/m \\ c_{eq_r}^{(ne)} &= c_{eq_r}(\Delta\theta_{SL} = \frac{\pi}{2}, \Delta\theta_{LW} = 0.1881) = 2.0274 * 10^3 Ns/m \end{aligned}$$

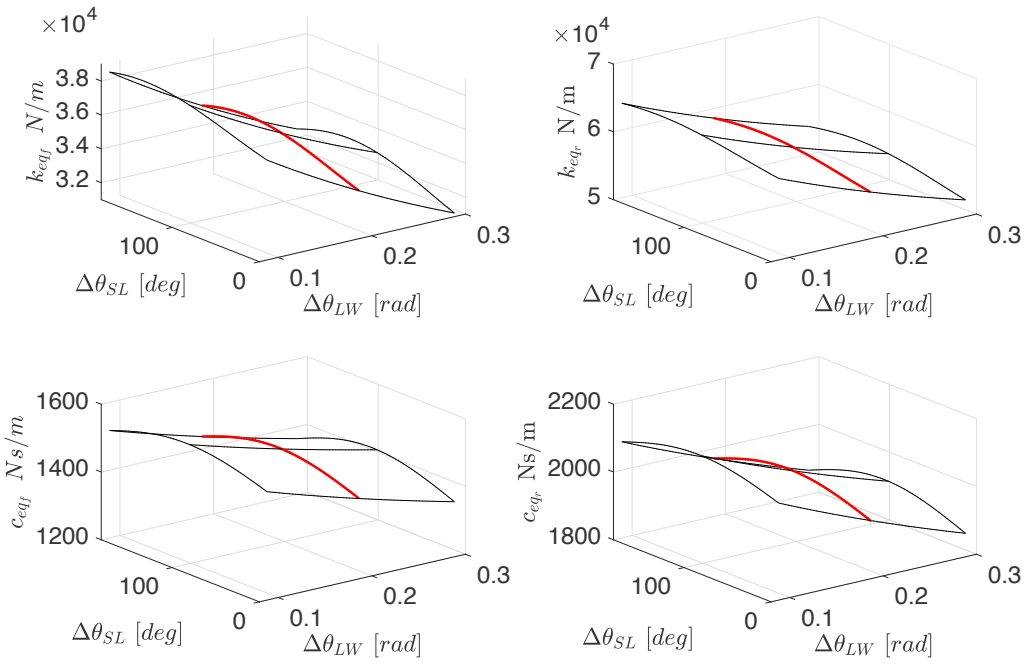

Fig. 6.4 Evolution of $k_{eq_{f/r}}$ (top row) and $c_{eq_{f/r}}$ (bottom row). The red lines represent the curves of $k_{eq_{f/r}}$ and $c_{eq_{f/r}}$ at the nominal equilibrium position in which $\Delta\theta_{LW} = 0.1881\,rad$.

The main input-output frequency responses of the hand-derived equivalent model at the trim state are shown in Figure 6.5.

The following points can be observed from the frequency response plot in Figure 6.5 at the trim state:

- The top row shows that the body acceleration at the centre of the mass displays the typical double-hump response to road disturbance: first at the sprung mass resonance frequency and later at the unsprung mass resonance frequency. The equation of calculating the unsprung mass resonance frequency is approximately given by $\sqrt{\frac{k_{t_{f/r}}}{m_u}}$, which is the same expression as the invariant point for sprung mass acceleration. Thus, regardless of how the active suspension control law (i.e. $\dot{z}_{lini}$) is chosen, the sprung mass acceleration will not be changed at the unsprung mass resonance frequency. Therefore, dynamic weighting functions should be selected to reduce the sprung mass acceleration at the sprung mass resonance frequency, and to avoid any deterioration in all three control objectives at the unsprung mass resonance frequency.

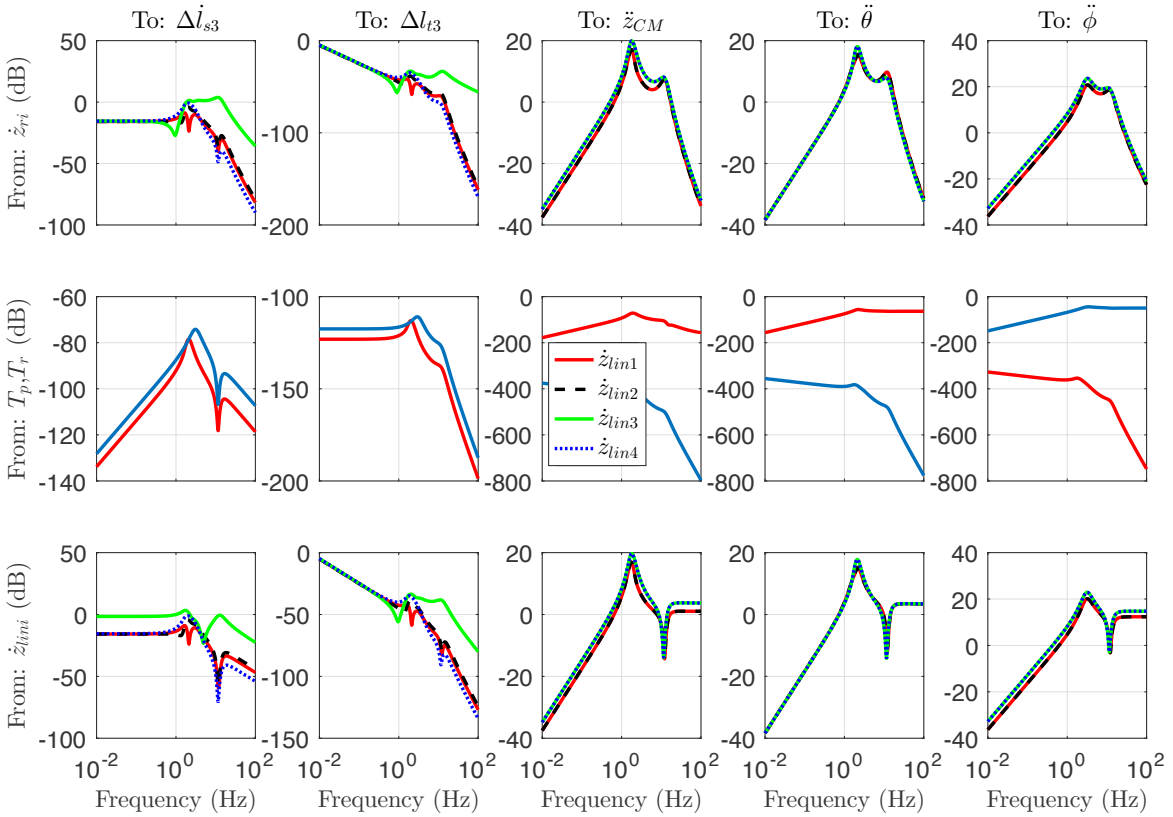

Fig. 6.5 Frequency response from the exogenous disturbances (i.e. road speed at four corners (top), pitch and roll torque at CM (middle), and the speeds for the equivalent linear actuators (bottom), to suspension velocity and tyre deflection at the rear left corner of the GT (left two columns), and vertical, pitching and rolling accelerations at CM (right three columns). The results are obtained at the nominal single-link angle $\theta_{SL}^{(ne)} = \theta_{SL}^{min} + 90°$.

- The left two columns are the output responses of the tyre deflection and suspension velocity at the rear left corner of the GT. It is observed that the green lines, associated with the exogenous disturbances at the rear left corner of the GT, have much higher frequency gain (average ∼30 dB) at the frequency range of interest (1-10 Hz). This indicates that the tyre and suspension responses at each corner of the GT are mainly affected by exogenous disturbance at that corner. Therefore, the dynamic weighting functions on tyre deflections and suspension velocities can inherit the idea that is used to tackle the quarter-car control problem in Chapter 4.

- The middle row shows that, at the centre of the sprung mass, frequency response of the vertical acceleration, and pitching acceleration have higher frequency gain

to the exogenous pitch torque disturbance T_p than the roll torque disturbance T_r. The opposite characteristics are observed for the frequency response of the rolling acceleration. As in [ISO 2613-1:1997] [82] the vertical body acceleration is considered as the main criteria for passenger ride comfort performance, the frequency weights on pitch torque could be selected larger than the weights on the roll torque to emphasise the ride comfort properties, by minimising the body vertical acceleration.

- The last row shows the results obtained for the case with speeds for the equivalent linear actuators as inputs, which will be chosen as the control efforts in the next section. Slopes at the low frequencies remain constant for suspension velocity which indicates that the SAVGS has the capability to provide attitude control at low frequency ranges (f $<$ 1 Hz), by a higher level controller that will be developed in the next chapter. At high frequencies, the suspension deflection and tyre deflection transfer function roll off at -40 dB/decade, which indicates that it is very hard to improve the road holding properties at high frequencies. On the other hand, the sprung mass transfer functions have a constant high frequency asymptote implying that ride comfort can be improved at a high frequency range within the space travel limits.

6.2 $\mathcal{H}_\infty$ control design

6.2.1 Control objectives

In this section, the control objectives are achieved by constructing a full-car $\mathcal{H}_\infty$ multi-objective control framework based on the hand-derived equivalent state-space formula, which is formulated as a disturbance rejection problem to exploit linearised dynamics of the closed-loop system. To emphasise the importance of the control objectives in the frequency ranges of interest, the closed-loop system is thus augmented by selecting frequency weights on the relevant input-output paths. The control objectives of this chapter are briefly summarised as follows:

1. In the low frequencies (f $<$ 2 Hz), the tracking of the single-link position commands as exogenous references, provided by higher level controllers should be considered. These references will be generated by the PID controller in the next chapter for good attitude control capabilities.

2. In the frequency range $2 \sim 8$ Hz, where humans are most sensitive to variation, significant reduction should be achieved in vertical body acceleration, pitching, and rolling acceleration at the centre of the sprung mass to improve passenger ride comfort. Vertical body acceleration is the prioritised control objective according to the description in [ISO 2613-1:1997] [82].

3. The gains of tyre deflections at each corner of the GT should be reduced in the frequency range of $1 \sim 5$ Hz for improvement in road holding properties.

4. The control efforts (the speeds for the equivalent linear actuators) should mainly work in frequencies lower than 20 Hz to prevent power consumption on very high frequencies for the region of non-interest. The magnitude of the speeds for the actuators should be limited to protect the gearbox and motor.

6.2.2 Robust control scheme

Figure 6.6 shows the closed-loop $\mathcal{H}_\infty$ control structure augmented with frequency weights, where the weighting function blocks and signal labelling will be described in this section. The thin blocks and signals are singular weighting functions and signals at the mass centre of the vehicle model. However, the bolded blocks and signals contain four weighting functions and signals at each of the four corners of the vehicle model. For example, frequency weights $\mathbf{W_{ref}}$ correspond to diag(W_{ref1}, W_{ref2}, W_{rer3}, W_{ref4}) and $\mathbf{b_I^T}$ is equal to [b_1, b_2, b_3, b_4].

The frequency weights on the exogenous disturbances and control objectives, W_d = diag($\mathbf{W_{ref}}, \ldots, \mathbf{W_{lp}}$) and W_z=diag($\mathbf{W_{act}}, \ldots, W_{cmr}$), are selected to emphasise the frequency regions of most significant disturbance strength and most importance to system performance, respectively. $\tilde{\mathbf{d}}$ and $\tilde{\mathbf{z}}$ are modelled as normalised signals $\mathbf{d}$ and $\mathbf{z}$ shaped by the weighting functions W_d and W_z, respectively, given as:

$$\tilde{\mathbf{d}} = \mathbf{W_d}\mathbf{d}, \quad \mathbf{z} = \mathbf{W_z}\tilde{\mathbf{z}}$$

With the frequency weights W_d and W_z augmented into the state-space representation, P_ω is ready for $\mathcal{H}_\infty$ controller design and analysis.

The selection of the frequency weights in W_d and W_z, exogenous disturbances, control objectives, and measurement signals for the $\mathcal{H}_\infty$ control synthesis are described as follows. The scaling factors in front of the weighting functions reflect the relative importance of each regulated input and output.

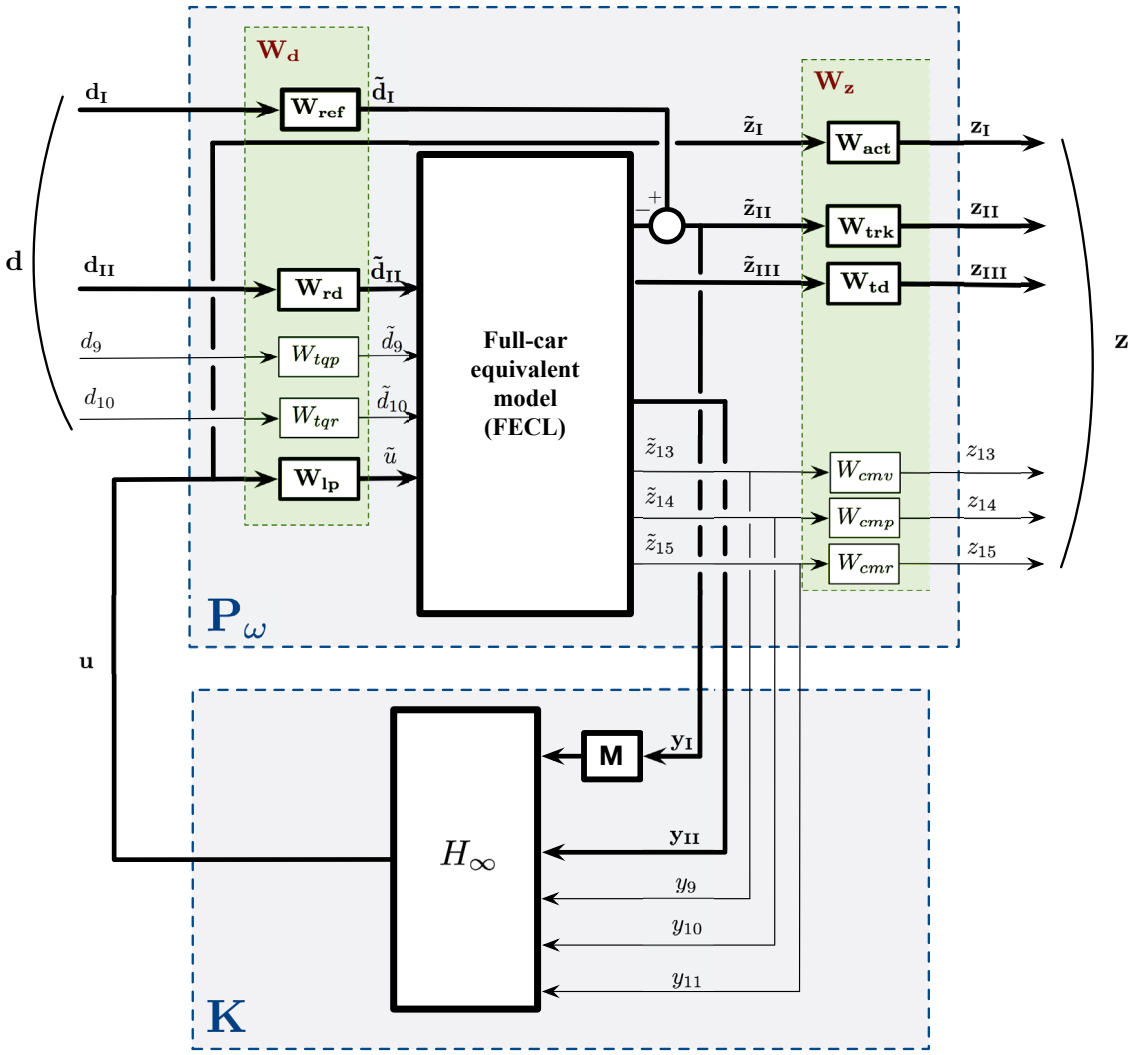

Fig. 6.6 Interconnection for $\mathcal{H}_\infty$ control synthesis.

Exogenous disturbances, d, and frequency weights

Ten inputs are considered in this chapter for the control synthesis, which can be categorised into three parts: 1) the rate of change of the road heights at each of the four corners of the vehicle model; 2) exogenous position commands for the single-links at each of the four corners of the vehicle model; and 3) pitch and roll torque at the centre of the sprung mass.

The exogenous references of the single-link position, $\tilde{\mathbf{d}}_\mathbf{I}^\mathbf{T}=[\tilde{d}_1, \tilde{d}_2, \tilde{d}_3, \tilde{d}_4]=[z_{lin1}^{(e)}, z_{lin2}^{(e)}, z_{lin3}^{(e)}, z_{lin4}^{(e)}]$, in low frequencies (f<2 Hz) are provided by the higher level controllers. These references will be generated by the PID controller in the next chapter to increase ground clearance and to compensate for road disturbance and load transfer during turn-

ing manoeuvres, and acceleration and braking. In this hand-derived equivalent model, the equivalent displacement $z_{lin\mathrm{i}}^{(e)}$ is the corresponding parameter to represent the single-link rotate angle. The frequency weights (i.e. $\mathbf{W_{ref}}$=diag(W_{ref1}, W_{ref2}, W_{rer3}, W_{ref4})) for the exogenous references are chosen as low pass filters with a cut-off frequency of 2 Hz and the zero frequency gain is defined related to the maximum equivalent displacement $z_{lin\mathrm{i}} \approx 0.02m$ corresponding to the maximum single-link rotation (i.e. $\Delta\theta_{SL} = 0°$ or 180°). This gives:

$$W_{ref1} = W_{ref2} = W_{ref3} = W_{ref4} = 0.02 * \frac{1}{\frac{1}{2*\pi*1}s + 1}$$

The rates of change in road heights, $\tilde{\mathbf{d}}_{\mathbf{II}}^{\mathbf{T}}$=[$\tilde{d_5}$, $\tilde{d_6}$, $\tilde{d_7}$, $\tilde{d_8}$]=[$\dot{z}_{r1}$, $\dot{z}_{r2}$, $\dot{z}_{r3}$, $\dot{z}_{r4}$], at each of the four corners of the vehicle model are considered as the main exogenous disturbances on the active suspension system. Bump, step and random road are the main excitations to evaluate through simulations in the literature, which introduce large amounts of energy from the wheel to the chassis in a wide range of spatial frequencies. Typically, 0.01 to 10 cycles/m are most relevant based on [ISO 8606:1995] [85]. The frequency weights (i.e. $\mathbf{W_{rd}}$=diag(W_{rd1}, W_{rd2}, W_{rd3}, W_{rd4})) selected for the road height changes are:

$$W_{rd1} = W_{rd2} = W_{rd3} = W_{rd4} = 0.25$$

The rotational motion during braking, accelerating and turning manoeuvres are captured in the model by the external pitch ($\tilde{d_9} = T_p$) and roll ($\tilde{d_{10}} = T_r$) torques acting at the centre of the sprung mass. The scaling factor of the frequency weights for pitch and roll torque are related to the maximum torques of the maximum lateral and braking accelerations, which are relative to the force causing rotational motions on the front/rear wheels times the perpendicular distance to the centre of the vehicle. The constant weights (i.e. W_{tqp} and W_{tqr}) selected for the pitch and road torque are:

$$W_{tqp} = 4350$$

$$W_{tqr} = 2700$$

To conclude, the 10 input vector representing the exogenous disturbances is defined as:

$$\tilde{\boldsymbol{d}}^{\boldsymbol{T}} = [\tilde{\boldsymbol{d}}_{\boldsymbol{I}}, \tilde{\boldsymbol{d}}_{\boldsymbol{II}}, \tilde{d_9}, \tilde{d_{10}}] = [z_{lin1}^{(e)}, z_{lin2}^{(e)}, z_{lin3}^{(e)}, z_{lin4}^{(e)}, \dot{z}_{r1}, \dot{z}_{r2}, \dot{z}_{r3}, \dot{z}_{r4}, T_p, T_r]$$

Control objectives, z, and frequency weights

The control objectives in this chapter, which have also been summarised in Section 6.2.1, are: 1) to minimise the tracking errors between the single-link position references that are provided by the higher level controller and the single-link angle outputs of the vehicle model. In the hand-derived equivalent model, z_{lin} is used to account for the effect of the single-link angle; 2) to improve ride comfort that is qualified through the vertical, pitching, and rolling accelerations; 3) to improve road holding by reducing the tyre deflections at the four corners of the vehicle model; and 4) to penalise the high speeds for the equivalent linear actuators, thus ensuring the power and torque limits of the actuators are not exceeded.

Weighting functions (i.e. $\mathbf{W_{act}}$=diag(W_{act1}, W_{act2}, W_{act3}, W_{act4})) are defined as high-pass filters to penalise high-frequency content of the speeds for the equivalent linear actuators $\tilde{\mathbf{z}}_\mathbf{I}^\mathbf{T}$=[$z_1$, z_2, z_3, z_4]=[$\dot{z}_{lin1}$, $\dot{z}_{lin2}$, $\dot{z}_{lin3}$, $\dot{z}_{lin4}$] and thus limit the control bandwidth:

$$W_{act1} = W_{act2} = W_{act3} = W_{act4} = 0.15 * \frac{\frac{1}{(2*\pi*10)^2}s^2 + \frac{2}{2*\pi*10}s + 1}{\frac{1}{(2*\pi*100)^2}s^2 + \frac{2}{2*\pi*100}s + 1}$$

Tracking errors, $\tilde{\mathbf{z}}_\mathbf{II}^\mathbf{T}$=[$z_5$, z_6, z_7, z_8]=[$z_{lin1}^{(e)} - z_{lin1}$, $z_{lin2}^{(e)} - z_{lin2}$, $z_{lin3}^{(e)} - z_{lin3}$, $z_{lin4}^{(e)} - z_{lin4}$], are considered as one control objective so that the vehicle's single-link angle is able to follow the desired reference signals provided by the higher level controller to tackle the low frequency attitude control problems. The frequency regions of the weighting functions for the tracking errors are given as low pass filters, which should not overlap the frequency weights for the control of acceleration and tyre deflection objectives over the frequency range 2∼10 Hz. The weights (i.e. $\mathbf{W_{trk}}$=diag(W_{trk1}, W_{trk2}, W_{trk3}, W_{trk4})) are chosen as:

$$W_{trk1} = W_{trk2} = W_{trk3} = W_{trk4} = 0.006 * \frac{\frac{1}{2*\pi*120}s + 1}{\frac{1}{2*\pi*0.3}s + 1}$$

The main control objectives in this chapter are to improve passenger ride comfort and road holding performance. For ride comfort, minimising the vertical $\tilde{z_{13}} = \ddot{z}_{CM}$, pitching $\tilde{z}_{14} = \ddot{\theta}$ and rolling $\tilde{z}_{15} = \ddot{\phi}$ acceleration at the centre of the sprung mass are the major targets of control synthesis. For road holding, the dynamic tyre deflections, $\tilde{\mathbf{z}}_\mathbf{III}^\mathbf{T}$=[$z_9$, z_{10}, z_{11}, z_{12}]=[Δl_{t1}, Δl_{t2}, Δl_{t3}, Δl_{t4}], at each corner of the vehicle model are also set to be penalised in some frequency range. According to [ISO:2631-1:1997] [82], the sensitive frequencies of the human body are 1∼2 Hz for rotational motions and 2∼10 Hz for vertical acceleration. It is also noted that, in [ISO:2631-1:1997] [82], vi-

bration on the vertical direction is defined as the principal factor related to the health and comfort of the passenger. On the other hand, the measurement of rotational vibrations is defined as an additional factor of vibration effects on comfort. Therefore, in this work, the gain on the vertical acceleration is selected to be higher than the pitching and rolling accelerations. In addition, as the SAVGS PID controller in the next chapter is designed as a roll focus controller, the gain on the pitching acceleration in this chapter is selected higher than the rolling acceleration to counterbalance the overall control. The ride comfort (i.e. W_{cmv}, W_{cmp} and W_{cmr}) frequency weights are chosen as low pass filter, and road holding (i.e. $\mathbf{W_{td}}$=diag(W_{td1}, W_{td2}, W_{td3}, W_{td4})) performance weights are selected as band-pass filter to penalise the disturbances between 1∼5 Hz:

$$W_{cmv} = 3 * \frac{1}{\frac{1}{2*\pi*20}s + 1}$$

$$W_{cmp} = 4.8 * \frac{1}{\frac{1}{2*\pi*1}s + 1}$$

$$W_{cmr} = 1.44 * \frac{1}{\frac{1}{2*\pi*1}s + 1}$$

$$W_{td1} = W_{td2} = 0.5 * \frac{\frac{1}{2*\pi*0.001}s + 1}{\frac{1}{(2*\pi)^2*5}s^2 + \frac{6}{2*\pi*5}s + 1}$$

$$W_{td3} = W_{td4} = \frac{\frac{1}{2*\pi*0.001}s + 1}{\frac{1}{(2*\pi)^2*5}s^2 + \frac{6}{2*\pi*5}s + 1}$$

To conclude, the 15 output vector representing the control objectives is defined as:

$$\begin{aligned}\tilde{\boldsymbol{z}}^{\boldsymbol{T}} &= [\tilde{\boldsymbol{z}}_{\boldsymbol{I}}, \tilde{\boldsymbol{z}}_{\boldsymbol{II}}, \tilde{\boldsymbol{z}}_{\boldsymbol{III}}, \tilde{z}_{13}, \tilde{z}_{14}, \tilde{z}_{15}] \\ &= [\dot{z}^*_{lin1},\ \dot{z}^*_{lin2},\ \dot{z}^*_{lin3},\ \dot{z}^*_{lin4},\ z^{(e)}_{lin1} - z_{lin1},\ z^{(e)}_{lin2} - z_{lin2},\ z^{(e)}_{lin3} - z_{lin3}, \\ &\quad z^{(e)}_{lin4} - z_{lin4}, \Delta l_{t1},\ \Delta l_{t2},\ \Delta l_{t3},\ \Delta l_{t4},\ \ddot{z}_{CM},\ \ddot{\theta},\ \ddot{\phi}]\end{aligned}$$

Measurement signals, y, and frequency weights

The measurement signals used by the feedback controller are chosen based on the availability of the sensors in the lab, and the literature review of common sensors is used for active suspension control. In summary, uniaxial accelerometers are used

to detect accelerations at the centre of the sprung mass with regards to passenger ride comfort, and LVDT linear position sensors are used to measure the suspension deflection velocity pertaining to road holding performance. Encoders are embedded to measure the single-link angle and are then converted to the equivalent displacement for calculating tracking errors.

In addition, to cancel the steady-state tracking error, free integrators (bolded block $\mathbf{M}$=diag(M_1, M_2, M_3, M_4) in Figure 6.6) are included before the tracking errors are fed back to the $\mathcal{H}_\infty$ controller. Thus, the transfer function of M for 'loop shaping' is absorbed into the final controller K such that the final controller is found by post-multiplying. The transfer functions of $\mathbf{M}$ have been selected as:

$$M_1 = M_2 = M_3 = M_4 = \frac{8}{s}$$

The 11 vectors of measurement signals are defined as:

$$\begin{aligned} \boldsymbol{y^T} &= [\boldsymbol{y_I}, \boldsymbol{y_{II}}, y_9, y_{10}, y_{11}] \\ &= [z^{(e)}_{lin1} - z_{lin1},\ z^{(e)}_{lin2} - z_{lin2},\ z^{(e)}_{lin3} - z_{lin3},\ z^{(e)}_{lin4} - z_{lin4}, \Delta\dot{l}_{s1},\ \Delta\dot{l}_{s2},\ \Delta\dot{l}_{s3},\ \Delta\dot{l}_{s4}, \\ &\quad \ddot{z}_{CM},\ \ddot{\theta},\ \ddot{\phi}] \end{aligned}$$

where

$\mathbf{y_I^T}$=$[z^{(e)}_{lin1} - z_{lin1},\ z^{(e)}_{lin2} - z_{lin2},\ z^{(e)}_{lin3} - z_{lin3}, z^{(e)}_{lin4} - z_{lin4}]$ and $\mathbf{y_{II}^T}$=$[\Delta\dot{l}_{s1}, \Delta\dot{l}_{s2}, \Delta\dot{l}_{s3}, \Delta\dot{l}_{s4}]$

Control efforts, u, and frequency weights

Due to the torque and current constraints of the inner position controllers K_{lsp} of the actuators [11] at the four corners of the vehicle, the rapid change of the single-link velocity will not be tracked precisely greater than a certain frequency (∼18 Hz). Thus, the nominal actuator dynamics are represented by the following first-order transfer functions $\mathbf{W_{lp}}$=diag(W_{lp1}, W_{lp2}, W_{lp3}, W_{lp4}):

$$W_{lp1} = W_{lp2} = W_{lp3} = W_{lp4} = \frac{1}{\frac{1}{2*\pi*17.8}s + 1}$$

The expression of the final control feedback signals to the vehicle plants are stated as follows:

$$\tilde{\boldsymbol{u}} = \mathbf{W_{lp}}\boldsymbol{u}$$

Thus, the control efforts are chosen as the reference speed of the equivalent actuators, i.e.,

$$\boldsymbol{u^T} = [u_1,\, u_2,\, u_3,\, u_4] = [\dot{z}^*_{lin1}, \dot{z}^*_{lin2}, \dot{z}^*_{lin3}, \dot{z}^*_{lin4}]$$

where $\tilde{\mathbf{u}}^{\mathbf{T}}$=$[\tilde{u}_1,\, \tilde{u}_2,\, \tilde{u}_3,\, \tilde{u}_4]$=$[\dot{z}_{lin1},\dot{z}_{lin2},\dot{z}_{lin3},\dot{z}_{lin4}]$.

The full-car linear $\mathcal{H}_\infty$ -controlled scheme in Figure 6.6 is formulated in MATLAB and controller $\mathbf{K}$ is obtained using `hinfsyn` by absorbing the integrator unit $\mathbf{M}$ into the $\mathcal{H}_\infty$ controller. The final controller is determined after several iterations by tuning the frequency weights and by adjusting the performance and the stability of the effectiveness of the proposed $\mathcal{H}_\infty$ controller in the nonlinear simulations. The Bode magnitude plot for the finalised $\mathcal{H}_\infty$ controller from 11 measurement signals $\mathbf{y}$ to the first control effort $u_1 = \dot{z}^*_{lin1}$ at the front left corner of the vehicle is shown in Figure 6.7. The Bode magnitudes from the same inputs to other control efforts at the other three corners have very similar results to the curves in Figure 6.7.The single-link position tracking error signals are low-pass filtered (see in red lines). Thus, the vehicle dealing with the control feedback signals from the higher level controller only in the low frequency range as desired. Bode plots of acceleration and suspension deflections velocity signals to the equivalent actuator velocity $\dot{z}^*_{lin1}$ at the front left corner with regards to passenger ride comfort and road holding performance are with 'bandpass' nature.

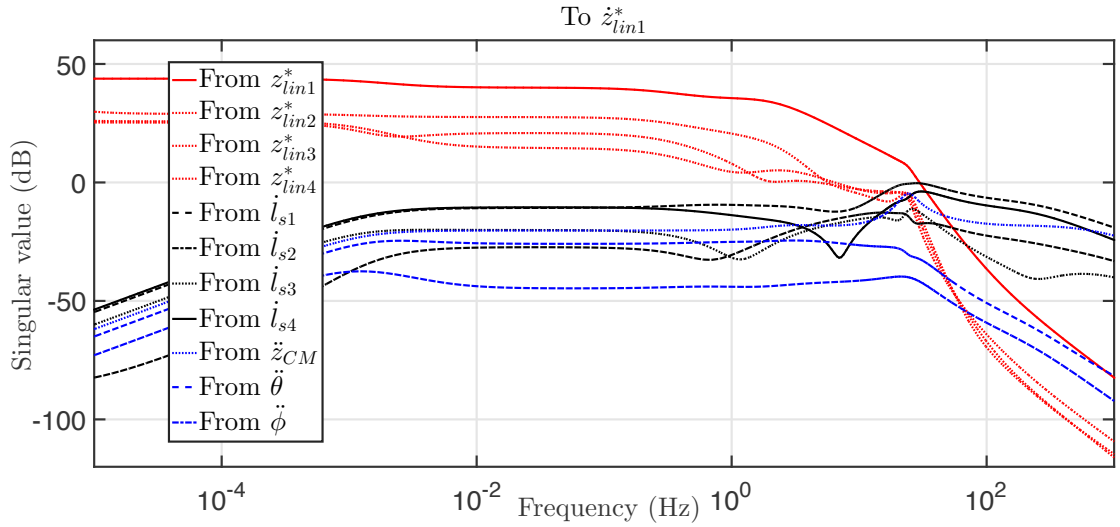

Fig. 6.7 Bode magnitude plot of controller, from 11 measurement signals $\mathbf{y}$ to the first control effort $u_1 = \dot{z}^*_{lin1}$ at the front left corner of the vehicle. The other three corners of the vehicle have very similar results to the shapes of these curves.

6.3 Nonlinear control scheme

In the last section, the proposed full-car linear $\mathcal{H}_\infty$ controller aims to minimise accelerations at the centre of sprung mass and tyre deflections for all corners of the vehicle in the context of high frequency vehicle dynamics, and to track the exogenous single-link position at low frequencies. To assess the performance of the proposed controller, it is installed on the nonlinear full-car SAVGS model (FC). The general nonlinear control scheme of this chapter is shown in Figure 6.8.

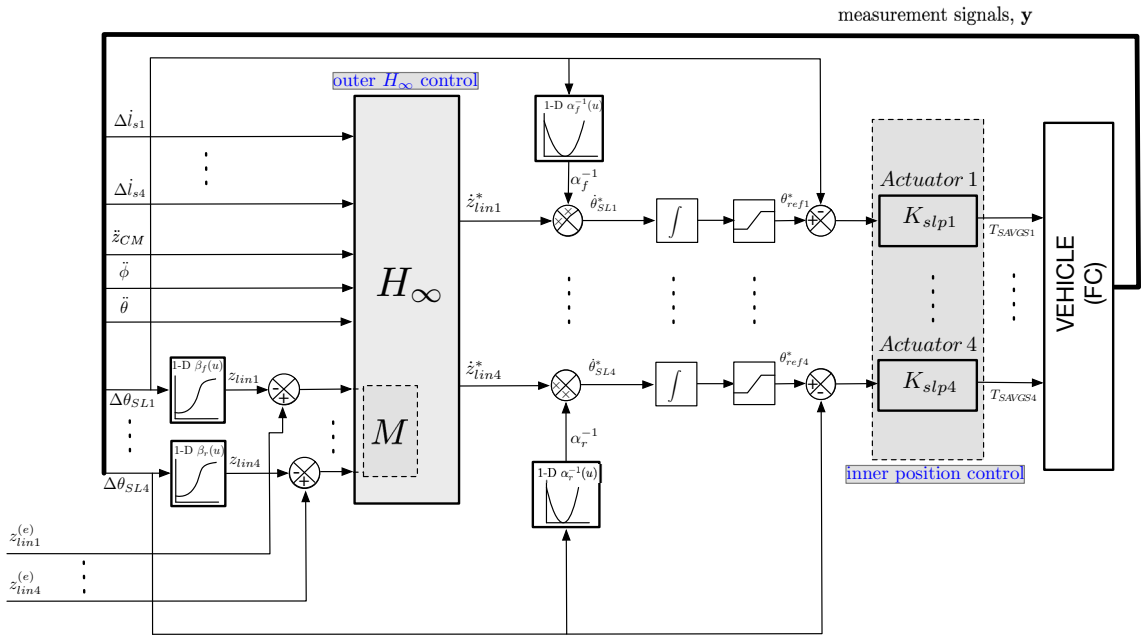

Fig. 6.8 General nonlinear control scheme (FE-SAVGS).

The closed-loop SAVGS involves two controllers which are connected in series to tackle multiple control objectives:

1. The inner position control contains the actuator (PMSM and gearbox) and the single-link position controller (K_{slpi}) at each corner of the vehicle. It measures the single-link tracking error (θ^*_{refi}-$\Delta\theta_{SLi}$) and then generates the torque $T_{\text{SAVGS}i}$ to follow the single-link position reference ($\theta^*{}_{refi}$). Meanwhile, the physical and design constraints (i.e., voltage, power, current, speed and single-link rotation limits) must also be satisfied at all times. The design of the inner position control of the SAVGS actuator and the details of the physical and design constraints have been explained in [9], and for the relevant schematic refer to Fig. 4.2.

θ^*_{refi} is obtained by integration of the control feedback of the proposed $\mathcal{H}_\infty$ controller. In practice, the SAVGS becomes ineffective when the single-link angle rotation is close to 180° , whereby the vehicle is approximately equivalent to the passive configurations and single-link offers negligible installation ratio changes. Therefore, saturation blocks are introduced between the integrators and the reference angles to guarantee the single-links operate within the chosen rotational limits ($\theta^*_{refi} \in [\theta^{(\min)}_{\mathrm{SL}}, \theta^{(\max)}_{\mathrm{SL}} - 20°]$ and $\theta^{(\max)}_{\mathrm{SL}} = \theta^{(\min)}_{\mathrm{SL}} + 180°$)

2. The outer $\mathcal{H}_\infty$ controller, which has been proposed in the last section, reads the measurement signals ($\mathbf{y}$) of the vehicle as the feedback inputs, and generates the reference single-link velocities ($\dot{\theta}^*_{\mathrm{SL}i}$) as control inputs to the vehicle plant.

   Equivalent parameters $\alpha_{f/r}$ and $\beta_{f/r}$ as a function of $\Delta\theta_{SLi}$ are used for the conversion from the reference angular speeds ($\dot{\theta}^*_{SL\mathrm{i}}$) and the angles ($\Delta\,\theta_{SL\mathrm{i}}$) for single-links to the reference linear speeds ($\dot{z}^*_{lin\mathrm{i}}$) and displacements ($z_{lin\mathrm{i}}$) for the equivalent linear actuators, respectively, giving the expressions as:

$$\begin{aligned} \dot{z}^*_{lin} &= \alpha(\Delta\theta_{SL})\dot{\theta}^*_{SL} \\ z_{lin} &= \beta(\Delta\theta_{SL}) \end{aligned}$$

   where the evolution of α_f and α_r is shown in Figure 6.5 (the red lines). β_f and β_r can be calculated through the integration of the equation (3.1). Figure 6.9 shows the evolution of β_f and β_r.

6.4 Simulation results and comparison

In this section, the nonlinear simulation results obtained for the GT car traveling on: 1) random roads with various road roughness, and 2) a smoothed bump at the left side wheels, are presented to assess the different full-car control schemes' steady-state and transient response characteristics, respectively. While the random road simulations describe the average control performance and the performance can be analysed in frequency domain, the smoothed bump emphasises the vehicle response on sudden event performance properties. The main vehicle and the SAVGS parameters for the nonlinear control scheme have been given in Tables 3.5 and 3.6 in Chapter 3. For a full-car vehicle, passenger weight changes are added close to the vehicle sprung

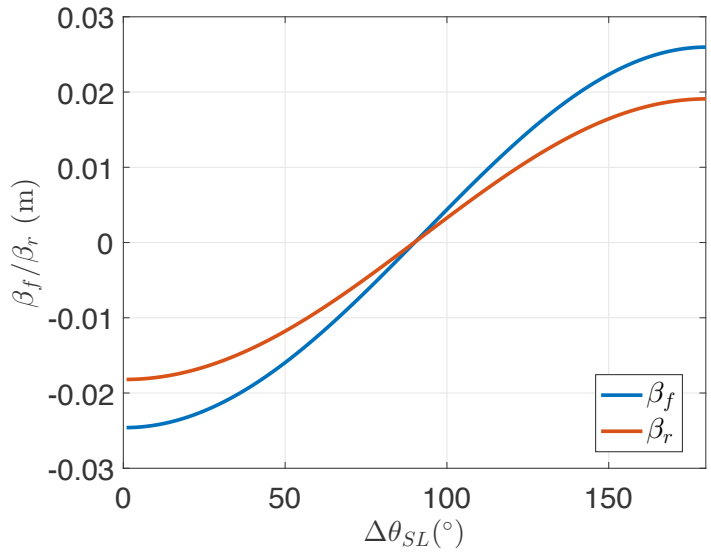

Fig. 6.9 Evolution of β_f and β_r as a function of $\Delta\theta_{SL}$.

mass centre. Hence, in this chapter, the improvement in vehicle acceleration at the centre of the sprung mass ($\ddot{z}_{CM}$) using of the $\mathcal{H}_\infty$ -controlled SAVGS systems is mainly examined. The tyre deflection and suspension deflection are also investigated for the road holding capability. Maximum allowable power, torque and single-link speed limits of the actuator (i.e. PMSM and gearbox) are applied to explore the potential of the SAVGS $\mathcal{H}_\infty$ -controlled scheme.

The following types of nonlinear control scheme have been considered in the simulations:

- Pure passive nonlinear full-vehicle system (PASSIVE).
- SAVGS $\mathcal{H}_\infty$ controller proposed in the last chapter developed based on the full-car AutoSim linearised model implemented to the passive nonlinear full-vehicle system (F-SAVGS).
- SAVGS $\mathcal{H}_\infty$ controller proposed in this chapter developed based on the full-car hand-derived equivalent model implemented to the passive nonlinear full-vehicle system (FE-SAVGS).

6.4.1 Response to random road profiles

The two full-car active control schemes and one passive nonlinear system have firstly been simulated when traveling with a constant speed of $100\,km/h$ in a longitudinal direction and a nominal angle offset $\Delta\theta_{SL}^{(ne)} = 90^\circ$. Two random roads, with the

same level of roughness are generated to excite the left and right side of the wheels in one simulation. Thus, the pitch motion of the vehicle can be assessed due to the delay of the responses on the front and rear wheels associated to the wheel base of the vehicle. Roll motion can be assessed due to the height difference between the left and right wheels according to the randomness of the two random road profiles on the two sides. $1km$ long random road sections with road class A and C (good quality road and poor quality road for the GT, see in Figure 3.10) that are generated based on the second approach in Section 3.3.3 in Chapter 3, with the values of the road parameters $n_0 = 0.1\,cycles/m$, $\Delta n = 0.005\,cycles/m$, $\omega = 2$. The class A road section contains road profile A1 and A2 on the right and left side of the vehicle respectively, and the class C road section contains road profile C1 and C2 on the right and left side of the vehicle respectively.

The PSDs for sprung mass vertical, pitching and rolling accelerations at the mass centre are presented in Figure 6.10. The main peaks ($\sim$2 Hz) in the PSDs of the vertical, pitching and rolling accelerations of controlled active suspension systems (i.e. FE-SAVGS and F-SAVGS) are significantly reduced for road A and C compared with the passive system. Specifically, regarding the vertical acceleration spectral (left column), which is the principal factor corresponding to ride comfort, the FE-SAVGS offers much better attenuation than the F-SAVGS in the frequency range of interest (1-8 Hz). At the sprung mass resonance frequency ($\sim$ 2 Hz), compared to the passive system, the FE-SAVGS achieves gain reductions of approximately 12.57 dB and 11.32 dB that are higher than 7.98 dB and 6.46 dB of the F-SAVGS, with respect to road roughness A and C. The pitching acceleration spectral (middle column) of the FE-SAVGS and F-SAVGS systems show similar improvements compared to the passive case. The rolling acceleration spectral of the FE-SAVGS system has a less gain reduction than the F-SAVGS system, which is expected due to: 1) rolling motion is the additional factor related to the health and comfort of the passenger compared to vertical acceleration; and 2) the PID controller for attitude control in the next chapter is defined as a roll focus controller to compensate for the rolling gain of the $\mathcal{H}_\infty$ control in this chapter.

The PSDs for the tyre deflections at four corners of the vehicle system with road class C are presented and compared in Figure 6.11. In the frequency range from 0.3 to the unsprung mass resonance frequency, a trade-off of attenuation and amplification is observed for the $\mathcal{H}_\infty$ controlled systems and passive systems. In the frequency range from 0.3 to 4 Hz, the FE-SAVGS controlled system shows the best attenuation of the amplitude spectra. The maximum reduction at sprung mass resonant frequency is up

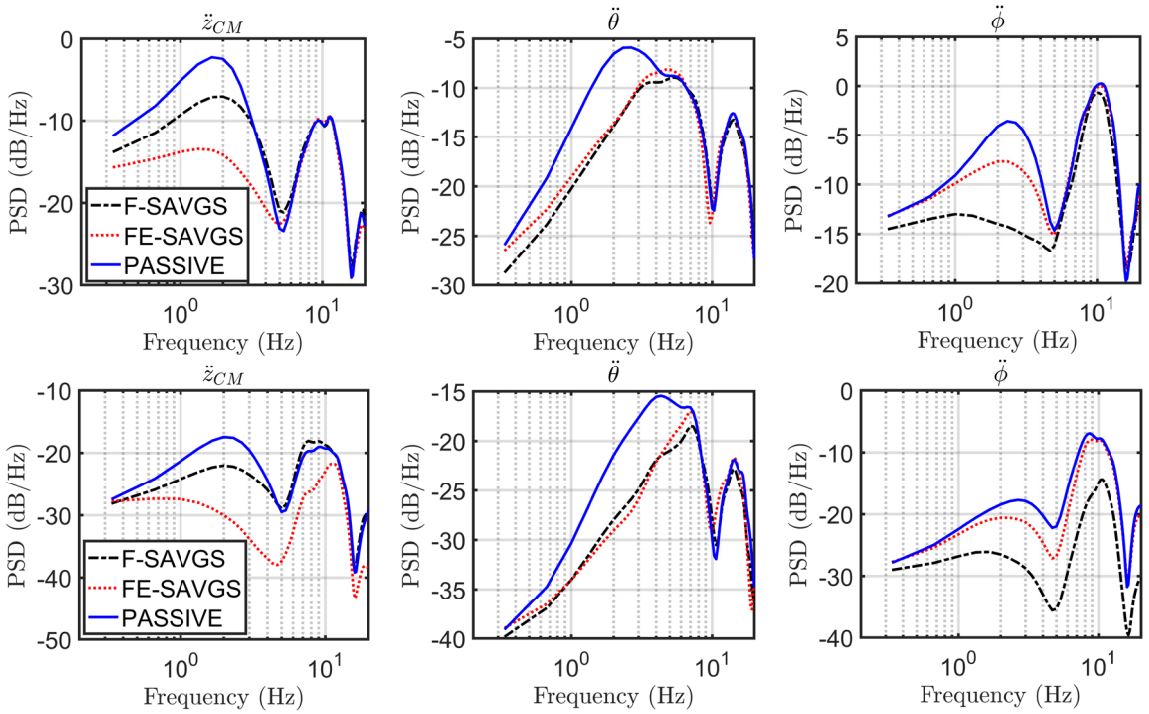

Fig. 6.10 PSDs for sprung mass vertical, pitching and rolling accelerations at the mass centre of the GT with road class A (bottom row) and C (top row).

to 3.03 dB and 8.75 dB for front and rear wheels. In the higher frequency range above 4 Hz, the FE-SAVGS and F-SAVGS controlled systems slightly amplify the responses. The tyre deflection PSDs for good quality road A are irrelevant to compare, as the tyre deflections on four corners of both active and passive systems are extremely small ($<$0.005 m).

Figure 6.12 shows the 5 s period simulation results of the FE-SAVGS and passive systems for random road class C. Figure 6.12(a) is the road profile C2 on the rear left wheel. The FE-SAVGS has a better ride comfort property compared with the passive system, due to the peak reduction at the sprung mass centre (Figure 6.12(b)-(d)). Most of the peaks for tyre deflections on the rear left wheel (Figure 6.12(e)) are also reduced, which demonstrates that the FE-SAVGS controlled system of this work is able to improve ride comfort without compromising road holding ability. The results of the other three wheels perform similarly. Figure 6.12(f) shows that the single-link angle is rotated actively within the allowable range (0-160°) to achieve the performance improvements above.

The pitch and roll angles for the random-profiled road are examined and very small rotational angles are found for random road class A and C. Specifically, the pitch angle

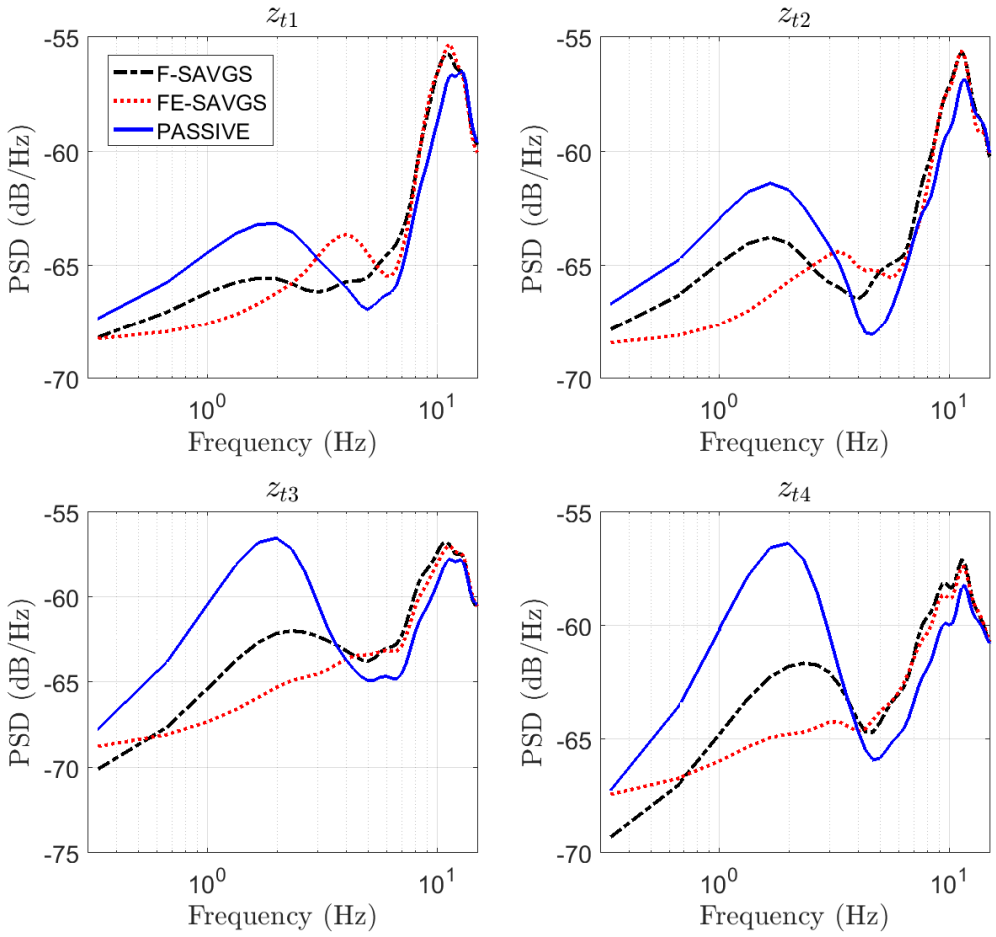

Fig. 6.11 PSDs for tyre deflections of four corners of vehicle systems with road class C.

for road class A and C are within $\pm 0.5°$ and $\pm 2°$, respectively. For the roll angle, road class A and C excited maximum roll angle does not exceed $\pm 0.1°$ and $\pm 0.5°$. Therefore, such small rotational angles will not affect the feeling of human comfort.

6.4.2 Response to a smoothed bump

To evaluate the transient response of the systems, the vehicle models are subjected to a one sided smoothed bump, with the bump only acting on the left wheels of the vehicle. This type of terrain excites both the pitch and roll motions of the sprung mass. The expression of the smoothed bump and the driving conditions of the vehicle in this section are identical to the situation in Section 4.10 in Chapter 3, where the bump height h=0.05 m and width w=2 m, at the forward speed V=20 km/h. where

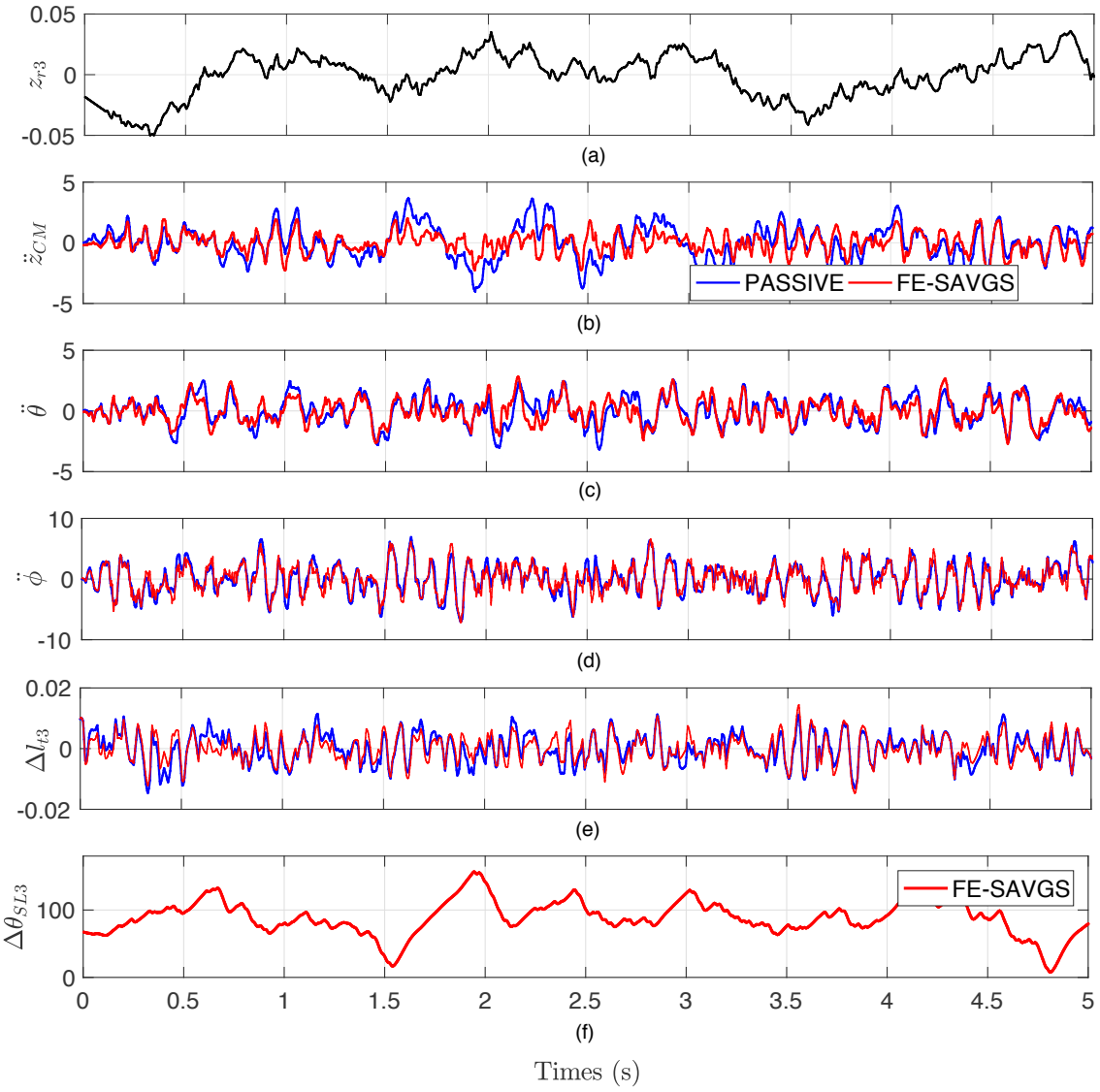

Fig. 6.12 Response time histories of vehicle systems for random class C during a 5 s period simulation.

the bump height h=0.05 m and width w=2 m, at the forward speed V=20 km/h. For the purpose of evaluating the pitch and roll mitigation, the systems only undergo bump disturbance through the left wheels of the vehicle. In time domain, the road profiles on the four tyres are given in Figure 6.13 (a).

The time histories of the vehicle models excited by this one sided smoothed bump are presented in Figure 6.13. It shows the mass centre accelerations (Figure 6.13 (b)-

(d)) and the tyre deflection at the rear left corner of the vehicle (Figure 6.13 (e)) to assess the ride comfort and road holding. By examining these plots, the FE-SAVGS and F-SAVGS exhibit better acceleration and tyre deflection attenuation with shorter settling time than passive suspension. The FE-SAVGS provides the best results in terms of superior peak reduction on vertical acceleration at the centre of the sprung mass without compromising road holding ability.

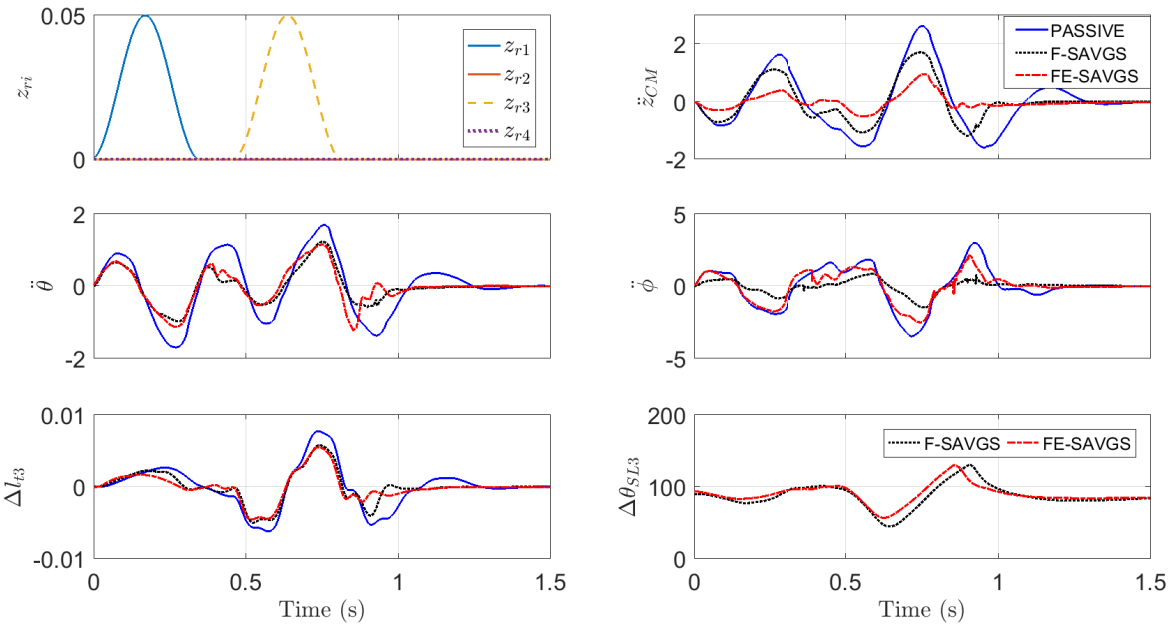

Fig. 6.13 Response time histories of vehicle systems for one side bump disturbances: (a) road inputs at four corners; (b) vertical accelerations at mass centre; (c) pitching accelerations; (d) rolling accelerations; (e) tyre deflection at rear left wheel; (f) single-link rotation for SAVGS controlled systems at rear left wheel.

6.4.3 Position controller performance

The inner position controller aforementioned in Figure 4.2 is designed to protect the PMSM and its servo-drive, to ensure the single-link rotates within its operational limits, and to set power and torque consumption by the controller. The operational limits in this chapter are identical to the constraints in Section 5.4.4, Chapter 5. The output torque-speed operating points for the actuators (i=1,...,4) are plotted in Figure 6.14 alongside the power, torque and speed constraint envelop. The most power consuming events, the poor quality random road C, is examined. Gaps between the operation points and the power constraints occur due to the power losses in the PMSM and gearbox, which are summarised in Table 5.5. Result shows that the operating points

locate within the designed constraints of the real system, therefore demonstrating the robustness behaviour of the overall controlled system.

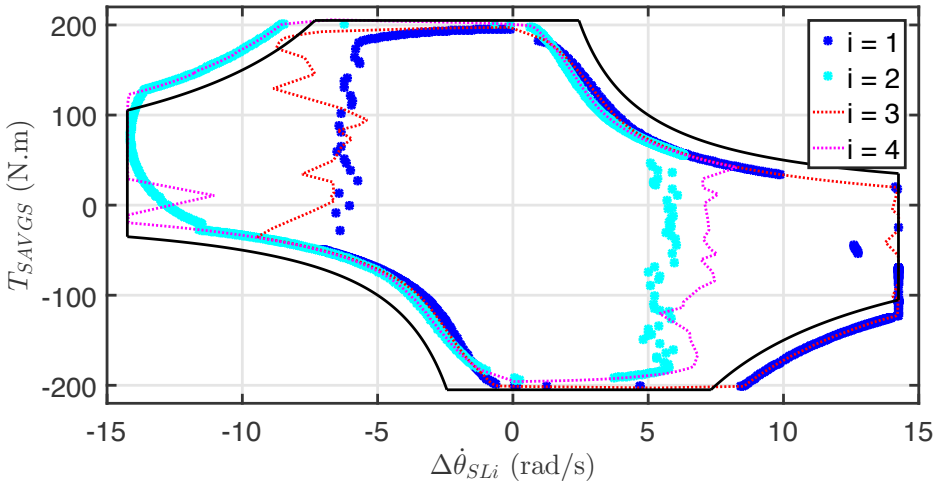

Fig. 6.14 Output torque vs. single-link velocity characteristics for random road class C (only shows the boundaries), presented in Figure 6.12. The black envelop is the actuator limit boundaries.

6.5 Conclusions

This chapter has explored the potential of the $\mathcal{H}_\infty$ control of the full-car SAVGS for ride comfort and road holding enhancement based on a new linear equivalent hand-derived full-car model. The dynamic equations are firstly obtained and include the SAVGS action through an equivalent linear displacement actuator. The equivalent parameters of the spring-damper unit are also calculated. Its main advantages over the linearised AutoSim full-car model used in Chapter 5 are: 1) it removes the main geometric nonlinearity associated with the single-link rotation when away from its equilibrium position; and 2) higher level reference commands for the single-link positions are introduced as exogenous inputs to follow the low frequencies signals provided by the PID controller in the next chapter for good attitude control ability. Through proper selection of the weighting functions, a multi-objective $\mathcal{H}_\infty$ controller was successfully obtained. The proposed controller was then applied to the nonlinear SAVGS full-car model. Comparing simulation results with the passive suspension and the SAVGS full-car $\mathcal{H}_\infty$ -controlled scheme developed in Chapter 5 to the random road and bump disturbances, the proposed controller showed the best performance in ride comfort and road holding ability. The robustness of the controller is then validated by

analysing the operation positions of the controlled system. The results show that the torque, power, and single-link rotational speed satisfy the constraints of the actuators (PMSM+gearbox). This indicates the robust behaviour of the proposed $\mathcal{H}_\infty$ controller in this chapter.

The next chapter develops an overall control framework to achieve the mitigation of attitude motions and comfort and road holding enhancement simultaneously. This can be achieved by blending the proposed controller in this chapter for high frequency vehicle dynamics control together with the attitude controller approach proposed in [10] for low frequency vehicle dynamics control. The attitude controller is a PID roll focus controller that provides single-link position references in low frequencies, which can be treated as the exogenous inputs (i.e. $\tilde{\mathbf{d}}_\mathbf{I}^\mathbf{T}=[\tilde{d}_1,\ \tilde{d}_2,\ \tilde{d}_3,\ \tilde{d}_4]=[z_{lin1}^{(e)},\ z_{lin2}^{(e)},\ z_{lin3}^{(e)},\ z_{lin4}^{(e)}]$) of the proposed controller in this chapter.

Chapter 7

Full-car overall control for combined attitude control, comfort and road holding improvement

Owing to the previous efforts and experience on SAVGS control in the context of high frequency vehicle dynamics in Chapters 4 and 5 that validated the effectiveness of $\mathcal{H}_\infty$ control application on the SAVGS quarter- and full- car configurations, and due to the previous work [12] that introduced a simplified hand-derived quarter-car linear model, it was managed to remove the main geometry nonlinearity associated with the single-link rotation when away from its equilibrium position, and a quarter-car $\mathcal{H}_\infty$ controller was then successfully synthesised.

Chapter 6, based on the foundation of previous studies, proposed an $\mathcal{H}_\infty$ control scheme of the full-car SAVGS configuration (FE-SAVGS) based on a full-car hand-derived model to demonstrate its performance improvements for passenger ride comfort and road holding ability, in the context of high frequency vehicle dynamics. The performance objectives are achieved by constructing a full-car linear $\mathcal{H}_\infty$ multi-objective control framework to minimise accelerations for the centre of the sprung mass and tyre deflection for all corners of the vehicle simultaneously. Extensive simulation results demonstrated that FE-SAVGS is the best $\mathcal{H}_\infty$ control approach on SAVGS from what has been tackled in the previous chapters due to: 1) In the frequency range of interest, FE-SAVGS offers much better attenuation performance for vertical sprung mass accelerations, which is the principal factor corresponding to ride comfort. It also achieves the superior tyre deflection reduction at the sprung mass resonance frequency. 2) The

proposed $\mathcal{H}_\infty$ controller in FE-SAVGS managed to remove the strong dependency that exists on the single-link angle, which indicates that the whole range of single-link motions is efficiently used for control. 3) Reference commands for the single-link positions are introduced as exogenous inputs that provide a possible solution to follow the low frequencies for the attitude control problem.

This chapter, aims to construct an overall control framework that achieves the mitigation of attitude motions and comfort, and road holding enhancement simultaneously. This is achieved by thoroughly blending the proposed controller in Chapter 6 for high frequency vehicle dynamics control together with the chassis attitude motions control approach based on the work already published in [12] for low frequency vehicle dynamics control. The overall control framework and the attitude control scheme is introduced in Section 7.1. In Section 7.2, a comprehensive set of manoeuvres is employed to test the performance, robustness, satisfaction of actuator, and suspension operating constraints of the overall SAVGS controlled framework with the attitude and $\mathcal{H}_\infty$ controller. Then, simulation results are ultimately compared with the results of the full-car model which is equipped with the $\mathcal{H}_\infty$ controller or the attitude controller separately. Finally, Section 7.3 has some conclusion remarks.

7.1 Overall control framework for comfort, road holding enhancement and attitude control

The overall SAVGS control framework is shown in Figure 7.1, which is the expansion of the nonlinear control scheme in Figure 6.8, in which the exogenous inputs for the single-link position references $z_{lin1}^{(e)}$ to $z_{lin4}^{(e)}$ are the outputs calculated by the attitude controller (outer PID controller) for the corresponding reference. The $\mathcal{H}_\infty$ controller and PID controller work collaboratively to tackle the ride comfort, road holding and attitude control objectives simultaneously.

7.1.1 Overall SAVGS control framework

The outer $\mathcal{H}_\infty$ controller for passenger ride comfort and road holding improvement in the context of high frequency vehicle dynamics and the inner loop controller for single-link position tracking have been covered in detail in Section 6.3.

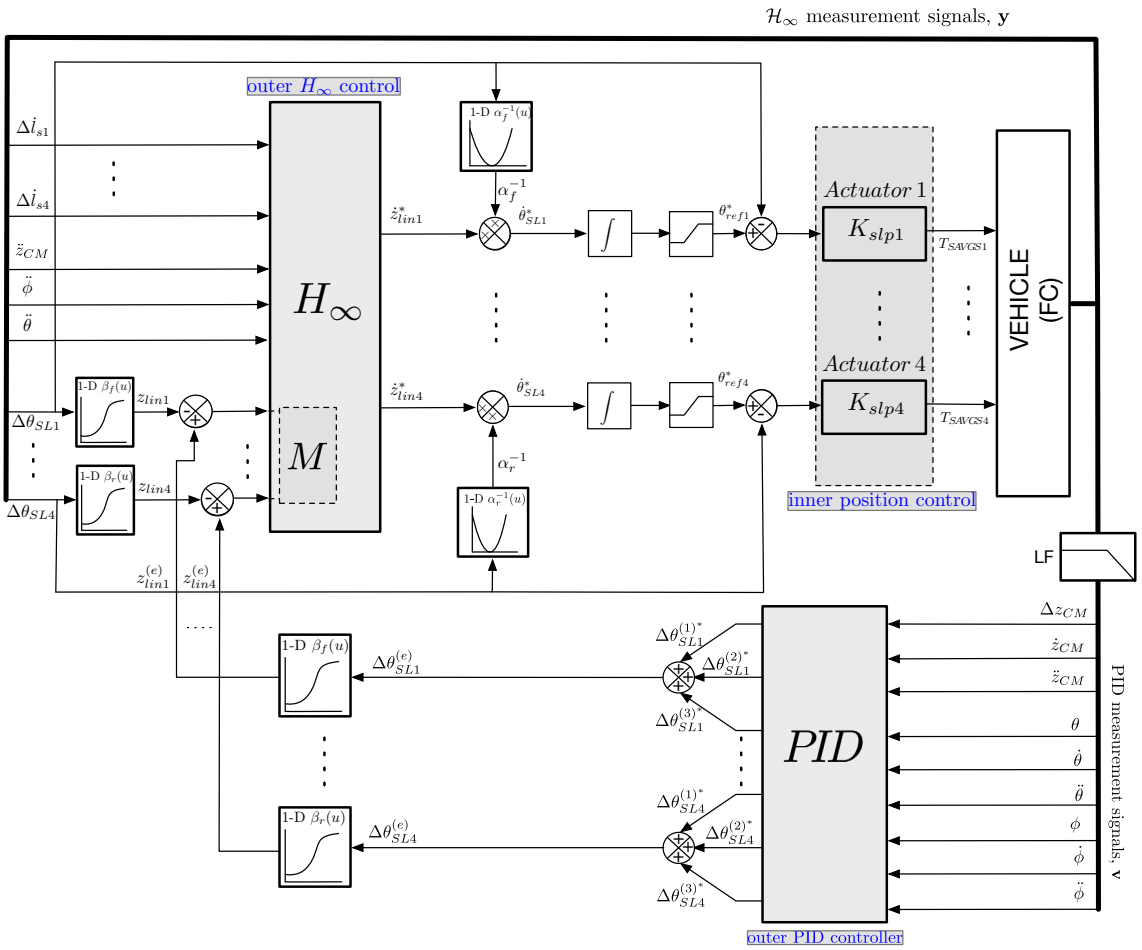

Fig. 7.1 Overall SAVGS control framework (FE-PID-SAVGS).

7.1.2 Attitude control

The attitude controller in this chapter is developed based on the previous idea in [10], which studied the effectiveness of the control of SAVGS attitude motions. In Figure 7.1, the outer PID controller calculates position references $(\Delta\theta^{(e)}_{SL1}, ..., \Delta\theta^{(e)}_{SL4})$ of the single-link actuator for each corner of the vehicle. For the corners $i = 1, ..., 4$, the position reference is the combination of three increments, where $\Delta\theta^{(1)^*}_{SLi}$ is associated with the vertical motions (heave) of the centre of the sprung mass (Δz_{CM}, $\dot{z}_{CM}$, and $\ddot{z}_{CM}$), $\Delta\theta^{(2)^*}_{SLi}$ is associated with the pitching rotations of the chassis (θ, $\dot{\theta}$, and $\ddot{\theta}$), and $\Delta\theta^{(3)^*}_{SLi}$ is associated with the rolling rotations of the chassis (ϕ, $\dot{\phi}$, and $\ddot{\phi}$).

Then, the position references $(\Delta\theta^{(e)}_{SL1}, ..., \Delta\theta^{(e)}_{SL4})$ of the single-link actuator for each corner of the vehicle are converted to the reference linear positions $(z^{(e)}_{lin1}, ..., z^{(e)}_{lin4})$ for the equivalent linear actuators, through the equivalent parameters $\beta_{f/r}$ as a func-

tion of $\Delta\theta_{SLi}$. Finally, the tracking errors $(z^{(e)}_{lin1} - z_{lin1}, ..., z^{(e)}_{lin4} - z_{lin4})$ are fed back to the $\mathcal{H}_\infty$ controller as exogenous inputs to ensure zero steady-state tracking errors for realistic control demands. As seen in Figure 6.7, as is desired, the transfer functions (red lines) from tracking error $(z^{(e)}_{lin1} - z_{lin1}, ..., z^{(e)}_{lin4} - z_{lin4})$ to the control efforts $(\dot{z}^*_{lin1}, ..., \dot{z}^*_{lin4})$ are shown with a low-pass nature which indicates that the position references for the control of attitude motions dominate at low frequency vehicle dynamics.

A low-pass filter (**LF** in Figure 7.1) is employed before the PID measurement signals, $\mathbf{v}$, for uncoupling the fast dynamics of the four actuators and emphasising the importance of the signals in the low frequencies. The time constant, τ, for the low-pass filter is chosen as 0.005s. The nominal height of the centre of the sprung mass is chosen as the reference for the heave control, and the reference for pitch and roll motions are set as constant zero. To calculate the outputs in terms of the vertical (heave), pitch and roll motions, the expressions of the PID controller in the time domain are given as follows [10]:

$$\begin{aligned}\Delta\theta^{(1)}_{SL1} = \Delta\theta^{(1)}_{SL2} &= +K^{(1)}_{p_f}\dot{z}_{CM} + K^{(1)}_{i_f}\Delta z_{CM} + K^{(1)}_{d_f}\ddot{z}_{CM} \\ \Delta\theta^{(1)}_{SL3} = \Delta\theta^{(1)}_{SL4} &= +K^{(1)}_{p_r}\dot{z}_{CM} + K^{(1)}_{i_r}\Delta z_{CM} + K^{(1)}_{d_r}\ddot{z}_{CM}\end{aligned} \tag{7.1}$$

$$\begin{aligned}\Delta\theta^{(2)}_{SL1} = \Delta\theta^{(2)}_{SL2} &= -K^{(2)}_{p_f}\dot{\theta} - K^{(2)}_{i_f}\theta - K^{(2)}_{d_f}\ddot{\theta} \\ \Delta\theta^{(2)}_{SL3} = \Delta\theta^{(2)}_{SL4} &= +K^{(2)}_{p_r}\dot{\theta} + K^{(2)}_{i_r}\theta + K^{(2)}_{d_r}\ddot{\theta}\end{aligned} \tag{7.2}$$

$$\begin{aligned}\Delta\theta^{(3)}_{SL1} = -\Delta\theta^{(3)}_{SL2} &= -K^{(3)}_{p_f}\dot{\phi} - K^{(3)}_{i_f}\phi - K^{(3)}_{d_f}\ddot{\phi} \\ \Delta\theta^{(3)}_{SL3} = -\Delta\theta^{(3)}_{SL4} &= -K^{(3)}_{p_r}\dot{\phi} - K^{(3)}_{i_r}\phi - K^{(3)}_{d_r}\ddot{\phi}\end{aligned} \tag{7.3}$$

The final overall controlled system is very sensitive to the selection of the control gains. The finalised control gains are obtained after several iterations to balance the performance of ride comfort, road holding and attitude motions control. When the $\mathcal{H}_\infty$ controller has been obtained, the principles when blending together the $\mathcal{H}_\infty$ control and attitude control include: 1) the low-pass cut-off frequency of the attitude controller in the frequency domain should not largely overlap with the band-pass frequency of the $\mathcal{H}_\infty$ controller, to ensure the different control objectives do not interfere with each other. This has been double secured by the low-pass natured trans-

fer functions from tracking errors to the control efforts (i.e., red lines in Figure 6.7) and the low-pass filter before the PID measurements signals (i.e. **LF** block in Figure 7.1); and 2) the gains of the PID controller cannot be set too large to cancel out the power drop of the cut-off frequency of the tracking errors to the reference single-link velocities (red lines in Figure 6.7). The selected control gains used in this chapter are given in Table 7.1.

Table 7.1 Attitude control gains

PID control	Eq.	Axle	P	I	D
Heave	(7.1)	F&R	0.1	2	1
Pitch	(7.2)	F&R	1	5	0.04
Roll	(7.3)	F&R	0.5	2.5	0.004

7.2 Simulation results and comparisons

In this section, the following types of nonlinear control scheme are considered for the simulations and comparisons:

- Pure passive nonlinear full-vehicle system (PASSIVE).
- The overall control framework proposed in this chapter, which aims to achieve the mitigation of attitude motions and comfort and road holding enhancement simultaneously (FE-PID-SAVGS).
- $\mathcal{H}_\infty$ -controlled SAVGS full-car system for comfort and road holding enhancement in the context of high frequency vehicle dynamics control proposed in Chapter 6, based on the full-car hand-derived equivalent model (FE-SAVGS).
- PID-controlled SAVGS full-car system for the low frequency attitude motions control based on previous work in [10] (PID-SAVGS).

To evaluate the effectiveness of the overall control of the SAVGS (FE-PID-SAVGS) on the dynamic response of the GT, six simulation results are carried out. Random roads and smoothed bump simulations are firstly obtained to assess the high frequency responses for ride comfort and road holding enhancement, which are compared with the $\mathcal{H}_\infty$ -controlled scheme (FE-SAVGS) in the last chapter. Then, the standard steady-state cornering and step steer manoeuvres are investigated to assess the attitude capabilities of roll mitigation and rapid transients, respectively. The results are

compared with vehicles equipped with attitude controller (PID-SAVGS) based on the previous work [10]. Finally, pure longitudinal acceleration and braking manoeuvres are simulated to study the pitch mitigation in low and high frequencies for the transient events and for the accelerating/decelerating process. Thus, PID-SAVGS and FE-SAVGS schemes are both employed for comparison purposes of this simulation.

The key parameters for the GT and the SAVGS for the nonlinear control scheme used in the simulations are given in Tables 3.5 and 3.6. Human sensitive frequencies for vibration are 2∼8 Hz. In the frequencies of interest for passenger ride comfort, the reduction in vertical vehicle acceleration at the centre of the sprung mass is the main criteria to be examined. Pitching and rolling acceleration is the additional criteria for ride comfort. Tyre deflection and suspension deflection are also investigated for road holding. For attitude motions control capability, roll and pitch angle mitigation are the main control objectives to be investigated. Unlike other active suspension systems, in which actuators with large strokes are placed in parallel with the spring-damper unit, the SAVGS in this project is placed in series with the spring-damper unit with a short single-link length (i.e., 15 cm for the front axle and 11 cm for the rear axle).Thus, the suspension deflection of the SAVGS is limited by its geometry and will not travel beyond the allowable bounds. As a consequence, the suspension deflection (suspension travel) has been dropped from the controller synthesis stage and this index will not be shown in the following simulation results. The overall controlled system must operate within the power, torque, voltage, current and speed constraints of the actuator during these simulations to prevent damage to the motor and gearbox. This will be examined at the end of this section.

7.2.1 Random road profiles

The overall controlled SAVGS system (FE-PID-SAVGS) traveling on random road profiles with a longitudinal forward speed of $100km/h$ is simulated to assess the ride comfort and road holding ability over the range of human sensitive frequency to vibration (2∼8 Hz). All simulations have been performed at nominal offset angles $\Delta\theta_{SLi}^{(ne)} = 90°$.

The road profiles used for this simulation are identical to the ones in Section 6.4.1, which are generated based on [85], and the road modelling details can be found in the second approach in Section 3.3.3. The power spectral density (PSD) representation of the road profiles is a shown in Figure 3.10. In summary, two random roads with the same level of roughness are generated to excite the left and right wheels of the vehicle in one simulation. Thus, together with vertical acceleration in the centre of the

sprung mass, pitching and rolling accelerations are also evaluated as the additional assessments for ride comfort. In this chapter, road section of class A and C, representing very good and poor quality road for the GT are used for vehicle excitation. In each case, the class A road section consists of road profiles A1 and A2 and class C road section consists of road profiles C1 and C2 on the right and left side of the wheels of the vehicle, respectively.

To understand the performance of the overall controlled system and the influence of the implementation of attitude control to the $\mathcal{H}_\infty$ -controlled SAVGS system, the response in frequency domain is compared with that of the original passive configuration (PASSIVE) and the $\mathcal{H}_\infty$ -controlled SAVGS system (FE-SAVGS). In Figure 7.2, the PSDs of the body vertical acceleration ($\ddot{z}_{CM}$), pitching ($\ddot{\theta}$) and rolling ($\ddot{\phi}$) accelerations are presented. Compared with the passive configurations (PASSIVE), significant magnitude reduction over the frequency range of interest for human sensitivity (2$\sim$8 Hz) is observed in the PSDs of the vertical and pitching accelerations of the overall controlled system (FE-PID-SAVGS). In the meantime, the rolling acceleration is not getting worse than the passive configuration by the implementation of the PID controller for other control objectives. Compared with the $\mathcal{H}_\infty$ -controlled SAVGS system (FE-SAVGS) proposed in the last chapter, the FE-PID SAVGS system performs as well in terms of magnitude reductions in the vertical and rolling accelerations. Especially for the vertical accelerations, which is the main criteria for the assessment of passenger ride comfort, the achieved acceleration gain reduction with respect to passive is up to approximately 12.47 dB and 9.65 dB at the resonant frequency near 2 Hz for road class C and A, respectively. The pitching accelerations' gain reductions are even improved by up to 5 dB and 6.5 dB in the in the range of 0.5 - 3Hz and 0.3 - 6Hz of road class C and A, respectively. These results indicate the improved ride comfort properties of the overall controlled SAVGS. Furthermore, implementation of the PID attitude control does not affect the positive performance improvement in vertical acceleration, as the main criteria for the assessment of passenger ride comfort.

To analyse the controlled systems in the time domain, the root mean square (RMS) for the sprung mass centre acceleration is used to assess system performance for the good and poor quality road (A and C). The results are summarised in Table 7.2. The RMS of the vertical sprung mass acceleration ($\ddot{z}_{CM}$) is consistently improved by $\sim$40% and $\sim$35% for road class A and C. Compared to the PASSIVE, the RMSs of the pitching and rolling accelerations improvement of the FE-PID-SAVGS is smaller than the results of the FE-SAVGS due to the combination of the PID controller in low frequencies for attitude motion control. As mentioned previously, vertical sprung

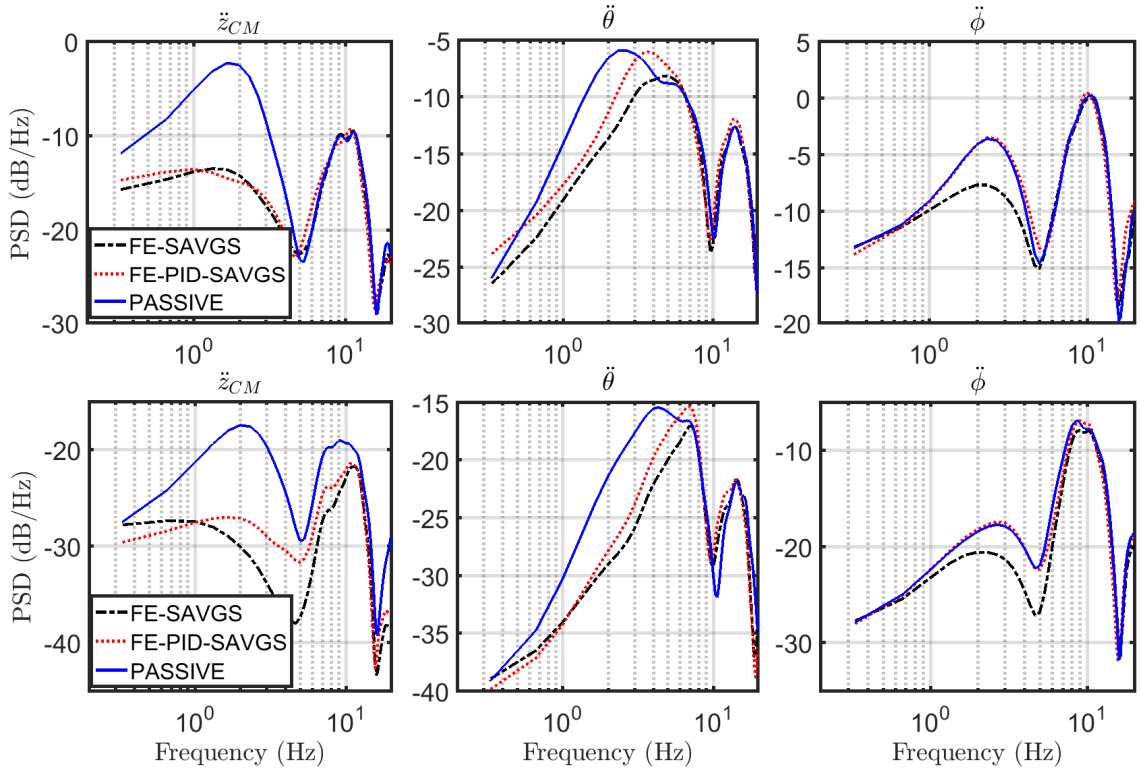

Fig. 7.2 PSDs for sprung mass vertical, pitching and rolling accelerations at the mass centre of the GT with random road sections of class C (top row) and A (bottom row).

mass acceleration ($\ddot{z}_{CM}$) is the main criteria for assessing passenger ride comfort and the FE-PID-SAVGS system performs much better on ride comfort, compared with the passive configurations.

The pitch and roll angles for the random-profiled roads are examined and very small rotational angles are found for random road class A and C. Specifically, the pitch angle for road class A and C are within $\pm 0.5°$ and $\pm 2°$, respectively. For the roll angle, the excited maximum roll angle of road class A and C did not exceed $\pm 0.1°$ and $\pm 0.5°$. Therefore, such small rotational angles will not affect the feeling of human comfort. The pitch and roll angle mitigation will be investigated in the step steer and steady-state cornering simulations for attitude motion control in the following sections.

Figure 7.3 presents 20 s-time response of the FE-PID-SAVGS and PASSIVE systems for random road class C. Random road class A has similar responses in the time domain. Figure 7.3(a) shows the random road profile acting on the rear left wheel of the vehicle systems in time domain, which refers to the green line of the PSDs plot for road profiles in frequency domain in Figure 3.10. It can be seen in Figures 7.3(b) and

Table 7.2 RMS of vertical, pitching and rolling accelerations ((%) = Performance Improvement (%) compared to Passive)

Road class A (A1 on left wheels, A2 on right wheels)					
	Passive	FE-SAVGS	(%)	FE-PID-SAVGS	(%)
$\ddot{z}_{CM}$	0.3171	0.1704	46.26	0.1917	39.55
$\ddot{\theta}$	0.3743	0.2963	26.18	0.3505	6.36
$\ddot{\phi}$	0.9395	0.8220	12.51	0.9019	4.00
Road class C (A1 on left wheels, A2 on right wheels)					
	Passive	FE-SAVGS	(%)	FE-PID-SAVGS	(%)
$\ddot{z}_{CM}$	1.1509	0.7635	33.66	0.7365	36.01
$\ddot{\theta}$	1.055	0.9136	13.40	1.0404	1.38
$\ddot{\phi}$	2.3015	2.1725	5.61	2.3125	-0.48

7.3(c) that the vertical acceleration at the sprung mass centre and tyre deflection at the rear left corner of the vehicle (the other three corners have similar results) have mostly reduced peaks once the overall control framework is employed, as compared to the passive configuration, which demonstrates the improved comfort and road holding properties of the controlled system. The last plot in Figure 7.3(d) illustrates the corresponding usage of the rear left single-link angle of the overall controlled SAVGS system, which is rotated actively within the allowable operation range (0∼160°) to improve system performance. The other three corners of the controlled system have similar single-link rotation results.

7.2.2 Smoothed bump

Simulation results for a smoothed bump at the left side wheels are presented to assess the overall full-car control schemes (FE-PID-SAVGS and FE-SAVGS) transient response characteristics compared to the passive configuration (PASSIVE), in the context of high frequency vehicle dynamics.

The expression of the smoothed bump and the driving conditions of the vehicle in this section are identical to the situation in Section 4.10 in Chapter 3, where the bump height h=0.05 m and width w=2 m, at the forward speed V=20 km/h. This bump only acts on the left side of the vehicle so that the attitude motions of the sprung mass can be assessed by analysing the pitching and rolling accelerations. Figure 7.4 presents the simulation results of the FE-PID-SAVGS, FE-SAVGS and PASSIVE systems. It can be observed that the FE-SAVGS performs slightly better than the FE-PID-SAVGS but the differences between these two SAVGS controlled systems are

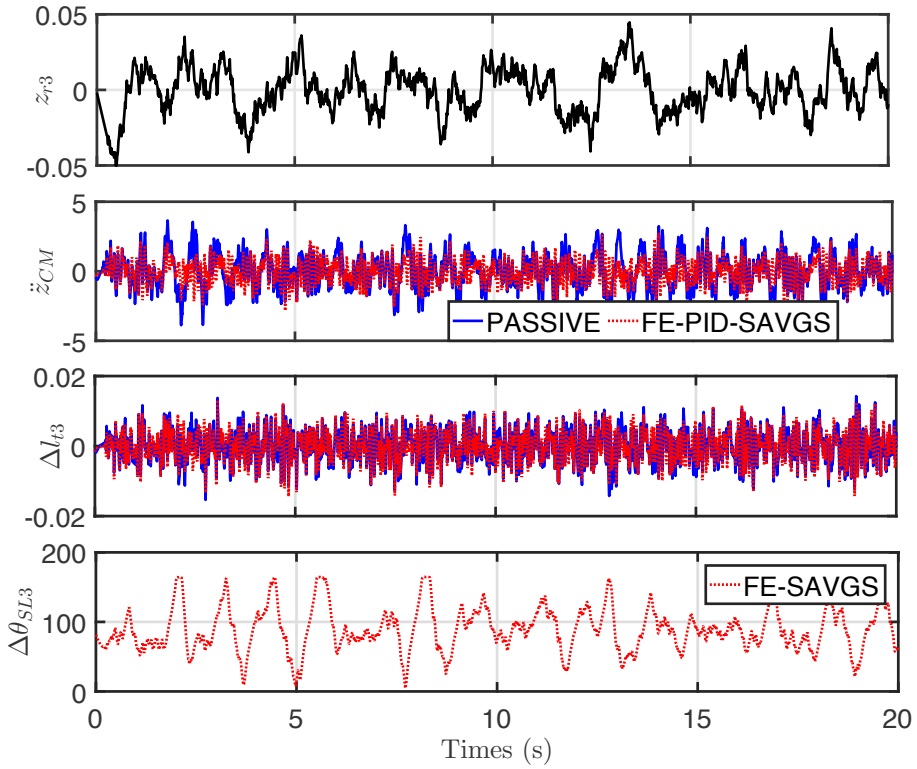

Fig. 7.3 Response time histories of vehicle systems for random class C during a 20 s period simulation.

very small. Both SAVGS controlled systems, compared with the passive configuration, offer good disturbance attenuation, smaller tyre deflection and quick response with shorter settling time, which proves better ride comfort and road holding properties.

7.2.3 Steady-state cornering

This open-loop test based on [ISO 4138:2004] [83] is employed to assess the potential of the PID-FE-SAVGS for roll mitigation, which will be compared with the PID-SAVGS system. According to this test, vehicles are driven on a circular path with a fixed radius of 100m. The driving speed remains constant at different speeds from 10 m/s to 30 m/s, which correspond to lateral accelerations from $1m/s^2$ to $10m/s^2$.

Figure 7.5 shows the roll reduction with respect to the response of the passive vehicle during the steady-state cornering test. It can be clearly seen that the overall controlled system (PID-FE-SAVGS) developed in this chapter offers as good roll mitigation performance, which is very similar as compared with the attitude controlled system (PID-SAVGS). This proves that the implementation of the $\mathcal{H}_\infty$ controller will

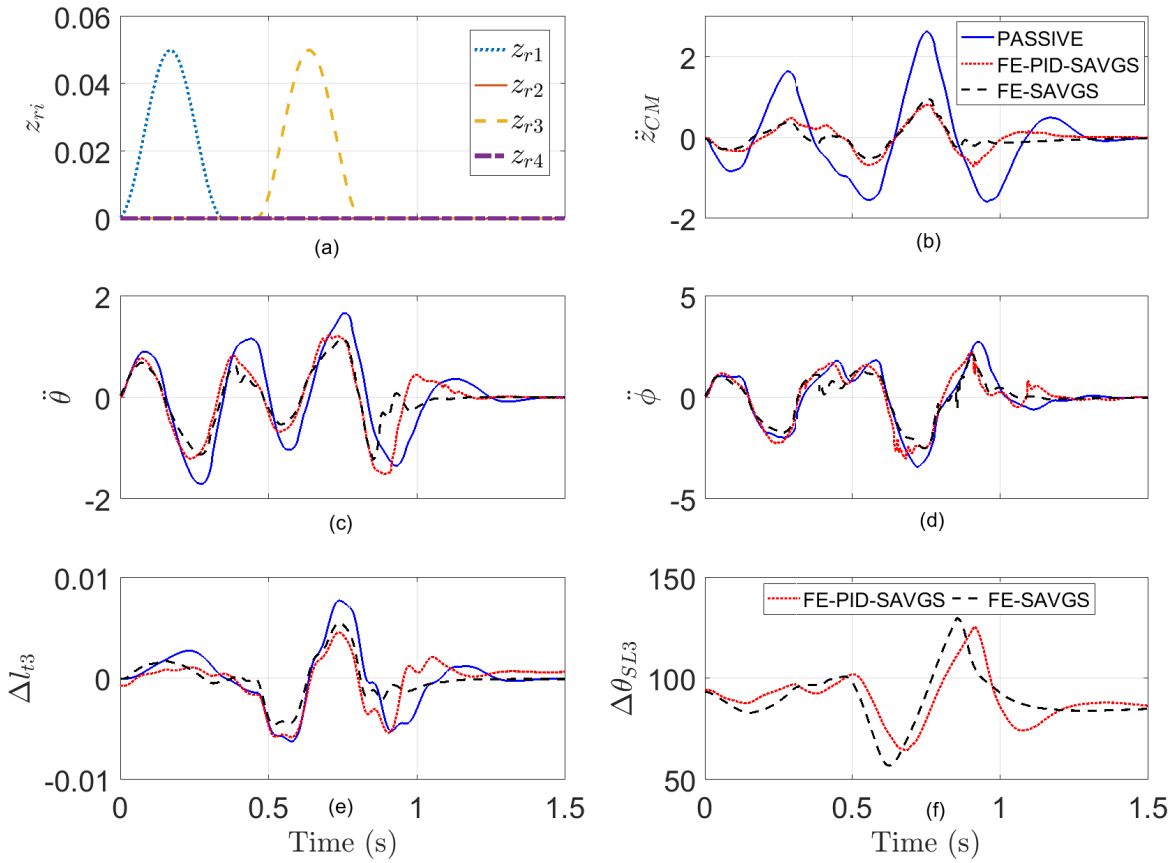

Fig. 7.4 Response time histories of vehicle systems for one sided bump disturbances: (a) road inputs at four corners; (b) vertical accelerations at mass centre; (c) pitching accelerations; (d) rolling accelerations; (e) tyre deflection at rear left wheel; (f) single-link rotation for SAVGS controlled systems at rear left wheel.

not affect the low frequency responses ($\ll$1 Hz) due to the controller's band pass nature for the ride comfort and road holding objectives. When the lateral accelerations are smaller than $5\,m/s^2$, which roll angles of the SAVGS controlled system are completely neutralised, and the roll reduction achieved is even $\sim$50% with the maximum expected lateral acceleration of 10 m/s^2.

7.2.4 Step steer

This open-loop test based on [ISO 7401:2011] [84] is used to assess the potential of the PID-FE-SAVGS for roll mitigation during rapid transient conditions, which will be compared with the PID-SAVGS system.

Vehicles are initially driving with a forward speed of 100km/h in a straight line. Then, a sudden steering wheel angle is applied at a constant rate of 500deg/s from

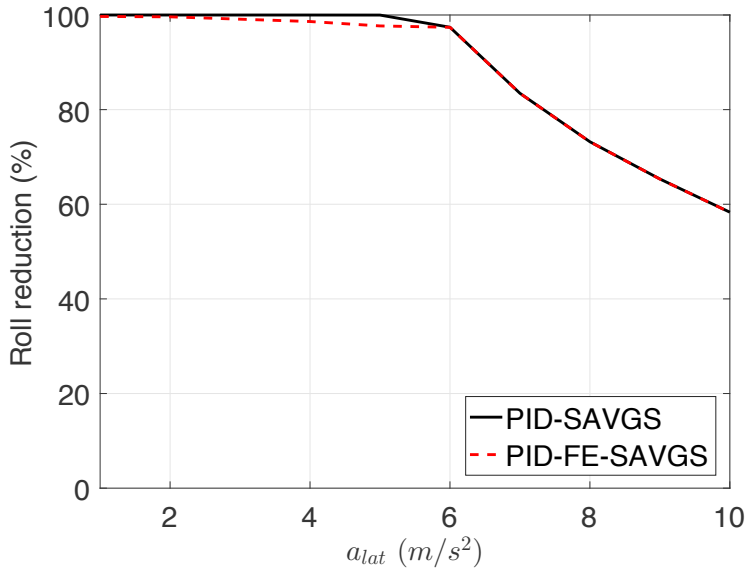

Fig. 7.5 Roll reduction during steady-state cornering at different lateral accelerations.

0°. The final change of the steering wheel angle, $\delta^{(ss)}$, is obtained by the passive configuration when maintaining a certain level of steady-state lateral acceleration, $a_{lat}^{(ss)}$ with a constant forward speed of 100km/h.

Figure 7.6 shows the reduction in peak roll angle during the step-steer test with respect to the response of the passive vehicle. It is noted that the PID-SAVGS provides attitude control as good as in the steady-state case in Figure 7.5. The differences between the FE-PID-SAVGS and PID-SAVGS controlled systems are due to the high frequency disturbance that occurs during the rapid transients which trigger the $\mathcal{H}_\infty$ controller whose main control objective is the attenuation of the vertical sprung mass acceleration in the high frequency range, rather than the attenuation of rolling acceleration. However, the FE-PID-SAVGS system also achieves a significant roll peak reduction, which is approximately ∼70% up to $5\,m/s^2$ and ∼50% up to $10\,m/s^2$.

7.2.5 Pure longitudinal accelerating and braking

The pure longitudinal accelerating and braking manoeuvre is used to assess the ability of the overall controlled system (FE-PID-SAVGS) for pitch mitigation in low and high frequency vehicle dynamics, PID-SAVGS and FE-SAVGS schemes are both also employed for the purpose of comparison.

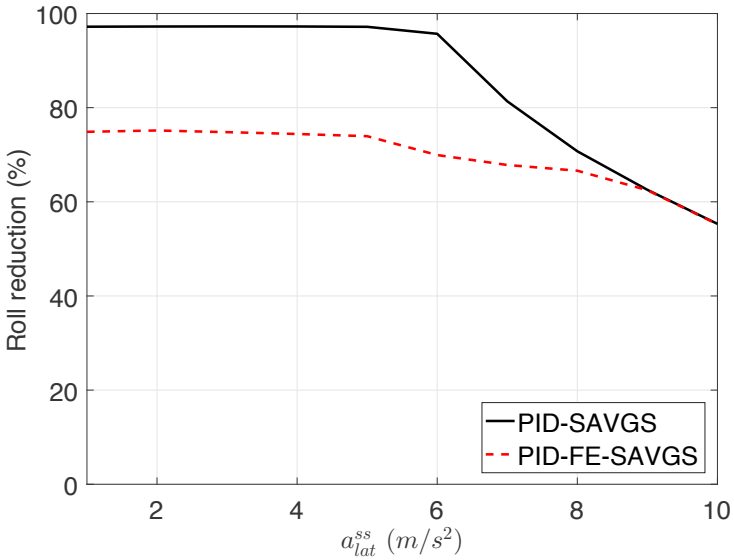

Fig. 7.6 Roll peak angle reduction for different lateral accelerations during step steer.

The evolution of the speed changing in this manoeuvre is given in Figure 7.7, which starts with a hard accelerating process from 1km/h to 75km/h in 5.7 s, keeps the speed for 2.8 s period and is followed by an emergency stop.

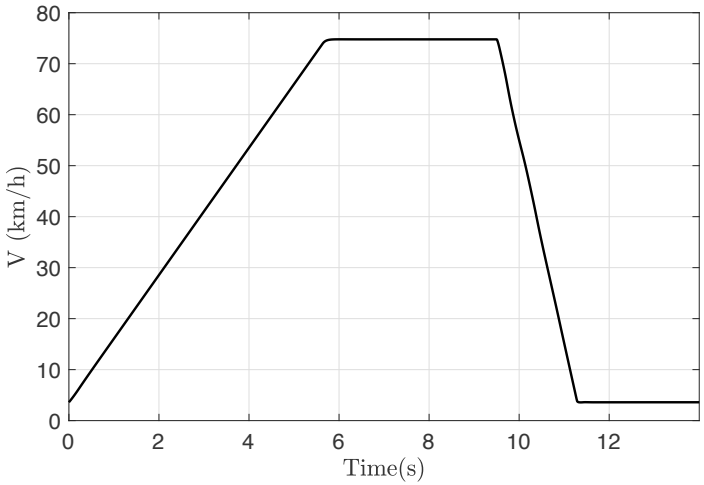

Fig. 7.7 Forward speed velocity profiles for the longitudinal accelerating and braking manoeuvre.

Time responses of the pure longitudinal accelerating and braking manoeuvre are shown in Figure 7.8. The attitude controlled scheme (PID-SAVGS), in Figure 7.8(a), is capable of maintaining a flat pitch angle during the acceleration phase and achieves significant ($\sim$ 50%) pitch angle correction during the emergency stop. However, the

responses in Figure 7.8(b) and 7.8(c) show that the PID-SAVGS performs best peak reduction at the begining of the transient event (∼9.5s) both for the pitching acceleration and the vertical sprung mass acceleration at the rear left corner of the vehicle. However, compared with other control schemes and passive system, it causes continues oscillation and longer setting time when the transient event finish. In contrast, the $\mathcal{H}_\infty$ controlled scheme (FE-SAVGS) offers good attenuation performance associated with the pitching accelerations and the vertical sprung mass acceleration at the rear left corner of the vehicles during the emergency stop with reduced peak acceleration and shorter settling time. However, in Figure 7.8(a), it shows that the FE-SAVGS is not working to correct the pitching angles during the acceleration phase and the emergency stop, due to the band-pass nature of the $\mathcal{H}_\infty$ controller which main control objective is the minimisation of sprung mass acceleration in the context of high frequency vehicle dynamics. Compared with the previous two approaches, the overall controlled system (FE-PID-SAVGS) is observed to have the best control performance as it achieves as good a pitch angle correction as the PID-SAVGS case in Figure 7.8(a) and shows better acceleration attenuation properties in Figure 7.8(b) and 7.8(c). Thus, this demonstrates once again that the full-car overall control scheme achieve the mitigation of attitude motions and ride comfort enhancement simultaneously.

7.2.6 Position controller performance

The aforementioned inner position controller in Figure 4.2 is designed to protect the PMSM and its servo-drive, to ensure the single-link rotates within its operational limits, and to set power and torque consumption by the controller. In this chapter, maximum allowable power flow from the PMSM in driving mode is set as 500 W and the power flow to the PMSM in regenerating mode is set as -1500 W, and the maximum torque limits (±200Nm) of the actuator are applied to explore the potential of the overall control scheme. The maximum single-link rotational velocity is set as $\pm 13 rad/s$.

The output torque-speed operating points for the actuators (i=1,...,4) are plotted in Figure 7.9 alongside the power, torque and speed constraint envelope. The most power consuming events, poor quality random road C and accelerating/braking manoeuvre are examined in 7.9(a) and 7.9(b), respectively. Gaps between the operation points and the power constraints occur due to power losses in the PMSM and gearbox, which are summarised in Table 5.5. This figure shows that the operating points are located within the designed constraints of the real system demonstrating the robustness behaviour of the overall controlled system. Furthermore, in these two power consump-

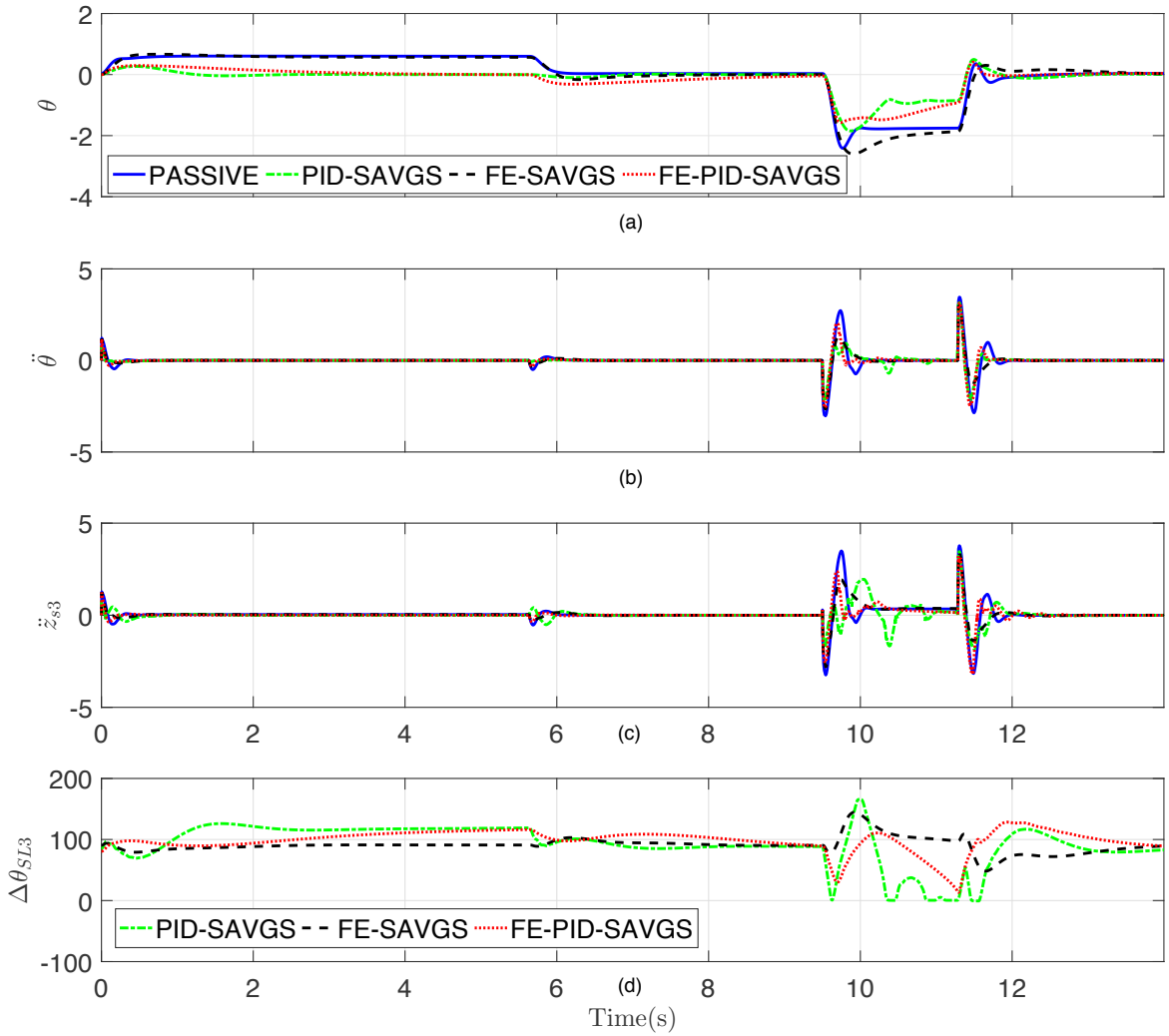

Fig. 7.8 Simulation results for the longitudinal and braking manoeuvre: (a) pitch angles; (b) pitching accelerations; (c) sprung mass vertical acceleration at the rear left wheel; and (d) single-link angle of the rear left wheel.

tion events, the single-link uses the full permitted region to achieve the maximum potential of the control of the SAVGS, without damage to the system stability. The average power consumption for one actuator of these two events is 452 W for random road class C and 27 W for accelerating and braking.

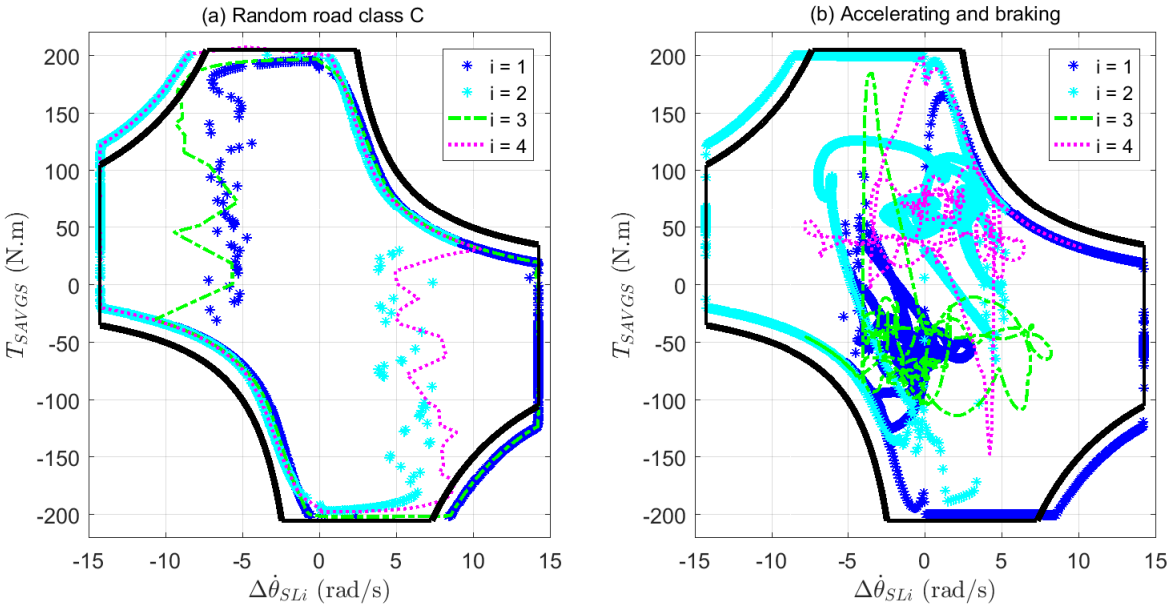

Fig. 7.9 Output torque vs. single-link velocity characteristics for: (a) random road class C (only shows the boundaries); (b) longitudinal acceleration and braking event of the nonlinear simulations, presented in Figures 7.3 and 7.8. Black envelope is the actuator limit boundaries.

7.3 Conclusions

This chapter constructed a full-car overall control framework for the combined attitude control, ride comfort and road holding enhancement. This is achieved through blending the full-car $\mathcal{H}_\infty$ -controlled scheme for high frequency vehicle dynamics control and the full-car chassis attitude motion control low frequency vehicle dynamics control together. The full-car $\mathcal{H}_\infty$ -controlled scheme of the SAVGS configuration based on a full-car hand-derived model has been proposed in Chapter 6, which showed performance improvement in comfort and road holding. This chapter developed an attitude controller with outputs that are used as the exogenous inputs for the $\mathcal{H}_\infty$ controller for single-link position tracking. The finalised control gains are selected after several iterations to balance the performance of ride comfort, road holding, and attitude motions control. Six events of simulation results are carried out with the overall con-

trolled scheme (FE-PID-SAVGS) to assess the control performance, demonstrate that, as compared with the $\mathcal{H}_\infty$ -controlled scheme (FE-SAVGS), the attitude controlled scheme (PID-SAVGS) and the passive configuration (PASSIVE): a) the full-car overall control scheme tackles the ride comfort, road holding and attitude control objectives simultaneously, due to the reduction of body acceleration and tyre deflection during the random road, smoothed bump and braking/accelerating manoeuvres with high frequency disturbance contents, as well as the significant roll and pitch mitigation during turning and braking/accelerating manoeuvres with low frequency disturbance contents; b) the working frequency of the $\mathcal{H}_\infty$ controller and the attitude controller inside the overall control framework do not largely overlapped with each other, which is suitable to tackle different control objectives as the measurement signals can be filtered and fed to the correct controller according to the frequency contents of the signals; c) the operating points of the overall controlled framework for all of the simulations are located within the designed constraints of the real system, already available on the market, which demonstrates the robustness of the overall controlled system.

Chapter 8

Conclusions and future work

8.1 Conclusions

This project has set out the aim of developing control strategies for the recently introduced Series Active Variable Geometry Suspension (SAVGS) concept. To this end, work on the $\mathcal{H}_\infty$ control synthesis from quarter- to full-vehicle single-link variant of the SAVGS control has been successfully carried out with promising results. The final overall SAVGS control framework obtained in this work achieves comfort and road holding, and chassis attitude motion enhancement for both the low- and high-frequency suspension functions simultaneously. Meanwhile, the physical and design constraints of the real mechanisms of the actuator in the real-world test rig, such as torque and power limitations, are all respected throughout all the simulations in this thesis. Thus, the results of this thesis lay the foundation for the success of the experimental study of the single-link variant of the SAVGS and the implementation of the control technique to other vehicle models.

This thesis, firstly, provides a comprehensive review of the basic disciplines related to automotive suspensions, placing a special focus on the characteristics and classification of active suspension. A brief review of previous SAVGS studies is supplied to contribute to better understanding of this new concept. In addition, several aspects of the performance indices that allow engineers to compare the different control strategies for active suspensions are discussed. The most widely employed control techniques for active suspension control problems are investigated, specifically emphasising on the $\mathcal{H}_\infty$ robust control strategy, which is used to solve multivariable problems in the frequency domain in this project. An explanation of the modelling process of both the nonlinear and linear vehicle models used throughout this project, including the quarter- and full- vehicle models developed for assessing vehicle performance in

the context of comfort, road holding, and attitude control and the linearised models developed for the control synthesis, then follows.

The controller design starts with the quarter-car single-link variant of the SAVGS control, which is achieved by constructing a linear $\mathcal{H}_\infty$ control scheme to reduce the impact of external road disturbance and load transfer on the vertical direction. The frequency weight selection and tuning process are discussed in detail, providing a reliable reference for frequency weight selection in the subsequent controller design process. The simulation results carried out using the nonlinear controlled system demonstrate that the SAVGS with the proposed $\mathcal{H}_\infty$ controller performs better in terms of ride comfort and road holding compared to the passive nonlinear quarter-car configuration, due to the reduction of body acceleration and tyre deflection of the high frequency suspension functions. During the simulations, very low power consumption is observed and actuator constraints, such as torque and speed limits, are all respected. The proposed $\mathcal{H}_\infty$ controller is also applied to test the full-car nonlinear model by equipping it at each corner of the vehicle. In addition, the results of the full-car SAVGS nonlinear model shows that the roll and pitch at high frequencies are fully under control with the implementation of the quarter-car $\mathcal{H}_\infty$ controller which implies a good performance in ride comfort and road holding, but it does not perform better than the full-car passive case in terms of the low frequency suspension functions. This finding motivates the design of a separate attitude controller for the control of chassis attitude motions that works collaboratively with the $\mathcal{H}_\infty$ controller to achieve multiple control objectives in Chapter 7.

This quarter-car control technique is then extended to the full-car SAVGS and its control by considering the pitching and rolling motions as additional objectives for the high frequency suspension functions. This is a significantly more complex control problem than that tackled in the quarter-car work, as the number of states, inputs and outputs of the full-car model is much larger and the SAVGS dynamics among the four corners of the vehicle interact. Two approaches to the full-car single-link variant of the SAVGS control are introduced in this thesis and presented in sequence in Chapter 5 and 6. Firstly, in Chapter 5, the full-car linear $\mathcal{H}_\infty$ multi-objective control framework based on the linearised AutoSim full-car model, which is linearised at the trim state of the vehicle that provides maximum control authority, is developed. Secondly, in Chapter 6, a full-car linear $\mathcal{H}_\infty$ multi-objective control framework is developed based on a new linear hand-derived equivalent full-car model that removes the main geometric nonlinearity associated with the single-link rotation of the AutoSim linearised full-car model. This approach achieves a higher level of robustness for single-link rotations,

especially when the single-link rotates away from its trim state. Thus, the full-car $\mathcal{H}_\infty$ controller proposed in Chapter 6 is selected as the final $\mathcal{H}_\infty$ controller to improve ride comfort and road holding properties in the context of high frequency vehicle dynamics. Simulations were conducted to test both control approaches, under various types of road disturbances, which demonstrates that the latter control approach has the best performance and robustness characteristics, while satisfying actuator and suspension operating constraints.

The overall control framework for the full-car single-link variant of the SAVGS control is presented in Chapter 7. This control framework is achieved by blending together an $\mathcal{H}_\infty$ controller and an attitude controller. The $\mathcal{H}_\infty$ controller chosen is the controller proposed in Chapter 6, in which extra exogenous inputs for tracking the single-link position commands of the attitude controller are included. The attitude controller is obtained after several iterations to balance the performance of the ride comfort, road holding, and chassis motions control to ensure that the different control objectives do not interfere with each other. Extensive simulation results, including random profiles, smoothed bump, steady-state cornering, step-steer and emergency braking are carried out to assess the overall control performance. Compared with the pure $\mathcal{H}_\infty$ -controlled scheme, pure attitude control scheme and the passive configuration, the full-car overall control scheme tackles the ride comfort, road holding and attitude control objectives simultaneously, due to the reduction of body acceleration and tyre deflection during the random road, smoothed bump and braking/accelerating manoeuvres with high frequency disturbance contents, as well as the significant roll and pitch mitigation during the turning and braking/accelerating manoeuvres with low frequency disturbance contents.

8.2 Future work

Based on this work on control strategies for Series Active Variable Geometry Suspension (SAVGS), the following is recommended for further research:

- Based on the outcomes of this thesis, the experimental validation of the single-link variant of the SAVGS control can be processed. In particular, a quarter-car test rig control has been published in [187], in which experiments are presented for the demonstration of the SAVGS practical feasibility, performance enhancement, and robustness behaviour of the controller. The experimental evaluation of the controller for the full-car SAVGS model could be explored on road tests.

- Vehicle uncertainties and parameter changes, such as damping coefficient, passenger mass, and actuator unmodelled nonlinearities, should be introduced into the $\mathcal{H}_\infty$ control synthesis and the overall control framework for improved system robustness, for example through the μ-synthesis framework.

- Other control methodologies for the single-link variant of the SAVGS control for the GT in this work, such as model predictive control (MPC) with previewed road information and fuzzy logic control, could also be investigated. In addition, the problem formulation in this thesis can also be expressed in terms of linear matrix inequalities (LMI) associated with its state-space realisation. It enables to characterise various properties of dynamic systems in the frequency domain in terms of LMIs.

- The control techniques used in this work could be applied to other vehicle models, for example the sport utility vehicles (SUV).

References

[1] Abdellari, E., Mehdi, D., and Saad, M. (2000). On the design of active suspension system by H_∞ and mixed H_2/H_∞: An lmi approach. In *American Control Conference, 2000. Proceedings of the 2000*, volume 6, pages 4041–4045. IEEE.

[2] AG, D. (2007). Special Feature: Innovation As A Tradition At Mercedes-Benz [Internet]. http://www.emercedesbenz.com.

[3] Al-Holou, N., Lahdhiri, T., Joo, D. S., Weaver, J., and Al-Abbas, F. (2002). Sliding mode neural network inference fuzzy logic control for active suspension systems. *IEEE Transactions on Fuzzy Systems*, 10(2):234–246.

[4] Alleyne, A. and Hedrick, J. K. (1995). Nonlinear adaptive control of active suspensions. *IEEE transactions on control systems technology*, 3(1):94–101.

[5] Aly, A. A. (2012). Car suspension control systems: basic principles. *International Journal of Control, Automation and Systems*, 1(1):41–46.

[6] Anon. (1998). Autosim 2.5+ reference manual, mechanical simulation corporation, 709 west huron, ann arbor mi.

[7] Anthony, M. (2001). *Discrete mathematics of neural networks: selected topics*. SIAM.

[8] Anubi, O. and Crane, C. (2011). Semi-global output feedback asymptotic tracking for an under-actuated variable stiffness mechanism. In *Proceedings of the 13th IFTOMM World Congress in Mechanism and Machine Science*.

[9] Arana, C., Evangelou, S. A., and Dini, D. (2012). Pitch angle reduction for cars under acceleration and braking by active variable geometry suspension. In *Decision and Control (CDC), 2012 IEEE 51st Annual Conference on*, pages 4390–4395. IEEE.

[10] Arana, C., Evangelou, S. A., and Dini, D. (2014). Car attitude control by series mechatronic suspension. In *19th IFAC World congress on Automatic Control*.

[11] Arana, C., Evangelou, S. A., and Dini, D. (2015). Series active variable geometry suspension for road vehicles. *Mechatronics, IEEE/ASME Transactions on*, 20(1):361–372.

[12] Arana, C., Evangelou, S. A., and Dini, D. (2017). Series active variable geometry suspension application to comfort enhancement. *Control Engineering Practice*, 59:111–126.

[13] Arana Remirez, C. (2015). *Active variable geometry suspension for cars*. PhD thesis.

[14] Ashari, A. E. (2004). Sliding-mode control of active suspension systems: unit vector approach. In *Control Applications, 2004. Proceedings of the 2004 IEEE International Conference on*, volume 1, pages 370–375. IEEE.

[15] Bei, S.-y., Chen, L., Chen, B.-l., and Liu, H.-m. (2008). On fuzzy-PID integrated control of automotive electric power steering and semi-active suspension. In *Intelligent Information Technology Application, 2008. IITA'08. Second International Symposium on*, volume 3, pages 847–851. IEEE.

[16] Biglarbegian, M., Melek, W., and Golnaraghi, F. (2008). A novel neuro-fuzzy controller to enhance the performance of vehicle semi-active suspension systems. *Vehicle System Dynamics*, 46(8):691–711.

[17] Blundell, M. (1999). The modelling and simulation of vehicle handling part 1: Analysis methods. *Proceedings of the Institution of Mechanical Engineers, Part K: Journal of Multi-body Dynamics*, 213(2):103–118.

[18] Blundell, M. (2000). The modelling and simulation of vehicle handling part 3: tyre modelling. *Proceedings of the Institution of Mechanical Engineers, Part K: Journal of Multi-body Dynamics*, 214(1):1–32.

[19] Blundell, M. and Harty, D. (2004). *The multibody systems approach to vehicle dynamics*. Elsevier.

[20] Bodie, M. O. and Hac, A. (2000). Closed loop yaw control of vehicles using magneto-rheological dampers. Technical report, SAE Technical Paper.

[21] Burton, A., Truscott, A., and Wellstead, P. (1995). Analysis, modelling-and control of an advanced automotive self-levelling suspension system. *IEE Proceedings-Control Theory and Applications*, 142(2):129–139.

[22] Butsuen, T. (1989). *The design of semi-active suspensions for automotive vehicles*. PhD thesis, Massachusetts Institute of Technology.

[23] Cao, D., Rakheja, S., and Su, C.-Y. (2007). Pitch attitude control and braking performance analysis of heavy vehicle with interconnected suspensions. Technical report, SAE Technical Paper.

[24] Cao, D., Song, X., and Ahmadian, M. (2011). Editors' perspectives: road vehicle suspension design, dynamics, and control. *Vehicle system dynamics*, 49(1-2):3–28.

[25] Cao, J., Li, P., and Liu, H. (2010). An interval fuzzy controller for vehicle active suspension systems. *IEEE Transactions on Intelligent Transportation Systems*, 11(4):885–895.

[26] Chantillyautomotive (2016). Suspension systems [Internet]. http://chantillyautomotive.com/suspension-systems/.

[27] Chen, H., Sun, P.-Y., and Guo, K.-H. (2003). A multi-objective control design for active suspensions with hard constraints. In *American Control Conference, 2003. Proceedings of the 2003*, volume 5, pages 4371–4376. IEEE.

[28] Chen, H.-H. F. and Guenther, D. A. (1989). Self-tuning optimal control of an active suspension. Technical report, SAE Technical Paper.

[29] Chen, K. and Beale, D. G. (2003). Base dynamic parameter estimation of a MacPherson suspension mechanism. *Vehicle System Dynamics*, 39(3):227–244.

[30] Cheng, C., Evangelou, S. A., Arana, C., and Dini, D. (2015). Active variable geometry suspension robust control for improved vehicle ride comfort and road holding. In *2015 American Control Conference (ACC)*, pages 3440–3446. IEEE.

[31] Cho, B. K. (1999). Active suspension controller design using MPC with preview information. *Journal of Mechanical Science and Technology*, 13(2):168–174.

[32] Cho, D. D. (1993). Experimental results on sliding mode control of an electromagnetic suspension. *Mechanical Systems and Signal Processing*, 7(4):283–292.

[33] Choi, S., Lee, H., and Chang, E. (2001a). Field test results of a semi-active ER suspension system associated with skyhook controller. *Mechatronics*, 11(3):345–353.

[34] Choi, S., Suh, M., Park, D., and Shin, M. (2001b). Neuro-fuzzy control of a tracked vehicle featuring semi-active electro-rheological suspension units. *Vehicle system dynamics*, 35(3):141–162.

[35] Constant, C. (2013). MacPherson and Pseudo MacPherson suspension [Internet]. http://www.car-engineer.com/mac-pherson-and-pseudo-mac-pherson-suspension/.

[36] Corriga, G., Sanna, S., and Usai, G. (1991). An optimal tandem active-passive suspension system for road vehicles with minimum power consumption. *Industrial Electronics, IEEE Transactions on*, 38(3):210–216.

[37] Crolla, D. (1996). Vehicle dynamics—theory into practice. *Proceedings of the Institution of Mechanical Engineers, Part D: Journal of automobile engineering*, 210(2):83–94.

[38] Crolla, D., Horton, D., Brooks, P., Firth, G., Shuttlewood, D., Woods, M., and Yip, C. (1994). A systematic approach to vehicle design using VDAS (Vehicle Dynamics Analysis Software). Technical report, SAE Technical Paper.

[39] Crosby, M., Harwood, R., and Karnopp, D. (1974). Vibration control using semi-active force generators. *Journal of engineering for industry*, 96(2):619–626.

[40] Demir, O., Keskin, I., and Cetin, S. (2012). Modeling and control of a nonlinear half-vehicle suspension system: a hybrid fuzzy logic approach. *Nonlinear Dynamics*, 67(3):2139–2151.

[41] Dingley, A. (1935). Sizaire sliding pillar suspension [Internet], https://commons.wikimedia.org/wiki.

[42] Donald, B. and Geoffrey, H. (1987). Car suspension and handling.

[43] Dorf, R. C. and Bishop, R. H. (2011). *Modern control systems*. Pearson.

[44] Doyle, J. C., Francis, B. A., and Tannenbaum, A. R. (2013). *Feedback control theory*. Courier Corporation.

[45] Doyle, J. C., Glover, K., Khargonekar, P. P., and Francis, B. A. (1989). State-space solutions to standard h/sub 2/and h/sub infinity/control problems. *IEEE Transactions on Automatic control*, 34(8):831–847.

[46] Ekoru, J. E., Dahunsi, O. A., and Pedro, J. O. (2011). PID control of a nonlinear half-car active suspension system via force feedback. In *AFRICON, 2011*, pages 1–6. IEEE.

[47] El-Demerdash, S., Selim, A., and Crolla, D. (1999). Vehicle body attitude control using an electronically controlled active suspension. Technical report, SAE Technical Paper.

[48] Elbeheiry, E. and Karnopp, D. (1996). Optimal control of vehicle random vibration with constrained suspension deflection. *Journal of Sound and Vibration*, 189(5):547–564.

[49] Elbeheiry, E. M., Karnopp, D. C., ElAraby, M. E., and Abdelraaouf, A. M. (1995). Advanced ground vehicle suspension systems-a classified bibliography. *Vehicle System Dynamics*, 24(3):231–258.

[50] Evangelou, S. A. (2010). Control of motorcycles by variable geometry rear suspension. In *Control Applications (CCA), 2010 IEEE International Conference on*, pages 148–154. IEEE.

[51] Evangelou, S. A., Dini, D., Meerschman, O. D., Tocatlian, A., C.Kneip, and Palas, C. (2012). Variable-geometry suspension apparatus and vehicle comprising such apparatus.

[52] Evers, W.-J., van der Knaap, A., Besselink, I., and Nijmeijer, H. (2008). Analysis of a variable geometry active suspension. In *International Symposium on Advanced Vehicle Control*, pages 350–355.

[53] Fateh, M. M. and Zirkohi, M. M. (2011). Adaptive impedance control of a hydraulic suspension system using particle swarm optimisation. *Vehicle System Dynamics*, 49(12):1951–1965.

[54] Fischer, D. and Isermann, R. (2004). Mechatronic semi-active and active vehicle suspensions. *Control engineering practice*, 12(11):1353–1367.

[55] Foda, S. G. (2001). Neuro-fuzzy control of a semi-active car suspension system. In *Communications, Computers and signal Processing, 2001. PACRIM. 2001 IEEE Pacific Rim Conference on*, volume 2, pages 686–689. IEEE.

[56] Fukao, T., Yamawaki, A., and Adachi, N. (1999). Nonlinear and H_∞ control of active suspension systems with hydraulic actuators. In *Decision and Control, 1999. Proceedings of the 38th IEEE Conference on*, volume 5, pages 5125–5128. IEEE.

[57] Gahinet, P. and Apkarian, P. (1994). A linear matrix inequality approach to H_∞ control. *International journal of robust and nonlinear control*, 4(4):421–448.

[58] Gáspár, P., Szaszi, I., and Bokor, J. (2003). Design of robust controllers for active vehicle suspension using the mixed μ synthesis. *Vehicle System Dynamics*, 40(4):193–228.

[59] Göhrle, C., Wagner, A., Schindler, A., and Sawodny, O. (2012). Active suspension controller using MPC based on a full-car model with preview information. In *American Control Conference (ACC), 2012*, pages 497–502. IEEE.

[60] Goran, M. and Smith, R. (1996). Insights gained from active suspension development. In *Proceedings of the 26th FISITA Congress*, pages 16–23.

[61] Green, M. and Limebeer, D. J. (2012). *Linear robust control*. Courier Dover Publications.

[62] Guclu, R. and Gulez, K. (2008). Neural network control of seat vibrations of a non-linear full vehicle model using PMSM. *Mathematical and Computer Modelling*, 47(11):1356–1371.

[63] Gysen, B., Paulides, J., Encica, L., and Lomonova, E. (2009). Slotted tubular permanent magnet actuator for active suspension systems. *Proc. LDIA*, pages 292–295.

[64] Gysen, B. L., Paulides, J. J., Janssen, J. L., and Lomonova, E. A. (2010). Active electromagnetic suspension system for improved vehicle dynamics. *IEEE Transactions on Vehicular Technology*, 59(3):1156–1163.

[65] Gysen, B. L., van der Sande, T. P., Paulides, J. J., and Lomonova, E. A. (2011). Efficiency of a regenerative direct-drive electromagnetic active suspension. *IEEE transactions on vehicular technology*, 60(4):1384–1393.

[66] Hać, A. (1985). Suspension optimization of a 2-DOF vehicle model using a stochastic optimal control technique. *Journal of sound and vibration*, 100(3):343–357.

[67] Hać, A. (1992). Optimal linear preview control of active vehicle suspension. *Vehicle system dynamics*, 21(1):167–195.

[68] Hac, A. and Bodie, M. O. (2002). Improvements in vehicle handling through integrated control of chassis systems. *International journal of vehicle autonomous systems*, 1(1):83–110.

[69] Halverson, H. (2003). 2003 Chevy Corvette - Cutting Edge Technology: A Look At The Corvette's Award-Winning Suspension Advancement [Internet]. http://www.superchevy.com/how-to/additional-tech/sucp-0311-2003-chevy-corvette/.

[70] Hanafi, D. (2010). PID controller design for semi-active car suspension based on model from intelligent system identification. In *Computer Engineering and Applications (ICCEA), 2010 Second International Conference on*, volume 2, pages 60–63. IEEE.

[71] Hassan, S. A. (1986). *Fundamental studies of passive, active and semi-active automotive suspension systems*. PhD thesis, University of Leeds.

[72] Hayakawa, K., Matsumoto, K., Yamashita, M., Suzuki, Y., Fujimori, K., and Kimura, H. (1999). Robust H_∞-output feedback control of decoupled automobile active suspension systems. *IEEE Transactions on Automatic Control*, 44(2):392–396.

[73] Hedrick, J. and Wormley, D. (1975). Active suspensions for ground transport vehicles-a state of the art review. Technical report.

[74] Hedrick, J. K. and Butsuen, T. (1990). Invariant properties of automotive suspensions. *Proceedings of the Institution of Mechanical Engineers, Part D: Journal of Automobile Engineering*, 204(1):21–27.

[75] Hillebrecht, P., Konik, D., Pfeil, D., Wallentowitz, H., and Zieglmeier, F. (1992). The active suspension between customer benefit and technological competition. In *Total Vehicle Dynamics. Volume 2.*

[76] Hollars, M. G., Rosenthal, D. E., Short, K., and Austin, A. (1991). Concurrent design and analysis of mechanisms. *Computers in Engineering*, pages 315–316.

[77] Hrovat, D. (1993). Applications of optimal control to advanced automotive suspension design. *Journal of Dynamic Systems, Measurement, and Control*, 115:328–328.

[78] Hrovat, D. (1997). Survey of advanced suspension developments and related optimal control applications. *Automatica*, 33(10):1781–1817.

[79] Hrovat, D. and Hubbard, M. (1987). A comparison between jerk optimal and acceleration optimal vibration isolation. *ASME Transactions on journal of Sound and Vibration*, 112(2):201–210.

[80] Hu, J., Bohn, C., and Wu, H. (2000). Systematic H_∞ weighting function selection and its application to the real-time control of a vertical take-off aircraft. *Control Engineering Practice*, 8(3):241–252.

[81] Huang, S.-J. and Lin, W.-C. (2003). Adaptive fuzzy controller with sliding surface for vehicle suspension control. *IEEE transactions on fuzzy systems*, 11(4):550–559.

[82] ISO 2631-1:1997 (1997). ISO 2631-1:1997, Evaluation of human exposure to whole-body vibration – Part 1: General requirements.

[83] ISO 4138:2004 (2004). ISO 4138:2004, Passenger cars – Steady-state circular driving behaviour – Open-loop test methods.

[84] ISO 7401:2011 (2011). ISO 7401:2011, Road vehicles – Lateral transient response test methods – Open-loop test methods.

[85] ISO 8608:1995 (1995). ISO 8606:1995, Mechanical Vibration-Road Surface Profiles- Reporting of Measured Data.

[86] ISO 8855:2011 (2011). ISO 8855:2011, Road vehicles - Vehicle dynamics and road-holding ability.

[87] Ivers, D. E. and Miller, L. R. (1991). Semi-active suspension technology. an evolutionary view. *ASME, NEW YORK, NY,(USA).*, 40:327–346.

[88] Jang, J.-S. and Sun, C.-T. (1995). Neuro-fuzzy modeling and control. *Proceedings of the IEEE*, 83(3):378–406.

[89] Jazar, R. (2008). *Vehicle Dynamics: Theory and Application*. Springer.

[90] Jones, W. (2005). Easy ride: Bose corp. uses speaker technology to give cars adaptive suspension. *IEEE Spectrum*, 42(5):12–14.

[91] Karnopp, D. (1983). Active damping in road vehicle suspension systems. *Vehicle System Dynamics*, 12(6):291–311.

[92] KARNOPP, D. (1987). Force generation in semi-active suspensions using modulated dissipative elements. *Vehicle System Dynamics*, 16(5-6):333–343.

[93] Karnopp, D. (1990). Design principles for vibration control systems using semi-active dampers. *Journal of Dynamic Systems, Measurement, and Control*, 112(3):448–455.

[94] Karnopp, D. (1995). Active and semi-active vibration isolation. *Transactions of the ASME-L-Journal of Vibration and Acoustics*, 117:177–185.

[95] Karnopp, D. (2009). How significant are transfer function relations and invariant points for a quarter car suspension model? *Vehicle system dynamics*, 47(4):457–464.

[96] Karnopp, D. and Margolis, D. (1984). Adaptive suspension concepts for road vehicles. *Vehicle System Dynamics*, 13(3):145–160.

[97] Keviczky, T. and Balas, G. J. (2006). Receding horizon control of an f-16 aircraft: a comparative study. *Control Engineering Practice*, 14(9):1023–1033.

[98] Kim, E.-S. (1996). Nonlinear indirect adaptive control of a quarter car active suspension. In *Control Applications, 1996., Proceedings of the 1996 IEEE International Conference on*, pages 61–66. IEEE.

[99] Klema, V. and Laub, A. (1980). The singular value decomposition: Its computation and some applications. *IEEE Transactions on automatic control*, 25(2):164–176.

[100] Kneppova, V., Kiffmeier, U., and Unbehauen, H. (1995). Weighting function selection in H_∞-optimal control with application to a thyristor-driven DC-motor. In *American Control Conference, Proceedings of the 1995*, volume 5, pages 3002–3006. IEEE.

[101] Koch, G., Fritsch, O., and Lohmann, B. (2010). Potential of low bandwidth active suspension control with continuously variable damper. *Control Engineering Practice*, 18(11):1251–1262.

[102] Kojima, H., Nakano, J., Nakayama, H., Kawashima, N., and Fujimoto, H. (1991). Development of new toyota electronic modulated suspension-two concepts for semi-active suspension control. Technical report, SAE Technical Paper.

[103] Kortüm, W. (1993). Review of multibody computer, codes for vehicle system dynamics. *Vehicle system dynamics*, 22(S1):3–31.

[104] Kumar, M. S. (2008). Development of active suspension system for automobiles using PID controller.

[105] Lanchester, F. (1936). Motor car suspension and independent springing. *Proceedings of the Institution of Automobile Engineers*, 30(2):668–762.

[106] Langlois, R. G. and Anderson, R. (1995). Preview control algorithms for the active suspension of an off-road vehicle. *Vehicle System Dynamics*, 24(1):65–97.

[107] Li, H., Yu, J., Hilton, C., and Liu, H. (2013). Adaptive sliding-mode control for nonlinear active suspension vehicle systems using T–S fuzzy approach. *IEEE Transactions on Industrial Electronics*, 60(8):3328–3338.

[108] Lin, J. and Lian, R.-J. (2011). Intelligent control of active suspension systems. *IEEE Transactions on industrial electronics*, 58(2):618–628.

[109] Lin, J.-S. and Kanellakopoulos, I. (1995). Nonlinear design of active suspensions. In *Decision and Control, 1995., Proceedings of the 34th IEEE Conference on*, volume 4, pages 3567–3569. IEEE.

[110] Martins, I., Esteves, J., Marques, G. D., and Da Silva, F. P. (2006). Permanent-magnets linear actuators applicability in automobile active suspensions. *IEEE Transactions on vehicular technology*, 55(1):86–94.

[111] Mastinu, G. and Ploechl, M. (2014). *Road and off-road vehicle system dynamics handbook*. CRC Press.

[112] Mehra, R. K., Amin, J. N., Hedrick, K. J., Osorio, C., and Gopalasamy, S. (1997). Active suspension using preview information and model predictive control. In *Control Applications, 1997., Proceedings of the 1997 IEEE International Conference on*, pages 860–865. IEEE.

[113] Merker, T., Girres, G., and Thriemer, O. (2002). Active body control (ABC) the DaimlerChrysler active suspension and damping system. Technical report, SAE Technical Paper.

[114] Miller, L. R. (1988a). Tuning passive, semi-active, and fully active suspension systems. In *Decision and Control, 1988., Proceedings of the 27th IEEE Conference on*, pages 2047–2053 vol.3.

[115] Miller, L. R. (1988b). Tuning passive, semi-active, and fully active suspension systems. In *Decision and Control, 1988., Proceedings of the 27th IEEE Conference on*, pages 2047–2053. IEEE.

[116] Milliken, W. F., Milliken, D. L., et al. (1995). *Race car vehicle dynamics*, volume 400. Society of Automotive Engineers Warrendale.

[117] Montazeri-Gh, M. and Kavianipour, O. (2014). Investigation of the active electromagnetic suspension system considering hybrid control strategy. *Proceedings of the Institution of Mechanical Engineers, Part C: Journal of Mechanical Engineering Science*, 228(10):1658–1669.

[118] Montazeri-Gh, M. and Soleymani, M. (2008). Genetic optimization of a fuzzy active suspension system based on human sensitivity to the transmitted vibrations. *Journal of Automobile Engineering*.

[119] Moradi, M. and Fekih, A. (2014). Adaptive PID-sliding-mode fault-tolerant control approach for vehicle suspension systems subject to actuator faults. *IEEE Transactions on Vehicular Technology*, 63(3):1041–1054.

[120] Morman, K. and Gianopoulus, F. (1982). Recent advances in the analytical and computational aspects of modeling active and passive vehicle suspensions. *Computational methods in ground transportation vehicles*, 50:75–115.

[121] Mousseau, C., Sayers, M. W., and Fagan, D. (1992). Symbolic quasi-static and dynamic analyses of complex automobile models. *Vehicle System Dynamics*, 20(sup1):446–459.

[122] Naude, A. and Snyman, J. (2003). Optimisation of road vehicle passive suspension systems. part 1. optimisation algorithm and vehicle model. *Applied Mathematical Modelling*, 27(4):249–261.

[123] Nicolas, R. (1991). Intelligent suspension system of lincoln MKZ to help mitigating pothole damage [internet]. http://www.car-engineer.com/intelligent-suspension-system-lincoln-mkz-help-mitigating-pothole-damage/.

[124] Olley, M. (1946). Road manners of the modern car. *Proceedings of the Institution of Automobile Engineers*, 41(1):523–551.

[125] Pfeiffer, F. (2008). *Mechanical system dynamics*, volume 40. Springer Science & Business Media.

[126] Poussot-Vassal, C., Sename, O., Dugard, L., Gaspar, P., Szabo, Z., and Bokor, J. (2008). A new semi-active suspension control strategy through LPV technique. *Control Engineering Practice*, 16(12):1519–1534.

[127] Priyandoko, G., Mailah, M., and Jamaluddin, H. (2009). Vehicle active suspension system using skyhook adaptive neuro active force control. *Mechanical systems and signal processing*, 23(3):855–868.

[128] Raiciu, T. (2009). How multi-link suspension works [internet], https://www.autoevolution.com/news/how-multi-link-suspension-works-7804.html.

[129] Rajamani, R. (2011). *Vehicle dynamics and control*. Springer Science & Business Media.

[130] Rajput, R. (2007). *A text book of Automobile Engineering*. Firewall Media.

[131] Ray, L. R. (1992). Robust linear-optimal control laws for active suspension systems. *Journal of dynamic systems, measurement, and control*, 114(4):592–598.

[132] Rubel, E., Haegele, K.-H., Panther, M., and Gatter, K. (1993). Semi-active suspension control. US Patent 5,189,615.

[133] Rumelhart, D. E., Hinton, G. E., Williams, R. J., et al. (1988). Learning representations by back-propagating errors. *Cognitive modeling*, 5(3):1.

[134] Ryan, R. (1990). Adams-multibody system analysis software. *Multibody Systems Handbook*, pages 361–402.

[135] Ryba, D. (1974). Improvements in dynamic characteristics of automobile suspension systems part 1. two-mass systems. *Vehicle System Dynamics*, 3(1):17–46.

[136] Sámek, D. and Dostál, P. (2008). Artificial neural networks in prediction and predictive control. In *Proceedings of the 22nd European Conference on Modelling and Simulation ECMS 2008*, pages 525–530.

[137] Sammier, D., Sename, O., and Dugard, L. (2003). Skyhook and h-infinity control of semi-active suspensions: Some practical aspects. *Vehicle System Dynamics*, 39(4):279–308.

[138] Sancibrian, R., Garcia, P., Viadero, F., Fernandez, A., and De-Juan, A. (2010). Kinematic design of double-wishbone suspension systems using a multiobjective optimisation approach. *Vehicle System Dynamics*, 48(7):793–813.

[139] Sato, M., Yokoyama, N., and Satoh, A. (2011). Gust alleviation control using robust MPC. In *Advanced Model Predictive Control*. InTech.

[140] Savaresi, S. M., Poussot-Vassal, C., Spelta, C., Sename, O., and Dugard, L. (2010a). *Semi-Active Suspension Control Design for Vehicles*. Elsevier Science.

[141] Savaresi, S. M., Poussot-Vassal, C., Spelta, C., Sename, O., and Dugard, L. (2010b). *Semi-active suspension control design for vehicles*. Elsevier.

[142] Sayers, M. (1990). Autosim user's manual, version 1.0 b8.

[143] Schiehlen, W. (2013). *Advanced multibody system dynamics: simulation and software tools*, volume 20. Springer Science & Business Media.

[144] Sharp, R. (1994). The application of multi-body computer codes to road vehicle dynamics modelling problems. *Proceedings of the Institution of Mechanical Engineers, Part D: Journal of Automobile Engineering*, 208(1):55–61.

[145] Sharp, R. and Hasan, S. (1987). Performance and design considerations for dissipative semi-active suspension systems for automobiles. *Proceedings of the Institution of Mechanical Engineers, Part D: Transport Engineering*, 201(2):149–153.

[146] Sharp, R. and Hassan, S. (1986a). An evaluation of passive automotive suspension systems with variable stiffness and damping parameters. *Vehicle System Dynamics*, 15(6):335–350.

[147] Sharp, R. and Hassan, S. (1986b). The relative performance capabilities of passive, active and semi-active car suspension systems. *Proceedings of the Institution of Mechanical Engineers, Part D: Transport Engineering*, 200(3):219–228.

[148] Sharp, R. and Hassan, S. (1987). On the performance capabilities of active automobile suspension systems of limited bandwidth. *Vehicle System Dynamics*, 16(4):213–225.

[149] Sharp, R. S. and Crolla, D. A. (1987). Road vehicle suspension system design - a review. *Vehicle System Dynamics*, 16(3):167–192.

[150] S.Levine, W. (2010). *Control System Advanced Methods*. CRC Press.

[151] Slotine, J.-J. E. and Li, W. (1987). On the adaptive control of robot manipulators. *The international journal of robotics research*, 6(3):49–59.

[152] Smith, M. C. and Walker, G. W. (2000). Performance limitations and constraints for active and passive suspensions: A mechanical multi-port approach. *Vehicle System Dynamics*, 33(3):137–168.

[153] Sobek, D. K., Ward, A. C., and Liker, J. K. (1999). Toyota's principles of set-based concurrent engineering. *Sloan management review*, 40(2):67.

[154] Society of Automotive Engineers. Vehicle Dynamics Committee (1978). *Vehicle Dynamics Terminology: SAE J670e : Report of Vehicle Dynamics Committee Approved July 1952 and Last Revised July 1976*. Handbook supplement.

[155] Strassberger, M. and Guldner, J. (2004). BMW's dynamic drive: an active stabilizer bar system. *IEEE control systems*, 24(4):28–29.

[156] Sun, W., Gao, H., and Kaynak, O. (2013a). Adaptive backstepping control for active suspension systems with hard constraints. *IEEE/ASME transactions on mechatronics*, 18(3):1072–1079.

[157] Sun, W., Zhao, Z., and Gao, H. (2013b). Saturated adaptive robust control for active suspension systems. *IEEE Transactions on Industrial Electronics*, 60(9):3889–3896.

[158] Sunwoo, M., Cheok, K. C., and Huang, N. (1991). Model reference adaptive control for vehicle active suspension systems. *IEEE Transactions on industrial electronics*, 38(3):217–222.

[159] Sutton, H. (1979). The potential for active suspension systems. *Automotive Engineer*, 4(2).

[160] Szászi, I., Bokor, J., and Gáspár, P. (2000). Mixed $H_2/\mathcal{H}_\infty$ control design for active suspension structures. *Periodica Polytechnica. Transportation Engineering*, 28(1-2):3.

[161] Tan, H.-S. and Bradshaw, T. (1997). Model identification of an automotive hydraulic active suspension system. In *American Control Conference, 1997. Proceedings of the 1997*, volume 5, pages 2920–2924. IEEE.

[162] Thompson, A. (1970). Design of active suspensions. *Proceedings of the Institution of Mechanical Engineers*, 185(1):553–563.

[163] Thompson, A. (1976). An active suspension with optimal linear state feedback. *Vehicle System Dynamics*, 5(4):187–203.

[164] Thompson, A. and Pearce, C. E. (1998). Physically realisable feedback controls for a fully active preview suspension applied to a half-car model. *Vehicle System Dynamics*, 30(1):17–35.

[165] Ting, C.-S., Li, T.-H. S., and Kung, F.-C. (1995). Design of fuzzy controller for active suspension system. *Mechatronics*, 5(4):365–383.

[166] Tseng, H. E. and Hrovat, D. (2015). State of the art survey: active and semi-active suspension control. *Vehicle system dynamics*, 53(7):1034–1062.

[167] Ulsoy, A., Hrovat, D., and Tseng, T. (1994). Stability robustness of LQ and LQG active suspensions. *Journal of dynamic systems, measurement, and control*, 116(1):123–131.

[168] Ulsoy, A. G., Peng, H., and Çakmakci, M. (2012). *Automotive control systems*. Cambridge University Press.

[169] Utkin, V. (1977). Variable structure systems with sliding modes. *IEEE Transactions on Automatic control*, 22(2):212–222.

[170] Valasek, M. and Kortüm, W. (2001). Semi-active suspension systems ii. *Mechanical Design Handbook*.

[171] van der Knaap, A. (1989). Design of a low power anti-roll/pitch system for a passenger car. *Delft University of Technology, Vehicle Research Laboratory, Report*, 89.

[172] Van der Sande, T., Gysen, B., Besselink, I., Paulides, J., Lomonova, E., and Nijmeijer, H. (2013). Robust control of an electromagnetic active suspension system: Simulations and measurements. *Mechatronics*, 23(2):204–212.

[173] Venhovens, P. T. and van der Knaap, A. (1995). Delft active suspension (das). background theory and physical realization. *Smart vehicles*.

[174] Wang, J., Wilson, D. A., Xu, W., and Crolla, D. A. (2005). Active suspension control to improve vehicl0e ride and steady-state handling. In *Decision and Control, 2005 and 2005 European Control Conference. CDC-ECC'05. 44th IEEE Conference on*, pages 1982–1987. IEEE.

[175] Wesselowski, K. and Cassandras, C. (2006). The elevator dispatching problem: Hybrid system modeling and receding horizon control. *IFAC Proceedings Volumes*, 39(5):136–141.

[176] Williams, D. A., Wright, P. G., and Davis, J. P. (1993). Control system for controlling the suspension of a land vehicle. US Patent 5,217,246.

[177] Wittenburg, J. and Wolz, U. (1985). MESA, VERDE: Ein computer programm zur simulation der michtlinearen dynamik von vielkorpersystemen. *Robotersysteme*, 1(1):7–18.

[178] Wright, P. and Williams, D. (1989). The case for an irreversible active suspension system. Technical report, SAE Technical Paper.

[179] Yagiz, N. and Sakman, L. (2005). Robust sliding mode control of a full vehicle without suspension gap loss. *Modal Analysis*, 11(11):1357–1374.

[180] Yakub, F. and Mori, Y. (2013). Model predictive control for car vehicle dynamics system-comparative study. In *Information Science and Technology (ICIST), 2013 International Conference on*, pages 172–177. IEEE.

[181] Yamashita, M., Fujimori, K., Hayakawa, K., and Kimura, H. (1994). Application of $\mathcal{H}_\infty$ control to active suspension systems. *Automatica*, 30(11):1717–1729.

[182] Yao, G., Yap, F., Chen, G., Li, W., and Yeo, S. (2002). Mr damper and its application for semi-active control of vehicle suspension system. *Mechatronics*, 12(7):963–973.

[183] Yoshimura, T., Kume, A., Kurimoto, M., and Hino, J. (2001). Construction of an active suspension system of a quarter car model using the concept of sliding mode control. *Journal of Sound and Vibration*, 239(2):187–199.

[184] Yoshimura, T., Nakaminami, K., Kurimoto, M., and Hino, J. (1999). Active suspension of passenger cars using linear and fuzzy-logic controls. *Control Engineering Practice*, 7(1):41–47.

[185] Yu, D. and Gomm, J. (2003). Implementation of neural network predictive control to a multivariable chemical reactor. *Control Engineering Practice*, 11(11):1315–1323.

[186] Yu, F. and Crolla, D. (1998). An optimal self-tuning controller for an active suspension. *Vehicle System Dynamics*, 29(1):51–65.

[187] Yu, M., Evangelou, S. A., and Dini, D. (2017). Model identification and control for a quarter car test rig of series active variable geometry suspension. In *20th IFAC World Congress*.

[188] Yue, C., Butsuen, T., and Hedrick, J. (1988). Alternative control laws for automotive active suspensions. In *American Control Conference, 1988*, pages 2373–2378. IEEE.

[189] Zames, G. (1981). Feedback and optimal sensitivity: Model reference transformations, multiplicative seminorms, and approximate inverses. *IEEE Transactions on automatic control*, 26(2):301–320.